

DEVELOPMENT OF A GLASS-CERAMIC FOR BIOMEDICAL
APPLICATIONS

A THESIS SUBMITTED TO
THE GRADUATE SCHOOL OF NATURAL AND APPLIED SCIENCES
OF
MIDDLE EAST TECHNICAL UNIVERSITY

BY

JONGEE PARK

IN PARTIAL FULFILLMENT OF THE REQUIREMENTS
FOR
THE DEGREE OF DOCTOR OF PHILOSOPHY
IN
METALLURGICAL AND MATERIALS ENGINEERING

FEBRUARY 2008

Approval of the thesis:

**DEVELOPMENT OF A GLASS-CERAMIC FOR BIOMEDICAL
APPLICATIONS**

submitted by **JONGEE PARK** in partial fulfillment of the requirements for the degree of **Doctor of Philosophy in Metallurgical and Materials Engineering Department, Middle East Technical University** by,

Prof. Dr. Canan Özgen
Dean, Graduate School of **Natural and Applied Sciences**

Prof. Dr. Tayfur Öztürk
Head of Department, **Metallurgical and Materials Engineering**

Prof. Dr. Abdullah Öztürk
Supervisor, **Metallurgical and Materials Engineering Dept., METU**

Examining Committee Members:

Prof. Dr. Muharrem Timuçin
Metallurgical and Materials Engineering Dept., METU

Prof. Dr. Abdullah Öztürk
Metallurgical and Materials Engineering Dept., METU

Prof. Dr. Bekir Karasu
Materials Science and Engineering Dept., Anadolu Univ.

Prof. Dr. Feza Korkusuz
Physical Education and Sports Dept., METU

Assist. Prof. Dr. Caner Durucan
Metallurgical and Materials Engineering Dept., METU

Date:

I hereby declare that all information in this document has been obtained and presented in accordance with academic rules and ethical conduct. I also declare that, as required by these rules and conduct, I have fully cited and referenced all material and results that are not original to this work.

Name, Last Name : Jongee Park

Signature :

ABSTRACT

DEVELOPMENT OF A GLASS-CERAMIC FOR BIOMEDICAL APPLICATIONS

Park, Jongee

Ph.D., Department of Metallurgical and Materials Engineering

Supervisor : Prof. Dr. Abdullah Ozturk

February 2008, 179 pages

The glass-ceramics containing apatite [$\text{Ca}_{10}(\text{PO}_4)_6(\text{O},\text{F}_2)$] and wollastonite [$\text{CaO}\cdot\text{SiO}_2$] crystals as the predominant crystalline phases, (A-W glass-ceramics) were produced through controlled crystallization of the glasses in the MgO-CaO-SiO₂-P₂O₅-F system. Phases formed in the crystallized counterpart of the glasses were identified by powder X-ray diffraction (XRD) analysis. The crystal morphology of the resultant glass-ceramics was examined using a scanning electron microscope (SEM). The crystallization kinetic parameters consisting of the activation energy for crystallization, (*E*), the Avrami parameter, (*n*), and frequency factor of the glass were determined with regard to small amount of TiO₂ additions using non-isothermal differential thermal analysis (DTA). The values for *E* and *n* for apatite and wollastonite were 460 kJ/mol and 433 kJ/mol, and 3.1±0.1 and 1.5±0.1, respectively. When 4 wt% TiO₂ was incorporated into the base glass, the values for *E* decreased to 408 and 320 kJ/mol for apatite and wollastonite, respectively; but the values for *n* increased from 3.1±0.1 to 3.3±0.1, and from 1.5±0.1 to 1.9±0.1 for apatite and wollastonite, respectively. TiO₂ is an effective nucleating agent in this glass system for promoting the precipitation of both apatite and wollastonite crystals.

Structure oriented changes in the indentation microhardness and tribological properties of the A-W glass-ceramics were evidenced. The microhardness at the free surface was 650 ± 12 H_V, but decreased with increasing depth distance from the free surface and attained 520 ± 8 H_V at a distance 0.5 mm below the free surface. The wear rate at the free surface was $0.7\pm 0.05 \times 10^{-4}$ mm³/Nm, but increased as the distance from the free surface increased and became $2.9\pm 0.15 \times 10^{-4}$ mm³/Nm at a distance 0.5 mm below the free surface. Tribological properties of the A-W glass-ceramics were compared with those of commercially available dental ceramics including IPS Empress 2[®], Cergo Pressable Ceramic[®], Cerco Ceram[®], Super porcelain EX-3[®], and bovine enamel. The wear rate, friction coefficient, and wear mechanisms of the A-W glass-ceramics were similar to currently used artificial dental materials.

Keywords: Apatite-wollastonite (A-W) glass-ceramic, Kinetics, Dental material, Tribology, Bioactivity.

ÖZ

BİYOMEDİKAL UYGULAMALAR İÇİN BİR CAM SERAMİĞİN GELİŞTİRİLMESİ

Park, Jongee

Ph.D., Metalurji ve Malzeme Mühendisliği Bölümü

Tez Yöneticisi : Prof. Dr. Abdullah Öztürk

Şubat 2008, 179 sayfa

Esas itibarıyla apatit [$\text{Ca}_{10}(\text{PO}_4)_6(\text{O},\text{F}_2)$] ve wollastonit [$\text{CaO}\cdot\text{SiO}_2$] kirstallerini içeren cam-seramikler, (A-W cam-seramikleri) $\text{MgO}\text{-CaO}\text{-SiO}_2\text{-P}_2\text{O}_5\text{-F}$ sistemindeki camların kontrollü olarak kristalleştirilmesi suretiyle üretildi. Camların kristalleşmiş hallerinde oluşmuş fazlar toz X-ışınları kırınım analiziyle belirlendi. Elde edilen cam-seramiklerin kristal morfolojileri tarama bir elektron mikroskobu (SEM) kullanılarak incelendi. Camın kristalleşme aktivasyon enerjisi, (E), Avrami parametresi (n), ve frekans faktöründen meydana gelen kristalleşme kinetik parametreleri düşük miktarda TiO_2 ilavelerine bağlı olarak sabit olmayan difransiyel termal analiz yöntemiyle belirlendi. Apatit ve wollastonit için belirlenen E ve n değerleri sırasıyla 460 kJ/mol ve 433 kJ/mol, ve 3.1 ± 0.1 ve 1.5 ± 0.1 idi. Başlangıç camına ağırlıkça %4 TiO_2 ilave edildiği zaman apatit ve wollastonit'in E değerleri sırasıyla 408 ve 320 kJ/mol'e düştü; fakat n değerleri sırasıyla 3.1 ± 0.1 'den 3.3 ± 0.1 'a ve 1.5 ± 0.1 'dan 1.9 ± 0.1 'a arttı. TiO_2 'nin bu cam sisteminde apatit ve wollastonit'in oluşmasını arttıran etkili bir çekirdekleyici unsur olduğu belirlendi.

A-W cam seramiklerin indentasyon mikrosertliğinde ve tribolojik özelliklerinde yapıya bağlı değişimler kanıtlandı. Yüzeydeki indentasyon mikrosertliği 650 ± 12 H_V idi. Fakat yüzeyden içeriye doğru derinlik mesafesi arttıkça azaldı ve yüzeyin 0.5 mm altındaki mesafede 520 ± 8 H_V oldu. Yüzeydeki aşınma hızı $0.7\pm 0.05 \times 10^{-4}$ mm^3/Nm idi, fakat yüzeyden içeriye doğru derinlik mesafesi arttıkça arttı ve yüzeyin 0.5 mm altındaki mesafede $2.9\pm 0.15 \times 10^{-4}$ mm^3/Nm oldu. A-W cam-seramiklerin tribolojik özellikleri ticari olarak elde edilebilir IPS Empress 2[®], Cergo Pressable Ceramic[®], Cerco Ceram[®], Super porcelain EX-3[®], ve dana dişi'nin tribolojik özellikleri ile karşılaştırıldı. A-W cam seramiklerin aşınma hızının, sürtünme katsayısının ve aşınma mekanizmalarının halen kullanılmakta olan yapay diş malzemelerinkilerine benzerdi.

Anahtar kelimeler: Apatit-wollastonit (A-W) cam-seramik, Kinetik, Diş malzemesi, Triboloji, Biyoaktivite.

ACKNOWLEDGMENTS

Praise the Lord. To Him who is worthy of all honor and glory.

First, I would like to express my deepest gratitude to Prof. Dr. Abdullah Öztürk, who is more than my PhD advisor. His knowledge, advice and encouragement throughout the entire stage of this dissertation will not be forgotten. Six years of studying under his guidance trained me to think critically and work scientifically from the academic view point. His support and understanding helped me to overcome difficult times during my years in METU. Thank you Sir.

I would want to acknowledge my committee members for imparting their knowledge and motivating me to achieve this goal. Thank you for your work and commitment.

My appreciation extends to my friends: Dr. Gürel Pekkan and Dr. Ahmet Çulhaoğlu, for their supportive and valuable discussions. I especially thank William Sawyer for his help in correcting my English. Thank you Friends.

Lastly, my special thanks goes to my family. Their constant support and love give me strength and cheer. To my beloved wife, Eunmi, and two sons, Haon and Hajun, who are always there to share in my successes and failures, your understanding, patience and support helped me complete this thesis. No words are adequate to express my heartfelt thankfulness for all you have done for me. I love you all.

TABLE OF CONTENTS

ABSTRACT	iv
ÖZ	vi
ACKNOWLEDGEMENTS	viii
TABLES OF CONTENTS	ix
LIST OF TABLES.....	xiv
LIST OF FIGURES.....	xvi
CHAPTER	
1. INTRODUCTION.....	1
1.1 INTRODUCTION.....	1
1.2 CHAPTER OVERVIEW	8
2. LITERATURE REVIEW	10
2.1 GLASS-CERAMIC.....	10
2.1.1 History and Applications	10
2.1.2 Glass-ceramic Process.....	11
2.1.2.1 Preparation of Glass	12
2.1.2.2 Shaping of Glass	12
2.1.2.3 Heat treatment of Glass	12
2.1.3 Phase Transformation by Manufacture Process	15
2.1.4 Kinetic Parameters	16
2.2 BIOACTIVE GLASS AND GLASS-CERAMIC	19
2.3 APATITE-WOLLASTONITE GLASS-CERAMIC.....	24
2.3.1 Composition and Properties	24
2.3.2 Effects of Various Additions.....	26
2.3.3 Reaction Kinetics of Bioactive Glass and Glass-ceramics.....	29
2.4 TEETH STRUCTURE.....	32
2.5 DENTAL CERAMICS	34
2.5.1 Sintered Porcelains.....	35
2.5.2 Glass-ceramics	36

2.6 TRIBOLOGY	38
2.6.1 Wear and Friction	39
2.6.2 Wear Simulation in Dentistry	40
2.6.3 Factors for Wear Simulation.....	42
2.7 PIN-ON-DISK TRIBOMETER	44
3. EXPERIMENTAL PROCEDURES.....	46
3.1 NUCLEATION AND CRYSTALLIZATION KINETICS OF A GLASS IN THE MgO-CaO-SiO ₂ -P ₂ O ₅ -F SYSTEM.....	46
3.1.1 Specimen Preparation.....	46
3.1.1.1 Glass Formation	46
3.1.1.2 Glass-ceramic Formation	48
3.1.2 Analyses	50
3.1.2.1 X-ray Diffraction.....	50
3.1.2.2 Scanning Electron Microscopy	50
3.1.2.3 Differential Thermal Analysis.....	50
3.2 THE EFFECT OF TiO ₂ ADDITION ON THE CRYSTALLIZATION KINETICS OF A GLASS IN THE MgO-CaO-SiO ₂ -P ₂ O ₅ -F SYSTEM	53
3.2.1 Specimen Preparation.....	53
3.2.1.1 Glass Formation	53
3.2.1.2 Glass-ceramic Formation	54
3.2.2 Analyses	54
3.2.2.1 X-ray Diffraction.....	54
3.2.2.2 Scanning Electron Microscopy	55
3.2.2.3 Differential Thermal Analysis.....	55
3.3 TRIBOLOGICAL PROPERTIES OF AN A-W GLASS-CERAMIC.....	57
3.3.1 Specimen Preparation.....	57
3.3.1.1 Glass Formation	57
3.3.1.2 Glass-ceramic Formation	57
3.3.1.3 Surface Grinding and Polishing	57
3.3.2 Analyses and Measurements	57
3.3.2.1 X-ray Diffraction.....	57

3.3.2.2 Scanning Electron Microscopy	58
3.3.2.3 Hardness	58
3.3.2.4 Tribology	58
3.3.2.5 Surface Profile.....	59
3.4 A COMPARISON OF TRIBOLOGICAL PROPERTIES OF A-W GLASS-CERAMICS WITH SELECTED DENTAL CERAMICS	62
3.4.1 Specimen Preparation.....	62
3.4.1.1 Preparation of A-W Glass-ceramics	62
3.4.1.2 Preparation of Commercial Dental Ceramics	62
3.4.2. Analyses and Measurements	64
3.4.2.1 Scanning Electron Microscopy	64
3.4.2.2 Hardness	64
3.4.2.3 Tribology	65
3.4.2.4 Surface Profile.....	65
3.5 TRIBOLOGICAL BEHAVIOR OF ALUMINA-ADDED A-W GLASS-CERAMICS	67
3.5.1 Specimen Preparation.....	67
3.5.1.1 Glass Formation	67
3.5.1.2 Glass-ceramic Formation	67
3.5.1.3 Simulated Body Fluid	68
3.5.2 Analyses and Measurements	70
3.5.2.1 X-ray Diffraction.....	70
3.5.2.2 Scanning Electron Microscopy	70
3.5.2.3 Hardness	70
3.5.2.4 Tribology	70
3.5.2.5 Surface Profile.....	71
3.6 BIOACTIVITY OF A-W GLASS-CERAMICS PRODUCED BY MELT-CASTING.....	73
3.6.1 Specimen Preparation.....	73
3.6.1.1 Glass Formation	73
3.6.1.2 Glass-ceramic Formation	73
3.6.1.3 Simulated Body Fluid	73

3.6.2. Analyses	74
3.6.2.1 X-ray Diffraction.....	74
3.6.2.2 Scanning Electron Microscopy	74
4. RESULTS AND DISCUSSION.....	76
4.1 NUCLEATION AND CRYSTALLIZATION KINETICS OF A GLASS IN THE MgO-CaO-SiO ₂ -P ₂ O ₅ -F SYSTEM.....	76
4.1.1 General	76
4.1.2 X-ray Diffraction Analysis	77
4.1.3 Scanning Electron Microscopy Analysis.....	83
4.1.4 Differential Thermal Analysis	89
4.2 THE EFFECT OF TiO ₂ ADDITION ON THE CRYSTALLIZATION KINETICS OF A GLASS IN THE MgO-CaO-SiO ₂ -P ₂ O ₅ -F SYSTEM	93
4.2.1 General	93
4.2.2 X-ray Diffraction Analysis	94
4.2.3 Differential Thermal Analysis	96
4.2.4 Scanning Electron Microscopy Analysis.....	103
4.3 TRIBOLOGICAL PROPERTIES OF A-W GLASS-CERAMICS	107
4.3.1 General	107
4.3.2 X-ray Diffraction Analysis	108
4.3.3 Scanning Electron Microscopy Analysis.....	109
4.3.4 Hardness and Wear Rate.....	110
4.3.5 Wear Rate	112
4.3.6 Surface Characterization	113
4.3.7 Friction Coefficient	115
4.4 A COMPARISON OF TRIBOLOGICAL PROPERTIES OF A-W GLASS-CERAMICS WITH SELECTED DENTAL CERAMICS	117
4.4.1 General	117
4.4.2 Hardness and Wear Rate.....	117
4.4.3 Surface Characterization	121
4.4.4 Friction Coefficient	128

4.5 TRIBOLOGICAL BEHAVIOR OF ALUMINA-ADDED A-W GLASS-CERAMICS	131
4.5.1 General	131
4.5.2 X-ray Diffraction Analysis	132
4.5.3 Hardness and Wear Rate.....	133
4.5.4 Friction Coefficient	136
4.5.5 Surface Characterization	138
4.6 BIOACTIVITY OF A-W GLASS-CERAMICS PRODUCED BY MELT-CASTING.....	143
4.6.1 General	143
4.6.2 X-ray Diffraction Analysis	144
4.6.3 Scanning Electron Microscopy	146
4.6.4 Electron Dispersive Spectroscopy Analysis.....	155
5. CONCLUSIONS	160
REFERENCES	163
CURRICULUM VITAE.....	177

LIST OF TABLES

TABLES

Table 1.1 Physical and mechanical properties of A-W glass-ceramic	3
Table 1.2 Failure loads obtained by detaching test between rabbit tibial bones and bioceramics after 8 weeks implantation	3
Table 2.1 Values of Avrami parameter (<i>n</i>) for various crystallization mechanisms	17
Table 2.2 Classification of bioceramics	20
Table 2.3 Composition (in wt %) of Bioglass® and selected glass-ceramics.....	22
Table 2.4 The evolution of bioactive glass and glass-ceramic implants	23
Table 2.5 Weight percentage of crystalline and glassy phases and their mechanical property in A-W glass-ceramic	26
Table 2.6 Mechanical properties of tooth.....	34
Table 2.7 Glass ceramics for dental restorations.....	38
Table 3.1 Starting materials, their manufacturer and catalog number.....	47
Table 3.2 Ingredients and batch composition of the glass.....	47
Table 3.3 Particle size of glass powders used for DTA.....	48
Table 3.4 Weight percent chemical composition of the glasses investigated.....	53
Table 3.5 Tribology test conditions	59
Table 3.6 The materials investigated and their manufacturer	63
Table 3.7 Ion concentration (mM) of SBF and human blood plasma	69
Table 3.8 Chemicals and their quantity in SBF in 1 liter of distilled water.....	69
Table 4.1 Comparison of 2θ and d-value of A-W glass-ceramic heat treated 1 h at 780 °C with those of the standard oxyapatite and fluorapatite	79
Table 4.2 Comparing of 2θ and d-value of standard wollastonite with A-W glass-ceramics heat treated 1 h at 780 °C followed by 30 min at various temperatures	81
Table 4.3 Kinetic parameters of the glass investigated in this study	92

Table 4.4 The value of the intensity of the (211) plane of apatite crystals for the glasses investigated.....	95
Table 4.5 Values of thermal parameters obtained from DTA for different heating rates for the glasses investigated.....	98
Table 4.6 Activation energy for crystallization (E), Avrami parameter (n) and frequency factor (ν) for apatite and wollastonite.....	100
Table 4.7 Knoop hardness, wear rate and friction coefficient of the A-W glass-ceramic	111
Table 4.8 Values of the hardness, wear rate and mean friction coefficient for the materials studied	118
Table 4.9 Knoop hardness, wear rate and friction coefficient in dry and in SBF	134

LIST OF FIGURES

FIGURES

Figure 2.1 Nucleation (N) and crystal growth (C) rate in dependence on temperature.....	13
Figure 2.2 Dependence of temperature on time during two-step heat treatment (A) and single-step heat treatment (B).....	13
Figure 2.3 Glass-ceramic from melt casting	15
Figure 2.4 Glass-ceramic from powder packing	16
Figure 2.5 Glass transition temperature (T_g), crystallization onset temperature (T_C), crystallization peak temperature (T_p) and width of the crystallization peak at half maximum (ΔT_f) from a DTA scan	18
Figure 2.6 Compositional dependence of bone bonding and soft-tissue bonding of bioactive glasses and glass-ceramics	21
Figure 2.7 Iliac spacers (left), artificial vertebrae (middle top), spinal spacers (middle bottom) and intervertebral spacers (right).....	25
Figure 2.8 Structure of tooth	32
Figure 2.9 Schematic representations of the wear modes	41
Figure 2.10 Geometry of pin-on-disk tribometer	45
Figure 3.1 Schedule of heat treatment for glass-ceramic formation	49
Figure 3.2 Flowchart showing the experimental procedure of the study on the nucleation and crystallization kinetics of a glass in the MgO-CaO-SiO ₂ -P ₂ O ₅ -F system.....	52
Figure 3.3 Flowchart showing the experimental procedure of the study on the effect of TiO ₂ addition on the crystallization kinetics of a glass in the MgO-CaO-SiO ₂ -P ₂ O ₅ -F system.....	56
Figure 3.4 Flowchart showing the experimental procedure of the study on tribological properties of an A-W glass-ceramic.....	61
Figure 3.5 Flowchart showing the experimental procedure of the study on a comparison of tribological properties of A-W glass-ceramics with selected dental ceramics	66
Figure 3.6 Flowchart showing the experimental procedure of the study on tribological behavior of alumina-added A-W glass-ceramics	72

Figure 3.7 Flowchart showing the experimental procedure of the study on bioactivity of A-W glass-ceramics produced by melt casting.....	75
Figure 4.1 XRD patterns obtained after heat treatment of the glass powders 1 h at different temperatures.....	78
Figure 4.2 XRD patterns obtained after heat treatment 1 h at 780 °C for the glass of different particle size.....	80
Figure 4.3 XRD patterns obtained after heat treatment of glass 1 h at 780 °C followed by 30 min at various temperatures. The particle size range of the glass powder is 500-850 μm.....	81
Figure 4.4 The variation of apatite-quartz intensity ratios of the glass heat treated 1 h at various temperatures.....	82
Figure 4.5 SEM image of the glass heat treated 1 h at 740 °C.....	83
Figure 4.6 SEM image of the glass heat treated 1 h at 760 °C.....	84
Figure 4.7 SEM image of the glass heat treated 1 h at 780 °C.....	84
Figure 4.8 SEM image of the glass heat treated 1 h at 800 °C.....	85
Figure 4.9 SEM image of the glass heat treated 1 h at 820 °C.....	85
Figure 4.10 SEM image of the A-W glass-ceramic heat treated 1 h at 780 °C followed by 30 min at 880 °C.....	87
Figure 4.11 SEM image of the A-W glass-ceramic heat treated 1 h at 780 °C followed by 30 min at 900 °C.....	87
Figure 4.12 SEM image of the A-W glass-ceramic heat treated 1 h at 780 °C followed by 30 min at 920 °C.....	88
Figure 4.13 SEM image of the A-W glass-ceramic heat treated 1 h at 780 °C followed by 30 min at 940 °C.....	88
Figure 4.14 SEM image showing the cracks induced by abnormal crystal growth in A-W glass-ceramic.....	89
Figure 4.15 DTA thermograms of glass with different particle size ranges. The measurements were done at the heating rate of 10 °C /min.....	90
Figure 4.16 DTA thermograms of the coarse glass powder (500-850 μm) measured at different heating rates.....	91
Figure 4.17 Kissinger plot of $\ln(\phi/T_p^2)$ vs $1/T_p$ of the glass with particle size range of 500-850 μm. (■ : 1 st exotherm, ○ : 2 nd exotherm).....	92
Figure 4.18 XRD patterns obtained after heat treatment 1 h at 780 °C for the glasses containing various amount of TiO ₂	95

Figure 4.19 XRD patterns obtained after heat treatment 1 h at 780 °C followed by 30 min at 900 °C for the glasses containing various amount of TiO ₂	96
Figure 4.20 DTA thermograms taken at the heating rate of 10 °C/min for the glasses investigated.....	97
Figure 4.21 The $\ln(\phi/T_p^2)$ vs $1/T_p$ curves for apatite	99
Figure 4.22 The $\ln(\phi/T_p^2)$ vs $1/T_p$ curve for wollastonite	100
Figure 4.23 Variation of the activation energy for crystallization with TiO ₂ additions	101
Figure 4.24 Variation of Avrami parameter with TiO ₂ additions	103
Figure 4.25 SEM micrographs of Glass 1 after heat treatment (a) at 780 °C for 1 h, and (b) at 780 °C for 1 h followed by 900 °C for 30 min.....	104
Figure 4.26 SEM micrographs of Glass 3 after heat treatment (a) at 780 °C for 1 h, and (b) at 780 °C for 1 h followed by 900 °C for 30 min.....	106
Figure 4.27 XRD patterns of the glass-ceramic. The patterns were taken from (a) the free surface, (b) 0.1 mm, (c) 0.3 mm and (d) 0.5 mm below the free surface.....	108
Figure 4.28 SEM micrographs taken from the cross sectional area, the free surface, and the interior part of the A-W glass-ceramic.....	109
Figure 4.29 Variation in microhardness and wear rate of the A-W glass ceramic with the depth distance from the free surface.....	112
Figure 4.30 SEM micrograph of the wear track obtained at the depth distance 0.5 mm below the free surface	114
Figure 4.31 Wear track profiles obtained for the free surface and for the subsurfaces.....	114
Figure 4.32 Variation in the friction coefficient of the glass-ceramic with sliding distance for the free surface and the subsurfaces.....	116
Figure 4.33 Knoop Hardness and wear rate of the materials investigated. The error bars indicate the \pm standard deviation of the data from the averages	119
Figure 4.34 SEM micrographs of representative wear tracks of the materials investigated	
(a) E2, (b) A-W GC1	122
(c) SPE1, (d) CCS1	123
(e) CPC, (f) A-W GC2.....	124
(g) CCS2, (h) SPE2	125
(i) BE.....	126

Figure 4.35 Wear track profiles obtained after tribological tests. (a) E2, (b) A-W GC1, (c) SPE1, (d) CCS1, (e) CPC, (f) A-W GC2 (g) CCS2, (h) SPE2, (i) BE	126
Figure 4.36 Variation in the friction coefficient with sliding distance for the materials studied.....	129
Figure 4.37 XRD patterns of the alumina-added A-W glass-ceramics sintered at various temperatures.....	133
Figure 4.38 Variation in the friction coefficient with sliding distance for the alumina-added A-W glass ceramics in dry condition.....	137
Figure 4.39 Variation in the friction coefficient with sliding distance for the alumina-added A-W glass ceramics in simulated body fluid.....	137
Figure 4.40 Variation in the friction coefficient with sliding distance for the commercial dental materials in dry condition simulated body fluid.....	138
Figure 4.41 SEM micrographs of the wear track for alumina-added A-W glass ceramics. The tracks were obtained after wear tests (a) in dry condition (b) in SBF	139
Figure 4.42 SEM micrographs of the wear track for commercial dental materials. The tracks were obtained after wear tests (a) in dry condition (b) in SBF	140
Figure 4.43 Wear track profiles for alumina-added A-W glass ceramics. The profiles were obtained after wear tests (a) in dry condition (b) in SBF	141
Figure 4.44 Wear track profiles for commercial dental materials. The profiles were obtained after wear tests (a) in dry condition (b) in SBF	142
Figure 4.45 XRD patterns obtained from the surface of the glass ceramic A before and after immersing in the SBF solution for 1, 10, and 20 days	145
Figure 4.46 XRD patterns obtained from the surface of the glass ceramic A-W before and after immersing in the SBF solution for 1, 10, and 20 days	145
Figure 4.47 SEM micrographs taken from (a) fracture surface, (b) surface of the coated later of sample A after being immersed in the SBF for 1 day	147
Figure 4.48 SEM micrographs taken from (a) fracture surface, (b) surface of the coated later of sample A after being immersed in the SBF for 10 days.....	148
Figure 4.49 SEM micrographs taken from (a) fracture surface, (b) surface of the coated later of sample A after being immersed in the SBF for 20 days.....	149

Figure 4.50 The variation of the surface apatite layer thickness with immerse duration for sample A	150
Figure 4.51 The variation of the crack length with immerse duration for sample A	151
Figure 4.52 SEM micrograph of sample A-W after being immersed in SBF for 1 day	152
Figure 4.53 SEM micrograph of sample A-W after being immersed in SBF for 10 days.....	152
Figure 4.54 SEM micrograph of sample A-W after being immersed in SBF for 20 days.....	153
Figure 4.55 The variation of the surface apatite layer thickness with immerse duration for sample A-W	154
Figure 4.56 EDS spectrum of the apatite layer on the surface of the sample A after being immersed 10 days	155
Figure 4.57 The variation of element composition with distance from the interface between glass-ceramic and apatite layer. The sample was immersed in SBF for 20 days	156
Figure 4.58 The change of Ca/P atomic ratio with distance from the interface between A glass-ceramic and apatite layer	157
Figure 4.59 EDS spectrum of the apatite layer on the surface of the sample A-W after being immersed 20 days	158
Figure 4.60 The variation of element composition with distance from the interface between A-W glass-ceramic and apatite layer. The sample was immersed in SBF for 20 days.	159
Figure 4.61 The variation of Ca/P atomic ration with distance from the interface between A-W glass-ceramic and apatite layer.....	159

CHAPTER 1

INTRODUCTION

1.1 INTRODUCTION

Glass-ceramics are polycrystalline solids prepared by controlled crystallization of glasses [1]. The process to produce a glass-ceramic involves first formation of a base glass and then application of an additional heat treatment to convert the glass into a glass-crystal mixture. The heat treatment results in the nucleation and growth of various kinds of crystalline phases with fine sizes in the base glass. The resultant glass-ceramic can display superior properties to the base glass and to the sintered ceramics. The key parameters in the heat treatment schedule are temperature and duration which lead maximum nucleation rate and crystal growth to obtain demanding properties. Uniform, reproducible, and fine-grain microstructure, absence of porosity, and wide-ranging properties which can be tailored by changes in composition and heat treatment [2,3] make glass-ceramics attractive for a wide variety of established uses. Moreover, the possibility of the utilization of standard glass-forming techniques, such as blowing, rolling, pressing and casting prior to crystallization heat treatment [1,4] enables manufacturers to produce complex shape parts.

Additional interest in glass-ceramics has developed due to their superior thermal, chemical, dielectric, mechanical, and biological properties. Because of these desirable engineering properties, they have found several applications as engineering materials and new uses constantly appear. Magnetic memory disk substrates, liquid crystal displays, nosecones of rockets, heat-resistant windows, telescope mirror blanks, biomaterials and consumer products such as household crockery are among the examples where glass-ceramics are successfully used [5].

Glass-ceramics have generated interest in the biomedical field, especially in the repair and replacement of natural bone and dental restoration, owing to their biocompatibility with living tissues [6-17]. Certain compositions of the glass-ceramics have shown bioactivity, generally defined as the ability to elicit favorable cellular response [18-22]. They have been considered as candidate material for the repair and reconstruction of diseased, damaged, or worn out parts of the hard tissues of the body. Some glass-ceramics have been marketed under commercial trade name such as Dicor[®] (mica glass-ceramic), Ceravital[®] (apatite-devitrite glass-ceramic) and Bioverit[®] (mica-apatite glass-ceramic) [23-31]. Among them the glass-ceramics containing apatite [$\text{Ca}_{10}(\text{PO}_4)_6(\text{O},\text{F}_2)$] and wollastonite [$\text{CaO}.\text{SiO}_2$] crystals (A-W glass-ceramics) as the predominant crystalline phases in the MgO-CaO-SiO₂ glass matrix have received great importance as biomaterial especially in the replacement of natural bone [32-43].

The discovery of A-W glass ceramics by Kokubo *et al.* in 1982 [32] has drawn great attention principally due to their biological ability to bond spontaneously to living bone in a short period, and their maintenance of high mechanical properties such as toughness and strength for a long period in a body environment [33,38]. Some of the physical and mechanical properties of A-W glass-ceramics are shown in Table 1.1. The apatite induces the biological ability of A-W glass-ceramic to bond spontaneously to living bone, while the wollastonite prevents straight propagation of cracks and promotes a reinforcing effect [34,35]. The bonding ability of A-W glass-ceramic to bone is superior to selected bioceramic materials as shown in Table 1.2. In vitro studies [38] reveal that A-W glass-ceramic binds to bone more tightly than hydroxyapatite, which is currently available for the repair of bone and joints defects, because it contains a glassy phase which releases more Ca ions in the early post implantation stage than does hydroxyapatite, and it releases silicate ions which may initiate crystallization of apatite as their nuclei on the surface of the implant [34].

Table 1.1 Physical and mechanical properties of A-W glass-ceramic [39,40].

Property	Value
Density (g/cm ³)	3.07
Bending strength (MPa)	215
Compressive strength (MPa)	1080
Young's modulus (GPa)	118
Vickers hardness (H _V)	680
Fracture toughness (MPa.m ^{0.5})	2.0

Table 1.2 Failure loads obtained by detaching test between rabbit tibial bones and bioceramics after 8 weeks implantation [38].

Bioceramic	Failure Load ± Standard deviation (kg)
Alumina	0.18 ± 0.018
Bioglass [®]	2.75 ± 1.80
Dense hydroxyapatite	6.57 ± 1.36
A-W glass-ceramic	7.44 ± 1.91

Properties of A-W glass-ceramics are influenced by the composition of the base glass and heat treatment schedule applied. The crystallization temperature of apatite crystals increases as the contents of MgO and SiO₂ increase, where MgO is more effective than SiO₂. The crystallization temperature of apatite crystals decreases as the contents of P₂O₅ and CaO increase, where P₂O₅ is more effective than CaO [44]. Moreover, as the Ca/P ratio in the base glass decreases, the melting temperature and hence the viscosity decreases. The melt becomes suitable for casting process. If the ratio of the Ca/P in the base glass is too low, bubbles are induced in the melt and the desirable chemical and mechanical properties of the resultant glass-ceramic decrease [45].

Minor additives such as Na_2O , B_2O_3 , Fe_2O_3 , CaF_2 and TiO_2 may also be incorporated in the chemical composition to modify or enhance the properties of A-W glass-ceramic. Previous studies have shown that adding Na_2O and P_2O_5 increase the rate of apatite formation in vitro test, but B_2O_3 , Fe_2O_3 , MgO and CaF_2 decrease the bioactivity [46,47]. Especially, the bioactivity is strongly dependent on the Al_2O_3 content [48]. The presence of Al_2O_3 inhibits the formation of Ca, P-rich layer, which in turn diminishes bone bonding ability, making the A-W glass-ceramic non-bioactive [37,41].

Because of the highly desirable engineering properties, A-W glass-ceramics have found special applications in clinic either in powder form as bone filler or in bulk material for fabricating iliac crest prostheses, artificial vertebrae, spinal spacers, and intervertebral spacers [39,40, 49,50]. Porous A-W glass-ceramics and composites containing A-W glass-ceramic powder have been also researched to extend the variety of potential applications [51-57]. Yamamuro [38] reported that A-W glass-ceramic has been used in spine and hip surgery of patients with extensive lesions or bone defects.

A-W glass-ceramics can be used as possible dental material in view of the fact that they possess similar mechanical properties to the natural teeth and commercial dental materials. The compressive strength and Vickers hardness of the natural teeth are 500 MPa and 338 H_V , respectively [58,59]. However, the utilization of A-W glass-ceramic for dental applications has been limited since it is bioactive and abrasive to the natural teeth. A-W glass-ceramic releases calcium ions when in contact with living tissues and supersaturates the surrounding fluid with calcium ions which triggers a precipitation of calcium and phosphate as apatite on the ceramic surface [40]. It is not desirable for a material to be used for dental restorations although the physical properties of the material are comparable to the natural teeth. Studies [37,48,60] have shown that through incorporation of small amount of Al_2O_3 to the composition of the base glass, non-bioactive high strength A-W glass-ceramic can be produced without changing the crystalline phases. Ohtsuki *et al.* [48] have publicized that CaO-SiO_2 glasses containing

Al_2O_3 do not form apatite crystals on their surfaces in simulated body fluid even after 30 days. A similar effect of Al_2O_3 on bioactivity has been reported for Ceravital-type apatite-containing glass ceramics in the system $\text{Na}_2\text{O-K}_2\text{O-MgO-CaO-SiO}_2\text{-P}_2\text{O}_5$ [61].

The wear of the restoration and of the opposing enamel is a serious concern in clinical applications, especially when enamel is in occlusal contact with a harder restoration [25]. Dental materials may be worn by enamel or they may cause aggressive wear of enamel. Attempts are being made to produce wear-friendly low-fusing ceramics with lower concentrations of crystal phase(s) and smaller crystal sizes to be used for the dental applications. Wear could be controlled by altering the microstructure of glass-ceramics [62]. Wear properties of this material must be determined clearly under adverse conditions if it is to be utilized in critical biomedical and dental applications. A clear understanding of the tribological behavior of A–W glass-ceramics is necessary for correlating the tribological properties, such as wear rate and friction coefficient, with structural characteristics of this material system. The understanding of tribological performance of this material could extend its employment to special dental applications such as veneers, inlays, onlays, crowns etc. Hence, studies carried out on the tribological behavior of A–W glass-ceramics have both scientific and technological significance.

Wear is the loss of material from one or both of two contacting surfaces because of the mechanical activity between them. It is a complicated process and is affected by properties such as ductility, hardness and ultimate strength [63-65]. The wear of dental ceramics includes diverse phenomena as abrasion, adhesion, erosion and fatigue [66-69]. In reality the various mechanisms usually act simultaneously and/or sequentially and often influence each other in a very complex way, with the result that wear processes tend to be very difficult to predict. Many wear test devices have been designed and used to simulate or, mimic human oral environment and mastication movement. Among the various techniques, pin-on-disk technique is a versatile tool for investigating the

tribological properties of materials and components. It is the most commonly employed and dependable technique [62,70-72] to determine the tribological behavior of materials. The specimen can be either pin or disk.

In spite of the good characteristics of A-W glass-ceramic, it is hard to prepare due to their high melting and forming temperatures. Precipitation of wollastonite crystals causes cracks, pores, or even fractures the bulk sample if the crystallization heat treatment is not properly performed. Oriented precipitation of wollastonite crystals in a long fibrous form tends to induce a fairly large amount of directional volume change, causing large cracks in the interior of the crystallized products [32]. Hence, the utilization of A-W glass-ceramic for dental applications necessitates a full understanding of the factors affecting the crystallization behavior. Otherwise the advanced properties may be degraded or totally ruined during processing or service. In spite of some investigations [33,73-75] on the formation, structure, and properties of A-W glass-ceramics, data on the crystallization kinetics of these materials are rare and sparse.

The nature of the crystallinity and distribution of the crystalline phase(s) formed during crystallization heat treatment depend on the kind and amount of nucleating agent used. It has been realized that TiO_2 is a good nucleation agent in many silicate glass systems [76,77]. However, for some glass systems TiO_2 acts in an opposite manner [78,79]. The role of TiO_2 as a nucleation agent in A-W glass-ceramic has been overlooked due to the fact that the chemical composition includes P_2O_5 and F to promote nucleation. Therefore, a study conducted on the role of TiO_2 as a nucleation agent in the MgO-CaO-SiO_2 glass system is essential to understand the crystallization behavior of A-W glass-ceramics.

This study was carried out with an effort to show that A-W glass-ceramics can be a new candidate material for dental applications. Attempts to control apatite and wollastonite crystallization, and to provide better understanding of the tribological behavior of this material system in dental applications are the primary motivations for this study. A comparison was made between the experimental results of this

study and the results of the previous studies published in the literature. The purposes of the study are;

- 1) To study the nucleation and crystallization mechanism of A-W glass-ceramics through kinetic characterization.
- 2) To study the tribological properties of A-W glass-ceramics produced by melt-casting.
- 3) To study the additive effect on the crystallization kinetics and tribological properties of A-W glass-ceramics.
- 4) To compare the tribological properties of A-W glass-ceramics with selected commercially available dental ceramics.
- 5) To study the bioactivity of the A-W glass-ceramics.

1.2 CHAPTER OVERVIEW

This dissertation is classified by chapters. Within each chapter, sections, tables, figures, equations and pages are sequentially numbered using the chapter number as a prefix. The dissertation contents are divided into six sections. Each section has slightly different experimental procedure and results and discussion, so experimental procedure (chapter 3), and results and discussion (chapter 4) are divided into six sections.

Chapter 2 provides necessary background on A-W glass-ceramic, nucleation and crystal growth, tribology and dental ceramics.

Chapter 3 explains the experimental procedures. In section 3.1, the experimental procedure for a study on the nucleation kinetics of a glass in the MgO-CaO-SiO₂-P₂O₅-F system by non-isothermal method was explained. The experimental procedure for a study on the effect of TiO₂ addition on the crystallization kinetics of a glass in the MgO-CaO-SiO₂-P₂O₅-F system was explained in section 3.2. In section 3.3 and 3.4, experimental procedures for a study on tribological properties of A-W glass-ceramics, and a comparison study of tribological properties of A-W glass-ceramics with selected dental ceramics, were explained, respectively. In section 3.5, the experimental procedure for a study on tribological behavior of alumina-added A-W glass-ceramics was explained. In section 3.6, the experimental procedure for a study on bioactivity of A-W glass-ceramic by melt casting was explained.

Chapter 4 presents the data obtained and discusses the results. Nucleation kinetics of a glass in the MgO-CaO-SiO₂-P₂O₅-F system was discussed in section 4.1. The crystallization mechanisms of apatite and wollastonite were examined, and their kinetic parameters were calculated and evaluated. In section 4.2, the effect of TiO₂ addition on the crystallization kinetics of a glass in the MgO-CaO-SiO₂-P₂O₅-F system was investigated. Addition of TiO₂ acted as a nucleation agent, promoting the crystallization of apatite and wollastonite. In section 4.3, tribological

properties of A-W glass-ceramics were evaluated. Because of different crystallization mechanisms, a unique morphology was acquired on the surface. The free surface was more wear resistant than the interior, since wollastonite whiskers were formed on the surface during heat treatment. Section 4.4 discusses the comparison of tribological properties of A-W glass-ceramics with selected dental ceramics. The wear rate and friction coefficient of A-W glass-ceramics were similar to commercial dental ceramics. In section 4.5, tribological behavior of alumina-added A-W glass-ceramics was investigated. Glass-ceramics were heat treated at different temperature and wear test were done in dry and saliva conditions. The tribological properties were affected by the heat treatment schedule and the wear test conditions. In section 4.6, bioactivity of A-W glass-ceramics formed by melt-casting was examined. Apatite formation ability on the surface of A-W glass-ceramics was studied by in vitro test using simulated body fluid.

Chapter 5 gives conclusions, based on the outcomes of the experimental results for each of the 6 sectional studies.

CHAPTER 2

LITERATURE REVIEW

2.1 GLASS-CERAMIC

2.1.1 History and Applications

Glass-ceramics are polycrystalline solids prepared by the controlled crystallization of glasses. Crystallization is accomplished by subjecting suitable glasses to a carefully regulated heat treatment schedule which results in the nucleation and growth of crystal phases within the glass. The concept of controlled crystallization of glass designates the separation of a crystalline phase from the glassy parent phase in the form of tiny crystals, where the number of crystals, their growth rate and thus also their final size are controlled by suitable heat treatment. The crystalline phases are entirely produced by crystal growth from a homogeneous glass phase. This specialty distinguishes glass ceramics from traditional ceramics where most of the crystalline material is introduced when the ceramic composition is prepared, although some recrystallization may occur or new crystal types may arise due to solid state reactions [4]. Glass-ceramics are also distinguished from glasses by the presence of major amounts of crystals since glasses are amorphous or non-crystalline.

An early attempt to obtain glass-ceramic knowledge was done by Reaumur, a French chemist [1]. He found that if glass bottles were packed into a mixture of sand and gypsum and then subjected to red heat for several days, they were converted into opaque objects. However, he could not control the crystallization process which is necessary for the production of true glass-ceramics. In 1959, about 200 years after Reaumur's experience, Corning glass workers developed the

glass-ceramics in their present form [17]. In principle, a metastable glass product is formed from liquid state by cooling it. During subsequent heat treatment, controlled crystallization occurs, with the nucleation and growth of internal crystals. Thus, a glass-ceramic is a multiphase solid containing a residual glass phase with a finely dispersed crystalline phase. The controlled crystallization of the glass results in the formation of tiny crystals that are evenly distributed throughout the glass. The number of crystals, their growth rate and thus their size are regulated by the time and temperature of the heat treatment.

Glass-ceramics have thermal, chemical, dielectric and biological properties that are generally superior to metals and organic polymers in many applications. Glass-ceramics are stable at high temperature, and are also unique in that they are one of the few classes of materials that can be made to exhibit zero, or even negative thermal expansion [2]. The material can also demonstrate resorbability or high chemical durability. Its electrical properties include a low dielectric constant, high resistivity, and high breakdown voltage, as well as superconductivity in particular cases [5]. Glass-ceramics are also biocompatible, and certain types of the material have also shown bioactivity, generally defined as the ability to elicit favorable cellular response [18-22]. Glass-ceramics are also widely used because they can be easily processed and machined using conventional tools, and they have high strength and toughness values compared to typical ceramics, which are usually very brittle. Because of these desirable engineering properties, they find uses in wide range of applications such as magnetic memory disk substrates, liquid crystal displays, nosecones of rockets, telescope mirrors, biomaterials and consumer products such as household crockery [5,9,22].

2.1.2 Glass-ceramic Process

The procedure for the preparation of glass-ceramic comprises the preparation of a homogeneous glass, the shaping of the glass to produce the required articles and finally, the application of a controlled heat treatment process to change the glass into a crystalline glass-ceramic.

2.1.2.1 Preparation of Glass

Glasses are made by heating together a mixture of raw materials, known as 'batch', at a sufficient high temperature to permit the materials to react with one another and to encourage the escape of gas bubbles from the melt [77]. Most glass batches melt homogeneously at temperatures between 1400 °C and 1600 °C. Inhomogeneities in the glass that have an unfavorable effect on the properties of the final product mostly appear more markedly in the crystallized material than in the original glass. It is thus necessary to pay attention to the homogeneity of the glass during batch preparation. In that regard, the purity of the starting materials is the most important. In glass-ceramics, materials of very high purity should be used since some types of impurity, even in quite small concentrations, could affect the crystallization characteristics of the glass [4].

2.1.2.2 Shaping of Glass

Upon completion of the melting process, the glass is cooled from the melting temperature to the working temperature where the glass has a higher viscosity. Various shaping methods, such as casting, rolling, drawing, pressing, and blowing are applied to the glass to produce the required shape and size of products [3].

2.1.2.3 Heat treatment of Glass

The objective of the heat treatment process is to convert the glass into a crystalline ceramic having properties superior to those of the base glass. The aim is to produce glass-ceramic containing crystals of small dimensions which are closely interlocked. Therefore, during heat treatment, not only the required physico-chemical properties must be attained, but also deformation, cracking or other detrimental effects must be avoided [2]. The production of large numbers of small crystals carries the requirement for efficient nucleation and this in turn means that careful control must be done over the nucleation stage of the heat treatment. Having nucleated the glass, it is necessary to raise the temperature further in order

to permit crystal growth of the nuclei. The crystallization process can be controlled in terms of the dependence of the nucleation and growth rates on temperature as shown in Figure 2.1. According to the heat treatment schedule, it can be divided into two processes; two-step heat treatment and single-step heat treatment as shown in Figure 2.2.

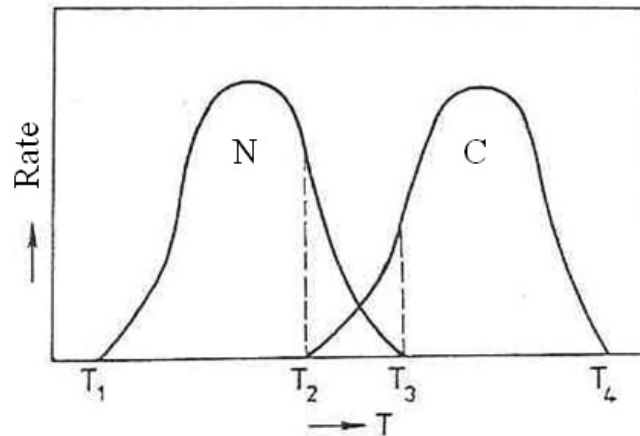


Figure 2.1 Nucleation (N) and crystal growth (C) rate in dependence on temperature [4].

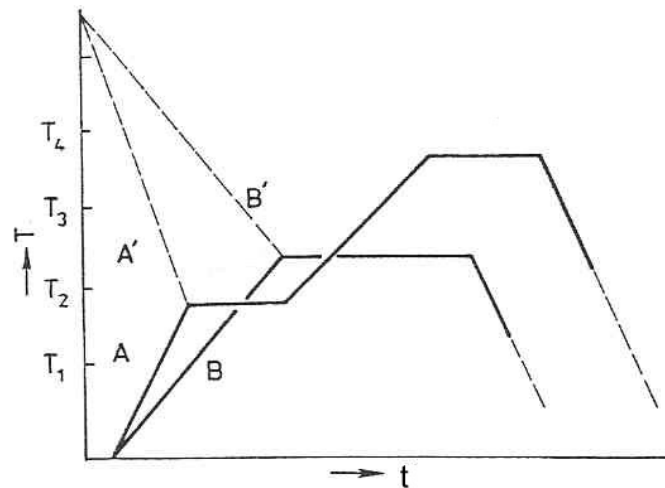


Figure 2.2 Dependence of temperature on time during two-step heat treatment (A) and single-step heat treatment (B) [4].

Two-step heat treatment: The crystallization process can be completely controlled if the nucleation and growth curves are separated. It means that the temperature difference (T_3-T_2) in Figure 2.1 is sufficiently small or negative. Then, the classical two-step heat treatment can be employed, as indicated by curve A in Figure 2.2. The product is heated to the nucleation temperature, selected between temperature T_1 and T_2 in Figure 2.1. After a certain time interval, the temperature is increased to the crystallization temperature between T_3 and T_4 , at which the crystallization is completed. The product is then cooled to room temperature. Normally, heating rates between 2 °C/min and 5 °C/min will be employed, although for thin glass-ware the rates as high as 10 °C/min can be used. The rate of cooling of the crystallized products can be around 10 °C/min depending on the thermal expansion characteristics of the crystal phases formed.

The two-step heat treatment can be modified if crystallization follows immediately after shaping. Then the temperature of the formed products does not fall to room temperature and procedure A can be used.

Single-step heat treatment: This procedure is used when nucleation occurs simultaneously with crystallization, when nucleation occurred already during product cooling, or during heating to the crystallization temperature [80]. At first, the nucleation and crystal growth curves must overlap partially in a certain temperature range ($T_2\sim T_3$) and controlled crystallization is limited. The single-step procedure is useful when a large amount of heat of crystallization is released, which unfavorable affect the course of the crystallization [80]. The procedure permits gradual, slow nucleus formation and growth, and distribution of the released heat over a longer time interval, as shown in curve B in Figure 2.2. Curve B means that the glass is cooled to the crystallization temperature directly from the melt.

2.1.3 Phase Transformation by Manufacture Process

Depending on manufacturing process, internally and externally nucleated glass-ceramics are produced. Figures 2.3 and 2.4 show the differences between these two. Internally nucleated glass-ceramics require the addition of a nucleation catalyst to the raw glass batch before melting. The melt is cast into a bulk glass and cooled. After cooling the formed bulk glass, it is given a heat treatment slightly above its transformation range to develop micro-heterogeneities upon which crystallization can subsequently begin (Figure 2.3 (a)) [5]. Further heat treatment produces a major phase change from glass to crystal that begins at the low energy surfaces of the tiny nuclei (Figure 2.3 (b)) and ends when the oxide raw materials of the major crystalline phases are depleted from the amorphous reservoir of the residual glass (Figure 2.3 (c)) [5]. In this process, bulk glass of precise shape can be formed and crystallized without significant distortion into a uniformly micro-crystalline ceramic.

On the other hand, externally nucleated glass-ceramics can be made in the powder packing process. Glass powder can be formed into shapes using press techniques with binders and plasticizers. Through the subsequent heat treatment, densification of the glass powder compact must occur prior to devitrification if a pore-free glass-ceramic is desired (Figure 2.4 (b)). The final result is a dense structure with a uniform crystal size normally finer than the grain size of the parent glass powder as shown in Figure 2.4 (c).

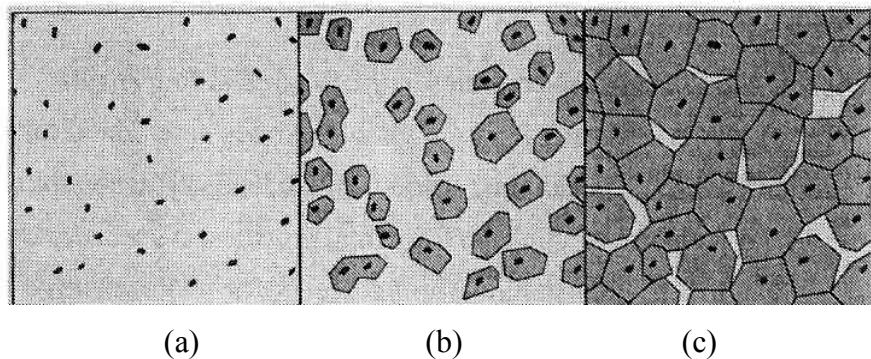


Figure 2.3 Glass-ceramic from melt casting [5].

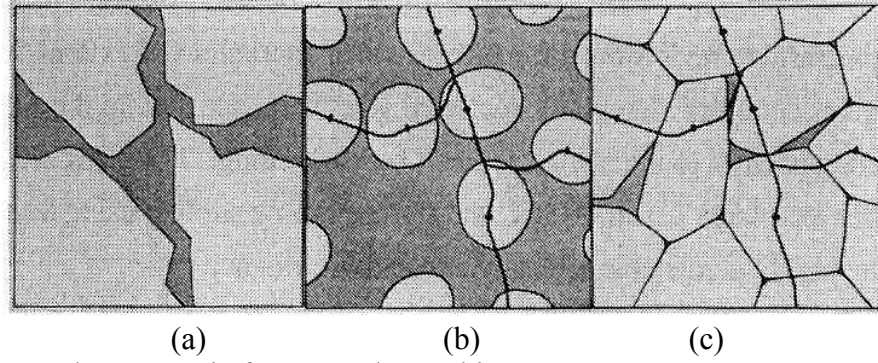


Figure 2.4 Glass-ceramic from powder packing [5].

2.1.4 Kinetic Parameters

The controlled transformation of glass into a polycrystalline material occurs during a predetermined heat treatment process. Properties and characteristics of the glass-ceramics can be varied by heating rate, time and temperature [2,4,80]. Parameters required for the heat treatment can be obtained from crystallization kinetic studies. Thermal analysis has been used to elucidate the nature of crystal growth using a differential thermal analyzer (DTA) [81-84].

The isothermal crystallization kinetic parameters are measured using the classical Johnson-Mehl-Avrami (JMA) equation [81].

$$x = 1 - \exp(-(kt)^n) \quad \text{Eq.1}$$

Taking natural logarithms and rearranging Eq.1, it can be obtained as follows;

$$\ln(1 - x) = n \cdot \ln(k) + n \cdot \ln(t) \quad \text{Eq.2}$$

where x is the volume fraction crystallized after time t , n is the Avrami parameter which depends on the growth direction number and the mechanism of nucleation and crystal growth as shown in Table 2.1, and k is the reaction rate constant.

Table 2.1 Values of the Avrami parameter (n) for various crystallization mechanisms [74,75].

Mechanism	n
Bulk crystallization	
Three-dimensional growth	3
Surface crystallization	
Two-dimensional growth	2
One-dimensional growth	1

Here, the reaction rate, k , can be expressed by the Arrhenius equation [81].

$$k = k_0 \exp\left(-\frac{E}{R T}\right) \quad \text{Eq.3}$$

where E is the activation energy for crystallization, R is the gas constant and T is the absolute temperature.

From the value of E , the value of the Avrami parameter n (the order of the crystallization reaction), is determined in accord with non-isothermal measurements using the method proposed by Augis and Bennett [82].

$$n = \frac{2.5}{\Delta T_f} \times \frac{T_p^2}{E/R} \quad \text{Eq.4}$$

where ΔT_f is the width of the crystallization peak at half maximum and T_p is crystallization peak temperature as seen in Figure 2.5. A sharp peak (small ΔT_f , large n) implies bulk crystallization, while a broad peak (large ΔT_f , small n) signifies surface crystallization. The Avrami parameter depends on the growth direction number and the mechanism of nucleation and crystal growth.

It should be noted that Eq.1 was derived with the assumption that nucleation and crystal growth were independent of time, which is valid only for isothermal conditions. Kissinger introduced equations to determine the crystallization activation energy from non-isothermal data. Later this approach was modified by others. This method is based on the dependence of the crystallization exotherm, T_p , and the heating rate, ϕ , as follows [83].

$$\ln\left(\frac{\phi}{T_p^2}\right) = \ln(v) - \ln\left(\frac{E}{R}\right) - \frac{E}{RT_p} \quad \text{Eq.5}$$

where v is the frequency factor for crystallization. A plot of $\ln(\phi/T_p^2)$ versus $1/T_p$ should yield a straight line whose slope and intercept may be used to calculate E and v , respectively.

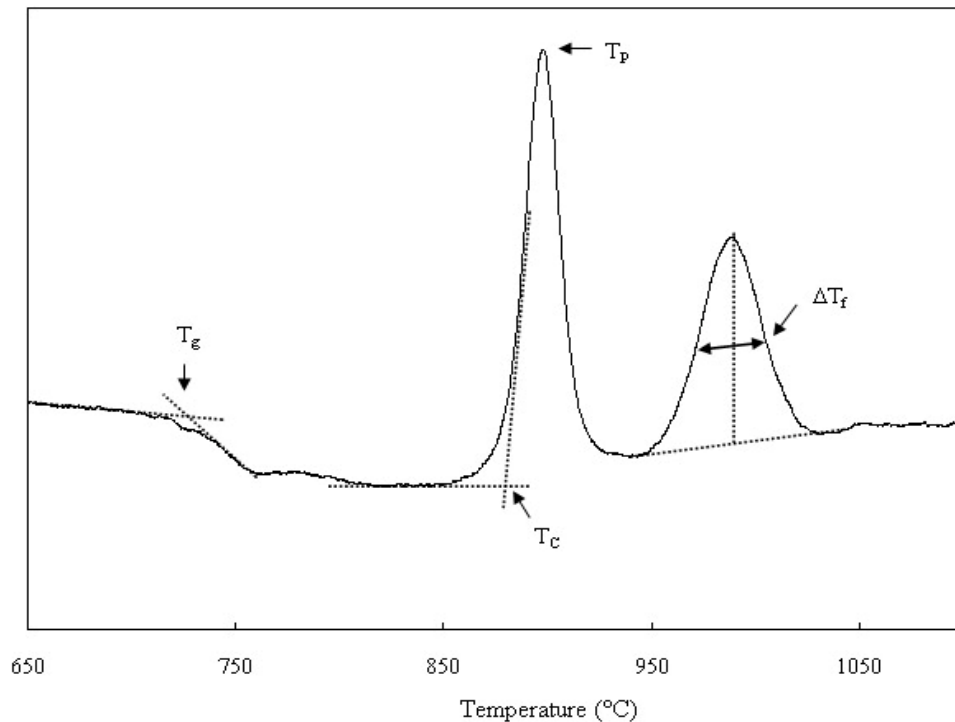


Figure 2.5 Glass transition temperature (T_g), crystallization onset temperature (T_c), crystallization peak temperature (T_p) and width of the crystallization peak at half maximum (ΔT_f) from a DTA scan.

2.2 BIOACTIVE GLASS AND GLASS-CERAMIC

Ceramics and glasses have been used for a long time in the medical industry for diagnostic instruments, thermometers, eye glasses, chemical wares and fiber optics for endoscopy. The implementation of ceramics as biomaterials was first cited in 1960 [85]. Ceramics and glasses have become candidates for the repair and reconstruction of diseased, damaged, or worn-out parts of the body, thus called bioceramics. The potential of bioceramics as implants is based on their compatibility with the physiological environment. The biocompatibility is related to their compositions that contain ions, such as sodium, potassium, calcium, magnesium, phosphorus, and ions showing limited toxicity to body tissues, such as aluminum, zirconium, and titanium, commonly found in the physiological environment [22,85-87].

Bioceramics are clinically used to repair hard tissues of the musculo-skeletal system, such as bones or teeth, joints, and to augment both hard and soft tissues. They can be used as bulk materials of a specific shape in many applications. Granule and powder bioceramics are also used for space fillers. In other cases, bioceramics can be used as a coating, or as a second phase in a composite producing a new material that improves both mechanical and biochemical properties [22,31].

Chemical reactivity and rate of tissue bonding are significantly controlled by composition and different phases present in the bioceramics. These materials are classified into three types, based on their chemical reactivity in physiological environment, as: nearly inert bioceramics, resorbable bioceramics, and surface reactive bioceramics. Reactivity and types of tissue attachment of the bioceramics with examples are summarized in Table 2.2.

Table 2.2 Classification of bioceramics [22,85,87].

Type of bioceramics	Chemical reactivity	Type of attachment	Example
Nearly inert	<ul style="list-style-type: none"> - biologically inactive - formation of fibrous tissue capsule of varying thickness around the material 	<ul style="list-style-type: none"> - bond grows into surface irregularities - press-fitting into defect - bone ingrowth (mechanical attachment) 	<ul style="list-style-type: none"> - high purity alumina ceramics - carbon - zirconia ceramics - hydroxyapatite coated metals
Surface reactive	<ul style="list-style-type: none"> - biologically active - formation of interfacial bond between material and tissue 	<ul style="list-style-type: none"> - attach directly by chemical bonding with the bone 	<ul style="list-style-type: none"> - hydroxyapatite - Bioglass[®] - Ceravital[®], Bioverit[®], Apatite-Wollastonite glass-ceramic
Resorbable	<ul style="list-style-type: none"> - biologically active - dissolve with the natural host tissue replacing the dissolved materials 	<ul style="list-style-type: none"> - slowly replaced by bone 	<ul style="list-style-type: none"> - calcium sulphate - trisodium phosphate - calcium and phosphate salts

Hench and his coworkers [21,22] discovered a glass (Bioglass[®]) that forms direct bonding to living bone within a certain range of composition as shown in Figure 2.6. The level of bioactivity is defined like $I_B=100/t_{0.5bb}$, where $t_{0.5bb}$ is the necessary time to bond to the bone to more than 50 % of the surface. In zone A, glasses are bioactive. In zone B, they behave almost like they are inert. In zone C, the glasses are resorbed in a time between 10 and 30 days. There is no technical interests in Zone D. All compositions in region A have a constant 6 wt% P₂O₅. A-W glass-ceramic has a higher P₂O₅ wt%. Region E (soft-tissue bonding) is inside the dashed line where $I_B>8$. [(*) 45S5 Bioglass[®], (▼)Ceravital[®], (●) 55S4.3 Bioglass[®]]

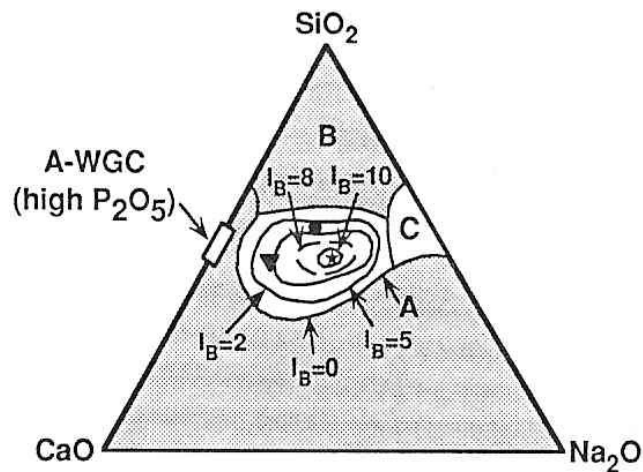


Figure 2.6 Compositional dependence of bone bonding and soft-tissue bonding of bioactive glasses and glass-ceramics [21,22].

The chemical bond between Bioglass[®] and living bone has been shown to depend on a high calcium and phosphorous concentration and to have a crystal structure similar to the human bone apatite [22,87,88]. This group developed several compositions of bioactive glasses (Table 2.3) which show different reactions in physiological environment. The compositions of Bioglass[®] also are compared with the other commercial glass-ceramics. The reactivity of the glass is lowered by increasing the silica content beyond 60 mole % and by adding multivalent cations, such as Al, Ti, Ta, Sb, Zr, into the glass. Substitution of fluorine ions for

oxygen ions is seen to slow down the reaction rate due to formation of stable fluorides which lower the solubility of surface reactive components. Therefore, the bioglasses of these compositions mechanically attach to the bone by formation of a fibrous capsule, similar to that seen in the case of bioinert implants.

Table 2.3 Composition (in wt %) of Bioglass[®] and selected glass-ceramics [29,87,89].

Component	Bioglass [®]			Ceravital [®]	Dicor [®]	Bioverit [®]
	45S5	45S5.4F	55S4.3			
SiO ₂	45	45	55	46.2	61.9	38.7
P ₂ O ₅	6	6	6			8.2
CaO	24.5	14.7	19.5	20.2	3.92	
Ca(PO) ₄				25.5		
CaF ₂		9.8				
MgO				2.9	15.4	27.7
MgF ₂						4.9
Na ₂ O	24.5	24.5	19.5	4.8		10.4
K ₂ O				0.4	15.4	6.8
Al ₂ O ₃					0.6	1.4
TiO ₂						1.9
Structure	Glass	Glass	Glass	Glass-ceramic	Glass-ceramic	Glass-ceramic

Though the Bioglass[®] forms a very strong bond to natural bone, unfortunately, its low mechanical strength (40~60 MPa) limits the application of this bioactive material to places with low loading. Requirements for load-bearing bioactive implants have led to a development of bioactive glass-ceramics. Controlled heat treatment on a suitable glass composition assists the formation of uniform, fine

crystals which in turn improves the mechanical properties. After the first glass-ceramic materials were developed, a large variety of different glass-ceramics have been developed on the basis of specific needs. The evolution of bioactive glass and glass-ceramic implants is outlined in Table 2.4.

Table 2.4 The evolution of bioactive glass and glass-ceramic implants.

Year (inventor)	Composition	Reference number
1969 (Hench and Wilson)	Na ₂ O-CaO-SiO ₂ -P ₂ O ₅	[22]
1972 (Grossman)	K ₂ O-MgO-SiO ₂ -Al ₂ O ₃ -F	[90]
1982 (Kokubo <i>et al.</i>)	MgO-CaO-SiO ₂ -P ₂ O ₅ -CaF ₂	[32]
1982 (Vogel <i>et al.</i>)	Na ₂ O-K ₂ O-CaO-MgO-F-Al ₂ O ₃ -SiO ₂ -P ₂ O ₅	[91]
1992 (Lin and Hon)	Na ₂ O-CaO-SiO ₂ -P ₂ O ₅	[92]
1994 (Liu and Chou)	MgO-CaO-SiO ₂ -P ₂ O ₅ -CaF ₂	[93]
2000 (Höland <i>et al.</i>)	Li ₂ O-K ₂ O-ZnO-CaO-SiO ₂ -P ₂ O ₅ -F	[94]

2.3 APATITE-WOLLASTONITE GLASS-CERAMIC

2.3.1 Composition and Properties

Glass can be converted into glass-crystal composites containing various kinds of crystalline phases with controlled sizes and contents by a suitable heat treatment. The resultant glass-ceramic can exhibit superior properties compared to that of parent glass and sintered crystalline ceramics. Through this process, in 1982 Kokubo *et al.* [32] invented a glass-ceramic composed of MgO 4.6, CaO 44.9, SiO₂ 34.2, P₂O₅ 16.3, CaF₂ 0.5 in weight percent, (wt%) later called A-W glass-ceramic. Upon heat treatment, two crystalline phases (apatite and wollastonite) were precipitated in the glassy phase [33,34]. It has been realized that growth of apatite and wollastonite crystalline phases in the parent glass is responsible for the substantial improvement in mechanical properties of this biomaterial.

A-W glass-ceramics are machined in various shapes, for example to make: iliac spacers, artificial vertebrae, spinal spacers and intervertebral spacers as shown in Figure 2.7. As seen in Table 1.1, A-W glass-ceramic has high bending strength even higher than that of human cortical bone (160 MPa), probably due to the precipitation of the wollastonite as well as apatite. It also presents high surface energy, high fracture toughness and high bending strength [40]. It has a roughened fracture surface, so wollastonite prevents straight propagation of cracks, promoting a reinforcing effect. However, surface crystallization of the wollastonite phase prohibits manufacture by melt-casting and products must be sintered from glass powders.

A-W glass-ceramic has been used in spine and hip surgery of patients with extensive lesions or bone defects due to its excellent mechanical strengths and capacity of binding to living bone. In vitro studies suggest that A-W glass-ceramic binds to bone more tightly than hydroxyapatite which is currently available for the repair of bone and joints defects. This is because it contains a glassy phase which releases more Ca ions in the early post implantation stage than does

hydroxyapatite, and releases silicate ions which may initiate crystallization of apatite as their nuclei on the surface of the implant.

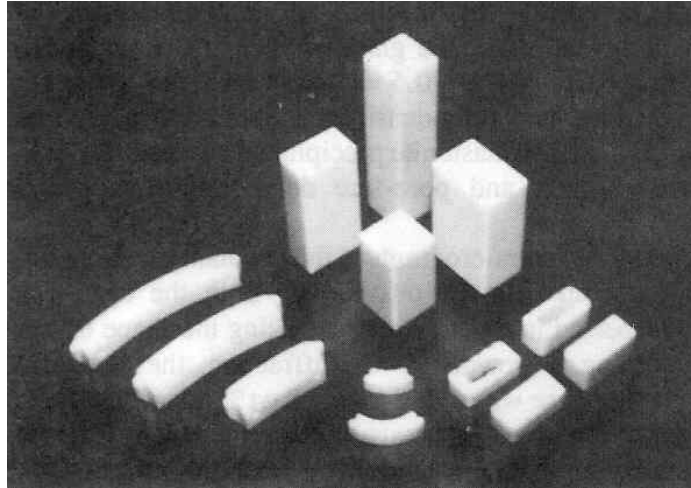


Figure 2.7 Iliac spacers (left), artificial vertebrae (middle top), spinal spacers (middle bottom) and intervertebral spacers (right) [40].

In a study on microstructure and mechanical properties of A-W glass-ceramic [35], three different crystals were precipitated during heat treatment. Glass phase was detected when the material was heated at 750 °C. With increasing the heating temperature to 870 °C, oxyfluorapatite [$\text{Ca}_{10}(\text{PO}_4)_6(\text{O},\text{F}_2)$] was detected. Wollastonite [$\text{CaO}\cdot\text{SiO}_2$] crystals started to be formed with apatite at 1050 °C. With increasing heating temperature to 1200 °C, a part of the apatite crystals were converted to whitlockite [$3\text{CaO}\cdot\text{P}_2\text{O}_5$]. The weight percentage of each crystalline and glassy phase, and their mechanical properties were listed in Table 2.5.

The content of the glassy phase decreased in the order of $G > A > A-W > A-W-CP$, where G, A, A-W and A-W-CP are the abbreviations used for the materials given in Table 2.5. Bending strength is considerably increased by precipitation of wollastonite crystals. A-W-CP has better mechanical properties than A-W and looks better as an implant. Machinability, however, is low and there was no significant difference between A-W and A-W-CP in the bonding strength in vivo test.

Table 2.5 Weight percentage of crystalline and glassy phases and their mechanical properties in A-W glass-ceramic [35].

Material	Apatite	Wollastonite	Whitlockite	Glass	σ_{air} (MPa)	σ_{N_2} (MPa)	K_{IC} (MPa.m ^{0.5})	E (GPa)	ν
G	0	0	0	100	72±25	120±20	0.8±0.1	89	0.28
A	35	0	0	65	88±12	141±26	1.2±0.1	104	0.27
A-W	35	40	0	25	178±20	193±12	2.0±0.1	117	0.27
A-W-CP	20	55	15	10	213±17	243±18	2.6±0.1	124	0.26

G: Glass, A: Apatite glass-ceramic, A-W: Apatite-wollastonite glass-ceramic, A-W-CP: Apatite-wollastonite-whitlockite glass-ceramic.

σ_{air} and σ_{N_2} are flexural strengths measured in air and nitrogen, respectively. ν is Poisson's ratio.

2.3.2 Effects of Various Additions

A small amount of CaF₂ was used in the composition to facilitate the sintering process, and to inhibit transformation of apatite to whitlockite at heat treatment temperature of 1200 °C [95]. Fluorine is considered to stimulate bone formation. A study on human bone apatite indicated that the presence of fluorine improves crystallinity of apatite [96]. This improvement might be caused by an increase in the number of nuclei which in turn enhances supersaturation of calcium phosphate. However, fluorine concentration has been limited in terms of effectiveness and toxicity. There is clear evidence for a dose-response relationship between fluorine concentration and caries-preventive effect, but there is also risk of dental fluorosis [97]. The excessive amount of fluorine will cause osteosclerosis and mottled tooth enamel. Therefore, the amount of fluoride incorporated in the glass composition must be limited if all the fluoride does not incorporate into the crystal structure [98].

Substitution of B_2O_3 for CaF_2 in A-W bioglass-ceramics was performed by Kitsugi *et al.* [99]. Experimental results show that mechanical properties, bone-bonding capability, and biocompatibility of the B_2O_3 modified A-W glass-ceramics are comparable with those of A-W glass-ceramics.

The effect of varying amounts of Al_2O_3 in A-W glass-ceramics on bone bonding behavior was studied by several researchers [37,41,61]. Results show that the presence of Al_2O_3 inhibits the formation of Ca, P-rich layers, which in turn diminishes bone bonding ability and reduces the reaction zone thickness.

When A-W glass-ceramic is implanted into a bone defect, it forms a thin layer, rich in Ca and P, on its surface and bonds to the surrounding bone through this apatite layer. The compositional and structural characteristics of this apatite are similar to those of apatite in natural bone [39]. It is expected that a bone-producing cell, osteoblast, would proliferate preferentially on the surface of the bone-like apatite layer. Consequently, the surrounding bone can grow directly on the surface apatite layer. When this occurs, a tight chemical bonding can form between the bone-like apatite layer and natural bone. As a result, A-W glass-ceramic can have a chemical bonding with the bone. This Ca, P-rich layer plays an essential role in forming the chemical bond of all bioactive materials which bond to bone [52].

The role of the residual glassy phase composition on bone bonding behavior was investigated by several research groups. Variation in a glass composition can either enhance or suppress bioactivity of the glass. Kitsugi *et al.* [42] compared chemical reactivity of A-W glass with 99.99 wt % SiO_2 glass by in vivo test. They noted that after implanting the SiO_2 glass in rabbits for 10 and 20 weeks, silica-gel layers and Ca, P-rich layers were not observed. On the other hand, formation of this chemical film was seen on the A-W glass 2 days after implantation. Kitsugi *et al.* [43] also showed that surface roughness of the A-W glass, abraded with alumina powder #2000, does not have significant effect on bond formation.

Ohura *et al.* [46] and Ebisawa *et al.* [47] studied bioactivity of P_2O_5 -free CaO-SiO₂ glasses with addition of various oxides and Ca-fluoride, i.e., Na₂O, B₂O₃, Al₂O₃, Fe₂O₃, P₂O₅, MgO, and CaF₂. Si-rich and Ca, P-rich layers were detected on all samples except that with Fe₂O₃ addition. It was observed from the in vitro test that the rate of apatite formation increased with Na₂O and P₂O₅ content, but decreased with B₂O₃, Fe₂O₃, MgO and CaF₂. In vivo tests showed that bioactivity of CaO-SiO₂ glasses increased with Na₂O and P₂O₅ additions, but decreased with B₂O₃, CaF₂, Al₂O₃, and Fe₂O₃ additions.

Ohtsuki *et al.* [48] investigated bioactivity of glasses in the system of CaO-SiO₂-Al₂O₃. After an in vitro test involving 7-30 days, formation of the Ca, P-rich layer was observed only on CaO-SiO₂-Al₂O₃ glasses in which Al₂O₃ content was less than 1.5 mol%. On the other hand, a Ca, P-rich layer was not detected on CaO-SiO₂-Al₂O₃ glasses containing more than 1.7 mol% Al₂O₃ or on SiO₂-free CaO-Al₂O₃ glass. The in vitro test showed that the bioactivity of the glass is suppressed by a certain amount of Al₂O₃ addition.

The effects of changes in glass composition on the crystallization behavior of apatite containing glass-ceramics in the system MgO-CaO-SiO₂-P₂O₅ were studied by Shyu and Wu [44]. These effects were described by several parameters. With increasing the contents of MgO and SiO₂, the crystallization temperature of apatite crystals increased, where MgO was more effective than SiO₂. With increasing the contents of P₂O₅ and CaO, the crystallization temperature of apatite crystals decreased, where P₂O₅ was more effective than CaO. However, the apatite nucleation rate and nucleation density increased with decreasing of the crystallization temperature without depending on the changes in the glass composition.

A-W glass-ceramic has been studied as filler in composite to improve the biocompatibility. The bone cements of bisphenol-a-glycidyl dimethacrylate (Bis-GMA) containing A-W glass-ceramic powder were soaked in simulated body fluid, and they showed a good bioactivity on the surface of the bone cement [53].

Moreover, A-W glass-ceramic powder promoted the osteoblastic differentiation of bone marrow cells intensively. A-W glass-ceramic powder has also been used in composites of polymethyl methacrylate (PMMA) [54,55] and polyethylene [56,57], and showed higher bioactive properties. The interface strength between bone and A-W glass-ceramic-coated implant was significantly higher than with non-coated implant. It means that histologically more bone tissue ingrowths occur in the A-W glass-ceramic coated implants. [7,100]

The ability to cast glass-ceramic is one of its process advantages. A-W glass-ceramic can be cast when it is heat treated at slightly over the melting temperature, because the viscosity decreases abruptly at that temperature. As the Ca/P ratio decreases, the melting temperature decrease and the viscosity also decreases [42]. It might be suitable for casing process. When the ratio of the Ca/P becomes too low, it will induce bubbles in the melt and the chemical and mechanical properties of the glass-ceramic product will decrease.

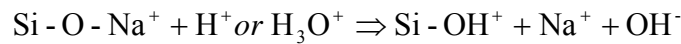
2.3.3 Reaction Kinetics of Bioactive Glass and Glass-ceramics

The ability to form a direct chemical bond to living tissues is a common characteristic among certain compositions of glasses, ceramics and glass-ceramics. The bonding at an implant-tissue interface is provided by the formation of a biologically active hydroxyl-carbonate apatite (HCA) layer, which has chemical constitutions and structure equivalent to the mineral phase in the natural bone. This type of bonding provides a strong adherence that resists substantial mechanical forces [85,86,91].

The base components are usually SiO_2 , Na_2O , CaO , and P_2O_5 . They have a certain compositional range to assure the bone bonding capability. For rapid formation of HCA layer, they contain less than 60 mole% SiO_2 , high Na_2O and CaO content, and a high $\text{CaO}/\text{P}_2\text{O}_5$ ratio [85,86].

Hench and his co-workers have developed kinetic concepts related to surface reactions from a series of investigations on several Bioglass[®] compositions. A sequence of at least five stages of reactions is proposed to describe the kinetics of bonding [86].

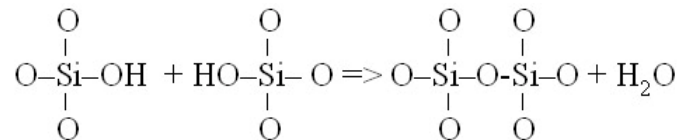
Stage 1: During immersing a bioactive glass in an aqueous solution, a leaching process takes place which involves ion exchange between cations (alkali or alkaline earth ions) from the glass, and hydrogen ions (H⁺ or H₃O⁺) from the solution. This reaction occurs very rapidly, within minutes of material exposure to body fluids, and creates a de-alkalinization of the surface layer with a net negative surface charge.



Stage 2: An alkaline interfacial pH leads to network dissolution by breaking of Si-O-Si- bonds. The silicate released into the solution thus forms silanol (Si-OH) at the glass-solution interface by the following reaction.



Stage 3: The hydrated silica (Si-OH) layer on the glass surface rearranges by condensation and re-polymerization reactions to form a SiO₂-rich gel layer.



Stage 4: Ca²⁺ and PO₄³⁻ groups that migrate from the glass to the surface through the silica-rich layer together with those from the solution form a calcium-phosphate (Ca,P)-rich layer. The Ca, P-rich layer is on the top of the silica gel layer in *in vitro* test, but immerses in the silica-gel layer for the *in vivo* test. These

dual films serve as an effective barrier for further leaching of cations. At this stage, the Ca, P-rich phase has an amorphous structure.

Stage 5: The amorphous CaO-P₂O₅ film crystallizes by incorporating OH⁻, CO₃²⁻, or F⁻ anions from the solution to form a mixture of hydroxyapatite, hydroxyl-carbonate apatite, hydroxyl-carbonate fluorapatite, or hydroxyfluorapatite.

Bioactive A-W glass-ceramic also bonds to living tissues through a similar mechanism. Kokubo [40] reported that calcium and silicate ions dissolved from A-W glass-ceramic into simulated body fluid (SBF). However, alumina-added A-W glass-ceramics hardly dissolved any ions into the SBF solution. Formation of HCA layer has been observed on A-W glass-ceramics, but not on alumina-added A-W glass-ceramics [37,39].

The effects of additives to bioactivity were discussed in section 2.3.2. The presence of hydrated silica-gel on the surface provides favorable sites for apatite nucleation. The calcium ions dissolved from the bioactive glass-ceramics together with the calcium and phosphate ions in the SBF solution form a Ca, P-rich layer on the provided nucleation sites. The thickness of the apatite layer increases with the soaking time, degree of supersaturation and temperature [40,101].

2.4 TOOTH STRUCTURE

A healthy tooth cut in half lengthways shows the layers of the tooth and its internal structure, as well as how the tooth relates to the gum and surrounding jaw bone in Figure 2.8. The tooth is divided into three parts: crown, neck and root. The crown is the part of the tooth that is visible above the gum (gingival). The neck is the region of the tooth that is at the gum line, between the root and the crown. The root is the region of the tooth that is below the gum. Some teeth have only one root, for example, incisors and canine teeth, whereas each molar and premolar has 4 roots per tooth [9,10,102].

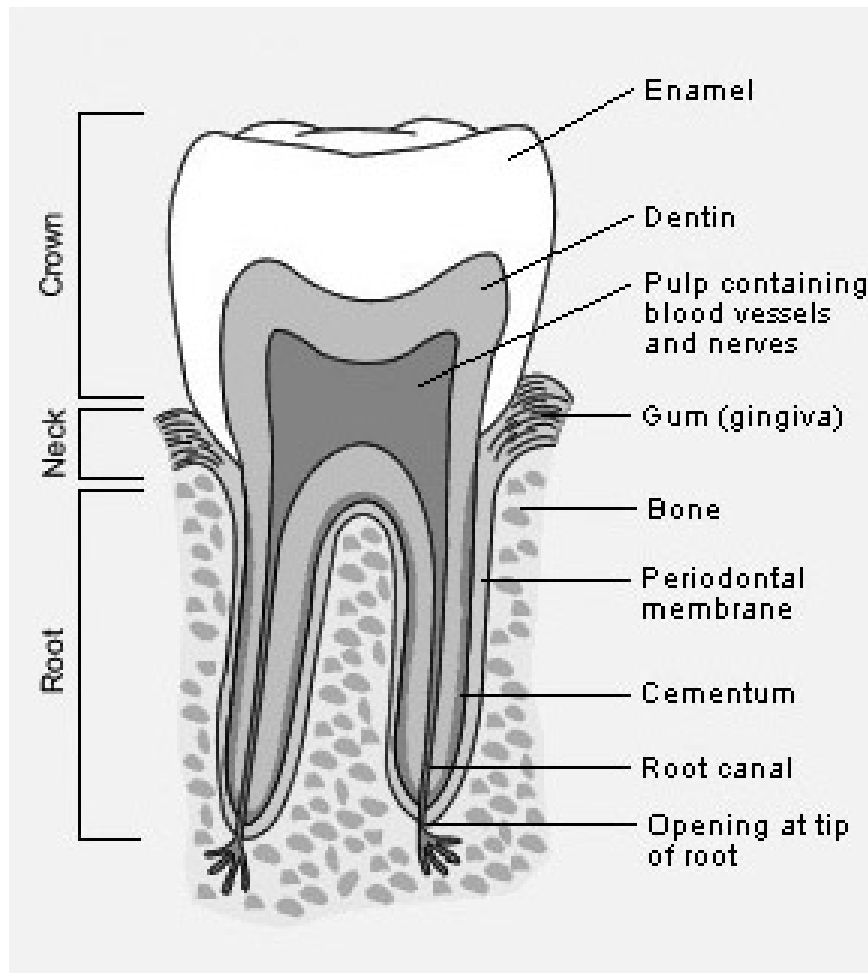


Figure 2.8 Structure of tooth [10].

The external region of the crown is enamel. It protects the underlying dentin. Enamel is the hardest substance in the human body, harder even than bone. It gains its hardness from tightly packed rows of calcium and phosphorus crystals within a protein matrix structure. Mature enamel is not considered to be a living tissue. So, when the tooth erupts, enamel can no longer be formed. This has important implications because any wear or loss of enamel due to decay, cannot be repaired by the body [10,102,103].

The internal region of the tooth is dentin. It is the major component of the inside of tooth, between the enamel and the dental pulp. Dentin is slightly softer than enamel. It contains collagen, water and hydroxyapatite crystals. Dentin is elastic and compressible in contrast to the brittle nature of enamel. The dentin is the main foundation of the tooth, supporting the enamel, providing protection to the pulp, and through its covering below the gums, giving rise to the attachment via a ligament to the surrounding bone. The tooth cannot, however, replace dentin that has been physically lost [56,102,104]. The mechanical properties of dentin are compared with those of enamel in Table 2.6.

Below the gum, the dentin of the root is covered with a thin layer of cementum, rather than enamel. Cementum is a hard bone-like substance onto which the periodontal membrane attaches. This membrane bonds the root of the tooth to the bone of the jaw. It contains elastic fibers to allow some movement of the tooth within its bony socket [10,59,102].

The pulp is the tissue that occupies the space in the center of the tooth, lying in the dentin. It is made of soft tissue and contains blood vessels to supply nutrients to the tooth, and nerves to enable the tooth to sense heat and cold. It also contains small lymph vessels which carry white blood cells to the tooth to help fight bacteria. The extension of the pulp within the root of the tooth is called the root canal. The root canal connects with the surrounding tissue via the opening at the tip of the root. This is an opening in the cementum through which the tooth's nerves supply and blood supply enter the pulp from the surrounding tissue [10,59].

Table 2.6 Mechanical properties of tooth [102].

	Enamel	Dentin
Fracture toughness (MPa.m ^{0.5})	0.7 ~ 1.3	1 ~ 2
Hardness (GPa)	4	0.5
σ_{UTS} (MPa)	-	70 ~ 80
Young's modulus (GPa)	60	5 ~ 17

2.5 DENTAL CERAMICS

As people retain their teeth for much longer than in the past, the need for aesthetically acceptable restorations is continuing to increase. In that sense, ceramic holds a special place in dentistry because it is still considered to produce aesthetically the most pleasing results. Its color, translucency and vitality cannot as yet be matched by any other materials such as resin or metal. This is reflected in the growing use by dentists of restorative procedures using ceramics. Ceramics will continue to be important restorative materials for many years to come [9].

The aesthetic appeal is not an only reason for dental application of ceramics. Ceramics possess several properties that make them suitable for use as dental materials. These properties include compressive strength, dimensional stability, radiopacity and durability with the oral environment [10,11]. Traditionally, dental ceramics are used in the construction of artificial teeth for dentures, crowns and bridges. Since the 1980s, however, the use of ceramics has been extended to include veneers, inlays/onlays, crowns and short span anterior bridges, since there have been tremendous advances in the mechanical properties and methods of these dental ceramics [12].

The first dental ceramic in dental application is porcelain. It dates from 1774, when a French pharmacy named Alexis Duchateau considered the possibility of replacing his ivory dentures with porcelain [12]. He succeeded to make the first

porcelain denture with the assistance of porcelain manufactures. Since then, many materials such as vulcanite, and recently polymethyl methacrylate, have helped to replace porcelain for dental applications. In 1963, Vita Zahnfabrik (Germany) introduced the first commercial porcelain [9].

Within the last few decades, a number of ceramics have been developed for dental applications. Each of these materials uses a different approach in attempting to improve the mechanical properties without being harmful to the aesthetic qualities of the ceramics. They can be clarified first according to the processing technique and second according to their major crystalline phase.

2.5.1 Sintered Porcelains

One of the most serious drawbacks with the early dental porcelains was their lack of strength and toughness, which seriously limited their use. The porcelain fractured from the fit surface outwards. One solution to overcome the problem is to provide the dental porcelain with support from stronger substructures, such as leucite, alumina, magnesia and zirconia.

Lucite-reinforced feldspathic porcelain was developed as a commercial name of Optec HSPTM (Jeneric/Pentro Inc.) containing up to 45 vol% tetragonal leucite [13]. The large amount of leucite in the material contributes to a high thermal contraction coefficient which leads mismatch between leucite and the glassy matrix and results in the development of tangential compressive stresses in the glass around the leucite crystals when cooled. These stresses can act as crack deflectors and contribute to increase the resistance of the weaker glassy phase to crack propagation.

Alumina-based core porcelain is a typical example of strengthening by dispersion of a crystalline phase [14]. Alumina has a high modulus of elasticity (350 GPa) and high fracture toughness (3.5 to 4 MPa.m^{0.5}) [14]. Its dispersion in a glassy matrix of similar thermal expansion coefficient leads to significant strengthening

of the core porcelain. Hi-Ceram (Vident) is a recent development of this technique.

Magnesia core porcelain was also developed [15]. Its high thermal expansion coefficient ($\sim 14.5 \times 10^{-6} / ^\circ\text{C}$) closely matches that of body and incisal porcelains designed for bonding to metal ($\sim 13.5 \times 10^{-6} / ^\circ\text{C}$). The flexural strength of unglazed magnesia core ceramic is twice as high (131 MPa) as that of conventional feldspathic porcelain (65 MPa). The magnesia core material can be significantly strengthened by glazing, that is by placing the surface under residual compressive stresses that have to be overcome before fracture can occur.

Zirconia fiber-reinforced porcelain was developed as commercial name of Mirage II (Myron Int.) [16]. Zirconia undergoes a crystallographic transformation from monoclinic to tetragonal at 1173 °C. Partial stabilization can be obtained by using various oxides such as CaO, MgO, Y_2O_3 and CeO, which allows the high-temperature tetragonal phase to be retained at room temperature. The transformation of partially stabilized tetragonal zirconia into the stable monoclinic form can also occur under stress and is associated with a slight particle volume increase. The result of this transformation is that compressive stresses are established on the crack surface, thereby arresting its growth.

2.5.2 Glass-ceramics

The unique properties of glass-ceramics allow them to be formed into complex shapes in the glassy state and to retain their finished dimensions during firing. Along with this, their aesthetic qualities, high strength and toughness, insensitivity to abrasion damage, chemical durability, thermal shock resistance, and polishability make them appropriate materials for use in dental restorations. Some of commercially available dental ceramics are listed in Table 2.7. The glass-ceramics used in dental applications are based on three different crystalline phases; fluoromica, leucite and lithia [17].

Dicor (Corning Glass Works) is a mica-based machinable glass-ceramic. The machinability of Dicor is made possible by the presence of a tetrasilicic fluoromica ($\text{KMg}_{2.5}\text{Si}_4\text{O}_{10}\text{F}_2$) as the major crystalline phase. These small crystals are interlocked with each other (named as 'house of cards' microstructure), resulting in greater mechanical strength and reinforcement [90]. Dicor is used in crowns, inlays, onlays and veneers. The flexural strength is in the region of 120-150 MPa.

The second glass-ceramic used for dental applications is a leucite (KAlSi_2O_6) crystalline-containing glass-ceramic. IPS Empress (Ivoclar Vivadent) is a representative leucite glass-ceramic which can be processed in various shapes and allow the manufacture of inlays and crowns [23,94]. As the glass-ceramic comprises a certain volume of glass phase, it can be pressed into a mold using the principle of viscous flow [11]. In addition to the pressing method, CAD/CAM procedures can also be used to manufacture leucite-based glass-ceramic restoration (ProCAD[®] in Table 2.8) [9,12,105]. All leucite glass-ceramic restorations are bonded to the tooth structure with a luting material, preferably an adhesive bonding system. The retentive pattern produced on the glass-ceramic surface is particularly advantageous in this respect.

IPS Empress 2 is a lithium disilicate glass-ceramic. It is based on the $\text{SiO}_2\text{-Li}_2\text{O}$ system and lithium disilicate ($\text{Li}_2\text{Si}_2\text{O}_5$) is the main crystalline which makes up some 70% of the volume of the glass-ceramic [94]. The microstructure of lithium disilicate glass-ceramic consists of many small interlocking plate-like crystals that are randomly oriented. The lithium disilicate crystals cause cracks to deflect, branch or blunt, therefore the propagation of cracks through this glass-ceramic is arrested by the crystals, providing a substantial increase in the flexural strength. The mechanical properties of this glass-ceramic are superior to that of the leucite glass-ceramic, with a flexural strength is in the region of 350-450 MPa and a fracture toughness approximately three times that of the leucite glass-ceramic [14,15].

Table 2.7 Glass ceramics for dental restorations.

Main crystalline phase	Application	Commercial name (manufacturer)	Reference number
feldspar	crowns, inlays, veneers	Duceram [®] (Degudent)	[106]
leucite	crowns, bridges	Optec OPC [®] (Jeneric Pentron)	[106]
leucite	crowns, inlays, veneers	IPS EMPRESS [®] (Ivoclar Vivadent)	[107]
leucite	crowns, inlays, veneers	ProCAD [®] (Ivoclar Vivadent)	[23]
leucite, fluoroapatite	crowns, bridges	IPS d.SIGN [®] (Ivoclar Vivadent)	[58]
lithium disilicate	crowns, bridges	IPS EMPRESS [®] 2 (Ivoclar Vivadent)	[107]
lithium metasilicate	crowns, inlays, veneers, bridges	IPS e.maz [®] (Ivoclar Vivadent)	[105]
mica	crowns, inlays	DICOR [®] MGC (Corning Inc.)	[108]
mica	crowns, inlays	DICOR [®] MGC (Corning Inc.)	[109]
porcelain	crowns, inlays, veneers	Super porcelain [®] EX-3 (Noritake Dental)	[110]

2.6 TRIBOLOGY

Tribology is the science and technology of interaction surfaces in relative motion and of related subjects and practices. ‘Tribology’ is derived from the Greek word ‘tribos’ meaning rubbing or sliding and was introduced only two decades ago. The nature and consequences of the interactions that take place at the moving interface control its wear, friction and lubrication behavior [111]. Understanding the nature of these interactions associated with the interfacial phenomena constitute the essence of tribology. Collection of all the mechanical, chemical and environmental parameters that can affect wear and wear behavior is referred to as

the tribo-system. Typical factors that can affect wear behavior are the properties of the materials, the nature of the relative motion, the ambient temperature, and the composition of the environment in which the wear occurs [62-64].

2.6.1 Wear and Friction

Wear is a progressive loss of material when two surfaces undergo relative movement under loads [63]. It is inevitable when two surfaces go through slip or sliding under load. The progressive loss results in the damage of the material and changes the surface characteristics. Wear testing has been used to rank wear resistance of materials for the purpose of optimizing material selection and development for a given application. In general, wear is evaluated by the amount of volume lost and the state of the wear surface. The degree of wear is described by wear rate which is defined as wear volume per unit distance and unit load [63].

$$W_R = \frac{V_{\text{loss}}}{F \cdot S} \quad \text{Eq.6}$$

In this equation, V_{loss} is the volume loss (mm^3), F is friction force (N) and S is the sliding distance (m). The experimental wear rates of metallic materials under different lubrication conditions show wide distribution in the range of 10^{-15} to 10^{-1} mm^3/Nm . For ceramics, such as Al_2O_3 , ZrO_2 , SiC and Si_3N_4 , under unlubricated sliding, the wear rates range from 10^{-9} to 10^{-2} mm^3/Nm , depending on operating conditions and material selections [111]. So, it can be said that the wear is not a property, but a system response.

Material-material interaction such as wear gives rise to the phenomenon of friction which resists to the relative motion between materials at the real area of contact [112]. In a system with no friction, there will be no wear. The magnitude or 'level' of friction is often expressed in terms of the coefficient of friction, μ , which is the force, F , to slide divided by the force or load, W , pressing the two solid bodies together.

$$\mu = F/W \quad \text{Eq.7}$$

Though exact values of friction cannot be predicted, general ranges of friction are rather easy to define. Very low friction can be achieved by rolling or elastic contact between solid surfaces that have low bonding force between them. Intermediate friction levels are found in materials that are moderately hard and not carefully cleaned. The highest friction is usually accompanied by much plastic flow in surfaces. Ceramic material pairs often have higher friction than do metals. Rubber has high friction when sliding against almost any other solids, and the friction is inversely related to the hardness of the rubber. However, the friction of rubber and plastics often varies in a manner that reflects their visco-elastic properties.

2.6.2 Wear Simulation in Dentistry

Wear is an important consequence of occlusal interactions in dentistry [64]. If not controlled, wear could lead to poor masticatory function with a concomitant reduction in quality of life and possible deterioration of systemic health. Restorative dental ceramics play an important part in wear, and differ significantly with respect to wear [65]. Dental ceramics may be worn by enamel or they may cause aggressive wear of enamel. The wear of dental ceramics includes diverse phenomena as abrasion, adhesion, erosion (tribochemical wear) and fatigue [66,67]. In reality the various mechanisms usually act simultaneously and/or sequentially and often influence each other in very complex ways, with the result that wear processes tend to be very difficult to predict [68]. Schematic representation of the wear modes is illustrated in Figure 2.9.

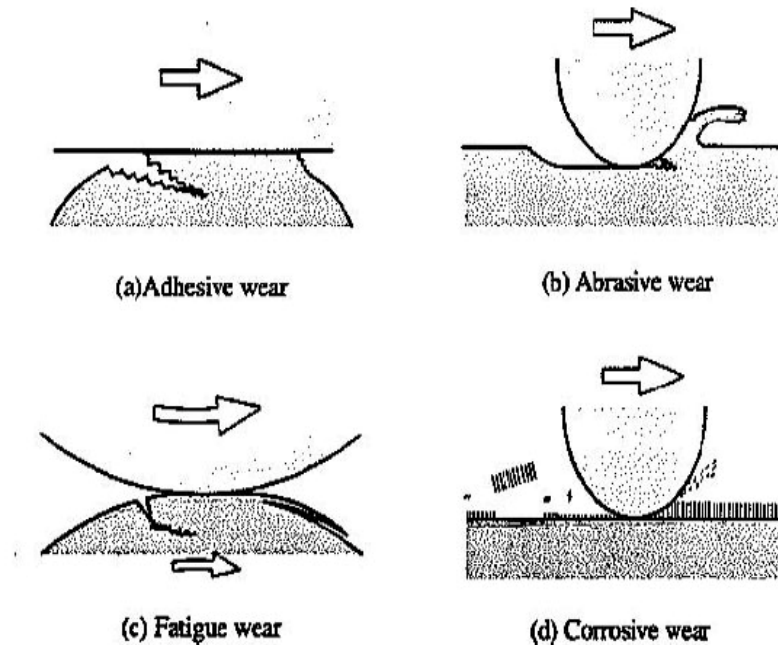


Figure 2.9 Schematic representations of the wear modes [111].

Adhesive wear occurs when there is a high attraction between surfaces such that ‘cold welds’ occur between the asperities [67]. It is schematically shown in Figure 2.9 (a). High adhesive shear stresses tear platelet-shaped wear particles out of the surface, which may remain attached to the antagonistic surface. In the mild case, this reduces the wear rate, and in the severe case can increase it.

Abrasion in dental literature is mainly caused by frictional surface interactions with toothbrush and paste, food bolus and fluid components during chewing [68]. This form of wear is considered an important mechanism of occlusal material loss in dental ceramics. It is divided into two different systems: two-body abrasion and three-body abrasion. Two-body abrasion occurs predominantly during non-masticatory tooth movement and is particularly in bruxism, while three-body abrasion occurs during mastication and is prevalent in person who eats an abrasive diet such as grained bread. If one surface is brittle, there is fracture of the asperities. If one surface is soft, then harder surface will plough into it, raising up chips which eventually fracture away as seen in Figure 2.9 (b).

Surface fatigue is a wear phenomenon that occurs in moving contact at cyclic load variations as shown in Figure 2.9 (c). Stress concentrates slightly below the surfaces, and then a network of subsurface cracks is created. Through the stress concentration, the cracks are very likely to grow and connect until the damaged area does not offer enough support for the superficial layer any more, which will then rapidly delaminate, leaving an extremely rough surface.

Dental erosion is caused when chemicals weaken the inter-molecular bonds of the surface and therefore potentiate the other processes [67,69]. To some extent this is not a wear process in its own right. In the mouth this effect is normally caused by acids. These acids weaken the surface, then they are rubbed away by the movement of the surfaces and immediately the underlying (previously unaffected) surface is attacked by the acid, as shown in Figure 2.9 (d).

2.6.3 Factors for Wear Simulation

Any laboratory investigation of the wear resistance of dental materials needs to consider oral conditions so that in vitro wear results can be correlated with in vivo findings. The factors affecting the wear simulation tests are; [62,65-72,74]

1. Antagonist: The choice of the countersample is a critical factor in establishing the pattern of tribological wear and in achieving an efficient in vitro wear testing system. Potential antagonists are listed below.

- Enamel
- Gold, ceramic and composite
- Stainless steel
- Annealed chromium-steel counterbodies
- Alumina
- Dental porcelain
- Steatite

2. Load: In the load, several variations are possible.
 - Contact loads: ranging from 1 ~ 100 N
 - Chewing force: 53 or 75.6 N maximum force
 - Abrasion load: 20 N
 - Attrition load: 90 N

3. Chewing frequency: It is related with the frequency of load cycles. The chewing frequency used in simulated wear studies varies from 1.2 to 1.7 Hz.

4. Sliding speed: The sliding speed (0.25 cm/s) during the in vitro study should be comparable with the in vivo situation.

5. Sliding distance: In order to compare results from different studies, the sliding distance should be taken into consideration. It ranges from 1 m to 600 m.

6. Temperature: It should be taken into account the temperature changes that can occur in the mouth. A constant temperature (20 °C, 37 °C) or thermocycling (5° to 55°C).

7. Food bolus during mastication: Several types of food bolus or slurry can be used during mastication movement simulating.
 - A slurry of water and un-plasticized polymethylmethacrylate beads
 - Polymethylmethacrylate powder
 - Hydroxyapatite slurry
 - Green carborundum slurry
 - Soft (CaCO₃) abrasive
 - Hard (SiC) abrasive
 - Millet-seed/PMMA-beads mixture

2.7 PIN-ON-DISK TRIBOMETER

Many wear test devices have been designed and used for different purposes. Some of them are quite simple while others are sophisticated in trying to mimic human oral environment and mastication movement. In principle, they can be classified into three types; scratch tests, two-body wear tests and three-body tests [70]. Scratch tests use a hard tip that slides on the sample surface to be studied. Two-body wear tests employ the relative movement between the sample and an abrasive surface. There are many variations of the geometric design and the selection of the abrasive surface. The most common variations are: pin-on-disk, pin-on-table, pin-on-belt, and pin-on-drum. Among them pin-on-disk is the most commonly employed technique [71]. The specimen can be either pin or disk. There are also different options for relative motion, such as circular, reciprocal and more complicated movements that simulate mastication. Three body tests employ a third-body medium between the two components in relative motion to mimic the function of food. Three-body system provided some correlation with clinical results, however, large variations were observed. Though the wear behavior of a particular product can be measured directly, the results are often difficult to interpret and to compare with other products because of a lack of detailed information about the formulation and processing of the material. Furthermore, the results of a particular in-vitro test often do not correlate with in-vivo studies [71].

The diversity of wear test methods being applied to materials has created problems in comparing results and in establishing a coherent wear technology based for these materials. Standardization of wear testing is a means to alleviate many of these problems. American Society for Testing and Materials (ASTM) is attempting to develop standard wear tests specifically suited for ceramic materials, either by modifying existing methods developed for other materials, or by developing new methods. One of the standards of wear test is ASTM G99-95A, entitled as ‘Standard Test Methods for Wear Testing with a Pin on Disc Apparatus’ [113].

Geometry of wear track, radius, and forces on disk is schematically shown in Figure 2.10. Rotating a test disk against a stationary test specimen pin (or ball) performs the test. The tribometer measures the tangential force between the two contacting surfaces and calculates the coefficient of friction as the ratio of the tangential force to the load. The results obtained from the test are usually expressed in the form of a wear rate, defined as the volume of material removed per sliding distance for a given load ($\text{mm}^3/\text{N.m}$) [70,71].

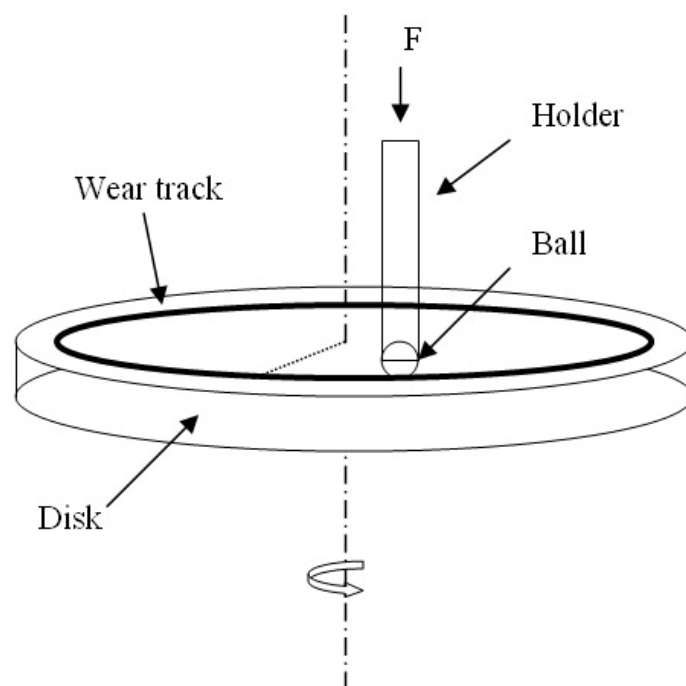


Figure 2.10 Geometry of pin-on-disk tribometer [72].

CHAPTER 3

EXPERIMENTAL PROCEDURES

3.1 NUCLEATION AND CRYSTALLIZATION KINETICS OF A GLASS IN THE MgO-CaO-SiO₂-P₂O₅-F SYSTEM

In this section, the experimental procedure for a study conducted on the nucleation and crystallization kinetics of a glass in the MgO-CaO-SiO₂-P₂O₅-F system that leads to formation apatite-wollastonite (A-W) glass-ceramic is explained.

3.1.1 Specimen Preparation

3.1.1.1 Glass Formation

A glass of the nominal composition of 4.6 MgO, 45.0 CaO, 34.0 SiO₂, 16.2 P₂O₅, and 0.2 F₂ in weight percent, wt%, was prepared from the mixtures of MgO, CaCO₃, SiO₂, CaHPO₄·2H₂O, and CaF₂. The chemical composition of this glass is the same as the glass developed by Kokubo *et al.* [32] to obtain A-W glass-ceramic. The starting materials used were extra pure grade powders to avoid any impurity effects, and purchased through local distributors. The manufacturer and catalog number of the starting materials are listed in Table 3.1. CaCO₃ and CaHPO₄·2H₂O are assumed to decompose into their stable oxides during firing as follows;

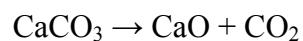


Table 3.1 Starting materials, their manufacturer and catalog number.

Starting material	Manufacturer	Item #
MgO	Merck	1.05862.1000
CaCO ₃	Merck	1.02066.1000
SiO ₂	Merck	1.13126.1000
CaHPO ₄ ·2H ₂ O	Merck	1.02146.9029
CaF ₂	Merck	1.02842.0100

The ingredients and batch composition of the glasses produced in this study are presented in Table 3.2. The batch composition is calculated by assuming that the batch materials are converted to their respective stable oxides during melting. The starting materials were carefully weighed (± 0.0001 g) to their proper amount in an analytical balance (Mettler Toledo, AB 204-S, Switzerland). The total weight of each batch was approximately 20 g. The batch was mixed and ground in an agate mortar with pestle. During mixing and grinding, distilled water was used. After mixing, the mixture was placed into an oven and dried at about 90 °C for at least 24 h.

Table 3.2 Ingredients and batch composition of the glass.

Ingredient	Batch composition (wt%)
MgO	3.40
CaCO ₃	42.07
SiO ₂	25.13
CaHPO ₄ ·2H ₂ O	29.03
CaF ₂	0.07

No heat treatment was applied to batches prior to melting. The batch was placed in a platinum crucible and melted in it at 1500 °C in an electrically heated muffle furnace. Melting took place in normal laboratory conditions without controlling the atmosphere. The melt was kept at this temperature for 1 h to ensure the homogeneity of the melt. Then, the melt was poured into a stainless steel plate to obtain glass blocks. The nominal dimensions of the blocks were approximately 30 × 30 × 7 mm in length × width × thickness, respectively. All glass blocks were annealed at 600 °C for 1 h.

After annealing, the glass blocks were heat treated at various temperatures for nucleation of the crystalline phase(s). Upon completion of the nucleation heat treatment, the glass blocks were crushed and ground in agate mortar with pestle, and then sieved through a series of screens for the differential thermal analysis. Particle size ranges prepared for this study are listed in Table 3.3. The glass particles are named coarse, medium and fine in accord with their size range.

Table 3.3 Particle size of glass powders used for DTA.

Identification	Size range of glass particle (µm)	Mesh number of screen
Coarse	500 – 850	#35 – #20
Medium	125 – 212	#120 – #70
Fine	< 45	< #325

3.1.1.2 Glass-ceramic Formation

The glass blocks and glass powders were heat treated at 740 °C to 820 °C, with 20 °C increment for the nucleation study. The heating rate was 5 °C/min and duration at the maximum temperature was 1 h. Cooling was done at a rate of 10 °C/min until 200 °C, and then the power of the furnace was turned off and the sample was furnace cooled to room temperature. The same heat treatment was

employed to all glass blocks and glass powders of different size. The glass blocks were used for microstructural studies and the glass powders were used for thermal and X-ray diffraction analyses.

Two-step heat treatment was performed to convert the glass blocks and glass powders to glass-ceramic. Figure 3.1 shows the heat treatment schedule for nucleation and crystal growth of the glass. Glasses were heat treated 1 h at T_1 for nucleation and then 30 min at $900\text{ }^\circ\text{C}$ for crystal growth with a heating rate of $5\text{ }^\circ\text{C}/\text{min}$. In this study, T_1 varied from $740\text{ }^\circ\text{C}$ to $820\text{ }^\circ\text{C}$ and T_2 varied from $880\text{ }^\circ\text{C}$ to $940\text{ }^\circ\text{C}$, with $20\text{ }^\circ\text{C}$ increments for both ranges. After holding the sample at T_2 for 30 min, the furnace was cooled until $200\text{ }^\circ\text{C}$ at a rate of $10\text{ }^\circ\text{C}/\text{min}$. The samples were furnace cooled from $200\text{ }^\circ\text{C}$ to room temperature with the power of the furnace turned off. The appearance of the blocks and powders after the heat treatment changed from transparent to opaque suggesting that microstructure morphology changed after heat treatment.

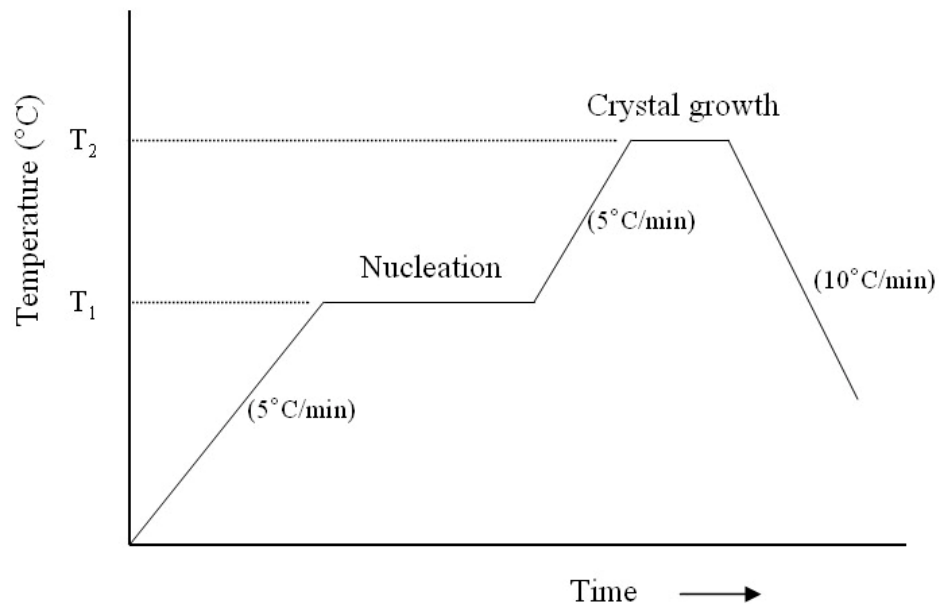


Figure 3.1 Schedule of heat treatment for glass-ceramic formation.

3.1.2 Analyses

3.1.2.1 X-ray Diffraction

Powder X-ray diffraction (XRD) was employed to identify phases formed during heat treatment in the crystallized counterparts of the glass. Measurements were done from $2\theta = 20$ to 50° with 0.02 step size, using Rikagu Geigerflex-DMAK/B (Japan) model operated at 40 kV and 20 mA utilizing Cu $K\alpha$ radiation. Quantitative X-ray analysis was employed using α -Quartz powder as an internal standard material. [114]

3.1.2.2 Scanning Electron Microscopy

A Jeol 6400 scanning electron microscope (SEM, Japan) was employed to examine the crystal morphology of the crystallized counterparts of the glass blocks. Prior to SEM analysis, the samples were mounted in epoxy resin and ground flat by using 240, 400, 800, and 1200 grit abrasive papers consecutively, and then polished with alumina powder solutions of 1 μm and 0.3 μm on a cloth to achieve a mirror-like surface finish. The polished samples were etched with 0.05 N HCl solution for 1 min, rinsed with distilled water, and then ultrasonic cleaned for 2 min. The samples were sputter coated with gold. Elemental analysis of the glass-ceramics was carried out using energy dispersive spectroscopy (EDS).

3.1.2.3 Differential Thermal Analysis

Thermal behavior of each particle size group of glass powders was determined by Differential Thermal Analysis (DTA) measurements. The differential thermal analyzer (Setaram Labsys, France) was operated at a heating rate of 10 $^\circ\text{C}/\text{min}$ with Al_2O_3 as reference material. Each run was made on 30 ± 0.1 mg sample in a platinum crucible. The measurements were made in flowing nitrogen atmosphere

up to a maximum temperature of 1100 °C. For particles of medium size, measurements were performed also with heating rates of 20 and 30 °C/min to determine the activation energy for crystallization and the Avrami parameter.

The crystallization peak temperature (T_p), the temperature of the exothermic peak maximum, the width of the crystallization peak at half maximum (ΔT_f), the width of the exothermic peak at half of the peak's height, (see Figure 2.5) and the heating rate (ϕ), were used to discern crystallization behavior of this glass system.

The flowchart showing the experimental procedure of this study was presented in Figure 3.2.

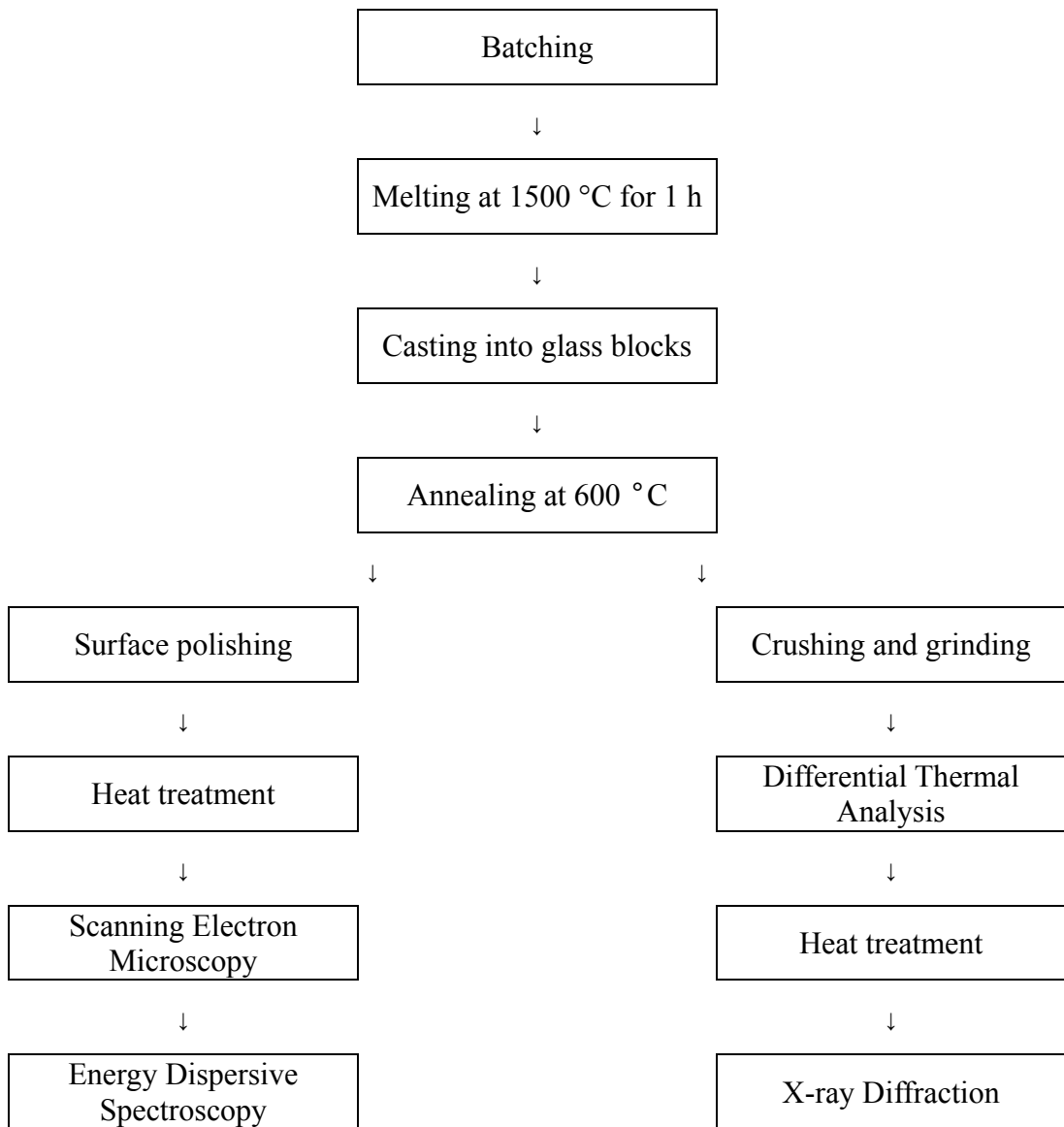


Figure 3.2 Flowchart showing the experimental procedure of the study on the nucleation and crystallization kinetics of a glass in the MgO-CaO-SiO₂-P₂O₅-F system.

3.2 THE EFFECT OF TiO₂ ADDITION ON THE CRYSTALLIZATION KINETICS OF A GLASS IN THE MgO-CaO-SiO₂-P₂O₅-F SYSTEM

In this section, the experimental procedure for a study conducted on the effect of TiO₂ addition on the crystallization kinetics of a glass in the MgO-CaO-SiO₂-P₂O₅-F system is explained.

3.2.1 Specimen Preparation

3.2.1.1 Glass Formation

The nominal compositions of the glasses investigated in this study are presented in Table 3.4. A glass of composition number 1, hereafter named as Glass 1, was selected as the base composition. The chemical composition of this glass is the same as the glass developed by Kokubo *et al.* [32] to obtain A-W glass-ceramic. In addition to this composition four other compositions of progressively higher TiO₂ content were formed and evaluated.

Table 3.4 Weight percent chemical composition of the glasses investigated.

Glass Number	MgO	CaO	SiO ₂	P ₂ O ₅	CaF ₂	TiO ₂
1	4.60	44.70	34.00	16.20	0.50	0
2	4.51	43.81	33.32	15.88	0.49	2
3	4.42	42.91	32.64	15.55	0.48	4
4	4.23	41.12	31.28	14.90	0.46	8
5	4.05	39.34	29.92	14.26	0.44	12

Glass batches were formed according to the procedure as described in section 3.1.1.1 using extra pure or reagent grade powders of the ingredients listed in Table 3.1. TiO₂ was supplied from Alfa Aesar, grade 036199 and added to glass composition in the batch. The total weight of each batch was approximately 20 g.

The batches were placed in a platinum crucible and melted in it at 1500 °C in an electrically heated muffle furnace. Melting took place in a normal laboratory conditions without controlling the atmosphere. The melt was kept at 1500 °C for 1 h to ensure the homogeneity of the melt prior to pouring into a stainless steel plate to obtain glass blocks. All glass blocks were annealed at 600 °C for 1 h.

After annealing, the glass blocks were heat treated at various temperatures for nucleation. Upon completion of the nucleation heat treatment, the glass blocks were crushed and ground in agate mortar with pestle, and then sieved through a series of screens for DTA. The particle size range used in this study was between 500 and 850 µm.

3.2.1.2 Glass-ceramic Formation

Two-step heat treatment was performed to convert the glass blocks and glass powders to glass-ceramic. The heat treatment was performed by heating the glasses 1 h at 780 °C for nucleation followed by 30 min at 900 °C for crystal growth. The heating rate was 5 °C/min. After holding 30 min at 900 °C, the furnace was cooled to 200 °C at a rate of 10 °C/min. The samples were furnace cooled from 200 °C to room temperature with the power of furnace turned off. The appearance of the blocks and powders after the heat treatment changed from transparent to opaque suggesting that microstructure morphology changed during the heat treatment.

3.2.2 Analyses

3.2.2.1 X-ray Diffraction

Powder XRD was employed to identify phases formed after heat treatment in the crystallized counterparts of the glass. The analyses were done according to the procedure as described in section 3.1.2.1.

3.2.2.2 Scanning Electron Microscopy

The crystal morphology of the crystallized counterparts of the glass blocks was examined by using SEM according to the procedure as described in section 3.1.2.2. Elemental analysis of the glass-ceramics was carried out using EDS.

3.2.2.3 Differential Thermal Analysis

Thermal behavior of the glass powders was determined by DTA measurements according to the procedure as described in section 3.1.2.3. DTA scans were obtained at heating rates of 5, 10, 15, and 20 °C/min in flowing nitrogen atmosphere. The value of the glass transition temperature T_g , crystallization onset temperature T_c , and peak maxima of the crystallization exotherm T_p , were determined from the DTA scans. The crystallization kinetic parameters were determined using Eq.2 and Eq.3 given in section 2.1.6.

The flowchart showing the experimental procedure of this study was presented in Figure 3.3.

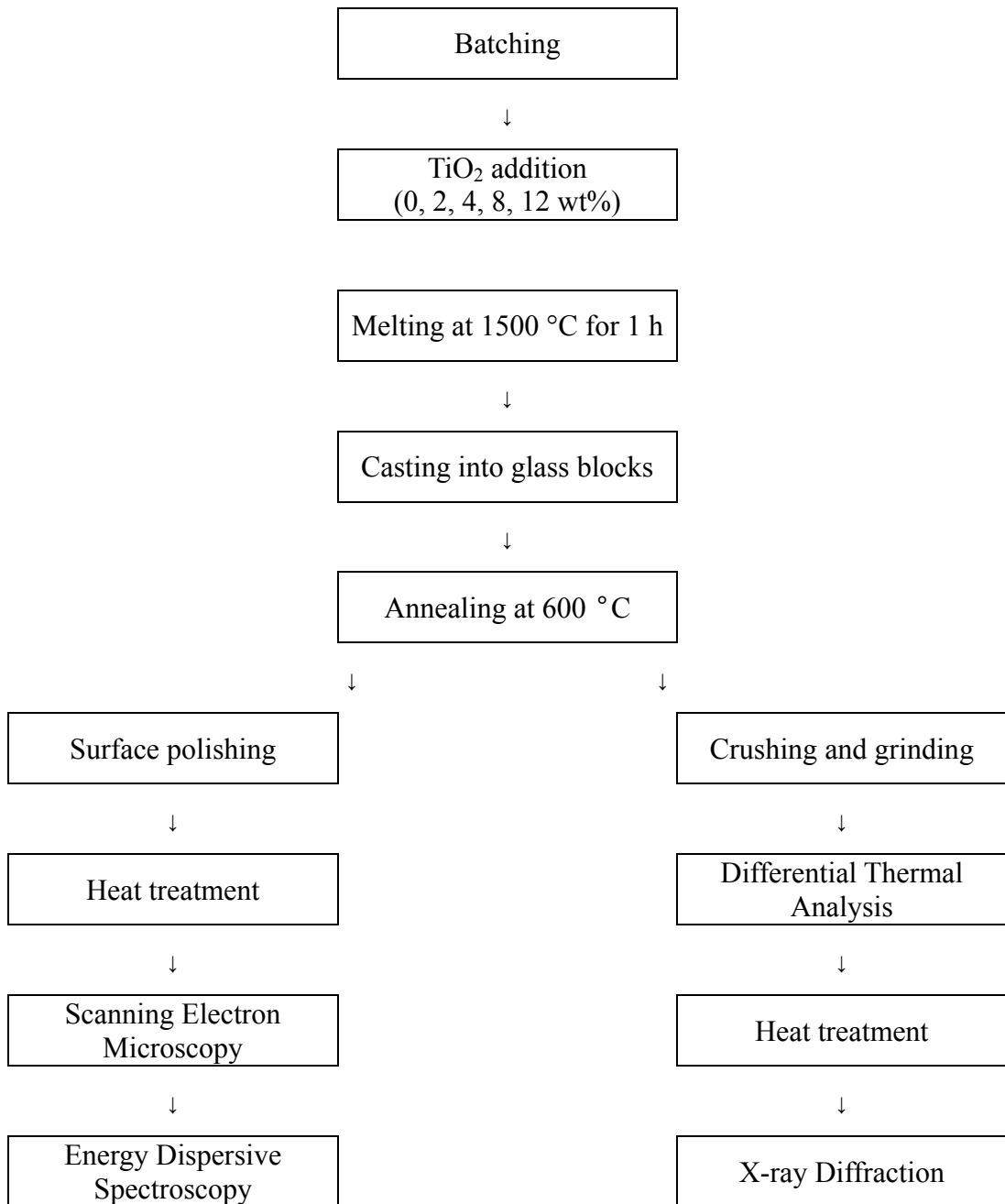


Figure 3.3 Flowchart showing the experimental procedure of the study on the effect of TiO_2 addition on the crystallization kinetics of a glass in the $\text{MgO-CaO-SiO}_2\text{-P}_2\text{O}_5\text{-F}$ system.

3.3 TRIBOLOGICAL PROPERTIES OF AN A-W GLASS-CERAMIC

In this section, the experimental procedure for a study conducted on tribological properties of an A-W glass-ceramic is explained.

3.3.1 Specimen Preparation

3.3.1.1 Glass Formation

Three glass blocks of Glass 1 in Table 3.4 were formed according to the procedure as described in section 3.2.1.1. Each glass blocks was annealed at 600 °C for 1 h prior to additional heat treatment to obtain bulk A-W glass-ceramics.

3.3.1.2 Glass-ceramic Formation

The glass blocks were converted to glass-ceramic according to the procedure as described in section 3.2.1.2.

3.3.1.3 Surface Grinding and Polishing

The surfaces of the glass blocks were ground flat by using 240, 400, 800, and 1200 grit abrasive papers consecutively, and then polished with the aid of 1 µm and 0.3 µm alumina powder solution on a cloth to achieve a mirror-like surface finish.

3.3.2 Analyses and Measurements

3.3.2.1 X-ray Diffraction

XRD analysis was performed to identify phases formed after heat treatment in the crystallized counterparts of the glass blocks. Analyses were performed on the free surface, and on the subsurfaces obtained at depth distances of 0.1, 0.3, and 0.5

mm below the free surface according to the procedure as described in section 3.1.2.1. Each subsurface was obtained by removing materials from the surface of the specimen through the grinding and polishing procedures as described in section 3.3.1.3. When the study of a surface was completed, the specimen was ground and polished until the next subsurface is obtained.

3.3.2.2 Scanning Electron Microscopy

SEM analysis was done to observe the wear track morphology on the surface and subsurfaces of A-W glass-ceramic samples according to the procedure as described in section 3.1.2.2. For taking SEM images of the wear tracks, the glass-ceramic samples were sputter coated with gold, and then subjected to SEM analysis without any surface cleaning or treatment, since they may have an effect on the wear traces.

3.3.2.3 Hardness

Microhardness measurements were performed on the free surface, and on the subsurfaces using a Knoop Hardness tester (Dukson tester, Willson, USA). Each sample was ground and polished as described in section 3.3.1.3. Testing surface and bottom of the sample were carefully polished to assure the surface parallelism prior to hardness measurements. At least five measurements were done at different locations of the flat surface through application of 500 gf for 15 s. The averages and the standard deviation of the measurements were calculated.

3.3.2.4 Tribology

Tribological tests were performed in accordance with ASTM G99-95A on the free surface and on the subsurfaces by means of a pin-on-disk type tribometer (CSM Instruments, Switzerland). A 5 mm diameter high purity zirconia ball (Asia Polishing Co., S. Korea) is chosen as the antagonist, since zirconia ball has recently achieved wide spread use in dentistry as a core and fixed partial dentures.

Some glass-ceramics are pressed onto a zirconia root canal post. The zirconia ball was fixed tightly in the ball holder. After each run, the zirconia ball was renewed to avoid any error from the change of surface roughness of zirconia ball. All specimens were clamped and supported on the sample stage tightly. Tribological tests were conducted under the conditions listed in Table 3.5. The duration of each run was approximately 6 h. To avoid the complication of tribo-chemical effects, lubrication was not applied.

Table 3.5 Tribology test conditions.

Parameter	Test condition
Ball Material	High purity commercial zirconia
Disc Material	A-W Glass-ceramic
Load	10 N
Sliding Speed	0.25 cm/s
Sliding Distance	50 m
Application Diameter	0.01 m
Acquisition frequency	1 Hz
Environment	Ambient laboratory atmosphere
Temperature	Room temperature
Lubrication	None

3.3.2.5 Surface Profile

After the completion of each individual tribological test, the surface profile of the sample was measured by using a stylus profilometer (Surtronic 3+, Taylor Hobson, England) to determine the wear track depth and wear area. The cross-sectional area of the wear track was calculated by averaging the wear area of four points of maximum mutual distance (90° spacing) on the wear track of the disk following the wear test by the software TalyProfile Lite version: 3.1.4 (Taylor Hobson,

England), from the profiles recorded at the four locations. The wear rate was calculated with the help of software TriboX2.0. The wear tests were repeated three times to assure the repeatability of the data.

The flowchart showing the experimental procedure of this study was presented in Figure 3.4.

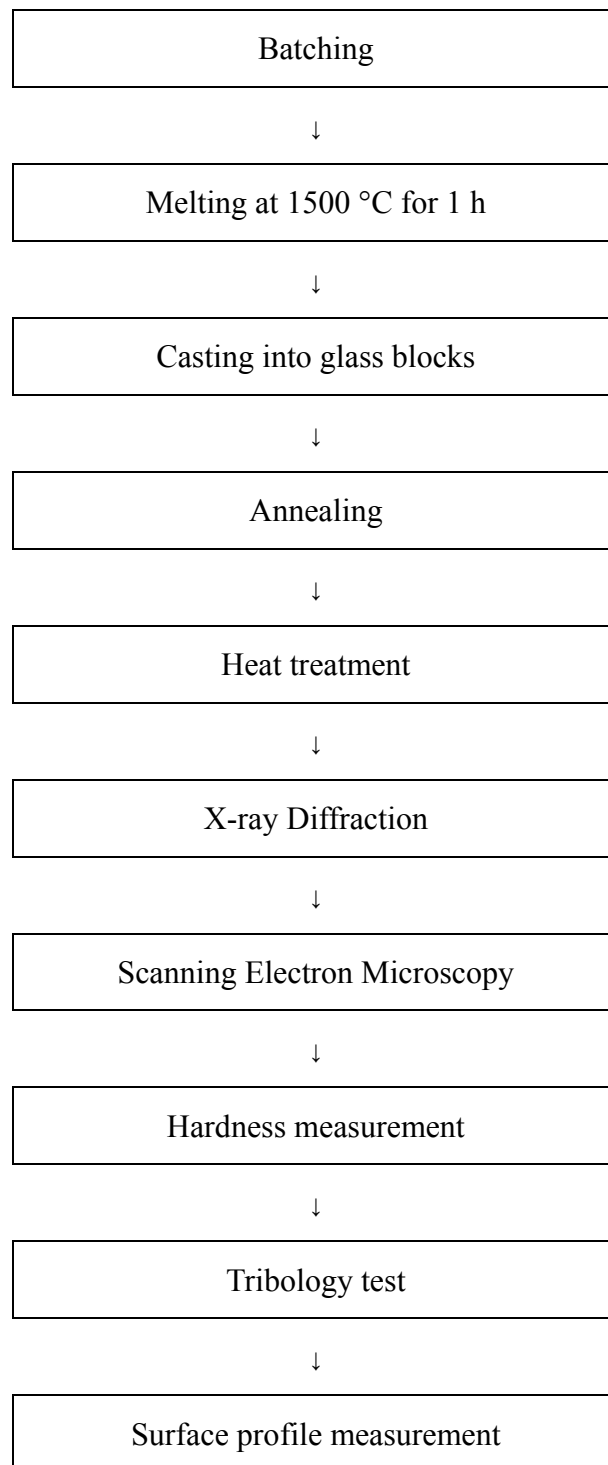


Figure 3.4 Flowchart showing the experimental procedure of the study on tribological properties of an A-W glass-ceramic.

3.4 A COMPARISON OF TRIBOLOGICAL PROPERTIES OF A-W GLASS-CERAMICS WITH SELECTED DENTAL CERAMICS

In this section, the experimental procedure for a study conducted on a comparison of tribological properties of A-W glass-ceramics with selected dental ceramics is explained.

3.4.1 Specimen Preparation

3.4.1.1 Preparation of A-W Glass-ceramics

The details for the preparation of the two kinds of A-W glass-ceramics (A-W GC1 and A-W GC2) used in this study were given in section 3.3.1. A-W GC1 is the sample upon which the tests were performed on the free surface and which contains both apatite and wollastonite phases. A-W GC2 is obtained by removing 0.5 mm from the free surface of the same sample through grinding and polishing, and consists of apatite phase only.

3.4.1.2 Preparation of Commercial Dental Ceramics

Six commercial dental materials were tested and evaluated together with the experimental A-W GC samples and bovine enamel (BE) which was used as reference material for comparison purpose. The details of the materials investigated and their manufacturers are listed in Table 3.8. The commercial dental materials are identified only for comparison purpose. They do not imply endorsement by the author or the institution where this research was conducted.

The materials were divided in three groups. i.e.; materials used as core (core materials) such as E2 and CPC, materials used as dentin porcelain (dentin porcelain materials) such as CCS1 and SPE1, and materials used as enamel porcelain (enamel porcelain materials) such as CCS2, and SPE2. Dentin and enamel porcelain materials contain different types and amounts of crystalline

phases such as leucite, lithium disilicate, alumina, mica, apatite etc., and different grain sizes [106], to reflect the need for increased color and opacity. Wear rates could be altered if these crystals become exposed [115].

Table 3.6 The materials investigated and their manufacturer.

ID Code	Material	Manufacturer	Lot no.
A-W GC1	A-W Glass-ceramic 1	This study	---
A-W GC2	A-W Glass-ceramic 2	This study	---
BE	Bovine Enamel	---	---
CCS1	Cergo ceram DC2 dentin porcelain	Degudent GmbH, Hanau, Germany	0312/5
CCS2	Cergo ceram S1 incisal material	Degudent GmbH, Hanau, Germany	08720
CPC	Cergo pressable ceramic Dentin A2, (Type 2, Class 1)	Degudent GmbH, Hanau, Germany	20459
E2	IPS Empress 2, Ingots 100, (Type 2, Class 1)	Ivoclar Vivadent, Schaan, Liechtenstein	G14847
SPE1	Super porcelain EX-3 A ₂ B dentin	Noritake Dental Supply Co., Aichi, Japan	002047
SPE2	Super porcelain EX-3 E ₂ enamel	Noritake Dental Supply Co., Aichi, Japan	004908

E2 and CPC glass ceramics are heat-pressed, lithium disilicate and leucite reinforced materials [107], and have been introduced for single unit restorations. E2 is used for fabrication of three-unit fixed partial dentures of the anterior region extending to the second premolar. SPE contains synthetic leucite and used to fabricate metal ceramic restorations. CCS is used as layering ceramic for zirconia based restorations. The SPE and CCS ceramics are low fusing and ultra low fusing ceramics, respectively [116].

The commercial dental ceramic materials were obtained in pressable ingots or powder forms from the manufacturers. Samples were prepared according to the instructions quoted by the manufacturers. Bovine lower central incisor teeth were

freshly extracted and their roots were separated. The crown parts were embedded in auto polymerizing acrylic resin (Akribel, Atlas Dental, Turkey) leaving the labial surfaces exposed. This process resulted in specimens with enamel surface of approximately 12 × 12 mm (length and width).

On preparation of the tribological test specimens for CCS and SPE ceramics, a matrix of vinyl polysiloxane (Elite H-D, Zhermack, Italy) was used as a mold to fabricate disk-shaped specimens with nominal dimensions of 12 × 2 mm (diameter and thickness). The test specimens for E2 and CPC ceramics were prepared according to “lost-wax” technique [107] using a pattern resin (GC Pattern resin, GC Corp., Japan) in the same nominal dimensions. The pressable ceramic specimens were heat-pressed at 920°C for E2, 980 °C for CPC. Other ceramics were fired at 830 °C for CCS1 and CCS2, and at 930 °C for SPE1 and SPE2.

3.4.2. Analyses and Measurements

3.4.2.1 Scanning Electron Microscopy

SEM analyses were done to observe the wear track morphology on the surfaces of A-W glass-ceramics, commercial dental ceramics and BE according to the procedure as described in section 3.1.2.2. For taking SEM images of the wear tracks, all samples were sputter coated with gold and then subjected to SEM without any surface cleaning or treatment.

3.4.2.2 Hardness

Hardness of all samples was measured according to the procedure as described in section 3.3.2.3. At least five measurements were done at different locations of the flat surface through application of 500 gf for 15 s. The averages and the standard deviation of the measurements were calculated.

3.4.2.3 Tribology

Tribological tests were performed according to the procedure as described in section 3.3.2.4 by the application of 10 N load, 0.25 cm/s rotating speed, 50 m sliding distance, and 1 cm wear track diameter. Details of the test conditions are seen in Table 3.5. The tribological tests were repeated three times to assure the repeatability of the data.

3.4.2.4 Surface Profile

After the completion of each individual tribological test, the surface profile of the samples was measured according to the procedure as described in section 3.3.2.4. The surface profile measurements were repeated three times to assure the repeatability of the data. Statistical analyses were performed using ANOVA and Tukey's HSD ($p < 0.05$).

The flowchart showing the experimental procedure of this study is presented in Figure 3.5.

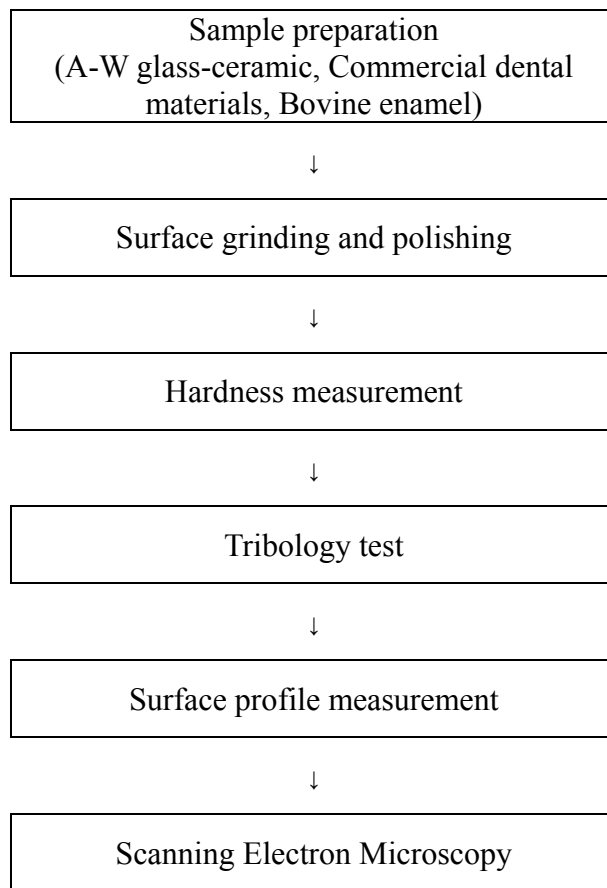


Figure 3.5 Flowchart showing the experimental procedure of the study on a comparison of tribological properties of A-W glass-ceramics with selected dental ceramics.

3.5 TRIBOLOGICAL BEHAVIOR OF ALUMINA-ADDED A-W GLASS-CERAMICS

In this section, the experimental procedure for a study conducted on tribological behavior of alumina-added A-W glass-ceramics is explained.

3.5.1 Specimen Preparation

3.5.1.1 Glass Formation

Alumina-added A-W glass-ceramic was prepared through powder packing process. A batch consisting of MgO 3.6, CaO 40.4, SiO₂ 33.2, P₂O₅ 16.5 and Al₂O₃ 6.3 in wt % was prepared from the mixture of MgO, CaCO₃, SiO₂, CaHPO₄·2H₂O, and Al₂O₃. This glass is the modified version of Kokubo's composition and has the same composition as the glass developed by Kitsugi *et al.*[41,52]. Glass batches were formed according to the procedure as described in section 3.1.1.1 using extra pure or reagent grade powders of the ingredients listed in Table 3.1. Al₂O₃ was supplied from Alfa Aesar, grade 039814 and added to glass composition in the batch. The total weight of each batch was approximately 20 g. Some of the materials are assumed to decompose into their stable oxide forms during melt. The decomposition reactions of them are the same as those explained in section 3.1.1.1.

The batch was melted and glass blocs were obtained according to the procedure as described in section 3.1.1.1. The glass blocks were colorless and indicated no unmolten batch materials or crystallinity. The glass blocks were crushed and ground in agate mortar with pestle, then sieved through a screen having an opening size of 45 μm.

3.5.1.2 Glass-ceramic Formation

The glass powders of less than 45 μm in size were mixed with isopropyl alcohol in the weight ratio of 1:1. Dried glass powder was pressed into a disc of 40 mm in diameter and 7 mm in thickness at a load of 40 kN by using a mounting press

(Struers, LaboPress-3, Denmark). The samples were prepared by sintering the disk shaped glass compacts at four different temperatures: 780 °C, 900 °C, 1000 °C, and 1100 °C. The heating rate up to the maximum temperature was 5 °C/min for all of the samples. Each sample was held at the maximum temperature for 2 h.

Two kinds of commercial dental restoration were prepared for comparison of tribological properties of alumina-added A-W glass-ceramics with those of commercial dental ceramics. The commercial dental materials Duceragold[®] (Degussa Dental GmbH, Germany) and IPS Empress[®] (Ivoclar Vivadent, Liechtenstein) were obtained in powder form from the manufacturers. The commercial dental materials are identified only for comparison purpose. They do not imply endorsement by the author or the institution where this research was conducted. Five samples of each were fabricated according to the instructions given by the manufacturers. The samples for Duceragold were prepared in disk-shape with nominal dimensions of 12 × 2 mm (diameter and thickness) by firing at 800 °C. The samples for IPS Empress were prepared in the same nominal dimensions by heat-pressing at 1075 °C.

Each sample was polished to mirror-like finish to assure the surface smoothness and parallelism prior to the tribological tests as described in section 3.3.1.3.

3.5.1.3 Simulated Body Fluid

The Simulated Body Fluid (SBF) was prepared according to the instructions given by Kokubo *et al.* [117]. It was buffered at a pH of 7.25 with Tri(hydroxymethyl) aminomethane and HCl solution. The ionic concentrations in SBF are given in Table 3.7. The chemicals used and their quantities in SBF are given in Table 3.8. In preparation of SBF, each chemical was added after assuring the previous chemical dissolved fully to avoid any unexpected chemical reactions among them. SBF solution was kept 6 h in refrigerator with a stopper in glass beaker prior to use in experiments. All samples were immersed in SBF 12 h before the wear test.

Table 3.7 Ion concentration (mM) of SBF and human blood plasma [40].

Ion	SBF (mM)	Blood Plasma (mM)
Na ⁺	142.0	142.0
K ⁺	5.0	5.0
Mg ²⁺	1.5	1.5
Ca ²⁺	2.5	2.5
Cl ⁻	147.8	103.0
HCO ³⁻	4.2	27.0
HPO ₄ ²⁻	1.0	1.0
SO ₄ ²⁻	0.5	0.5

Table 3.8 Chemicals and their quantity in SBF in 1 liter of distilled water [117].

Chemical	Quantity (g)	Manufacturer
NaCl	7.996	Merck
NaHCO ₃	0.350	Merck
KCl	0.220	Merck
K ₂ HPO ₄	0.174	Merck
MgCl ₂ ·2H ₂ O	0.305	Merck
CaCl ₂ ·2H ₂ O	0.368	Merck
Na ₂ SO ₄	0.071	Merck
Tri(hydroxymethyl)aminomethane	6.057	Merck
1M HCl	40 (ml)	Merck

3.5.2 Analyses and Measurements

3.5.2.1 X-ray Diffraction

Powder XRD was employed to identify phases formed after different heat treatment schedule of the glass. The analyses were done according to the procedure as described in section 3.1.2.1.

3.5.2.2 Scanning Electron Microscopy

The crystal morphology of the crystallized counterparts of the glass blocks was examined by using SEM according to the procedure as described in section 3.1.2.2. Elemental analysis of the glass-ceramics was carried out using EDS.

3.5.2.3 Hardness

Hardness of all of the samples was measured according to the procedure as described in section 3.3.2.3. At least five measurements were done at different locations of the flat surface through application of 500 gf for 15 s. The averages and the standard deviation of the measurements were calculated.

3.5.2.4 Tribology

Tribological tests were performed according to the procedure as described in section 3.3.2.4 by the application of 10 N load, 0.25 cm/s rotating speed, 50 m sliding distance, and 1 cm wear track diameter. Details of the test conditions are seen in Table 3.5. The tribological tests were repeated three times to assure the repeatability of the data.

All specimens were immersed in SBF for 12 h before the wear test started, and clamped and supported on the sample stage located at the bottom of the wear cell filled with SBF. The level of SBF in the wear cell was maintained such that the

specimen remained immersed in the fluid during the entire duration of the test.

3.5.2.5 Surface Profile

After the completion of each individual tribological test, the surface profile of the samples was measured according to the procedure as described in section 3.3.2.4. The surface profile measurements were repeated three times to assure the repeatability of the data.

The flowchart showing the experimental procedure of this study is presented in Figure 3.6.

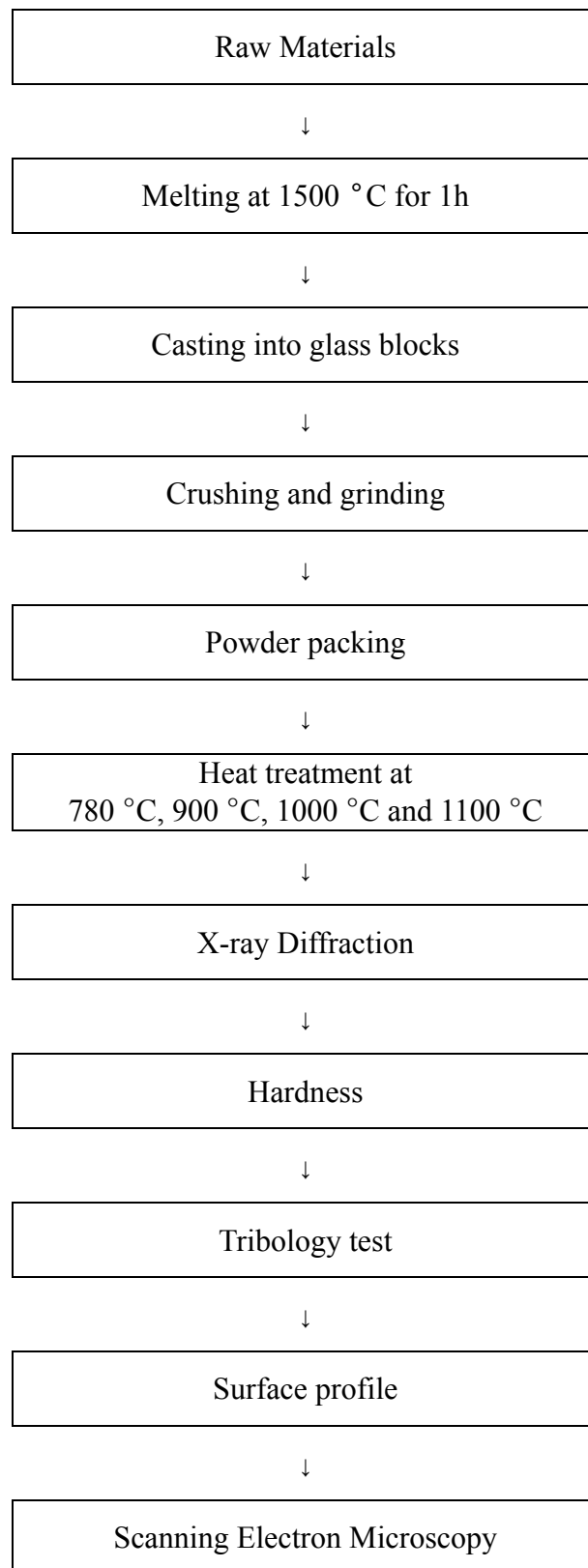


Figure 3.6 Flowchart showing the experimental procedure of the study on tribological behavior of alumina-added A-W glass-ceramics.

3.6 BIOACTIVITY OF A-W GLASS-CERAMICS PRODUCED BY MELT-CASTING

In this section, the experimental procedure for a study conducted on bioactivity of A-W glass-ceramic produced by melt casting is explained.

3.6.1 Specimen preparation

3.6.1.1 Glass Formation

Three glass blocks of Glass 1 in Table 3.4 were formed according to the procedure as described in section 3.2.1.1. The glass blocks were annealed 1 h at 600 °C prior to additional heat treatment to obtain bulk A-W glass-ceramics.

3.6.1.2 Glass-ceramic Formation

The annealed bulk glasses were cut into the size of 5×5×5 mm (width × length × thickness) using low speed diamond precision cutter. Two types of glass-ceramic samples were prepared. One is the apatite-only containing glass-ceramic (named as A glass-ceramic) and the other is apatite-wollastonite containing glass-ceramic (A-W glass-ceramic). The first sample, A glass-ceramic, was produced by heating the bulk glass at 780 °C for 1 h with a heating rate of 5 °C/min. The second sample, A-W glass-ceramic, was prepared by heating 1 h at 780 °C followed by 30 min at 900 °C. On both samples, after holding at each temperature for the times given, the furnace was cooled at a rate of 10 °C/min until 200 °C. The samples were then cooled from 200 °C to room temperature with the power of furnace turned off.

3.6.1.3 Simulated Body Fluid

In vitro bioactive test of the A-W glass-ceramic has been done using SBF solution which was prepared according to the instructions given in section 3.5.1.3. Each

sample was put in the beaker filled with 200 ml of SBF solution. The beakers were put in the water bath and the temperature was set at 37 °C. The samples were immersed for 1, 10 and 20 days and then collected at the end of each immersion time. They were carefully rinsed with distilled water, so that the coated layer should not be detached, then dried in an oven at 90 °C for 1 h. During the immersion, the SBF solution in the beaker was renewed every 48 h.

3.6.2. Analyses

3.6.2.1 X-ray Diffraction

XRD was employed to identify phases formed on the surface of samples after being immersed in SBF for certain duration as described in section 3.1.2.1.

3.6.2.2 Scanning Electron Microscopy

SEM was used to observe the surface morphology of the samples collected at the end of each immersion time according to the procedure as described in section 3.1.2.2. Elemental analysis of the glass-ceramics was carried out using EDS.

The flowchart showing the experimental procedure of this study is given in Figure 3.7.

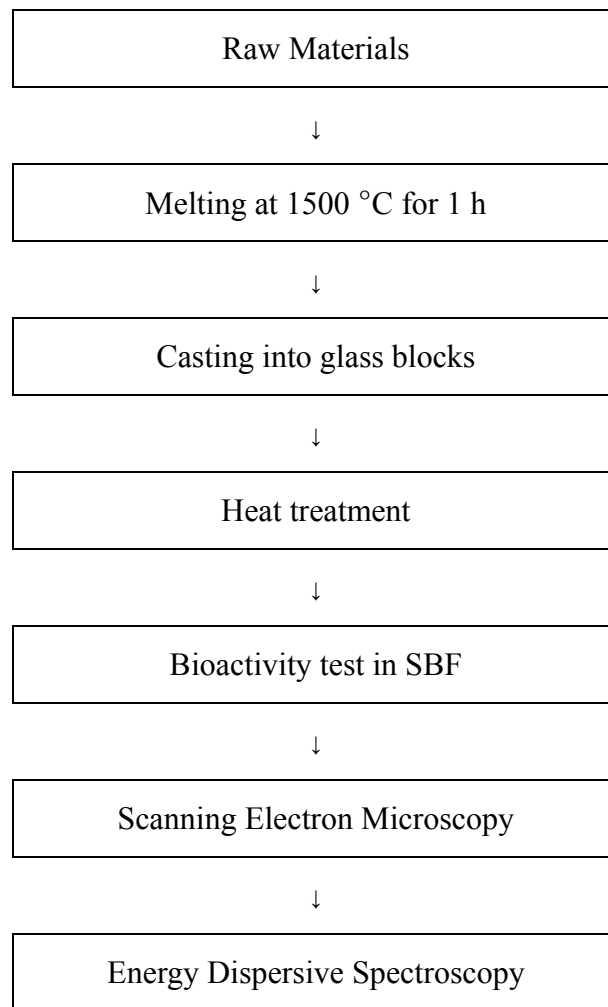


Figure 3.7 Flowchart showing the experimental procedure of the study on bioactivity of A-W glass-ceramics produced by melt casting.

CHAPTER 4

RESULTS AND DISCUSSION

4.1 NUCLEATION AND CRYSTALLIZATION KINETICS OF A GLASS IN THE MgO-CaO-SiO₂-P₂O₅-F SYSTEM

4.1.1 General

In this section, the data gathered from the experimental study conducted on the nucleation and crystallization kinetics of a glass in the MgO-CaO-SiO₂-P₂O₅-F system that leads to formation of Apatite-Wollastonite (A-W) glass-ceramic are presented. The results are discussed and compared with the results of the previous studies published in the literature.

Although there have been some investigations [34,44,74] on the formation, structure, and properties of A-W glass-ceramics, data on the crystallization kinetics of these materials are rare. A good understanding of the crystallization kinetics of A-W glass ceramics is necessary if these materials are to be technologically useful for special biomedical applications.

The purpose of the present research is to determine the crystallization kinetic parameters namely; activation energy, Avrami parameter, and frequency factor of a glass in the MgO-CaO-SiO₂-P₂O₅-F system using non-isothermal Differential Thermal Analysis (DTA). Results were supplemented by the phase and microstructural analyses to elucidate the behavior observed. X-ray Diffraction (XRD) and Scanning Electron Microscopy (SEM) were employed to get better understanding on types of crystals formed and microstructure developed during crystallization heat treatment.

The glass blocks obtained in the MgO-CaO-SiO₂-P₂O₅-F system according to the procedure described in section 3.1.1 were colorless and indicated no unmolten batch materials or crystallinity. The blocks were heat treated at various temperatures to determine the optimum nucleation temperature. Also, different heat treatment schedules were applied to find out the optimum temperature and duration to obtain A-W glass-ceramics through melt casting process.

4.1.2 X-ray Diffraction Analysis

XRD patterns obtained after heat treatment of the glass particles in the range of 500-850 μm (coarse particles) at temperatures of 740 °C, 760 °C, 780 °C, 800 °C, and 820 °C for 1 h at constant heating rate of 5 °C /min are presented in Figure 4.1. The XRD pattern obtained after heat treatment of the glass at 740 °C illustrates the pattern of an amorphous structure. No peaks are seen but a hump at low diffraction angle (2θ) values is clearly visible, which is an indicator of short range order [118]. When the glass is heat treated at 760 °C, the XRD pattern illustrates the peaks at definite 2θ values. These peaks are due to the reflection of intensity beam from definite crystallographic planes in crystal(s). The XRD analysis suggested that the intensity peaks match with the oxyapatite [Ca₁₀(PO)₄O] phase (JCPDS # 89-6495) or fluoroapatite [Ca₁₀(PO)₄(F)₂] phase (JCPDS # 15-0876). Only apatite phase, growing out of the amorphous matrix is observed in the patterns taken at temperatures from 740 °C to 780 °C. It can be identified as oxyfluoroapatite [Ca₁₀(PO)₄(O,F)₂] phase [40]. The peak belonging to a second crystal starts to appear at 800 °C. The intensity peak at 2θ of ~30.5° is attributed to the formation of the β-wollastonite (CaSiO₃) phase (JCPDS # 10-489) which is more clearly seen in the pattern obtained after heat treatment of the glass at 820 °C. The optimum temperature for the nucleation was taken as 780 °C at which maximum nucleation rate of the apatite phase is obtained without formation of the wollastonite phase. The results are in accord with the findings of Shyu and Wu [44] who have taken nucleation temperature as 755 °C for a glass system of similar chemical composition.

The 2θ and d -values of the glass-ceramics obtained after heat treatment of the glass at different temperatures match very well with those of oxyapatite or fluorapatite. The values of 2θ and d for oxyfluorapatite are listed along with the standard values of fluorapatite and oxyapatite in Table 4.1. It is seen that the 2θ values of the glass-ceramics have shifted to lower angles as compared to those of the standard oxyapatite and fluorapatite phases. Klein and Hurlbut [119] reported that apatite shows extensive solid solution with respect to anions as well as cations. The (PO_4) groups may be partially replaced by (SiO_4) groups in this glass causing the apatite structure to expand. As a result, the d -values are bigger than those for the standard apatite compounds.

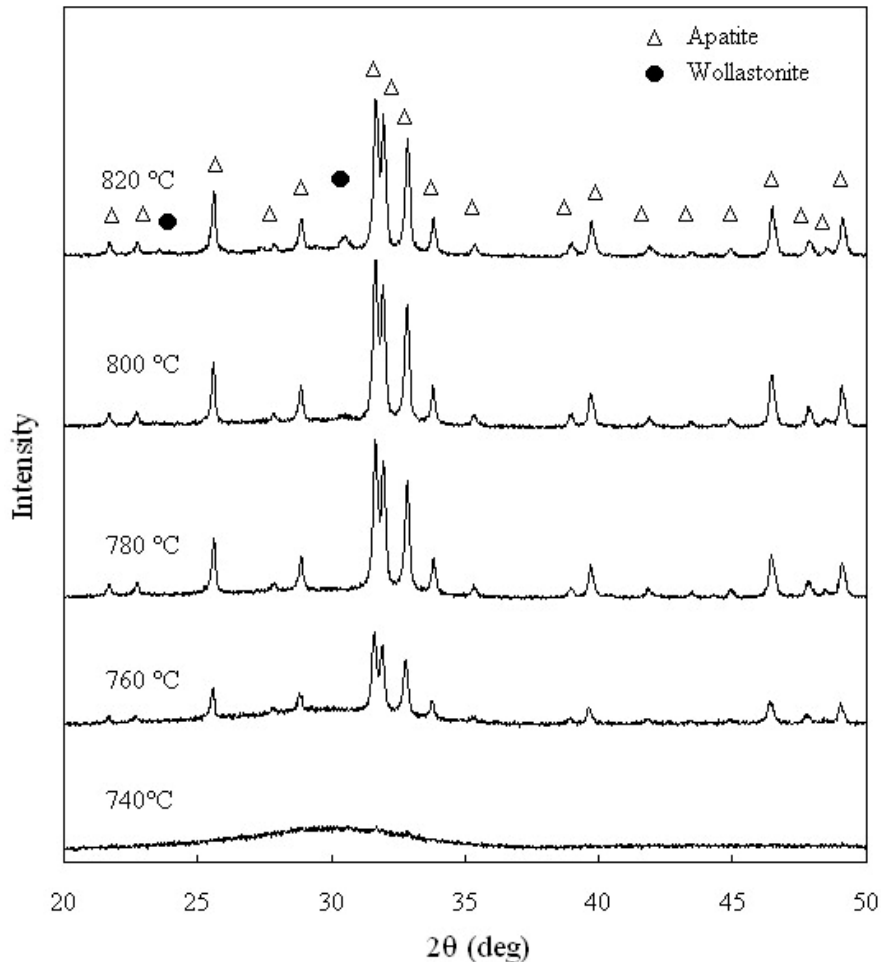


Figure 4.1 XRD patterns obtained after heat treatment of the glass powders 1 h at different temperatures.

Table 4.1 Comparison of 2θ and d -values of the A-W glass-ceramic heat treated 1 h at 780 °C with those of the standard oxyapatite and fluorapatite.

h k l	A-W glass-ceramic		Oxyapatite (JCPDS # 89-6495)		Fluorapatite (JCPDS # 15-0876)	
	2θ	d (Å)	2θ	d (Å)	2θ	d (Å)
2 0 0	21.700	4.0920	21.898	4.0841	21.902	4.0550
1 1 1	22.720	3.9106	22.902	3.8900	22.949	3.8720
0 0 2	25.580	3.4795	25.879	3.4405	25.863	3.4420
2 1 1	31.640	2.8255	31.773	2.8168	31.936	2.8000
1 1 2	31.940	2.7997	32.196	2.7794	32.267	2.7720
3 0 0	32.820	2.7266	32.902	2.7227	33.127	2.7020
2 0 2	33.820	2.6482	34.048	2.6313	34.141	2.6240
1 3 0	39.700	2.2685	39.818	2.2654	40.040	2.2500
2 2 2	46.440	1.9537	46.711	1.9450	46.865	1.9370

Three different size ranges of glasses were heat treated at 780 °C for 1 h in order to see the effects of particle size of the powder on nucleation. Figure 4.2 shows the XRD patterns obtained after heat treatment of the glasses of different particle size of the 500-850 μm . All patterns show peaks matching with the apatite phase, growing out of the amorphous matrix. As the particle size of the glass powder decreases, the intensity of the peaks increases, implying that the proportion of crystallinity increases with fine glass particles. Formation of small amount of wollastonite phase was detected only in the pattern obtained with the glass powders of less than 45 μm size.

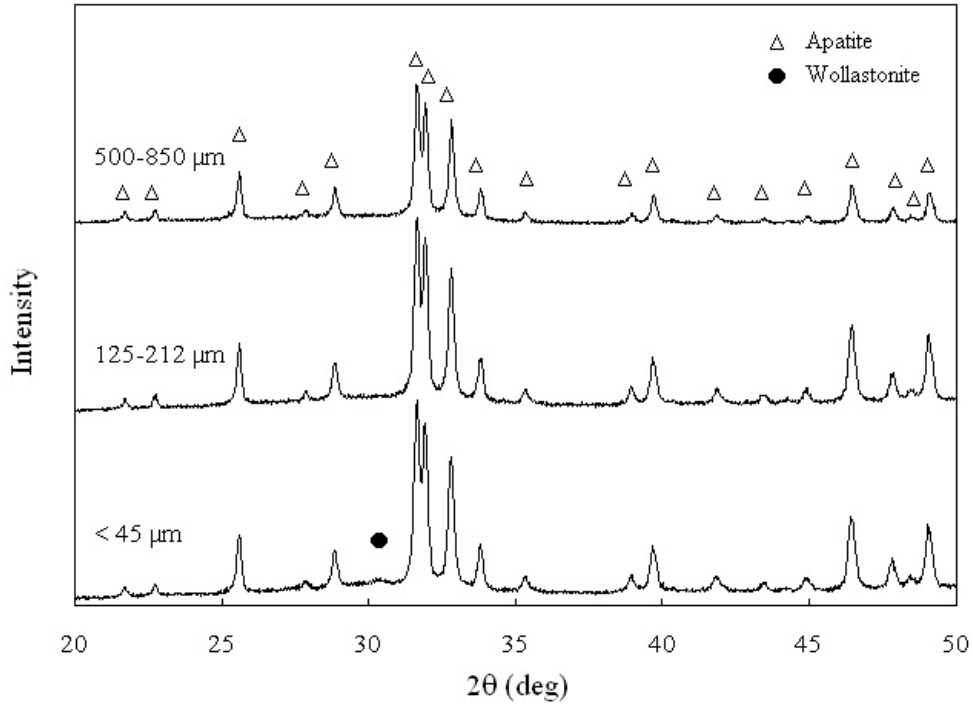


Figure 4.2 XRD patterns obtained after heat treatment 1 h at 780 °C for the glasses of different particle size.

Figure 4.3 shows the XRD patterns of the glass-ceramics obtained after heat treatment 1 h at 780 °C followed by 30 min at temperatures of 880 °C, 900 °C, 920 °C, and 940 °C, sequentially. The XRD patterns suggest that two crystalline phases, wollastonite and apatite, precipitated until the growth temperature of 940 °C. The peak intensity of the (320) plane of wollastonite crystals at 2θ of $\sim 30.5^\circ$ increased, implying that more and more of wollastonite phase precipitated with increasing growth temperature. On the other hand, the density of apatite phase decreased with increasing growth temperature. The lattice parameters of (320) plane of wollastonite is comparable to those of the standard wollastonite. The 2θ and d -values of standard wollastonite are 30.088 and 2.97 Å while those of the A-W glass-ceramics vary between 30.40 and 30.54, and between 2.9247 and 2.9379 Å, respectively. The (320) peak of the A-W glass-ceramics has higher 2θ value as compared to those of the standard wollastonite as seen in Table 4.2. Lower d -values of the A-W glass-ceramics as compared to those of the standard wollastonite might be caused by substitution of smaller Mg ions for Ca ions [88].

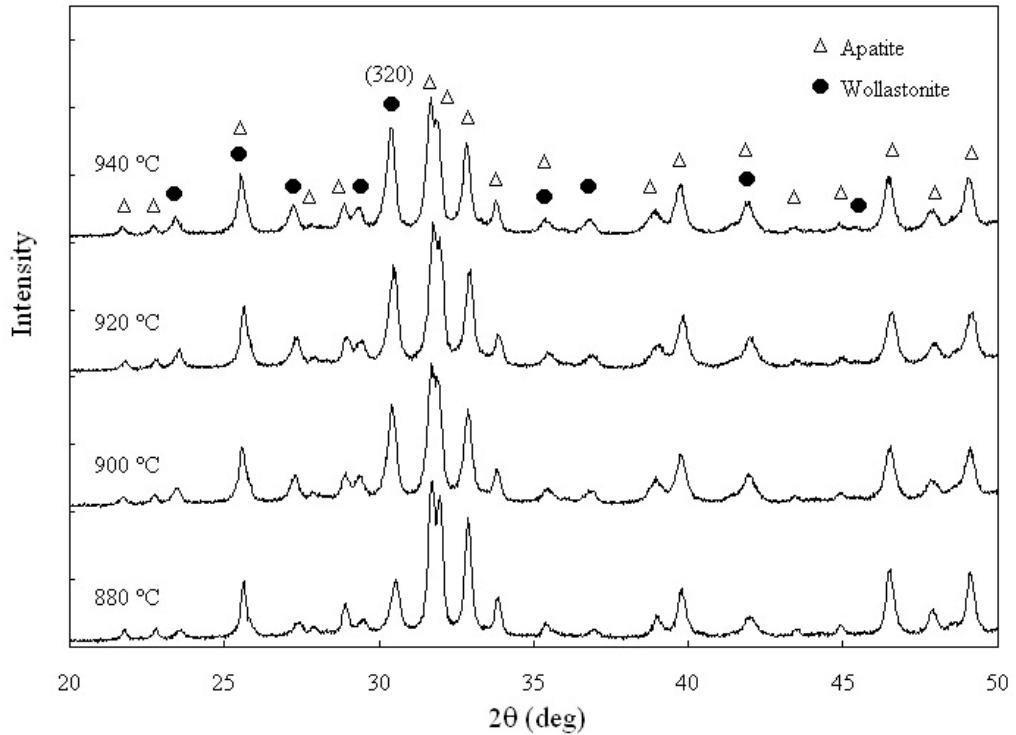


Figure 4.3 XRD patterns obtained after heat treatment of glass 1 h at 780 °C followed by 30 min at various growth temperatures. The particle size range of the glass powder is 500-850 μm.

Table 4.2 Comparison of 2θ and d-value of standard wollastonite with A-W glass-ceramics heat treated 1 h at 780 °C followed by 30 min at various temperatures.

Parameter	Wollastonite (JCPDS # 10-0489)	A-W glass-ceramics			
		880 °C	900 °C	920 °C	940 °C
2θ	30.088	30.54	30.40	30.46	30.40
d (Å)	2.9700	2.9247	2.9304	2.9341	2.9379

Quantitative XRD analysis was done using α -quartz as an internal standard. The variation of apatite to quartz intensity ratio (I_A/I_Q) with temperature is shown in Figure 4.4. The ratio is 0.17 at 740 °C, but increases to a maximum value of 0.55 at 780 °C, and then decreases and becomes 0.34 at 820 °C. The variation curve shows a feature similar to a typical nucleation rate curve as shown in Figure 2.1. The interpretation of the increase in ratio followed by a decrease with increasing temperature is that the atomic mobility of atoms increases with temperature, allowing nucleation by phase separation to occur at 780 °C. At the lower temperatures, atomic mobility is more sluggish, and structural rearrangement and nucleation mechanisms are prohibited. At the higher temperatures, the atomic mobility may increase into the range where less stable phase separation can be happen, however the temperature has entered into the range where the crystal growth occurs.

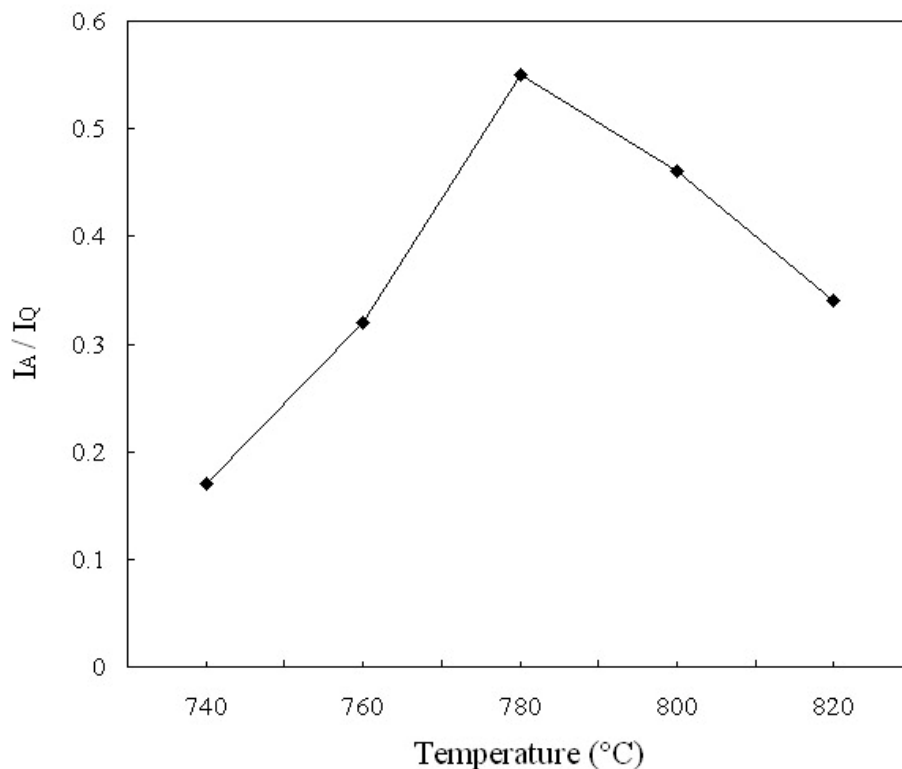


Figure 4.4 The variation of apatite-quartz intensity ratio of the glass heat treated 1 h at various temperatures.

4.1.3 Scanning Electron Microscopy Analysis

SEM images in Figures 4.5 to 4.9 show the microstructure of the glasses heat treated 1 h at temperatures of 740 °C, 760 °C, 780 °C, 800 °C, and 820 °C, respectively. The crystals are not clearly seen in Figure 4.5 implying that the proportion of crystallinity is not enough in glassy matrix. This finding is in agreement with the XRD data presented in Figure 4.1. The crystal size and density increase as the growth temperature is increased. The crystal size in the sample heat treated at 760 °C is approximately 2 μm as seen in Figure 4.6, but becomes maximum at about 5 μm when the temperature is increased up to 780 °C as seen in Figure 4.7. This crystal has been identified as apatite phase by XRD analysis and grows as a rice shape. The growth of apatite crystals has eventually consumed the glassy phase surrounding them. At 800 °C, however, the crystals became agglomerated. The crystals did not enlarge but stuck to each other as shown in Figure 4.8. When the growth temperature is increased to 820 °C, the crystals enlarged abnormally as shown in Figure 4.9.

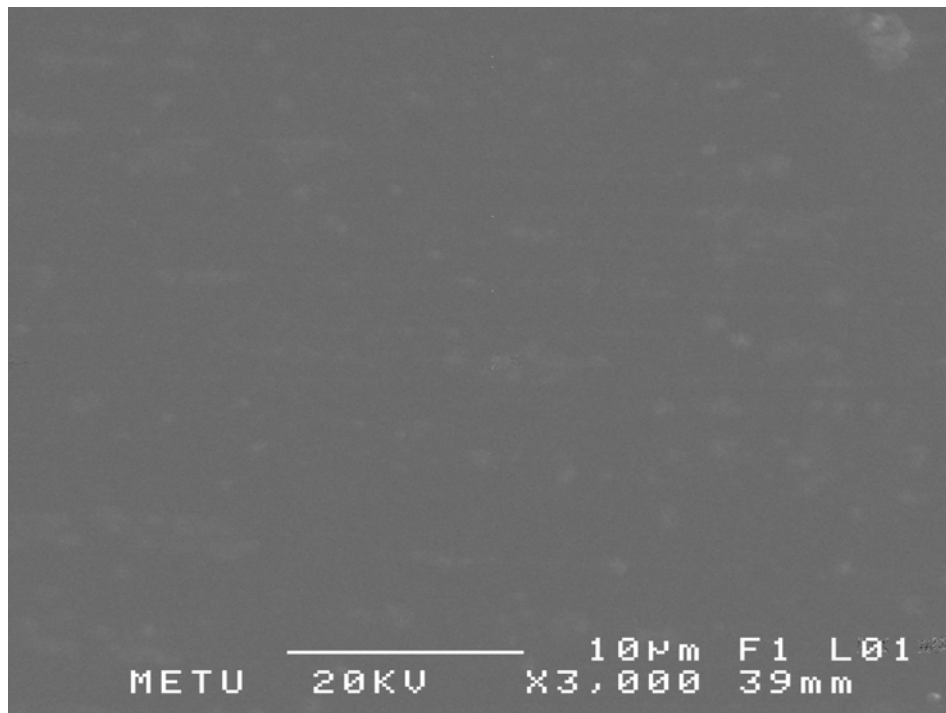


Figure 4.5 SEM image of the glass heat treated 1 h at 740 °C.

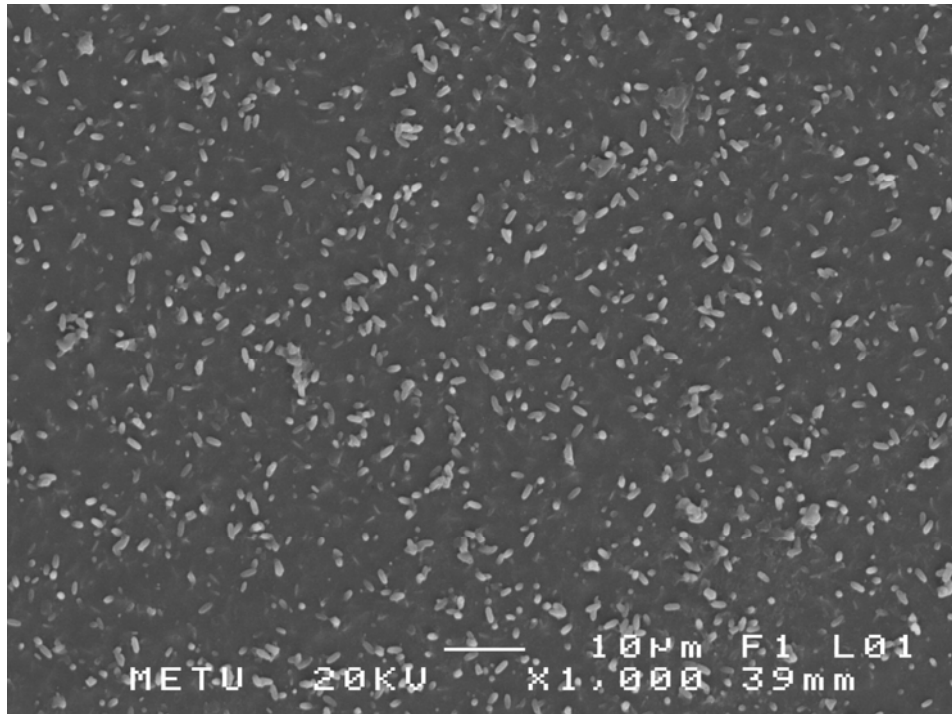


Figure 4.6 SEM image of the glass heat treated 1 h at 760 °C.

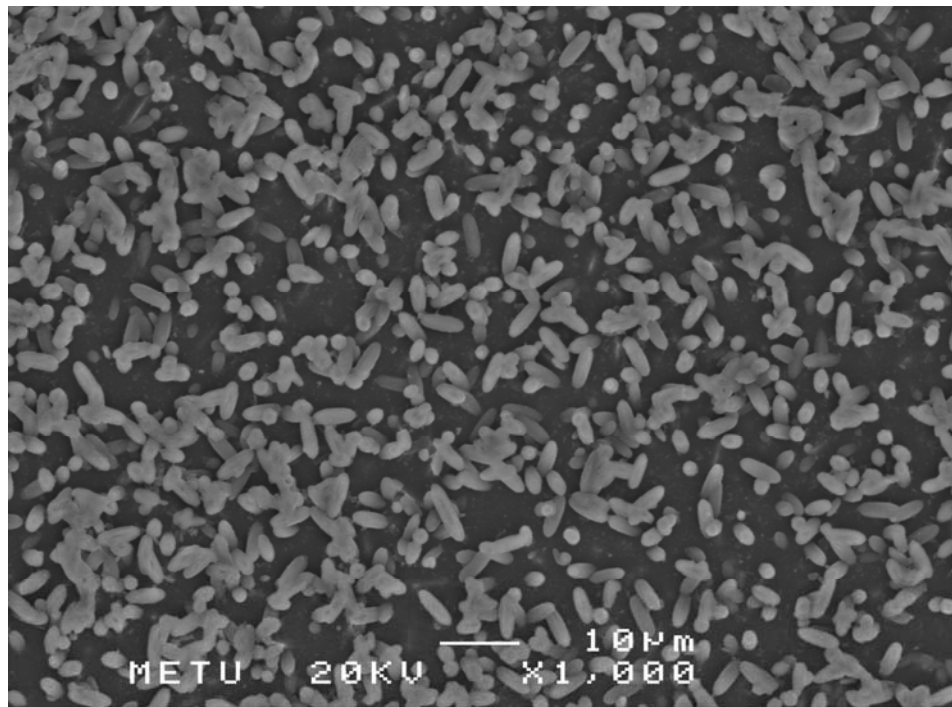


Figure 4.7 SEM image of the glass heat treated 1 h at 780 °C.

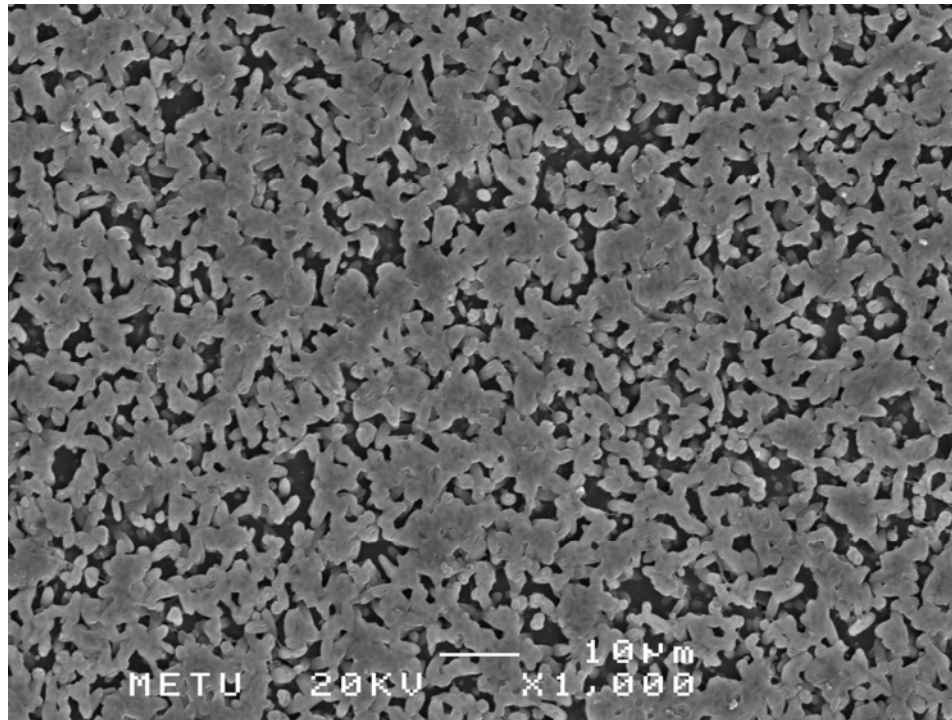


Figure 4.8 SEM image of the glass heat treated 1 h at 800 °C.

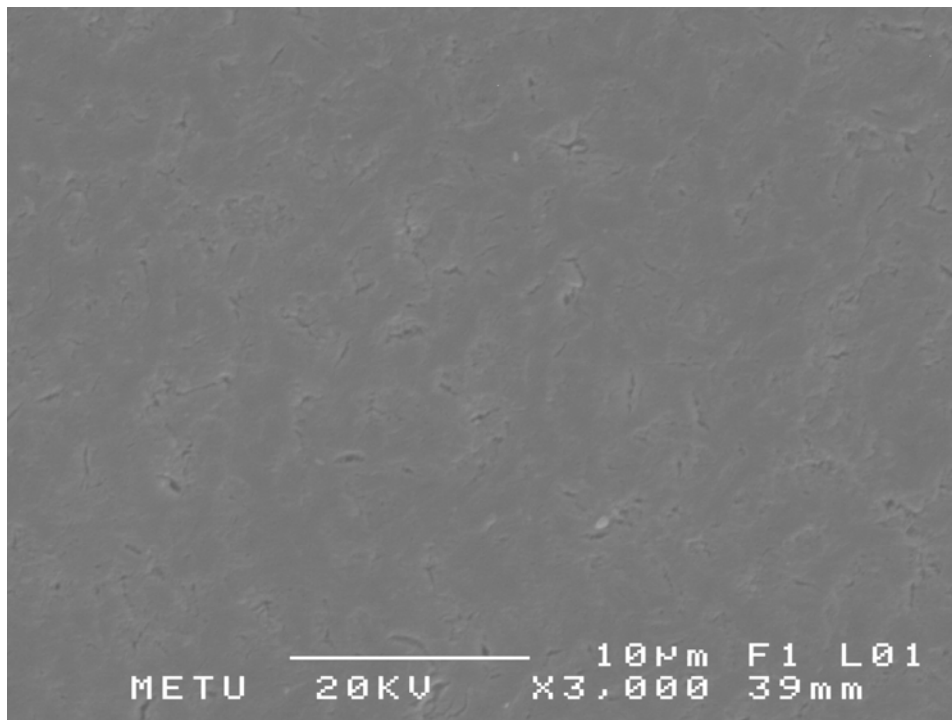


Figure 4.9 SEM image of the glass heat treated 1 h at 820 °C.

SEM micrographs in Figures 4.5 to 4.9 agree very well with the findings on nucleation rate data presented in Figure 4.4. At lower temperatures, the apatite crystal size and density were not enough, but with increasing temperatures, the crystal size and density increased and formed a maximum at 780 °C. Nevertheless, the crystal growth has been observed at higher temperatures.

SEM micrographs in Figures 4.10 to 4.13 show microstructure of the glasses heat treated 1 h at 780 °C followed by 30 min at 880 °C, 900 °C, 920 °C, and 940 °C, respectively. All of the micrographs show dendritic growth of crystals in web-like microstructure. Similar microstructure has been observed by other researchers [33,34,44]. There are not many microstructural differences with increasing growth temperature. Quite dense and well developed crystals were obtained at 900 °C as seen in Figure 4.11. The crystal size increased slightly and became thicker at 920 °C and 940 °C as shown in Figures 4.12 and 4.13, respectively.

Abnormal crystal growth induced internal stress and caused the formation of cracks. When growth temperature was increased to 920 °C, the cracks started to be formed in the interior of bulk A-W glass-ceramic as shown in Figure 4.14.

After the XRD and SEM analyses, the optimum crystal growth temperature was taken as 900 °C.

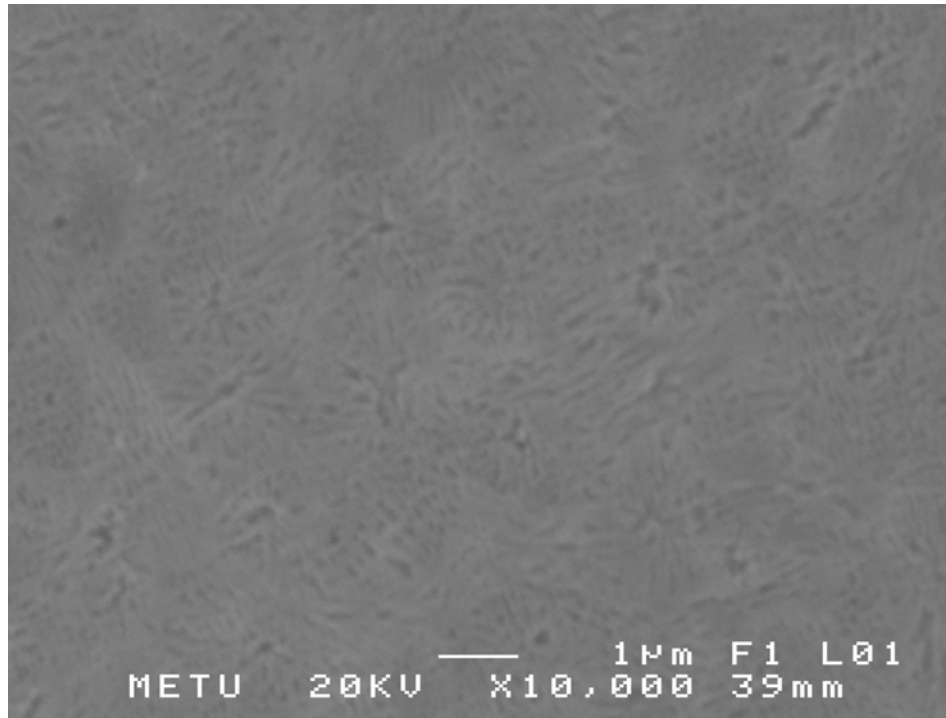


Figure 4.10 SEM image of the A-W glass-ceramic heat treated 1 h at 780 °C followed by 30 min at 880 °C.

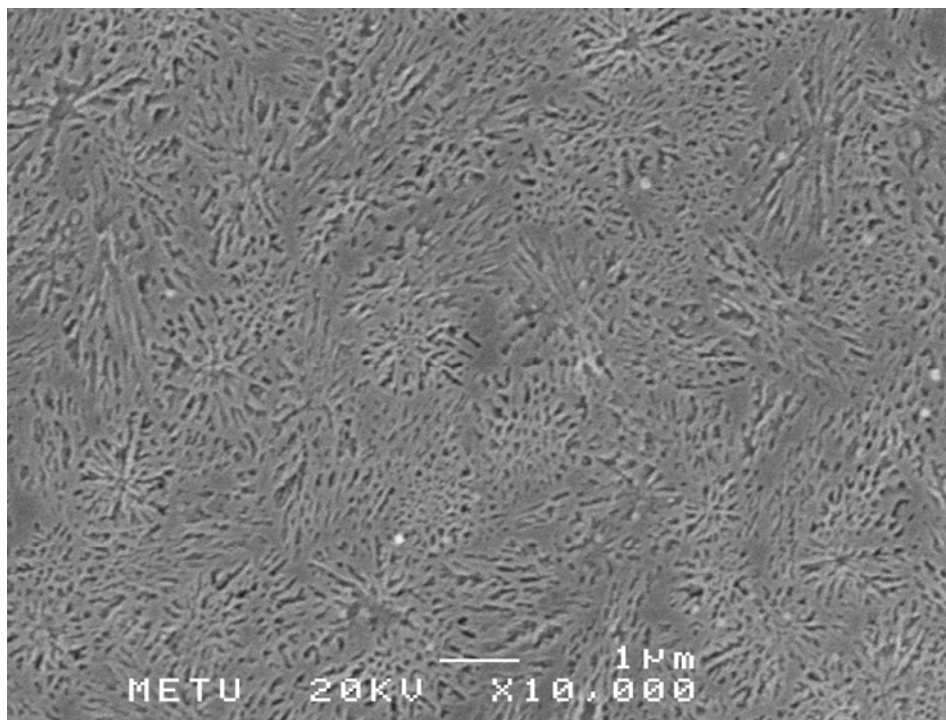


Figure 4.11 SEM image of the A-W glass-ceramic heat treated 1 h at 780 °C followed by 30 min at 900 °C.

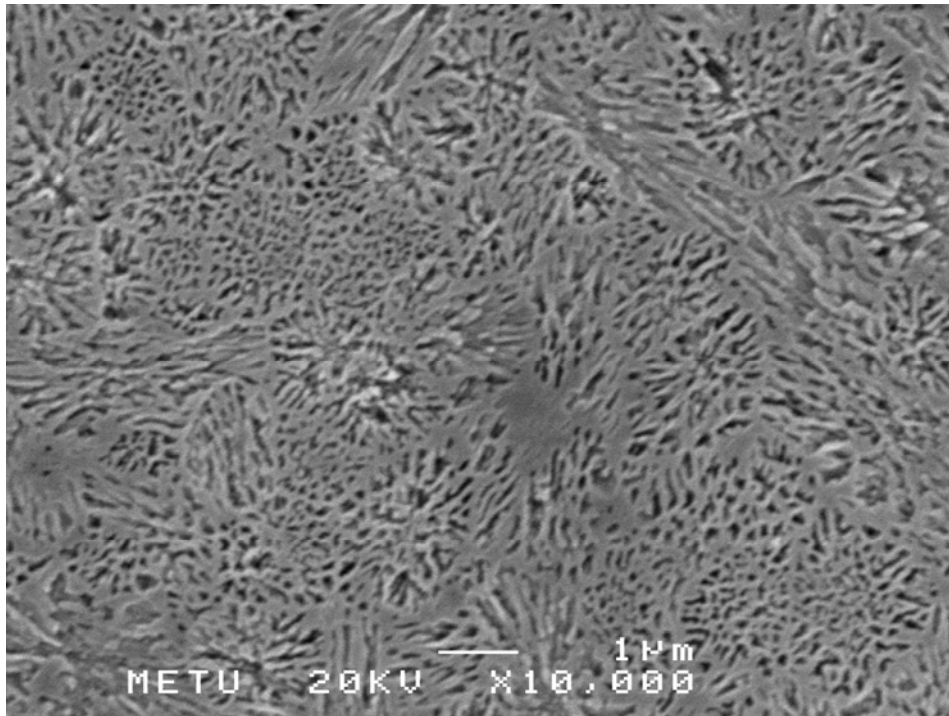


Figure 4.12 SEM image of the A-W glass-ceramic heat treated 1 h at 780 °C followed by 30 min at 920 °C.

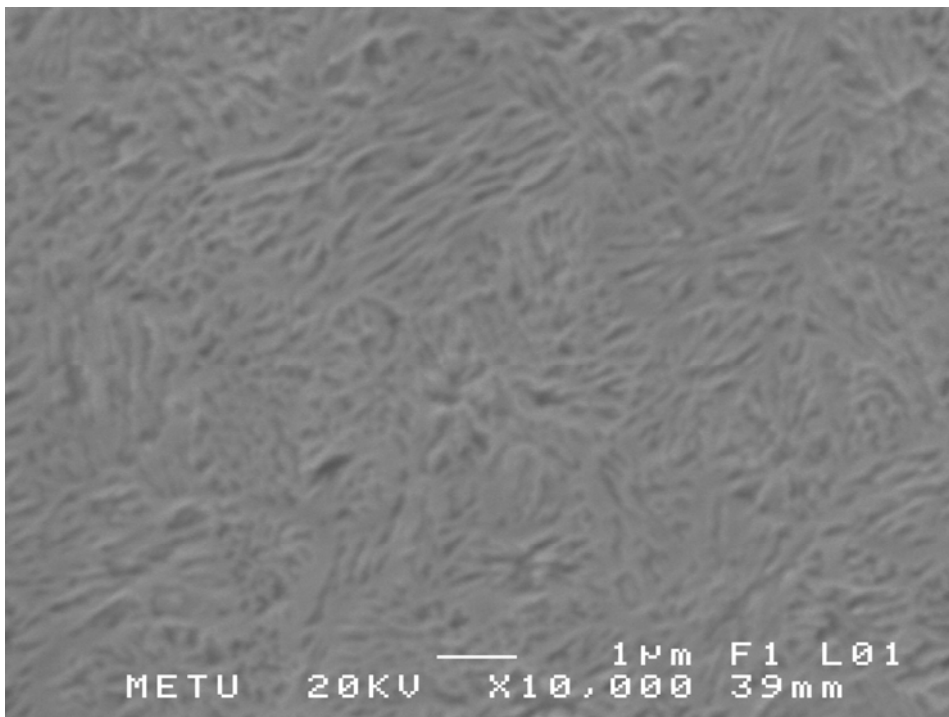


Figure 4.13 SEM image of the A-W glass-ceramic heat treated 1 h at 780 °C followed by 30 min at 940 °C.

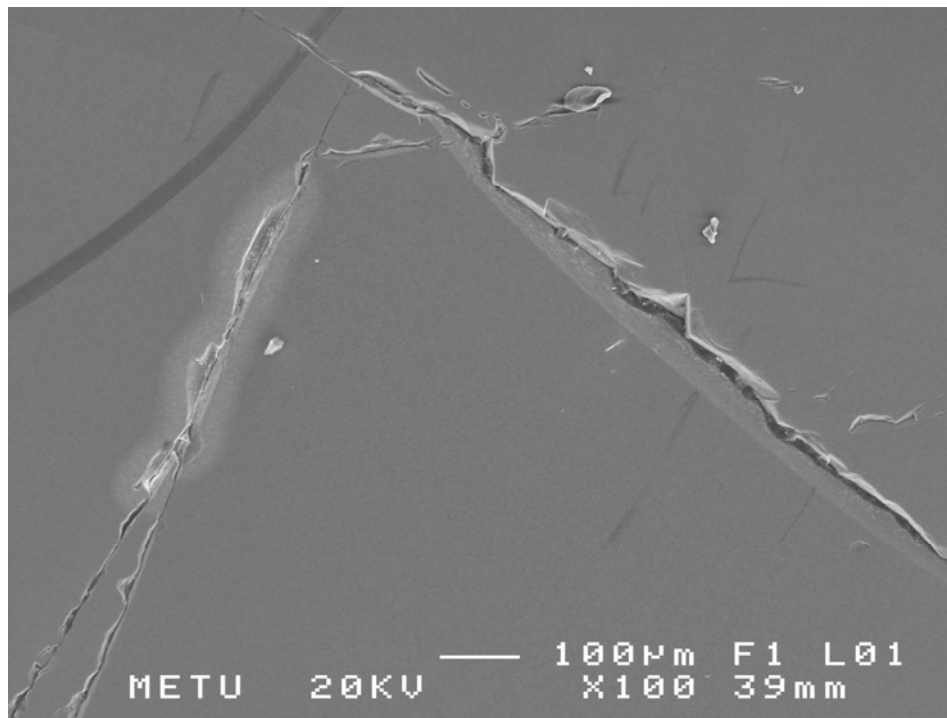


Figure 4.14 SEM image showing the cracks induced by abnormal crystal growth in the A-W glass-ceramic.

4.1.4 Differential Thermal Analysis

DTA thermograms of the glasses with different particle sizes are shown in Figure 4.15. The thermograms were obtained at a heating rate of 10 °C/min. All DTA curves have two exothermic peaks corresponding to crystallization of apatite and wollastonite phases [22]. The glass with coarse particles, in the size range of 500-850 µm, has the peak temperature of the first exotherm at 897 °C and the peak temperature of the second exotherm at 995 °C. The peak temperature of the first and second exotherm are observed between temperatures of 896 °C and 895 °C, and 944 °C and 923 °C for the glasses with medium and fine particles, respectively. No significant change in the peak temperature of the first exotherm was detected but; the peak temperature of the second exotherm clearly shifted to lower temperatures, from 995 °C to 923 °C, as particle size of glass powder is decreased.

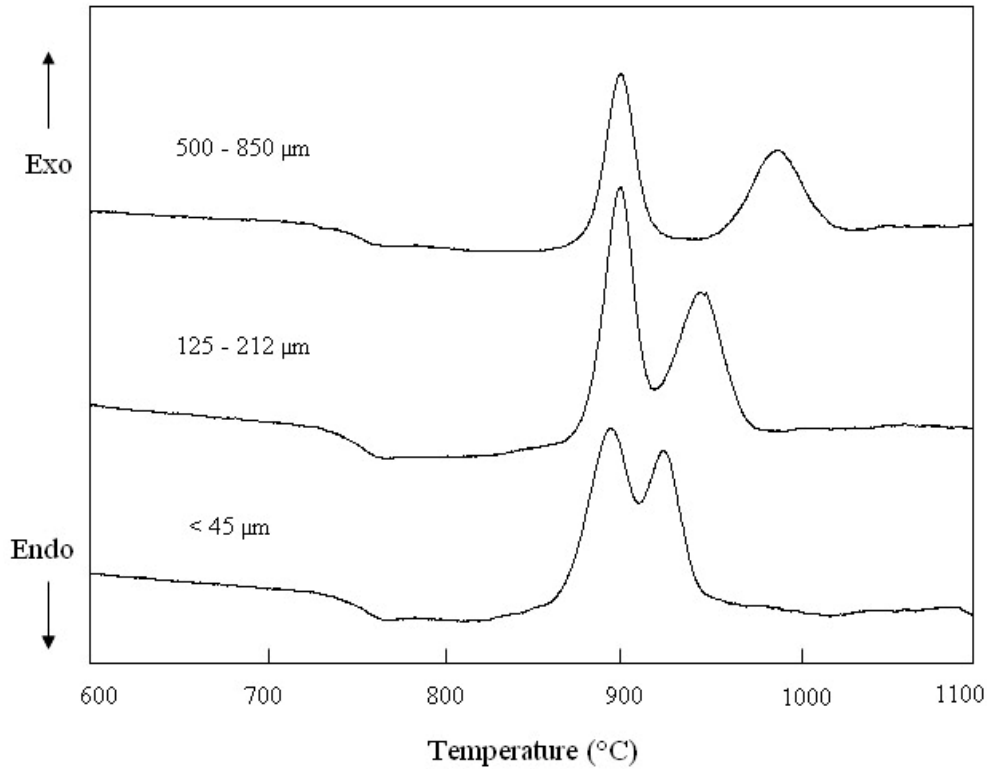


Figure 4.15 DTA thermograms of glass with different particle size ranges. The measurements were done at the heating rate of 10 °C /min.

The decrease in peak temperature was attributed to an increase in the surface area with decreasing particle size. The second exothermic peak is more strongly dependent on particle size of the glass powder. The results suggest that wollastonite phase crystallizes by surface crystallization mechanism. The apatite crystallization is not affected by particle size, implying that bulk crystallization mechanism dominates. The shape of the peak is another evidence of crystallization mechanism. The relatively sharp and narrow shape characterizes bulk crystallization mechanism, while the relatively broad and smooth shape is the characteristic of surface crystallization mechanism [83].

DTA thermograms taken at heating rates of 10, 20 and 30 °C/min for the glass of coarse particles are shown in Figure 4.16. Crystallization peak temperature, T_p , varies with heating rate, ϕ . It is clear that T_p increases also with increasing heating rate.

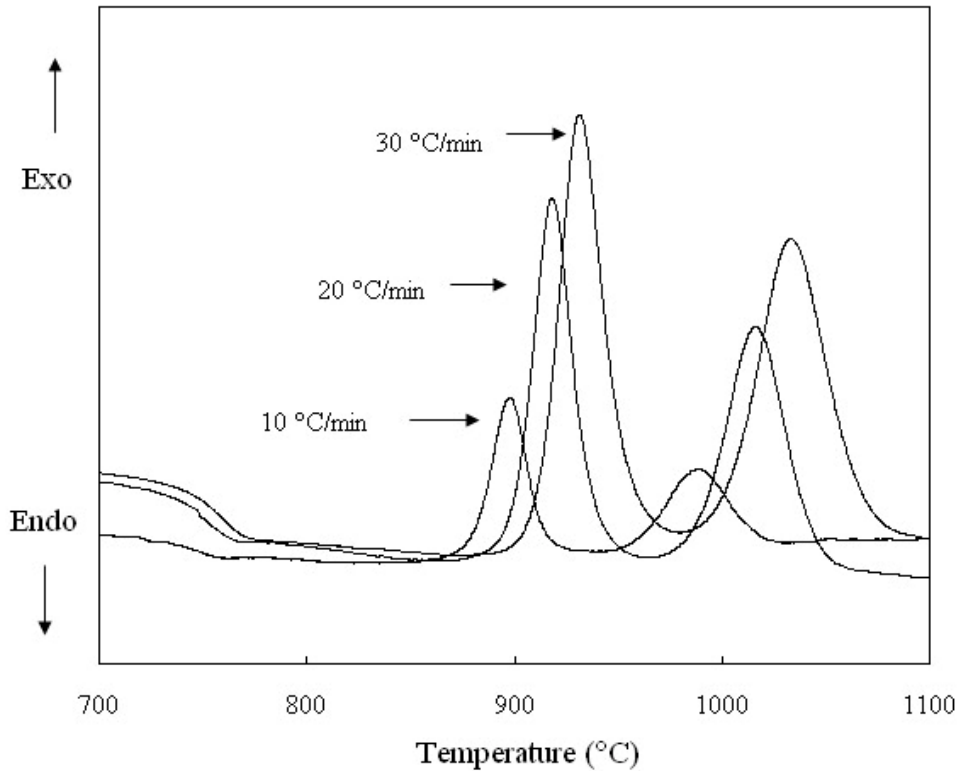


Figure 4.16 DTA thermograms of the coarse glass powder (500-850 μm) measured at different heating rates.

Figure 4.17 shows the Kissinger plot of $\ln(\phi/T_p^2)$ vs $1/T_p$. The data points were calculated using Eq. 5. The slope of the plot represents the activation energy for crystallization and the intercept is the frequency factor of each exotherm. The values of the kinetic parameters are listed in Table 4.3. The activation energy for crystallization of the first exotherm (apatite) is 460 kJ/mol, and that of the second exotherm (wollastonite) is 443 kJ/mol. The Avrami exponent, n , is about 3 for apatite phase and 2 for wollastonite phase. The values of n prove that the crystallization mechanism of apatite is bulk crystallization and that of wollastonite is surface crystallization.

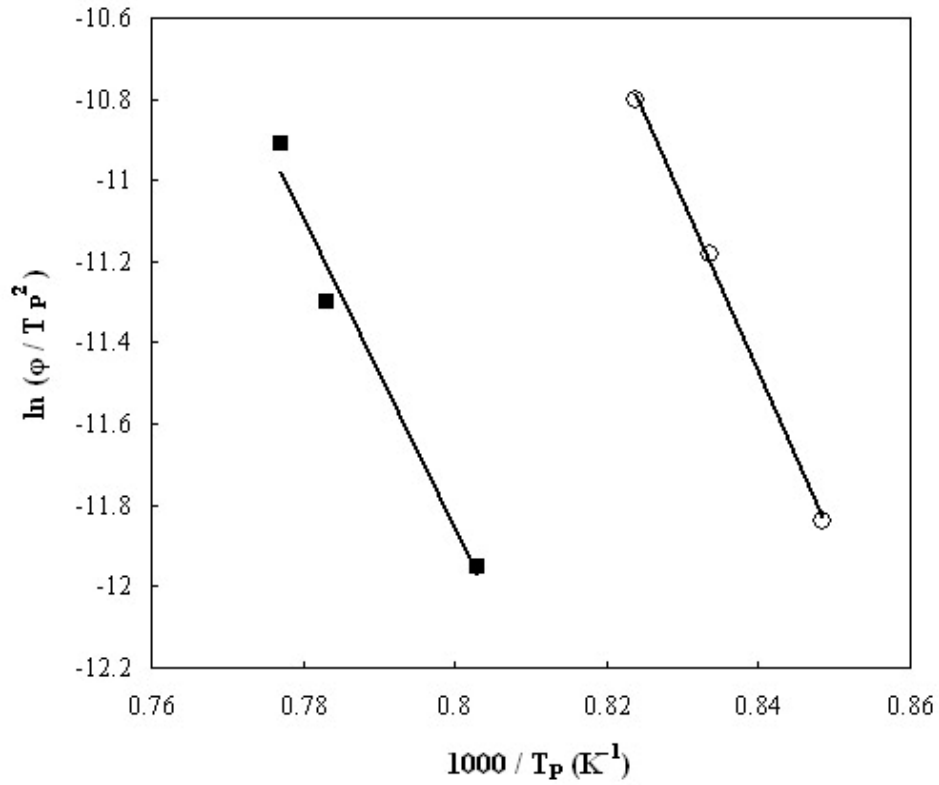


Figure 4.17 Kissinger plot of $\ln(\phi/T_P^2)$ vs $1/T_P$ of the glass with particle size range of 500-850 μm . (\blacksquare : 1st exotherm, \circ : 2nd exotherm).

Table 4.3 Kinetic parameters of the glass investigated in this study.

Heating rate (°C /min)	1 st exotherm E = 460 kJ/mol v = 1.74×10^{22} /s		2 nd exotherm E = 443 kJ/mol v = 2.25×10^{17} /s	
	T _P (°C)	n	T _P (°C)	n
10	895	3.1	1016	1.5
20	896	3.6	1037	1.8
30	897	3.5	1048	1.7

4.2 THE EFFECT OF TiO₂ ADDITION ON THE CRYSTALLIZATION KINETICS OF A GLASS IN THE MgO-CaO-SiO₂-P₂O₅-F SYSTEM

4.2.1 General

In this section, the data gathered from the experimental study conducted on the effect of TiO₂ addition on the crystallization kinetics of A-W glass in the MgO-CaO-SiO₂-P₂O₅-F system were presented. The results are discussed and compared with the results of the previous studies published in the literature.

Previous studies [76,77] have revealed that TiO₂ is a good nucleation agent in many silicate systems. However, the role of TiO₂ as a nucleation agent in A-W glass-ceramics has been overlooked due to the fact that the chemical composition includes P₂O₅ and F to promote nucleation. The effect of TiO₂ on the crystallization kinetics and tribological properties of this system has not been reported in the open literature.

The purpose of the present research is twofold. The first one is to investigate the role of TiO₂ as a nucleating agent in the MgO-CaO-SiO₂-P₂O₅-F system. The second one is to determine the influence of small amount of TiO₂ additions on the crystallization kinetics of a glass in this system using non-isothermal differential thermal analysis. Results were supplemented by the phase and microstructural analyses to elucidate the behavior observed.

The glass blocks obtained in the MgO-CaO-SiO₂-P₂O₅-F system according to the procedure as described in section 3.2.1 were colorless and indicated no unmolten batch materials or crystallinity. The blocks were carefully heat treated 1 h at 780 °C for nucleation followed by 30 min at 900 °C for crystal growth to obtain A-W glass-ceramics through melt casting process. The appearance of the blocks changed after the heat treatment from transparent to opaque suggesting that microstructure morphology changed after heat treatment.

4.2.2 X-ray Diffraction Analysis

The XRD pattern of the crystallized counterpart of the as-prepared glasses (glass ceramics) suggested that apatite (JCPDS card # 89-6495) and wollastonite (JCPDS #10-489) were precipitated in these glasses upon crystallization heat treatment.

Figure 4.18 shows the XRD patterns of the glasses containing various amount of TiO_2 . The patterns were obtained after heat treatment of the glasses listed in Table 3.4 1 h at 780 °C. It is clearly seen that TiO_2 content in the glass composition did not have a profound effect on the number of the crystalline phases precipitated. Only one kind of crystal, namely apatite, was detected even though the amount of TiO_2 incorporated into the base glass is increased up to 12 wt%. Nevertheless, the intensity of the (211) plane of apatite crystals at 2θ of $\sim 31.6^\circ$ varied with small amount of TiO_2 additions. The intensity increased with increasing TiO_2 content in the glass, formed a maximum at 4 wt% TiO_2 addition and then decreased slightly with further increase in TiO_2 content. The values of the intensity of the (211) plane of apatite crystals for the glasses investigated are listed in Table 4.4.

Figure 4.19 illustrates the XRD patterns obtained after heat treatment 1 h at 780 °C followed by 30 min at 900 °C for the glasses containing various amounts of TiO_2 . Precipitation of wollastonite phase is clearly seen in the patterns. The patterns suggest that apatite and wollastonite precipitated mutually in these glasses when exposed to a growth temperature of 900 °C. However, crystallization of wollastonite was more dominant in Glass 3 as compared to Glass 1. The peak intensity of the (320) plane of wollastonite crystals at 2θ of $\sim 30.5^\circ$ in Glass 3 is evidently higher than in any other glass. The intensity of the (320) plane increased from Glass 1 and became maximum in Glass 3, then started to decrease up to Glass 5. The tendency for wollastonite phase was the same as apatite phase. These results reveal that a small amount of TiO_2 additions to the base glass promoted the crystallization of apatite and wollastonite although the effect was more dominant for wollastonite.

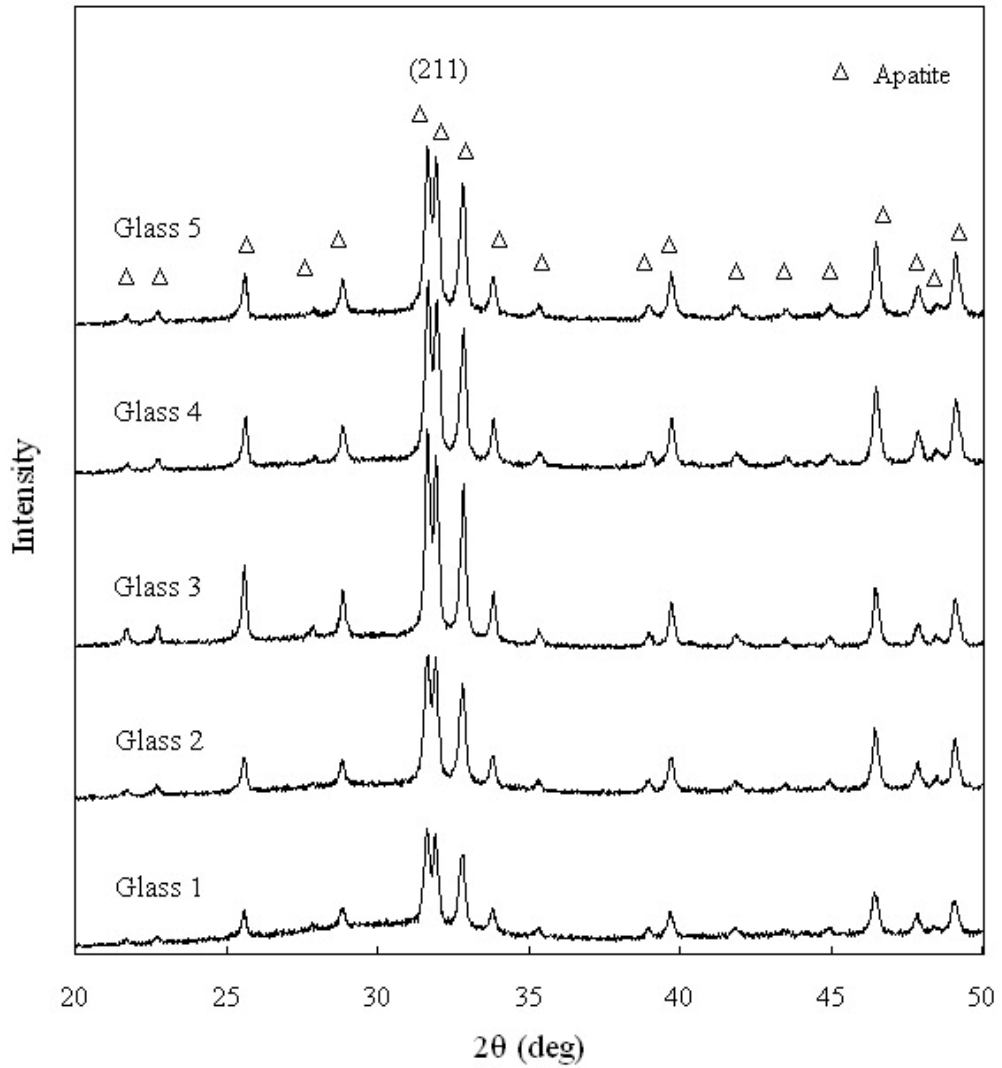


Figure 4.18 XRD patterns obtained after heat treatment 1 h at 780 °C for the glasses containing various amount of TiO₂.

Table 4.4 The values of the intensity of the (211) plane of apatite crystals for the glasses investigated.

	Glass 1	Glass 2	Glass 3	Glass 4	Glass 5
Intensity (CPS)	2131	2538	3873	3361	3146

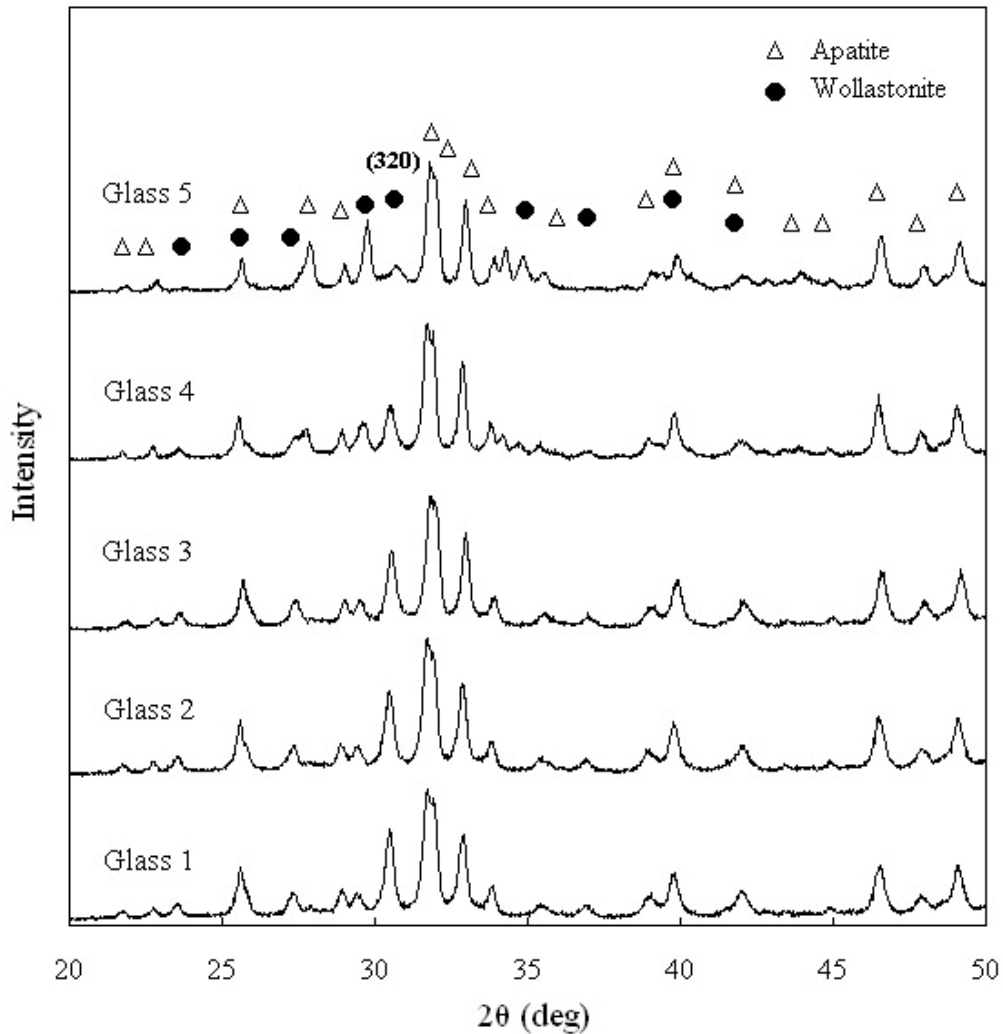


Figure 4.19 XRD patterns obtained after heat treatment 1 h at 780 °C followed by 30 min at 900 °C for the glasses containing various amount of TiO₂.

4.2.3 Differential Thermal Analysis

Representative DTA thermograms taken at a heating rate of 10 °C/min for the glasses containing various amount of TiO₂ are shown in Figure 4.20. The thermograms exhibit two well defined crystallization exotherms suggesting that at least two crystalline phases are being formed when this glass is reheated. The XRD analyses identified that the first exothermic peak, which occurred in the temperature range of 860 to 930 °C, is for the crystallization of apatite, and the second exothermic peak, which occurred in the temperature range of 950 to

1050 °C, is for the crystallization of wollastonite. The findings are in accordance with those reported in the literature [34,75]. The crystallization peak for apatite is narrow and sharp but that for wollastonite is broad, indicating that the two crystalline phases have different crystallization mechanisms. Ray and Day [83] reported that a sharp peak is characteristic of the bulk crystallization process; whereas, a broad peak reflects the process of surface crystallization.

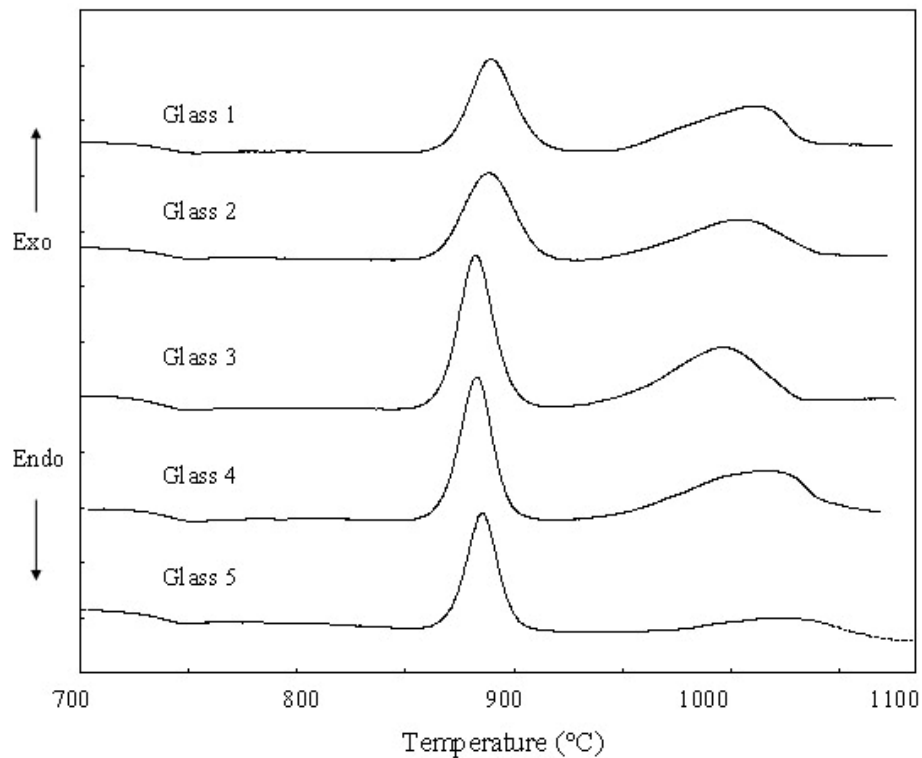


Figure 4.20 DTA thermograms taken at the heating rate of 10 °C /min for the glasses investigated.

Influence of the heating rate and TiO₂ addition on the glass transition temperature, T_g, and peak maxima of the crystallization exotherm, T_p, as well as the thermal stability parameter, T_c-T_g, is tabulated in Table 4.5 for the glasses investigated. The incorporation of a small amount of TiO₂ to Glass 1 had an effect on the thermal parameters. That is; for a given heating rate the T_g, T_c, T_p, and T_c-T_g of the phases crystallized varied as seen in Table 4.5. The values of the thermal

parameters decreased until 4 wt% TiO₂ addition and then increased with further TiO₂ additions. The temperature difference T_c-T_g is used as an indication of the thermal stability of glasses: the higher the value of this difference, the more the delay in the nucleation process and hence the greater the stability of the glass [120,121]. From that point of view, crystallization tendency of the glasses improved up to 4 wt% TiO₂ addition but became worse when TiO₂ concentration was increased further.

Table 4.5 Values of the thermal parameters obtained from DTA for different heating rates for the glasses investigated.

Sample	$\dot{\phi} = 5^{\circ}\text{C}/\text{min}$					$\dot{\phi} = 10^{\circ}\text{C}/\text{min}$					$\dot{\phi} = 15^{\circ}\text{C}/\text{min}$					$\dot{\phi} = 20^{\circ}\text{C}/\text{min}$				
	T _g	T _{pA}	T _{pW}	T _{cA} -T _g	T _{cW} -T _g	T _g	T _{pA}	T _{pW}	T _{cA} -T _g	T _{cW} -T _g	T _g	T _{pA}	T _{pW}	T _{cA} -T _g	T _{cW} -T _g	T _g	T _{pA}	T _{pW}	T _{cA} -T _g	T _{cW} -T _g
Glass 1	731	884	989	118	195	734	895	1016	127	216	735	909	1022	133	217	737	917	1031	139	226
Glass 2	731	881	987	116	186	732	893	1013	127	210	734	906	1018	133	215	736	913	1029	138	217
Glass 3	726	875	982	115	186	730	886	1003	125	206	733	897	1016	131	210	735	904	1025	134	214
Glass 4	728	876	998	118	189	731	888	1020	126	209	735	898	1029	131	211	737	906	1052	135	224
Glass 5	730	876	999	119	189	732	891	1025	130	216	735	900	1039	134	218	738	908	1061	136	232

(Subscript A and W designate the crystallization exotherms of apatite and wollastonite, respectively.)

Several researchers [121-123] have realized that TiO₂ acts as the glass network former in the form of [TiO₄], whereas others [124,125] have found that TiO₂ acts as the glass modifier in the form of [TiO₆]. TiO₂ would be normally expected to have a co-ordination number of six because of the size (0.68 Å) of the titanium ion [80]. However, the titanium ions may have a co-ordination number of four in order to take part in the glass network structure and to be compatible with the silicate network at high temperature [121]. During rapid cooling of the melt, TiO₂ may be “frozen in” with co-ordination number of four, so if there is a reheating on the glass, the tendency will be for TiO₂ to assume the co-ordination number of six and in doing this it will no longer be able to occupy network-forming positions [80]. The tetrahedral [TiO₄] enhances the glass formation ability by networking with [SiO₄] groups, and does not induce the formation of any non-bridging oxygen ions. However, octahedral [TiO₆] exists in six-fold coordination and

loosens the glass network. This may be one of the reasons for the initial decrease and subsequent increase in the thermal parameters with increasing TiO_2 additions. From the DTA results obtained, it is obvious that TiO_2 functioned in the $\text{MgO-CaO-SiO}_2\text{-P}_2\text{O}_5\text{-F}$ system as the glass network modifier and broke up the random network of glass producing the non-bridging oxygens when it is added to the base glass up to 4 wt%. Nevertheless, it functioned as the glass network former enhancing the glass formation when further additions were made.

Figures 4.21 and 4.22 show the $\ln(\phi/T_p^2)$ vs $1/T_p$ plots for apatite and wollastonite, respectively. The solid lines are the least squares fit of the data points. The kinetic parameters E and v were determined from the slope and intercept, respectively, of a modified form of JMA plots. Values of n were computed from Eq.4. The values of the kinetic parameters for apatite and wollastonite for the glasses investigated were presented in Table 4.6. The maximum uncertainty in measurements was calculated using error analysis as ± 15 kJ/mol and ± 0.1 , for E and n , respectively.

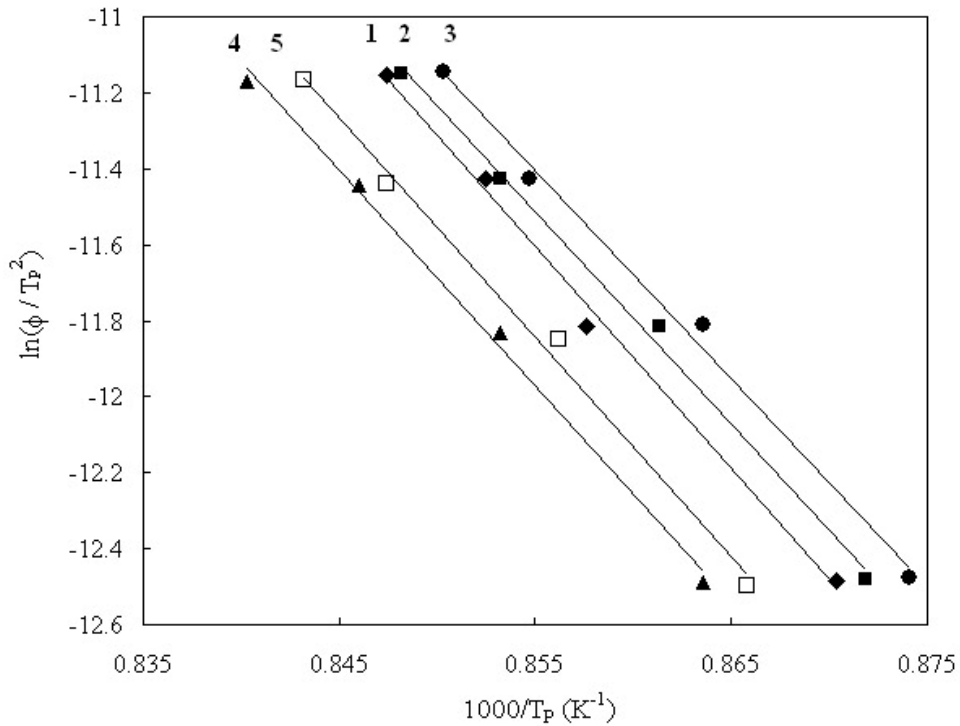


Figure 4.21 The $\ln(\phi/T_p^2)$ vs $1/T_p$ curves for apatite. Numbers on the curves correspond to the glass numbers given in Table 3.4.

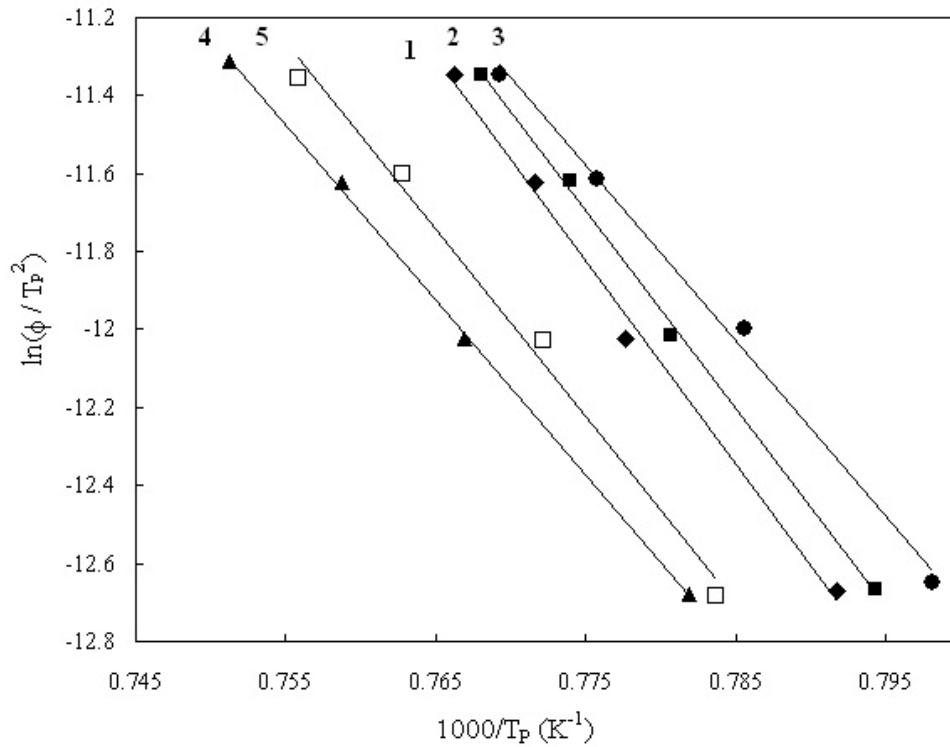


Figure 4.22 The $\ln(\phi/T_p^2)$ vs $1/T_p$ curve for wollastonite. Numbers on the curves correspond to the glass numbers given in Table 3.4.

Table 4.6 Activation energy for crystallization (E), Avrami parameter (n), and frequency factor (ν) for apatite and wollastonite.

Sample	$E \pm 15$ (kJ/mol)		$n \pm 0.1$		ν (s^{-1})	
	A	W	A	W	A	W
Glass 1	460	443	3.1	1.5	1.74×10^{22}	2.25×10^{17}
Glass 2	425	395	3.2	1.5	2.31×10^{21}	4.14×10^{16}
Glass 3	408	320	3.3	1.9	9.24×10^{17}	8.32×10^{11}
Glass 4	414	351	3.3	1.8	9.59×10^{19}	2.67×10^{12}
Glass 5	426	417	3.3	1.5	2.28×10^{21}	6.55×10^{15}

A and W designate apatite and wollastonite, respectively.

The variation of E for apatite and wollastonite with TiO₂ additions is graphically shown in Figure 4.23. Both phases exhibit similar behavior with increasing TiO₂ additions. The E of apatite and wollastonite first decreases and forms a minima at about 4 wt% TiO₂ addition and then increases with further TiO₂ additions.

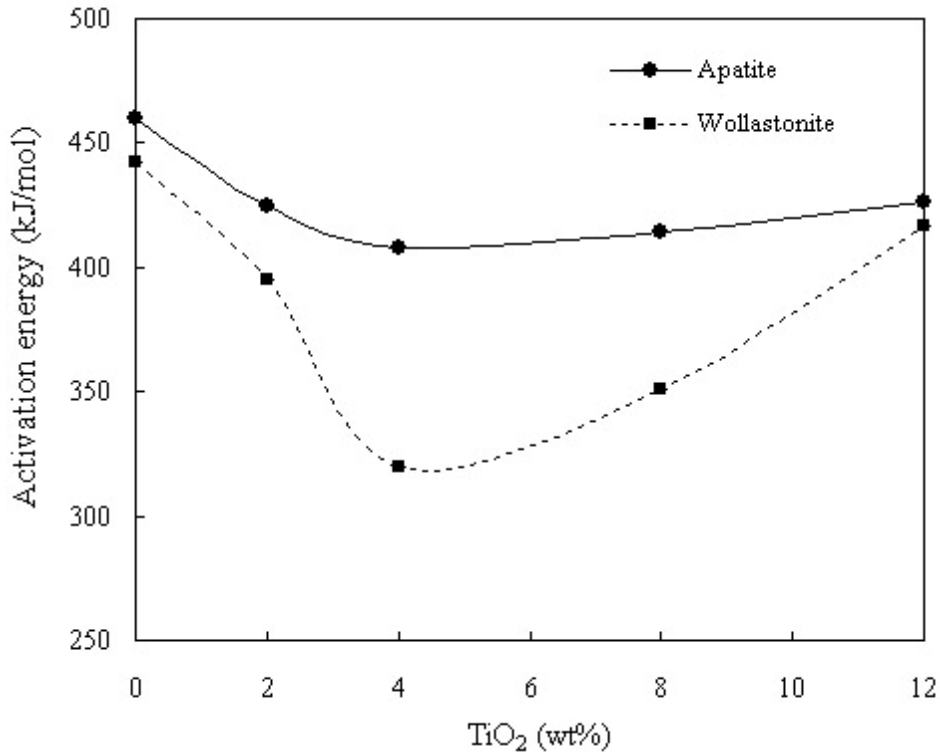


Figure 4.23 Variation of the activation energy for crystallization with TiO₂ additions.

The initial decrease until 4 wt% TiO₂ addition followed by an increase in the E of apatite and wollastonite supports the explanation for the possible effect of TiO₂. As seen in Table 4.6, the E for apatite and wollastonite is 460±15 kJ/mol and 443±15 kJ/mol, respectively in Glass 1, and becomes 408±15 kJ/mol and 320±15 kJ/mol, respectively in Glass 3. The decrease in E with 4 wt% TiO₂ addition is interpreted as the indication of the increasing tendency for crystallization [126]. Although it is difficult to find the physical meaning of the activation energy precisely when bulk and surface crystallization occur simultaneously, lower value of E in Glass 3 as compared to Glass 1 imply that Glass 3 is less stable and has a

higher tendency to devitrification. It is evident that TiO_2 promotes the crystallization of not only apatite but also wollastonite. Consequently, it is an effective nucleation agent for the glasses in the $\text{MgO-CaO-SiO}_2\text{-P}_2\text{O}_5\text{-F}$ system.

The variation of the n for apatite and wollastonite with TiO_2 additions is shown in Figure 4.24. The n of apatite and wollastonite tends to increase with TiO_2 additions, forms maxima at about 4 wt% TiO_2 addition and then decreases with further TiO_2 additions. The n is a crystal growth index which can describe the crystallization reaction mechanism and ability of a glassy material to crystallize. The crystallization process becomes easier when the value for n is higher [126]. When n is less than 3, surface crystallization is the dominant crystallization mechanism whereas; n greater than 3 means bulk crystallization mechanism is dominant [83]. The values for the n for apatite and wollastonite in Glass 1 are 3.1 ± 0.1 and 1.5 ± 0.1 , respectively. It is obvious that apatite prefers to crystallize through bulk crystallization three-dimensional growth mechanism and wollastonite crystallizes through surface crystallization two-dimensional growth mechanism. The values for the n for apatite and wollastonite increased from 3.1 ± 0.1 to 3.3 ± 0.1 , and from 1.5 ± 0.1 to 1.9 ± 0.1 , respectively when 4 wt% TiO_2 was incorporated. As shown in Figure 4.24, the n for apatite and wollastonite show a similar trend with increasing TiO_2 additions. In effect, TiO_2 additions tended to change the crystallization mechanisms of apatite from two-dimensional bulk crystallization to three-dimensional bulk crystallization. The incorporation of a small amount of TiO_2 (up to 4 wt%) encouraged the crystallization mechanisms of wollastonite from one-dimensional surface crystallization to two-dimensional surface crystallization while further additions had a tendency towards one-dimensional surface crystallization.

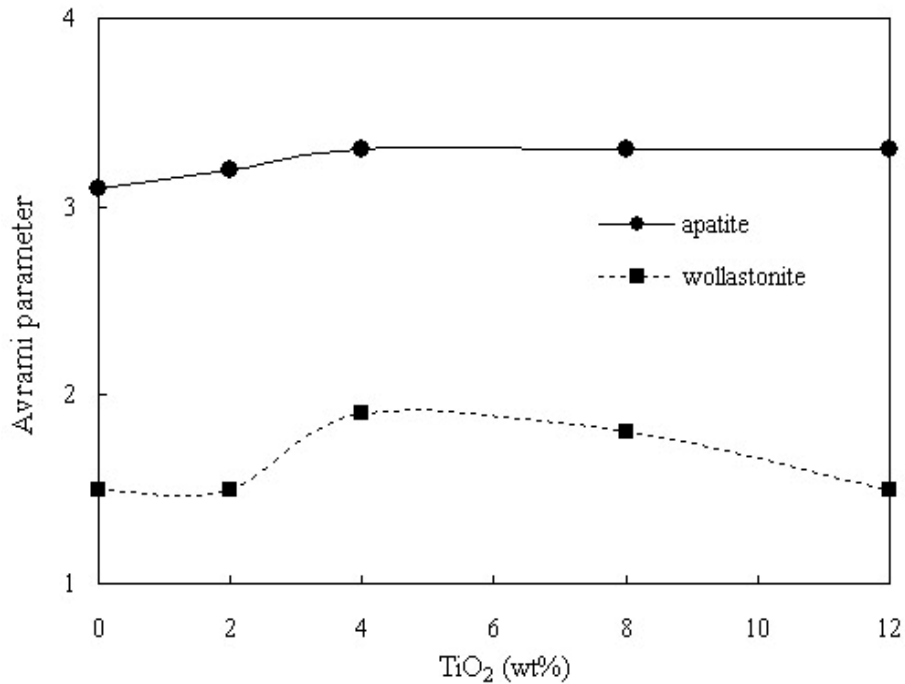
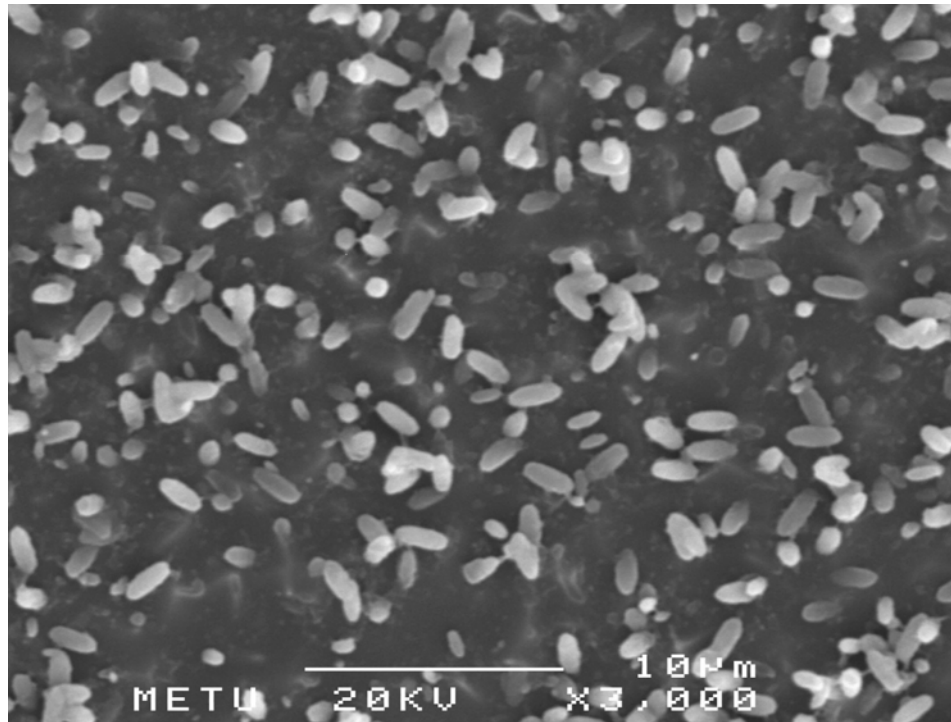


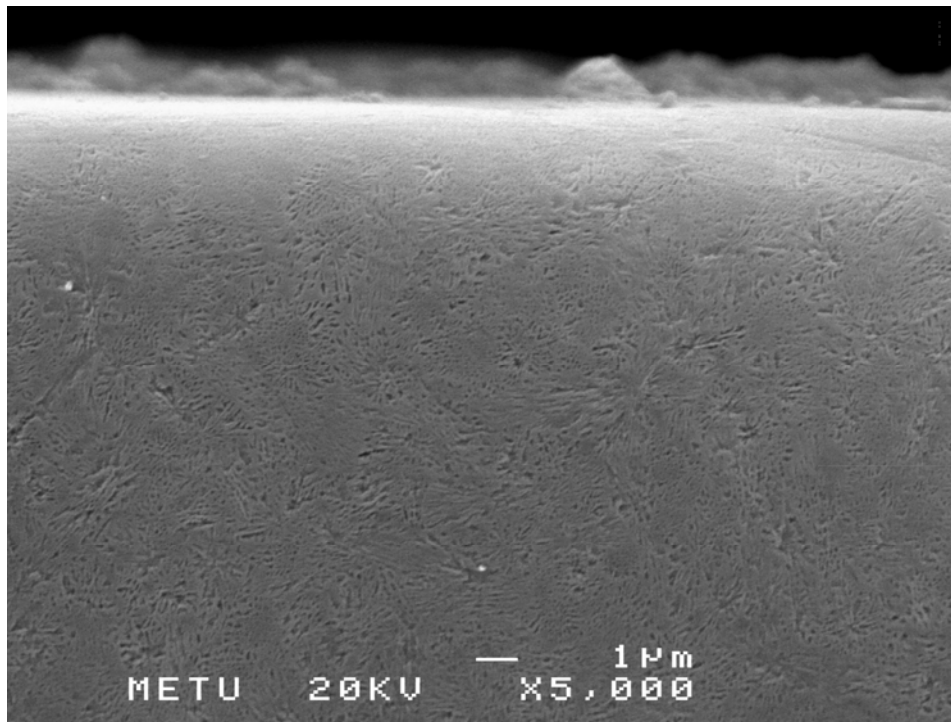
Figure 4.24 Variation of Avrami parameter with TiO₂ additions.

4.2.4 Scanning Electron Microscopy Analysis

SEM micrographs in Figures 4.25 and 4.26 show typical microstructure of the crystallized counterparts of Glass 1 and Glass 3, respectively. The micrograph in Figure 4.25(a) reveals that apatite crystals are uniformly precipitated by consuming the glass matrix surrounding them. The nominal length of the rice-shaped crystals is approximately 2 μm . As the heat treatment temperature increased, the crystals grew and appeared in web-like microstructure. Dendritic growth of the apatite crystals in the glass ceramic has been also observed by Kokubo [34]. The apatite crystals are well precipitated in Glass 3. The length of the crystals in Glass 3 is more or less the same with that in Glass 1, but the number of apatite crystals per unit volume increases. The results are compatible with the results of the XRD study presented in section 4.2.2. The rich precipitation of apatite in this glass is attributed to the decrease in the E of apatite with increasing TiO₂ addition. In addition to apatite crystals, the wollastonite crystals are formed as needle shape after heat treating the glass 1 h at 780 °C followed by 30 min at 900 °C.



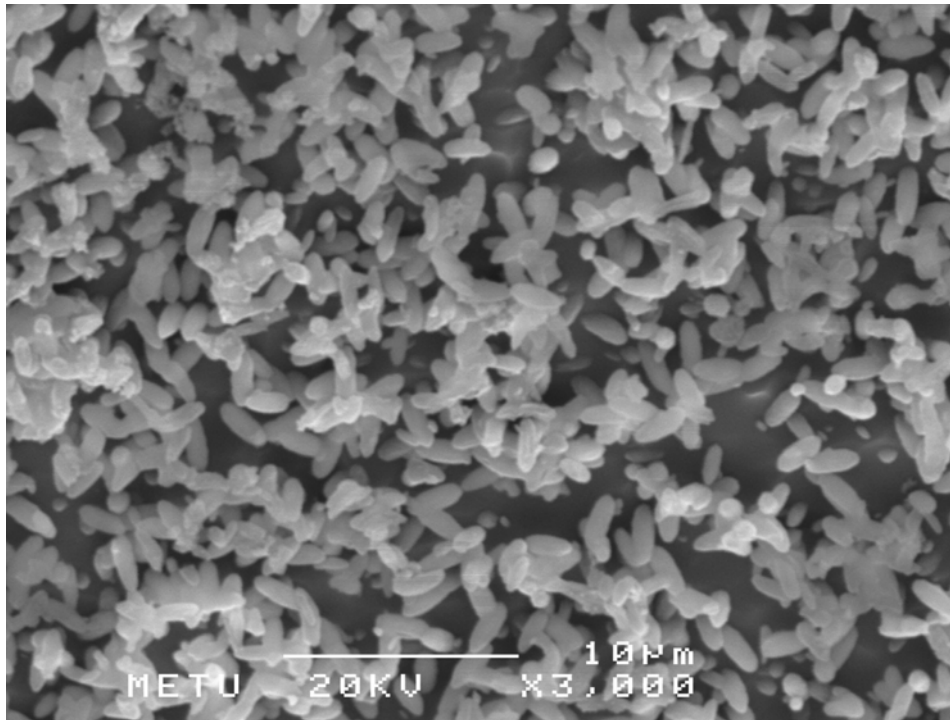
(a)



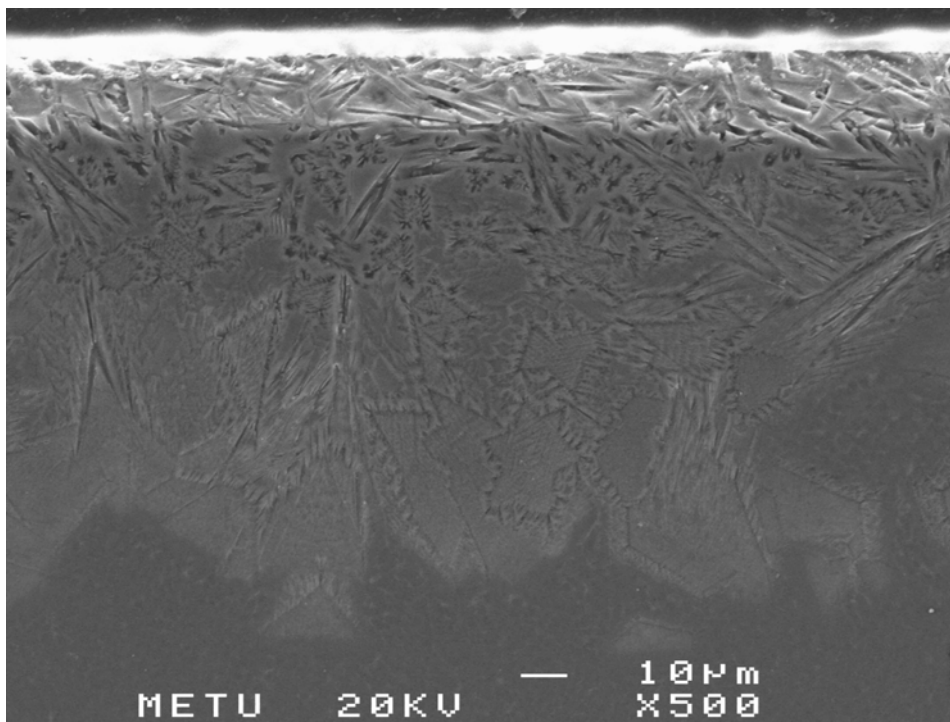
(b)

Figure 4.25 SEM micrographs of Glass 1 after heat treatment (a) at 780 °C for 1 h, and (b) at 780 °C for 1 h followed by at 900 °C for 30 min.

In view of the fact that wollastonite crystallizes through surface crystallization mechanism, the crystals grow from the surface towards the interior as shown in Figure 4.26 (b). The needle-like wollastonite crystals have not been observed in Glass 1 because they are crystallized between apatite grains. However, extensive crystallization of wollastonite has been observed in Glass 3 because it has low E for wollastonite. It is obvious that addition of as small as 4 wt% TiO₂ to Glass 1 encouraged apatite and wollastonite crystallization.



(a)



(b)

Figure 4.26 SEM micrographs of Glass 3 after heat treatment (a) at 780 °C for 1 h, and (b) at 780 °C for 1 h followed by at 900 °C for 30 min.

4.3 TRIBOLOGICAL PROPERTIES OF A-W GLASS-CERAMICS

4.3.1 General

In this section, the data gathered from the experimental study conducted on the tribological properties of Apatite-wollastonite (A-W) glass-ceramics is presented. The results are discussed and compared with the results of the previous studies published in the literature.

Determination of the tribological properties, namely wear rate and friction coefficient of A-W glass-ceramic are of importance since the understanding of tribological performance can extend the utilization of this material to special dental applications. In spite of some investigations [34,44,74,75] on the formation, structure, and mechanical properties of A-W glass-ceramics, the data on the tribological properties are rare and sparse. A good understanding of the tribological behavior of A-W glass ceramics is necessary for correlating the tribological properties with structural characteristics of the system. Hence, studies carried out on the tribological behavior of A-W glass ceramics have both scientific and practical significance.

The purpose of this investigation is to determine the tribological properties and to evaluate the structural characteristics on tribological behavior of A-W glass-ceramic produced by melt casting process. Microhardness and tribological property measurements were supplemented with microstructural analyses to explain the behavior observed.

The glass pieces obtained in the MgO-CaO-SiO₂-P₂O₅-F system according to the procedure as described in section 3.3.1 were colorless and indicated no unmolten batch materials or crystallinity. The pieces were carefully heat treated 1 h at 780 °C for nucleation followed by 30 min at 900 °C for crystal growth to obtain A-W glass-ceramics through melt casting process.

4.3.2 X-ray Diffraction Analysis

Figure 4.27 illustrates the XRD patterns obtained from the free surface, and the subsurfaces; 0.1, 0.3, and 0.5 mm below the free surface, after heat treatment of a bulk glass sample 1 h at 780 °C followed by 30 min at 900 °C. A preferred orientation with (002) plane of the wollastonite crystal (JCSRD # 10-489) along with the apatite crystal (JSPD card #89-6495) is detected on the free surface as seen in Figure 4.27(a). The preferred orientation of the wollastonite crystals changes to a texture with (320) plane at the depth distance of 0.1 mm below the free surface as seen in Figure 4.27(b). After removing a layer of 0.3 mm from the free surface, the texture vanishes. The XRD pattern shown in Figure 4.27(c) suggests that apatite and wollastonite phases precipitated randomly at the depth distance of 0.3 mm below the free surface. Polishing the surface until 0.5 mm below the free surface has diminished the layer at which wollastonite phase existed. Figure 4.27(d) illustrates the XRD pattern of the interior region where only apatite phase is detected.

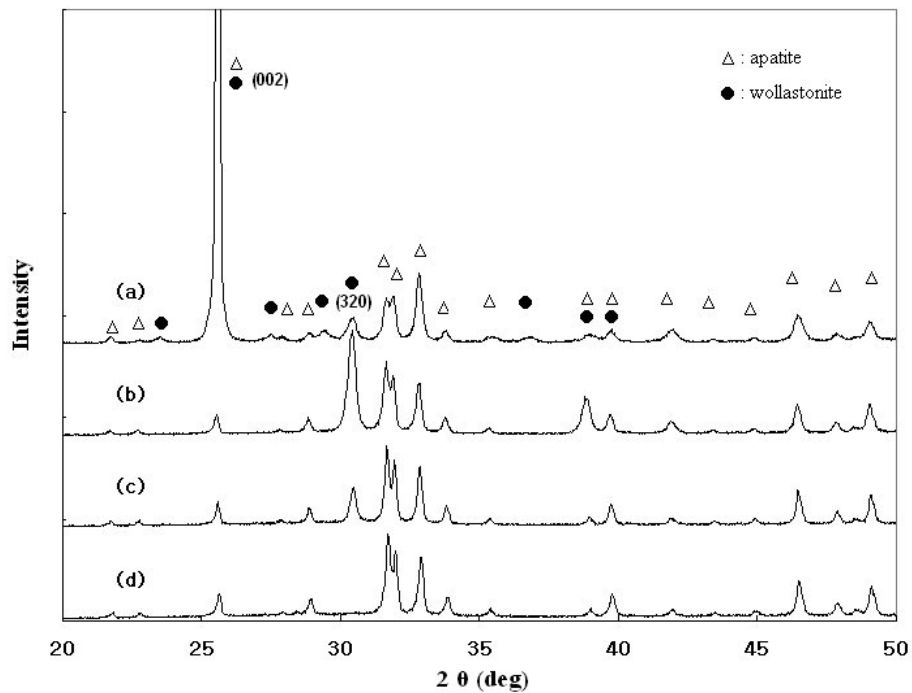


Figure 4.27 XRD patterns of the glass-ceramic. The patterns were taken from (a) the free surface, (b) 0.1 mm, (c) 0.3 mm and (d) 0.5 mm below the free surface.

4.3.3 Scanning Electron Microscopy Analysis

Figure 4.28 illustrates the micrographs taken from the cross-section and interior parts of the A-W glass-ceramic studied. The micrographs reveal that glass-ceramic has a dense and heterogeneous microstructure consisting of apatite and wollastonite crystals randomly distributed throughout the glass matrix. The preferred orientation of the wollastonite crystals with elongated needle-shaped grains is observed in the free surface. A typical characteristic of surface crystallization, in which crystals grow from the free surface towards interior, is apparent. The thickness of the layer at which wollastonite phase with preferred orientation has precipitated along with apatite phase is approximately 350 μm .

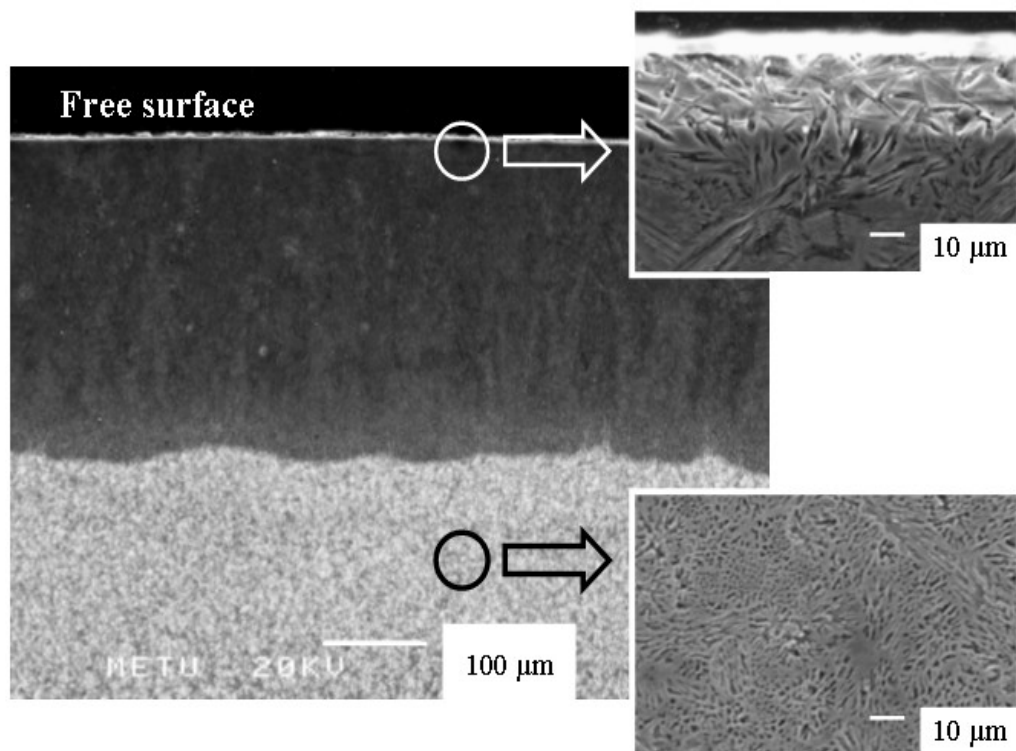


Figure 4.28 SEM micrographs taken from the cross sectional area, the free surface, and the interior part of the A-W glass-ceramic.

The effect of orientation decreases and become random as the depth distance from the free surface increases. Apatite which crystallizes in dendric form is the only phase present at a subsurface of 0.5 mm below the free surface. The dendritic growth of the crystals in the interior part of the specimen is also shown at a larger magnification in Figure 4.11 in section 4.1.3. The microstructure obtained from the interior part of the sample resembles that reported by Kokubo and his co-workers [33,34].

As stated in section 4.2, apatite and wollastonite have different crystallization mechanisms. Apatite has precipitated in bulk because of its three-dimensional bulk crystallization mechanism, whereas wollastonite prefers to precipitate from the free surface through a two-dimensional surface crystallization mechanism. A typical characteristic of this crystal growth is that crystals grow with vertical orientation to the surface [33]. This nature brings a unique surface crystallization effect on the A-W glass ceramics without adding any additives or surface treatments. The surface crystallization process affects the properties of the material in a different manner on the surface and in the interior. Hence, structure-oriented, depth-dependent changes in properties are anticipated.

4.3.4 Hardness and Wear Rate

The values for the microhardness, wear rate, and friction coefficient as determined at the free surface and at the subsurfaces are presented in Table 4.7. The microhardness of the free surface was about 650 ± 12 H_V, but decreased gradually with increasing depth distance from the free surface. Eventually, it attained a value of 520 ± 8 H_V at the subsurface of 0.5 mm below the free surface. The \pm signs next to the determination point indicate the standard deviation of the data from the averages. The microhardness value of the free surface (650 ± 12 H_V) was comparable to, but slightly lower than that (680 H_V) of the commercially available A-W glass-ceramic (Cerabone[®]) designed for use in hard tissue replacements [37,38]. The value for the subsurface of 0.5 mm below the free surface (520 ± 8 H_V) was close to that (540 H_V) for a commercial dental porcelain material (IPS

Empress 2) used in dentistry for core material [107]. The microhardness values suggest that the A-W glass ceramic produced in this study may be successfully utilized as core material in dentistry.

Table 4.7 Knoop hardness, wear rate, and friction coefficient of the A-W glass-ceramic.

Depth distance from the free surface (mm)	Knoop hardness (H _v)	Wear rate ($\times 10^{-4}$ mm ³ /N.m)	Mean friction coefficient (μ)
Free surface	650 \pm 12	0.7 \pm 0.05	0.75
0.1	601 \pm 12	1.8 \pm 0.10	0.87
0.3	550 \pm 10	2.1 \pm 0.15	0.89
0.5	520 \pm 8	2.9 \pm 0.15	0.95

The variation of KH and wear rate with the depth distance from the free surface is shown in Figure 4.29. The presence and proportion of wollastonite crystals as well as their orientation lead to an increase in microhardness of the A-W glass-ceramic. The results are in strong agreement with the findings of Kokubo *et al.*[35] who concluded that the mechanical strength of the bioactive glass is only slightly increased by precipitation of the apatite crystal but remarkably increased by precipitation of the wollastonite crystal. Accordingly, a higher value of hardness is expected on the surface than interior of the A-W glass-ceramic.

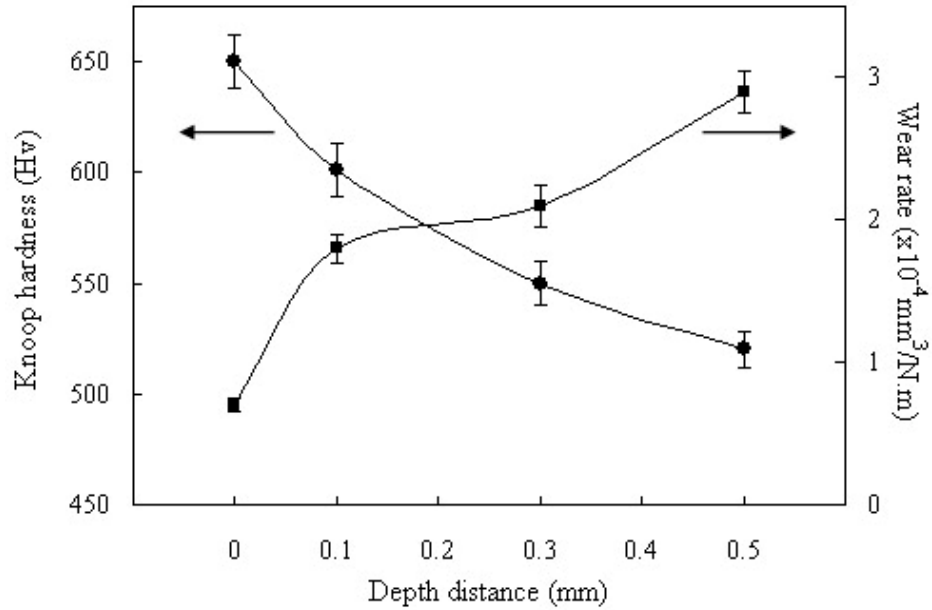


Figure 4.29 Variation in microhardness and wear rate of the A-W glass ceramic with the depth distance from the free surface.

4.3.5 Wear Rate

Mean roughness (Ra) of the polished surfaces prior to the wear tests was about $0.15 \pm 0.01 \mu\text{m}$. The average values of wear rate obtained for the free surface and for the subsurface of 0.5 mm below the free surface were $0.7 \pm 0.05 \times 10^{-4} \text{ mm}^3/\text{Nm}$, and $2.9 \pm 0.15 \times 10^{-4} \text{ mm}^3/\text{Nm}$, respectively. The standard deviation of the data indicates a good repeatability of the data points. As shown in Figure 4.29, the wear rate increased gradually with increasing depth distance from the free surface. The presence and proportion of wollastonite phase had an intense effect on the wear rate of the A-W glass-ceramic. The wear resistance of the material decreased as the proportion of wollastonite decreased. Results reveal that wear resistance of the glass-ceramic has been enhanced through the improvements in hardness of the free surface by the surface crystallization process as compared to in situ glass-ceramic. The results of the tribological tests match with the microhardness results, implying an inverse relation between the hardness and wear rate of the A-W glass ceramic.

Unfortunately, no wear rate data are available in the open literature for A-W glass ceramics with which the results of this study can be compared directly. However, a comparison can be made between the wear rate of a commercial mica-containing glass-ceramic (Dicor[®]) designed for use in dental restoration of occlusal surfaces and the A-W glass ceramic studied. The wear rate of the free surface ($0.7 \pm 0.05 \times 10^{-4} \text{ mm}^3/\text{Nm}$) of the A-W glass-ceramic studied is lower than that ($2.6 \times 10^{-3} \text{ mm}^3/\text{Nm}$) of the Dicor[®] [62] even though the tribology test conditions were rather harsher than in [62].

4.3.6 Surface Characterization

Figure 4.30 shows a typical SEM micrograph of the wear track obtained at the depth distance 0.5 mm below the free surface of the A-W glass-ceramic. Wear debris in the form of glass-ceramic particles or blocks were observed on the wear track, implying that abrasive and adhesive wear mechanisms have occurred during wear test. Since the microhardness of the glass-ceramic ($\sim 650 \text{ H}_V$) is much lower than that of the zirconia counterface ($\sim 1300 \text{ H}_V$) used against it, deep ploughing grooves, ridges and chips are also observed, which demonstrates features of abrasive and adhesive wear [62]. More ploughed marks were observed on the wear track as the depth distance from the free surface increased. Wear track profiles shown in Figure 4.31 reveal that the depth and width of the wear track as well as the wear area increased steadily with increasing depth distance from the free surface.

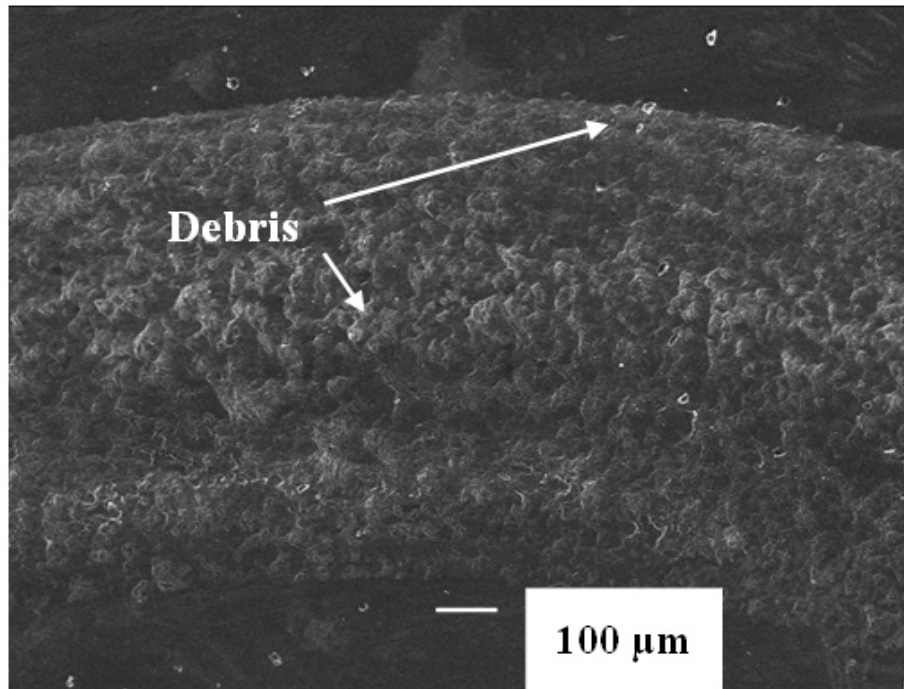


Figure 4.30 SEM micrograph of the wear track obtained at the depth distance 0.5 mm below the free surface.

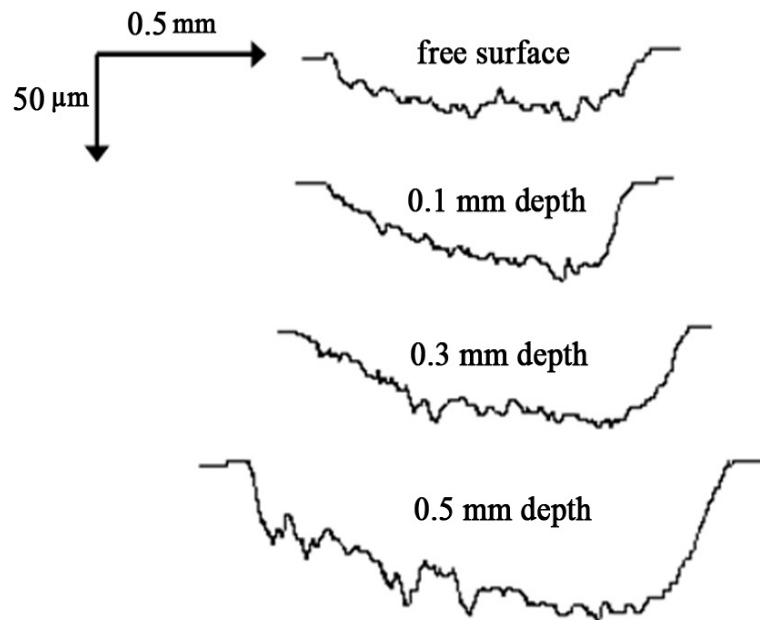


Figure 4.31 Wear track profiles obtained for the free surface and for the subsurfaces.

The existence of wollastonite phase resulted in an increase in the wear resistance due to the behavior of wollastonite like a filler reinforcing matrix [127]. Whisker-like wollastonite grains generate unique resistance to wear. Another reason is attributed to the formation of compressive stress induced from the surface crystallization process. Furthermore, the improvement is magnified as the wollastonite crystals position in one direction due to preferred orientation. In general, surface crystallization can improve the mechanical properties by two processes [128]. First, surface crystals can be of different thermal expansion or density from the interior so that a compressive stress is created in the surface layers. Second, the growth of surface crystals encapsulates surface flaws so that extra energy is required to cause flaw propagation.

4.3.7 Friction Coefficient

Figure 4.32 shows the variation in the friction coefficient of the glass-ceramic with sliding distance obtained for the free surface and for the subsurfaces. The mean friction coefficient (μ) of the glass-ceramic ranged between 0.75 μ and 0.95 μ . The μ at the free surface was about 0.75 μ and increased slightly with increasing depth distance from the free surface and reached to 0.95 μ at a distance 0.5 mm below the free surface. As seen in Figure 4.32, the μ of the free surface and of the depth distance 0.5 mm below the free surface are distinctly different from each other. On the other hand, the μ at the depth distances 0.1 mm below and 0.3 mm below the free surface are more or less the same. It is apparent that the μ is affected by the distribution of crystallized phases in the glass-ceramic. The results are in good agreement with the wear rate results.

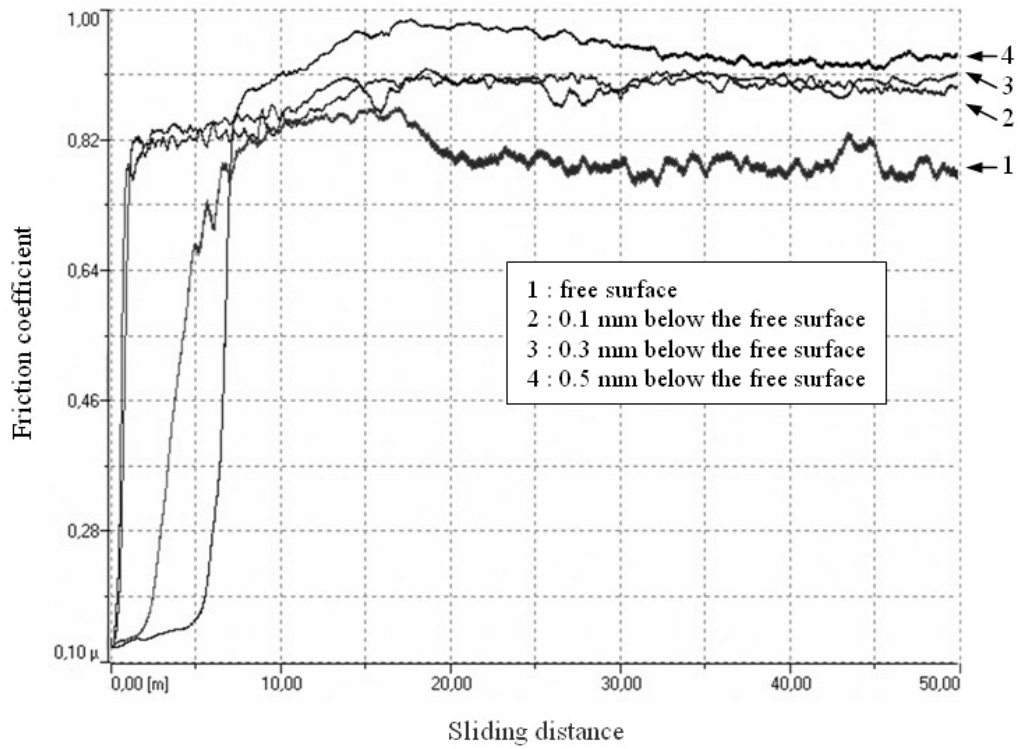


Figure 4.32 Variation in the friction coefficient of the glass-ceramic with sliding distance for the free surface and the subsurfaces.

4.4 A COMPARISON OF TRIBOLOGICAL PROPERTIES OF A-W GLASS-CERAMICS WITH SELECTED DENTAL CERAMICS

4.4.1 General

In this section, the data gathered from the experimental study conducted on comparison of tribological properties of A-W glass-ceramics with selected dental ceramics is presented. The results are discussed and compared with the results of the previous studies published in the literature.

The development of restorative materials that have wear resistance similar to enamel is desirable and would be a significant addition to clinical dental practice. It has been recognized in section 4.3 that the microhardness and wear resistance of the A-W glass-ceramics are comparable to currently used dental materials. The purpose of this present study is to compare the tribological properties of the A-W glass-ceramics with those of six different commercial dental ceramics. A series of tribological tests were conducted to evaluate the tribological similarities between the materials studied. Hardness of the materials was also measured since it is considered one of the important properties in selecting materials for restorative dentistry.

The glass pieces obtained in the MgO-CaO-SiO₂-P₂O₅-F system according to the procedure as described in section 3.1.1 were colorless and indicated no unmolten batch materials or crystallinity. The pieces were carefully heat treated 1 h at 780 °C for nucleation followed by 30 min at 900 °C for crystal growth to obtain the A-W glass-ceramics through melt casting process.

4.4.2 Hardness and Wear Rate

Values of Knoop hardness (KH), wear rate, and mean friction coefficient for all of the materials investigated are presented in Table 4.8. The numbers in parentheses indicate the standard deviation of the data from the averages. Values of KH and

wear rate for the materials investigated are also displayed graphically in Figure 4.33. KH values of the materials investigated varied from 322(13) H_V (for BE) to 671(5) H_V (for E2). KH value of A-W GC1 was close to that of E2, being the second highest among the materials investigated. KH value of A-W GC2 was almost the same as that of CPC though there was not a significant difference from the values for CCS1, CCS2, and SPE2. However, all values of the ceramic materials investigated were considerably higher than that of BE. The values for E2 and AW GC1 were more than twice the value measured for BE. The results reveal that the dentin porcelain and core materials exhibited relatively higher hardness than the enamel porcelain materials.

Table 4.8 Values of the hardness, wear rate, and mean friction coefficient for the materials studied.

Material	Knoop hardness (H _V)	Wear rate (×10 ⁻⁴ mm ³ /N.m)	Mean friction coefficient (μ)
E2	671 (±5)	0.18 (±0.01)	0.56
A-W GC1	650 (±12)	0.75 (±0.05)	0.75
SPE1	546 (±10)	2.38 (±0.26)	0.86
CCS1	527 (±9)	2.59 (±0.03)	0.83
CPC	521 (±3)	2.75 (±0.03)	0.84
A-W GC2	520 (±8)	2.93 (±0.15)	0.95
CCS2	514 (±5)	3.38 (±0.08)	0.85
SPE2	509 (±8)	3.44 (±0.10)	0.88
BE	322 (±13)	3.64 (±0.12)	0.89

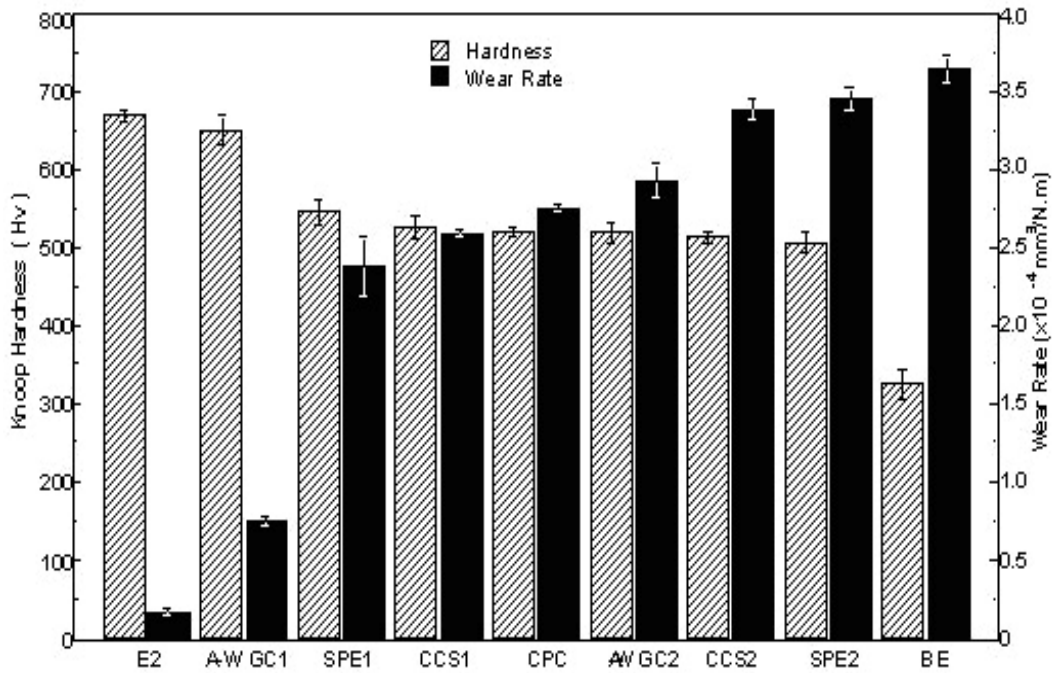


Figure 4.33 Knoop Hardness and wear rate of the materials investigated. The error bars indicate the \pm standard deviation of the data from the averages.

Wear rate of the materials studied varied from $0.18(\pm 0.01) \times 10^{-4} \text{ mm}^3/\text{N.m}$ (for E2) to $3.64(\pm 0.10) \times 10^{-4} \text{ mm}^3/\text{N.m}$ (for BE). The wear rate of A-W GC1 was considerably higher than that of E2, but still second lowest among the materials studied. The wear rate of A-W GC2 was more or less the same as the wear rate of the dentin porcelain materials such as CPC and CCS1.

The hardness values measured for A-W GC1 and A-W GC2 are in accord with the values reported for A-W glass-ceramics in the literature [74]. The hardness values measured for CCS2 and SPE2 were lower than CCS1 and SPE1, and were a bit lower than the values reported for low-fusing ceramics [58,129]. The hardness values measured for E2 and CPC were a little higher than the values reported in the literature [116,130] although the difference is not much. Hardness is considered one of the important properties in selecting materials for restorative dentistry since it delineates the abrasiveness of a material to which the natural dentition may be submitted [130]. Based on the similarities of hardness values between A-W GC2 and commercially produced dentin porcelain materials such as

CCS1 and CPC, A-W GC2 might be more compatible in direct contact with the natural dentition than A-W GC1. Ideally, an aesthetic restoration should wear at approximately the same rate as the enamel it replaces, and should not increase the wear rate of an opposing enamel surface [131]. All-ceramics have been widely used in dental restorations for the past two decades due to their aesthetics, structural durability, chemical inertness, biological compatibility, adequate strength, fracture toughness, and wear resistance [58,132].

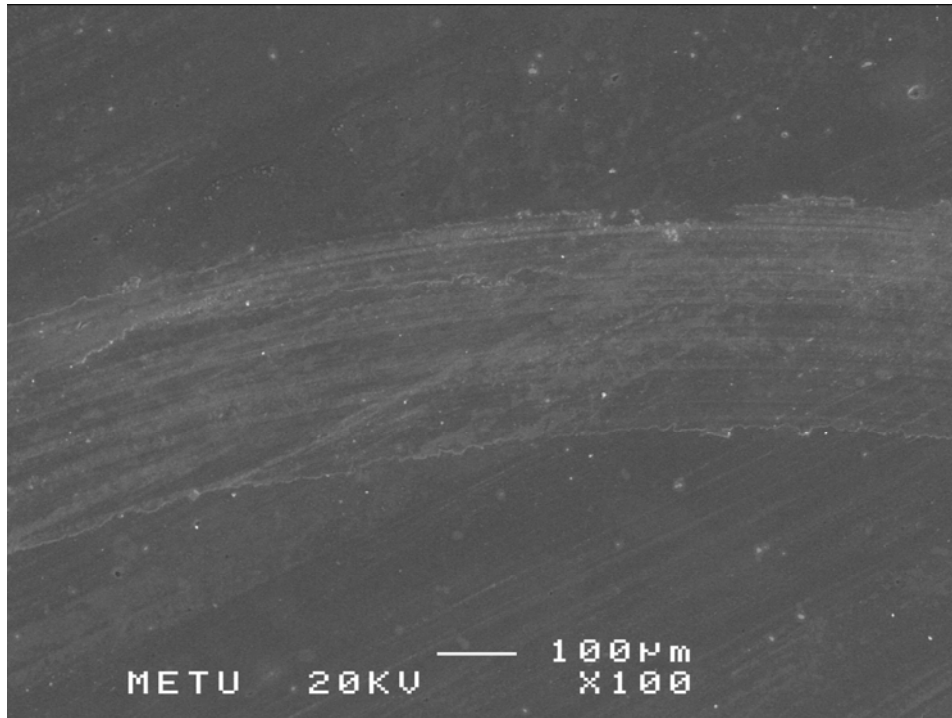
The results reveal that there is a difference between the hardness of A-W GC1 and A-W GC2. The difference of 25% in the values of the hardness of A-W glass-ceramics is due to structural variation between surface and interior crystal morphology as presented in section 4.3. It is obvious that wollastonite content and orientation of grains in the surface had a profound effect on the hardness. Similar results in E2 have been recently reported by Albakry *et al.* [130] who concluded that hardness anisotropy is seen in E2 following pressing due to the alignment of crystals.

Mean roughness (Ra) of the polished surfaces of the samples prior to the tribological tests was $0.15 \pm 0.01 \mu\text{m}$. E2 demonstrated the least wear among the materials studied. The wear rate of CPC was in the range of CCS1 and SPE1. Wear rate of CCS1, CPC and AW GC2 were more or less the same. No comparative data in the literature were found for the direct assessment of the results obtained on the wear rate of these materials, since there is only limited information and the test conditions are not identical. Hacker *et al.* [131] noted that all-ceramic low-fusing porcelain wore enamel less than conventional feldspathic porcelain Ceramco. It has been reported [115] that low fusing porcelains may cause less antagonist enamel wear than conventional porcelains because of their lower fusing temperatures. However, Clelland *et al.* [133] suggested that variations in ceramic composition and microstructure may affect the opposing enamel wear, but that low-fusing temperatures do not necessarily guarantee low enamel wear.

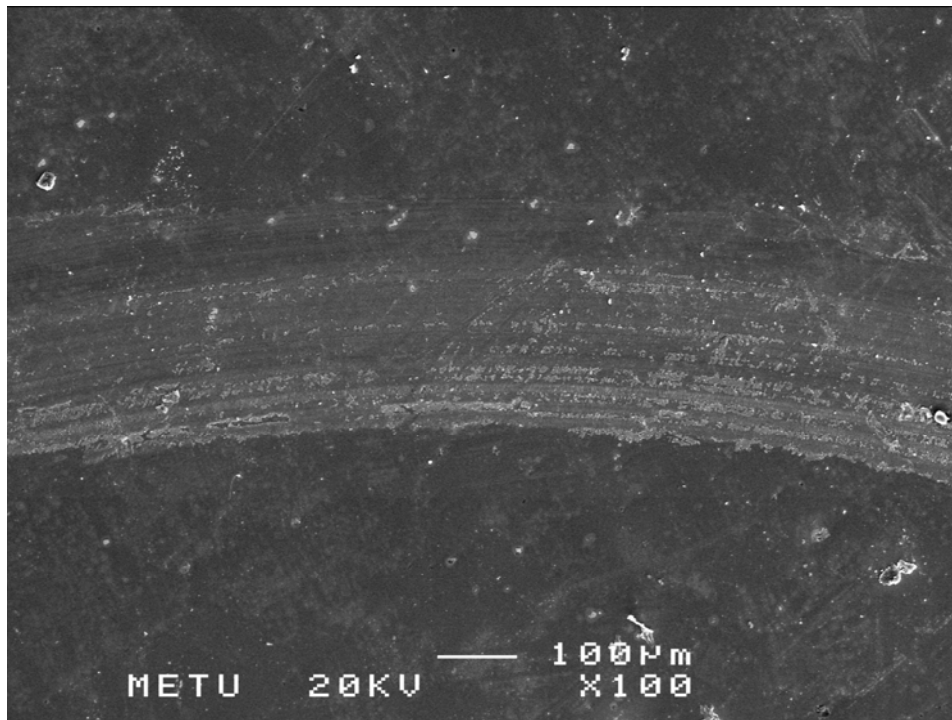
4.4.3 Surface Characterization

SEM micrographs taken from the wear track of the materials investigated are shown in Figure 4.34. The regions within the wear track appear quite coarse and rough as compared to the areas which were not exposed to wear. Microcracks and deep ploughing grooves are observed on the wear tracks of some of the samples. Materials having lower hardness exhibited relatively wider and deeper wear tracks. This situation is seen separately in the surface profile of wear tracks obtained after wear tests in Figure 4.35.

The SEM micrographs presented in Figure 4.34 illustrate the differences between the failure modes at the wear surfaces. Wear tracks of all specimens were seen clearly. Figure 4.34 (a) shows the wear track of E2. It is relatively harder than other samples, so the wear track is narrow and shallow as well. A-W GC1 (Figure 4.34 (b)) shows similar wear track aspect with E2. According to the length of wear track, the CPC and dentin porcelain materials shows more wear resistance than enamel porcelain materials. It is probable that, in the absence of a lubricant, ceramic particles removed from the surface become part of the abrasive system and contribute to an increase in roughness rather than smoothing of the surface.

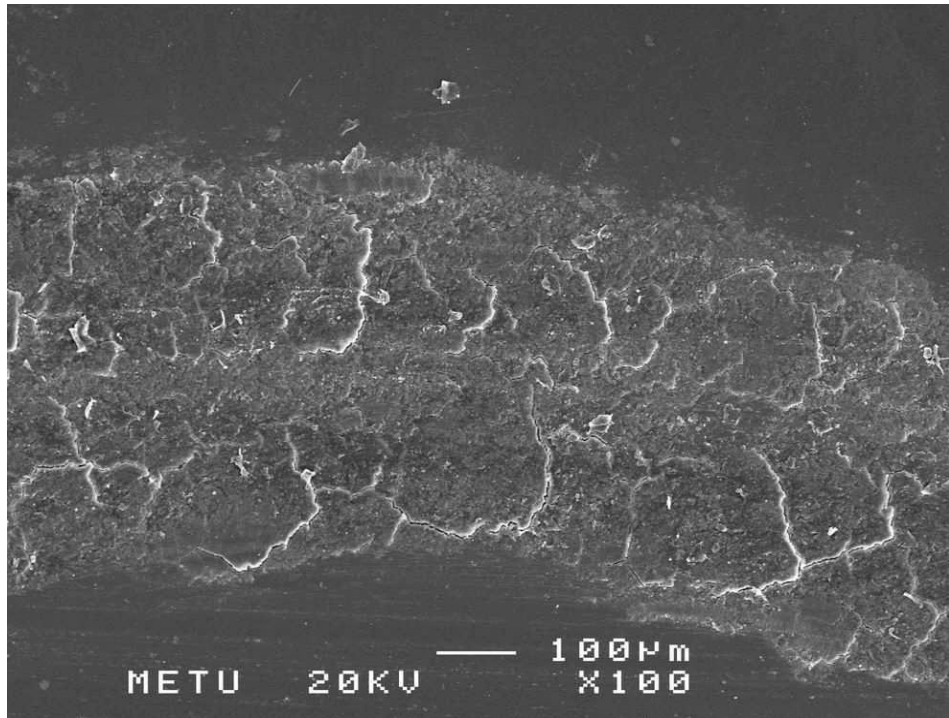


(a) E2

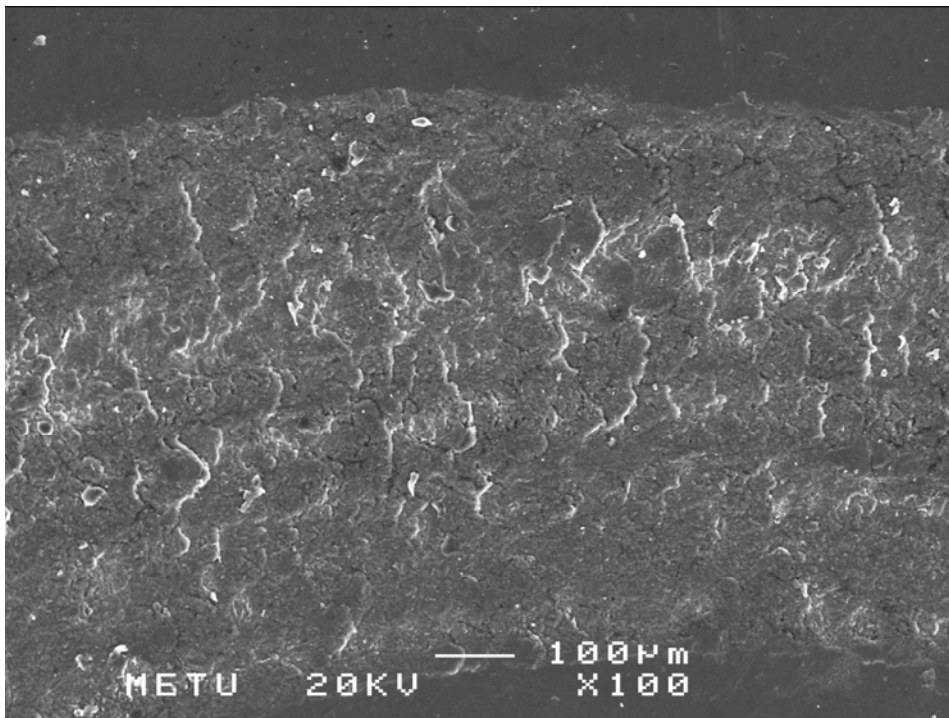


(b) A-W GCl

cont.

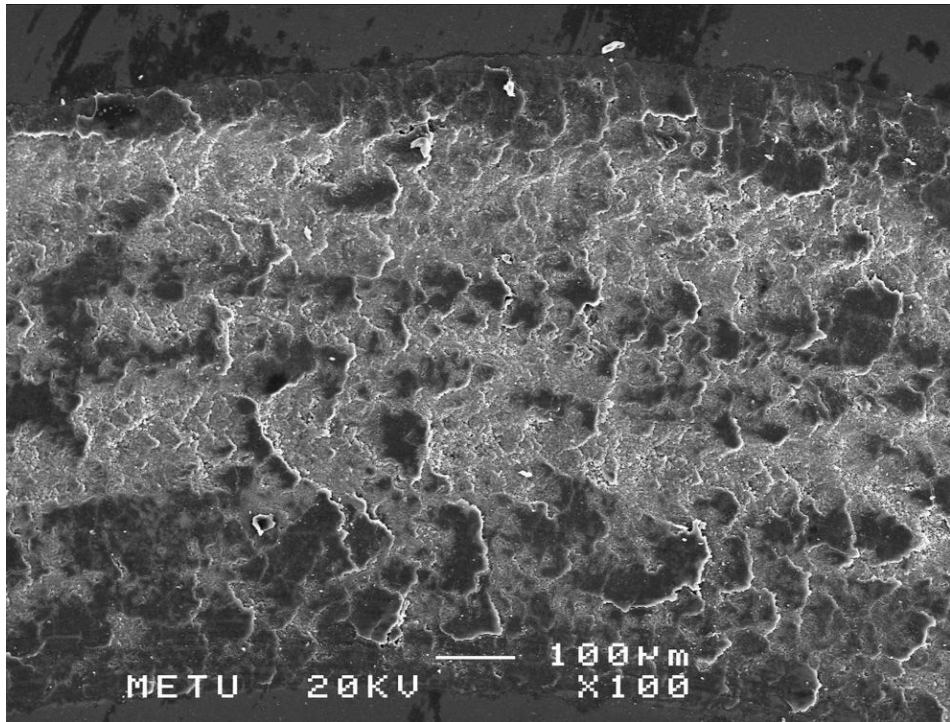


(c) SPE1

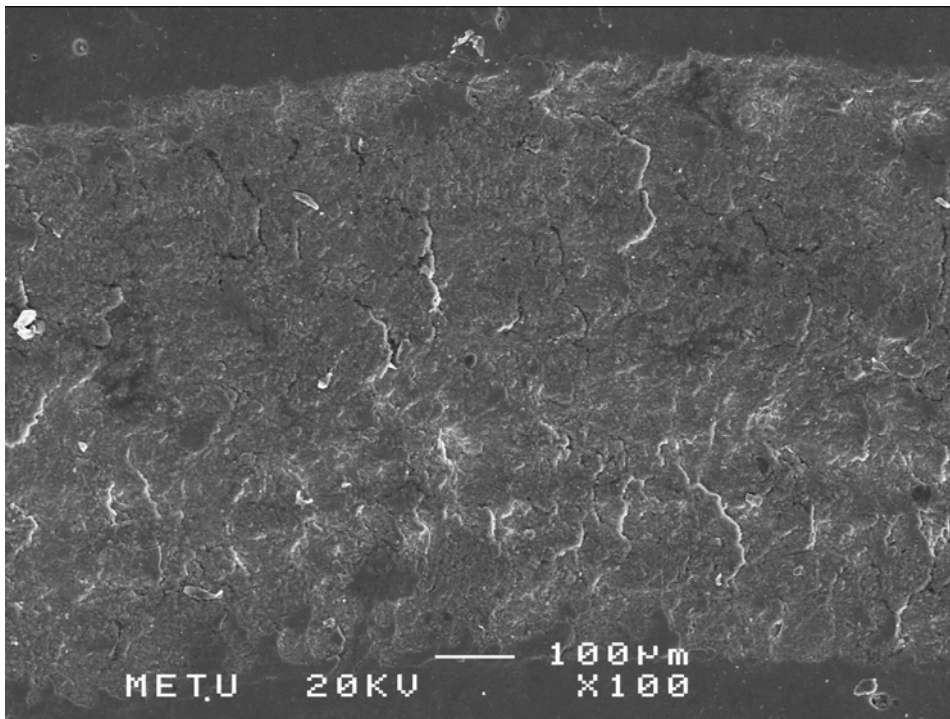


(d) CCS1

cont.

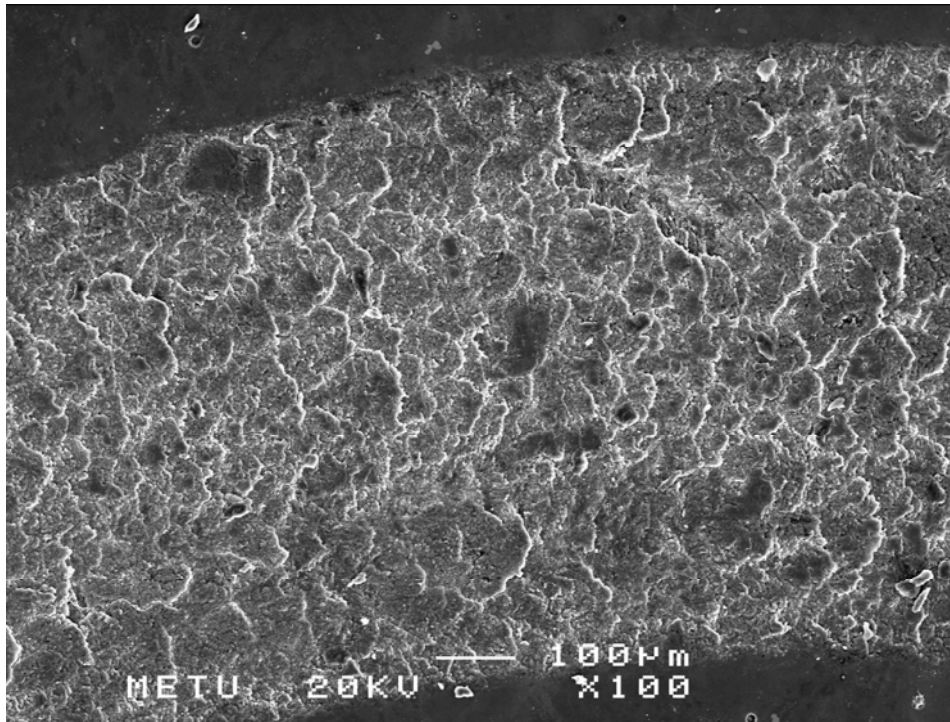


(e) CPC

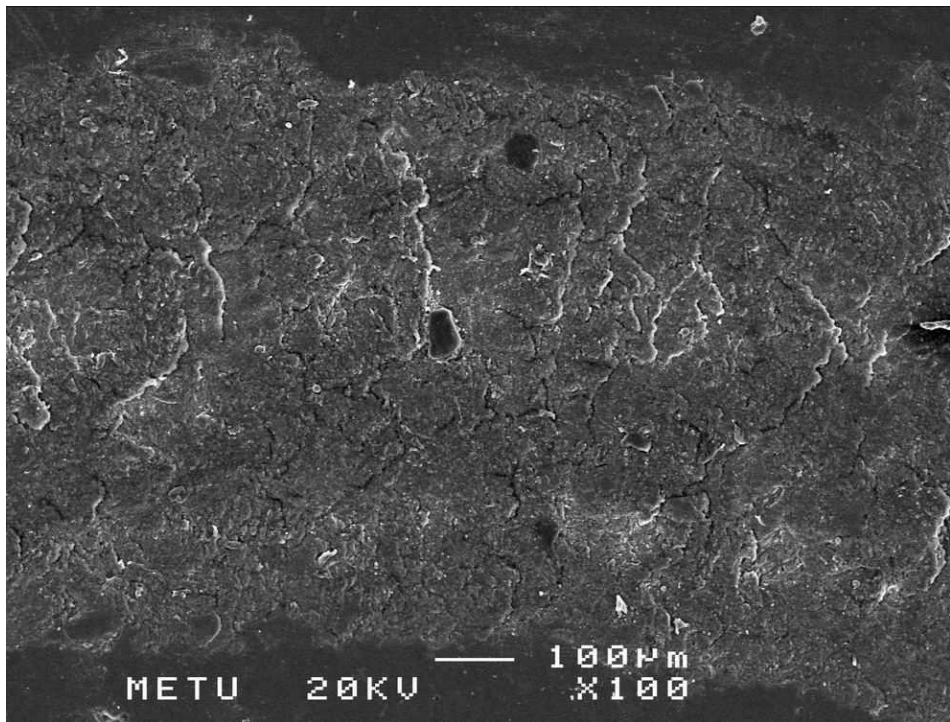


(f) A-W GC2

cont.

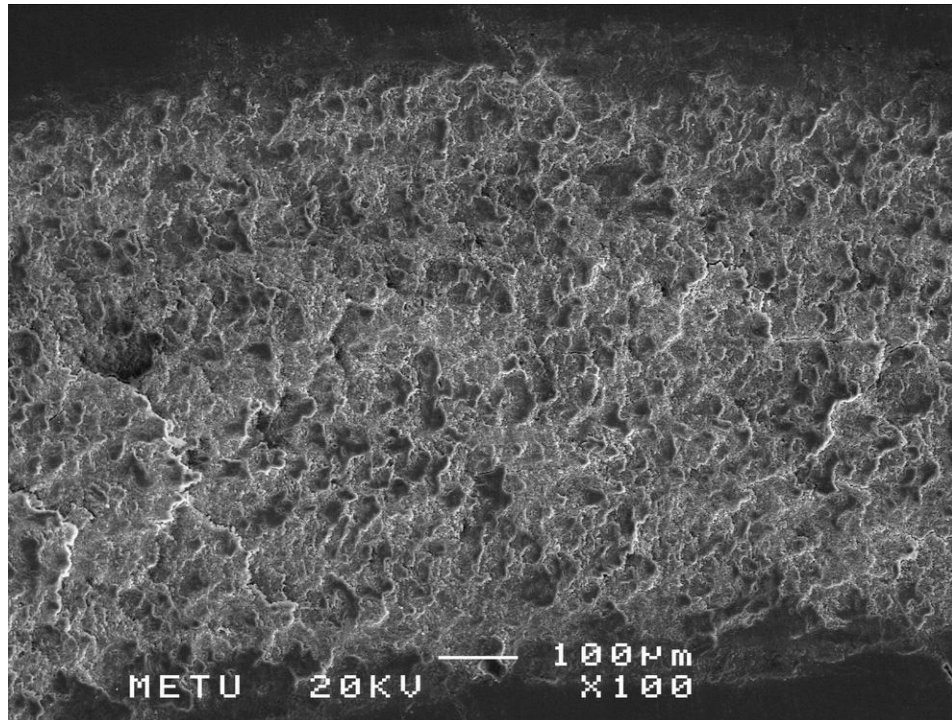


(g) CCS2



(h) SPE2

cont.



(i) BE

Figure 4.34 SEM micrographs of representative wear tracks of the materials investigated.

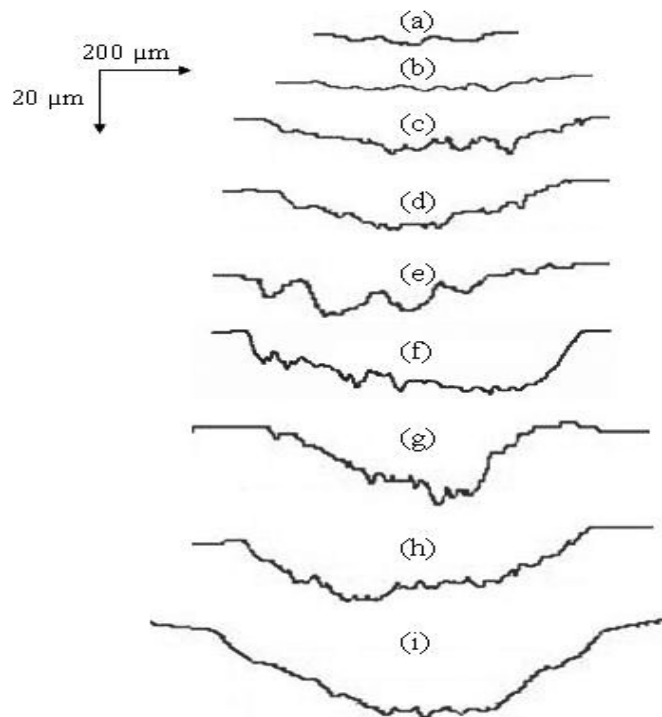


Figure 4.35 Wear track profiles obtained after tribological tests. (a) E2, (b) A-W GC1, (c) SPE1, (d) CCS1, (e) CPC, (f) A-W GC2 (g) CCS2, (h) SPE2, (i) BE.

Wear occurs through several mechanisms, including abrasion, corrosion, adhesion, and fatigue, and when these mechanisms combine, severe wear may result [66-68]. The surface profiles of the worn tracks of the specimens suggested that different wear mechanisms have occurred during the wear test. One of the wear mechanisms involved in E2 and A-W GC1 was abrasion, caused by the propagation of the fissures on the surface and the loss of material. The deep ploughing grooves, ridges and chips observed on the wear tracks demonstrate the features of abrasive and adhesive wear [62]. The profiles of the other dental ceramics suggest that fatigue wear, caused by fissure nucleation on the subsurface and its propagation as a result of the repeated cycles, was also involved. When compared, the profiles of enamel porcelain materials demonstrate wider grooves, indicating that lower hardness results in less surface protection during wear testing.

It is shown that the wear rates of A-W GC1 and A-W GC2 are quite different. The difference is attributed to the variation of wollastonite content and the orientations of crystals in these materials. In terms of wear properties, A-W GC2 might be a choice for dentin material while A-W GC1 for core material. Both materials should not have a direct contact with natural dentition since it could increase the wear rate of an opposing enamel surface.

The results of this study suggest that there is a good correlation between the hardness and wear rate data. That is, the materials become more wear resistant as they are harder. Although similar results have been reported by Borgioli *et al.* [134], several studies have found no correlation between hardness and wear due to the complexity of the wear process [62,66,67]. It is claimed that the relationship of wear to hardness is not valid for materials that are brittle in nature [70,115]. When ceramic slides against ceramic or enamel, wear does not occur by plastic deformation, as with metals, but by fracture [65]. Wang *et al.* [70] concluded that the results of any particular test would be a function of the hardness and stability of the abrasive counterface used and that the mechanisms of failure may vary with test conditions. Results of wear rate for the commercial dental materials studied

are within the ranges of the values published in the literature [62,130,133] although a zirconia ball was used as a counterface material and the test conditions were not identical.

4.4.4 Friction Coefficient

The mean friction coefficient (μ) of the materials studied varied from 0.56 μ (for E2) to 0.95 μ (for A-W GC2). The μ of A-W GC1 was close to that of CCS1, being the second lowest among the materials studied. Representative curves showing the variation of μ of the materials studied with sliding distance are illustrated in Figure 4.36. The μ of the materials was minimal at the beginning of the testing but, increased rapidly and reached a steady state with increasing sliding distance. It is evident that A-W GC1 displays a lower μ than the other materials studied, except E2. However, A-W GC2 has the highest μ of all the materials studied. In general, materials comprising higher hardness exhibited relatively lower μ and lower wear rate than those having lower hardness. Materials having lower hardness exhibited relatively wider and deeper wear tracks. This was apparent from the surface profile of wear tracks obtained after wear tests. (See Figure 4.35)

Results of μ for the commercial dental materials investigated are within ranges of the values published in the literature [62,130] although zirconia ball was used as a countersample material and the test condition was not identical. No information is available in the literature on μ of A-W glass ceramics. Reeh *et al.* [135] reported μ between enamel-to-enamel surfaces was about 0.9 μ under water lubrication. Tillitson *et al.* [136] found μ from 0.5 to 0.6 when testing hemispherical BE countersamples against flat BE surfaces and obtained μ of 0.5 to 0.9 when testing similar BE countersamples against flat porcelain discs under wet conditions.

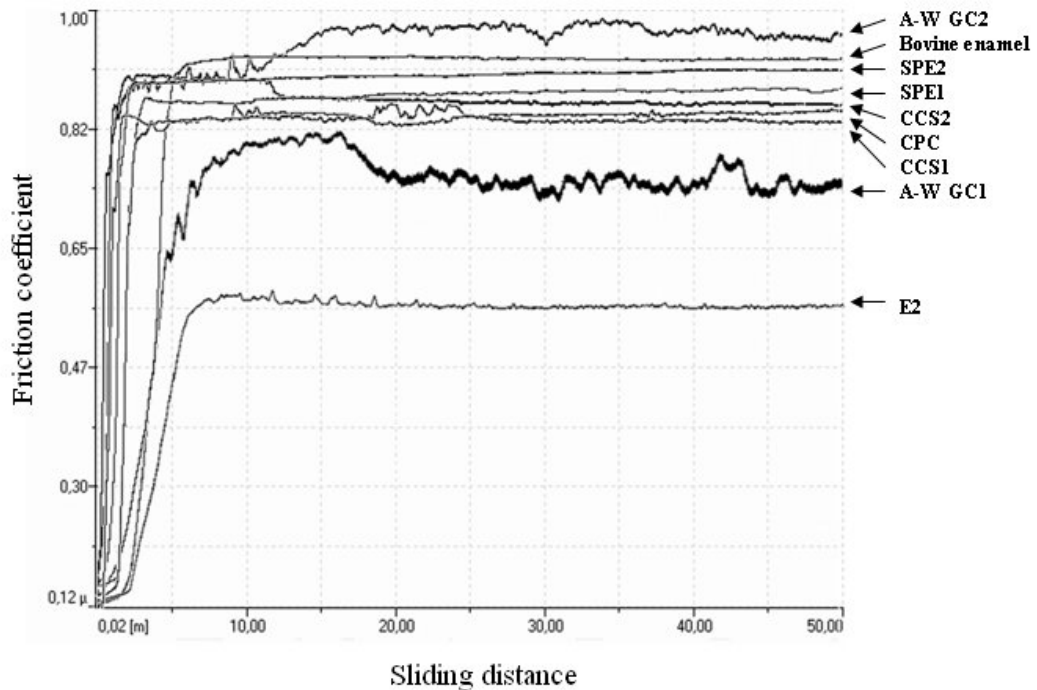


Figure 4.36 Variation in the friction coefficient with sliding distance for the materials studied.

Representative curves showing the variation of the friction coefficient with sliding distance presented in Figure 4.36 reveal that μ of the materials studied is minimal at the beginning of the testing due to the point-contact between the sphere and plane [137]. After the planar surface began to break down, μ increased rapidly with higher contact area and the formation of particles which cause a 3-body abrasion wear process. After a distance that ranges from 1-5 m, μ reached a steady state level according to the materials. Friction coefficient is a very important parameter that reflects the intrinsic interaction characteristics of a tribology system [70,137,138]. A-W GC1 and A-W GC2 would be appropriate materials for use in restorative dentistry due to their values of μ which are similar to those of the commercially available dental materials.

The present study describes a rapid measurement of tribological properties including specific wear rate and μ under well-controlled environmental conditions for commercial and potential dental ceramic materials in order to identify the

effect of specific material properties on the possible modes of material failure caused by the wear of the selected material surfaces. However, the physical factors and relationships that govern the wear of ceramics and tooth structures are complex, and no simple explanation can adequately describe this phenomenon. It is almost impossible to assess quantitatively or even qualitatively the relative impacts of all the components in any in vitro tribological system in determining its in vivo wear simulating characteristics. Furthermore, due to the differences in motion between the pin-on-disk tribometer and the occlusal motion in the oral cavity (continuous sliding vs. reciprocating), it is not clear whether the mechanisms causing the observed wear behavior would occur in vivo. Therefore, the results of the present study will not necessarily correlate with a specific clinical study.

4.5 TRIBOLOGICAL BEHAVIOR OF ALUMINA-ADDED A-W GLASS-CERAMICS

4.5.1 General

In this section, the data gathered from the experimental study conducted on tribological behavior of alumina-added A-W glass-ceramics is presented. The results are discussed and compared with the results of the previous studies published in the literature.

It has been presented in section 4.4 that the A-W glass-ceramics produced in this study possess similar tribological properties to commercial dental materials currently used in crown and bridge work. They have potential use as a material in dental applications if their shortcoming due to their bioactivity could be overcome. Previous studies [36,37,48] have shown that non-bioactive high strength apatite-wollastonite glass ceramic can be produced, without changing the crystalline phases, by adding small amount of Al_2O_3 to the composition of the base glass. However, tribological behavior of alumina-added A-W glass-ceramics has not been reported anywhere else. Determination of the tribological behavior of alumina-added non-bioactive A-W glass-ceramic in dry and in simulated body fluid (SBF) conditions is of importance since the understanding of tribological performance of this material in various experimental conditions could extend its utilization in special dental applications such as veneers, inlays, onlays, crowns etc. Hence, studies carried out on the tribological behavior of alumina-added non-bioactive A-W glass-ceramics have both scientific and technological significance.

The purposes of the present study were to produce non-bioactive A-W glass-ceramic by sintering glass powder compacts in the $\text{MgO-CaO-SiO}_2\text{-P}_2\text{O}_5\text{-Al}_2\text{O}_3$ system at different sintering temperatures, and to determine its tribological properties in dry and artificial saliva conditions. Hardness of the materials was also measured since it is considered one of the important properties in selecting the materials for restorative dentistry. Results of the alumina-added A-W glass-

ceramics were compared with the results of selected commercial dental materials to evaluate the tribological similarities among these materials and to elucidate the appropriateness of the alumina added A–W glass-ceramics for dental applications.

The glass pieces obtained in the MgO-CaO-SiO₂-P₂O₅-Al₂O₃ system according to the procedure as described in section 3.5.1 were colorless and indicated no unmolten batch materials or crystallinity. The pieces were crushed, ground, compacted, and sintered at various temperatures to obtain A–W glass-ceramic by powder packing.

4.5.2 X-ray Diffraction Analysis

The XRD patterns obtained after sintering the glass at different sintering temperatures are shown in Figure 4.37. The patterns illustrate that the glass ceramics are composed of a mixture of glass and crystalline phases. The proportion of the glassy phase decreases and that of crystalline phases increases with increasing sintering temperatures. The sample sintered at 780 °C, designated as A780, consisted of only apatite [Ca₁₀(PO₄)₆(O,F)₂]: JCPDS # 89-6495] crystals. The samples sintered at 900 °C and 1000 °C, designated as AW900 and AW1000, respectively, were composed of apatite and β-wollastonite (CaO·SiO₂) crystals (JCPDS # 10-489). In the XRD pattern of the sample sintered at 1100 °C, designated as AW1100, the crystals of whitlockite (3CaO·P₂O₅: JCPDS # 9-169) in addition to apatite and wollastonite were detected. AW1100 showed the biggest (320) plane of the wollastonite crystal implying that more and more wollastonite precipitated as the sintering temperature increased. However, the (211) plane of apatite crystal showed maximum height in AW1000 and then decreased in AW1100 since some of apatite crystals were converted to whitlockite crystals during sintering at 1100 °C. The findings are in good agreement with those reported in the literature [34,35,44].

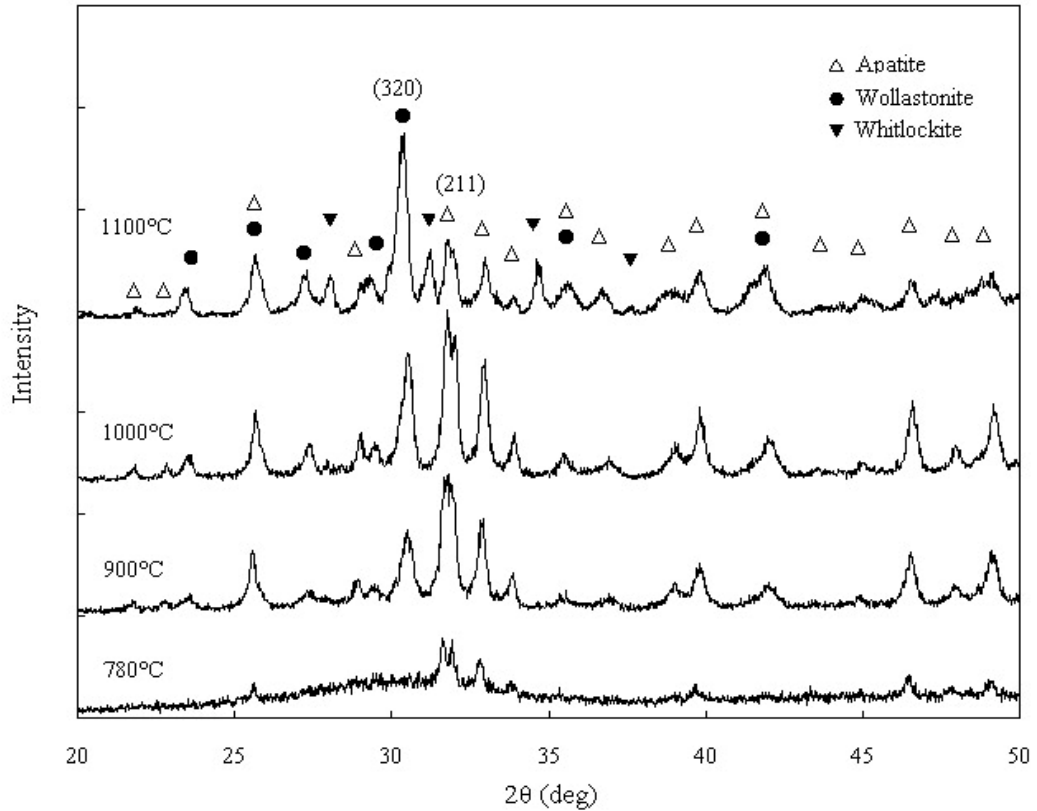


Figure 4.37 XRD patterns of the alumina-added A-W glass-ceramics sintered at various temperatures.

4.5.3 Hardness and Wear Rate

Values of Knoop hardness (KH), wear rate, and mean friction coefficient for the materials investigated are presented in Table 4.9. KH values of the materials investigated varied from 304.1(±7.9) H_V for A780 to 505(±6.1) H_V for AW1100. The values in the parentheses next to the average hardness indicate the ± standard deviation of the data from the averages. Hardness of the glass ceramics increased with increasing sintering temperature. This is attributed to the precipitation of more and more wollastonite and whitlockite crystals with increasing sintering temperature. Wollastonite crystal has a surface crystallization mechanism and it grows in column shape from surface to interior [74]. The existence of wollastonite crystals results in an increase in the mechanical properties due to the whisker-like shape of grains which act as a filler reinforcing matrix. Kokubo *et al.* [33] reported that the presence of wollastonite crystals can effectively increase the

fracture surface energy of the crystallized product, even when they are present as fine dendrites rather than long fibers. Hardness value, which has been used as an indication for the relative ability of a material to resist scratching and abrasion and the relative ease of finishing and polishing, has also been considered one of the important properties in selecting the materials for restorative dentistry since it delineates the abrasiveness of a material to which the natural dentition may be submitted [130]. As seen in Table 4.9, KH for the glass-ceramics containing apatite and wollastonite crystals was comparable to the values for the commercially produced dental materials, Duceragold and IPS Empress.

Table 4.9 Knoop hardness, wear rate and friction coefficient in dry and in SBF.

Material	Knoop hardness (H _v)	Wear rate (×10 ⁻⁴ m ³ /N.m)		Mean friction coefficient (μ)	
		in dry	in SBF	in dry	in SBF
A780	304.1 (±7.9)	41.37	2.74	0.93	0.85
AW900	419.6 (±14.6)	11.16	2.17	0.89	0.82
AW1000	478.1 (±7.9)	9.66	1.55	0.87	0.76
AW1100	505.0 (±6.1)	1.68	0.96	0.72	0.62
Duceragold	490.9 (±9.7)	2.26	1.33	0.88	0.78
IPS Empress	427.6 (±6.7)	2.89	1.41	0.82	0.75

Wear rate of the materials investigated varied from 0.96×10⁻⁴ mm³/N.m (for AW1100 in SBF) to 41.37×10⁻⁴ mm³/N.m. (for A780 in dry) depending on the tribological test environment. All materials had lower wear rate in SBF than in dry condition. This is due to the lubricating action of SBF which took apart the wear debris in the form of glass-ceramic particles or blocks formed on the wear surface during testing. However, in dry condition, ceramic particles removed from the surface became part of the abrasive system, established a 3-body abrasion wear process and contributed to an increase in roughness rather than smoothing of the surface [67].

As seen in Table 4.9, wear rate of the alumina-added A-W glass-ceramics decreased with increasing sintering temperature both in dry and in SBF conditions. Wear rate for the sample sintered at 780 °C was $41.37 \times 10^{-4} \text{ mm}^3/\text{N}\cdot\text{m}$ and $2.74 \times 10^{-4} \text{ mm}^3/\text{N}\cdot\text{m}$ in dry and in SBF conditions, respectively and decreased to $1.68 \times 10^{-4} \text{ mm}^3/\text{N}\cdot\text{m}$ and $0.96 \times 10^{-4} \text{ mm}^3/\text{N}\cdot\text{m}$ in dry and in SBF conditions, respectively when the sintering temperature is increased to 1100 °C. The decrease in wear rate with increasing sintering temperature is attributed to the fact that the glass-ceramic becomes denser and harder as sintering temperature is increased due to the change in the kind and amount of crystals precipitated during sintering. As presented earlier in section 4.4, the glass-ceramic becomes more wear-resistant as it gets harder. The results of the wear tests in accord with the results of the hardness tests, implying an inverse relation between the hardness and wear rate of the alumina-added A-W glass ceramics.

There is yet no publication in the open literature reporting the results of wear rate data for the alumina-added A-W glass ceramics. Therefore the values of wear rate obtained in this study could not be compared directly. However, when a comparison is made between the wear rate of the alumina-added A-W glass ceramic studied and that of the commercial dental materials, it is seen that, wear rate for AW1100 was lower than the values for Duceragold and IPS Empress either in dry condition or in SBF. Though wear rate for the glass ceramics sintered at lower temperatures was considerably higher than the values for Duceragold and IPS Empress in dry condition, but the difference was less in SBF. Seghi *et al.* [139] stated that ideally, an aesthetic restoration should wear at approximately the same rate as the enamel it replaces, and should not increase the wear rate of an opposing enamel surface. Therefore, AW1000 would be an alternative choice for materials used in restorative dentistry in the regions where direct contact with natural dentition occurs since it meets the requirements of the aesthetic restoration. However, AW1100 may be used as core material since it is harder and could increase the wear rate of an opposing enamel surface.

4.5.4 Friction Coefficient

Mean friction coefficient (μ) of the materials investigated ranged from 0.62 μ (for AW1100 in SBF) to 0.93 μ (for A780 in dry) depending on the tribological test conditions. The materials had relatively lower μ in SBF than in dry condition given that SBF played a role of lubricant between the ball and surface of the material during the test.

In general, materials comprising higher hardness exhibited relatively lower μ than those having lower hardness, implying an inverse relation between μ and hardness of the alumina-added A-W glass ceramics.

Variation in μ with sliding distance in dry condition and in SBF for the alumina-added A-W glass ceramics is shown in Figures 4.38 and 4.39, respectively. Variation in μ with sliding distance in dry condition and in SBF for the commercial dental materials is shown in Figure 4.40. Representative curves illustrate that μ of the materials studied is minimal at the beginning of the testing due to the point-contact between the ball and sample. After the planer surface begin to break down, μ increases rapidly with higher contact area and the formations of wear particles which cause a 3-body abrasion wear process [67]. After a sliding distance ranging from 1 to approximately 30 m, μ reached a steady state level for the alumina added A-W glass ceramics as seen in Figure 4.38 and 4.39. The sliding distance at the beginning of the steady state level increased with increasing sintering temperature of the alumina-added A-W glass ceramics. The commercial dental materials investigated showed similar behavior. The sliding distances at the beginning of the steady state level for the commercial dental materials were about 2 m in dry condition and 5 m in SBF as seen in Figure 4.40.

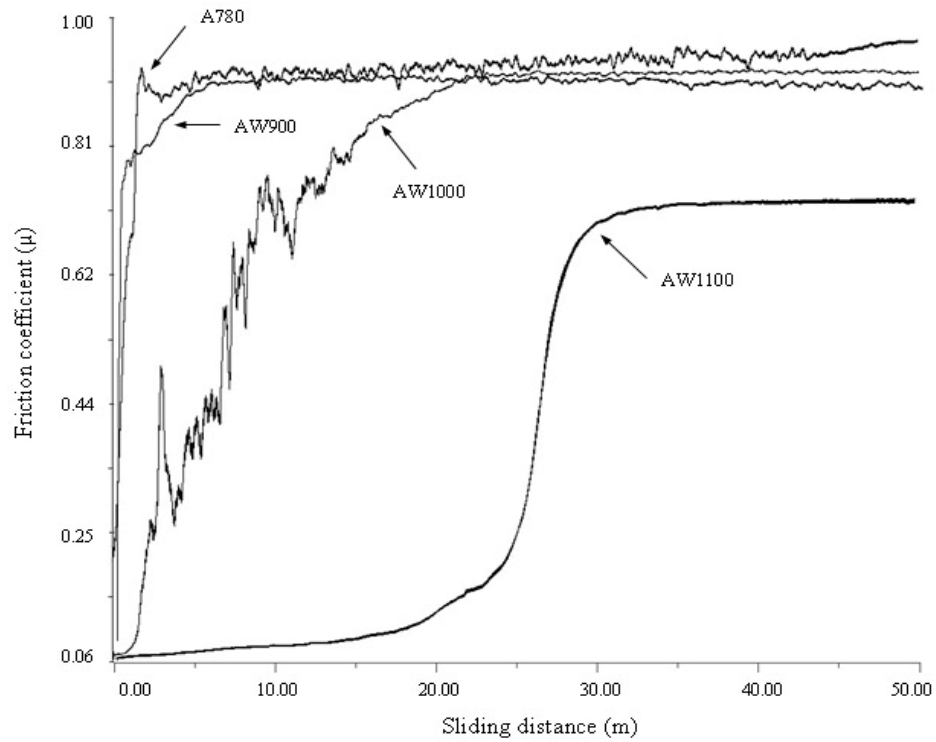


Figure 4.38 Variation in the friction coefficient with sliding distance for the alumina-added A-W glass ceramics in dry condition.

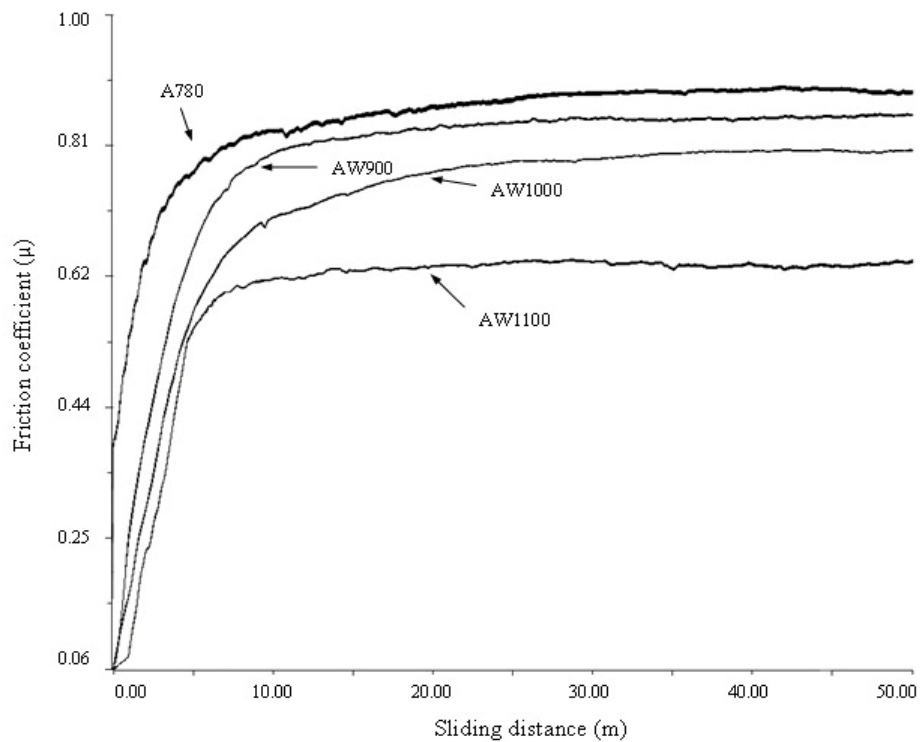


Figure 4.39 Variation in the friction coefficient with sliding distance for the alumina-added A-W glass ceramics in simulated body fluid.

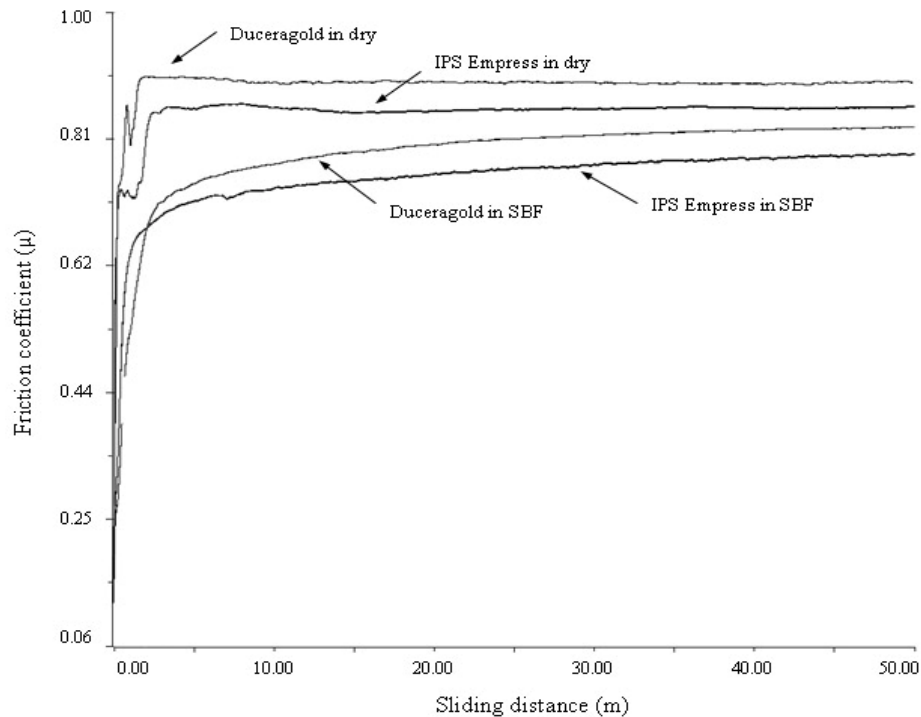
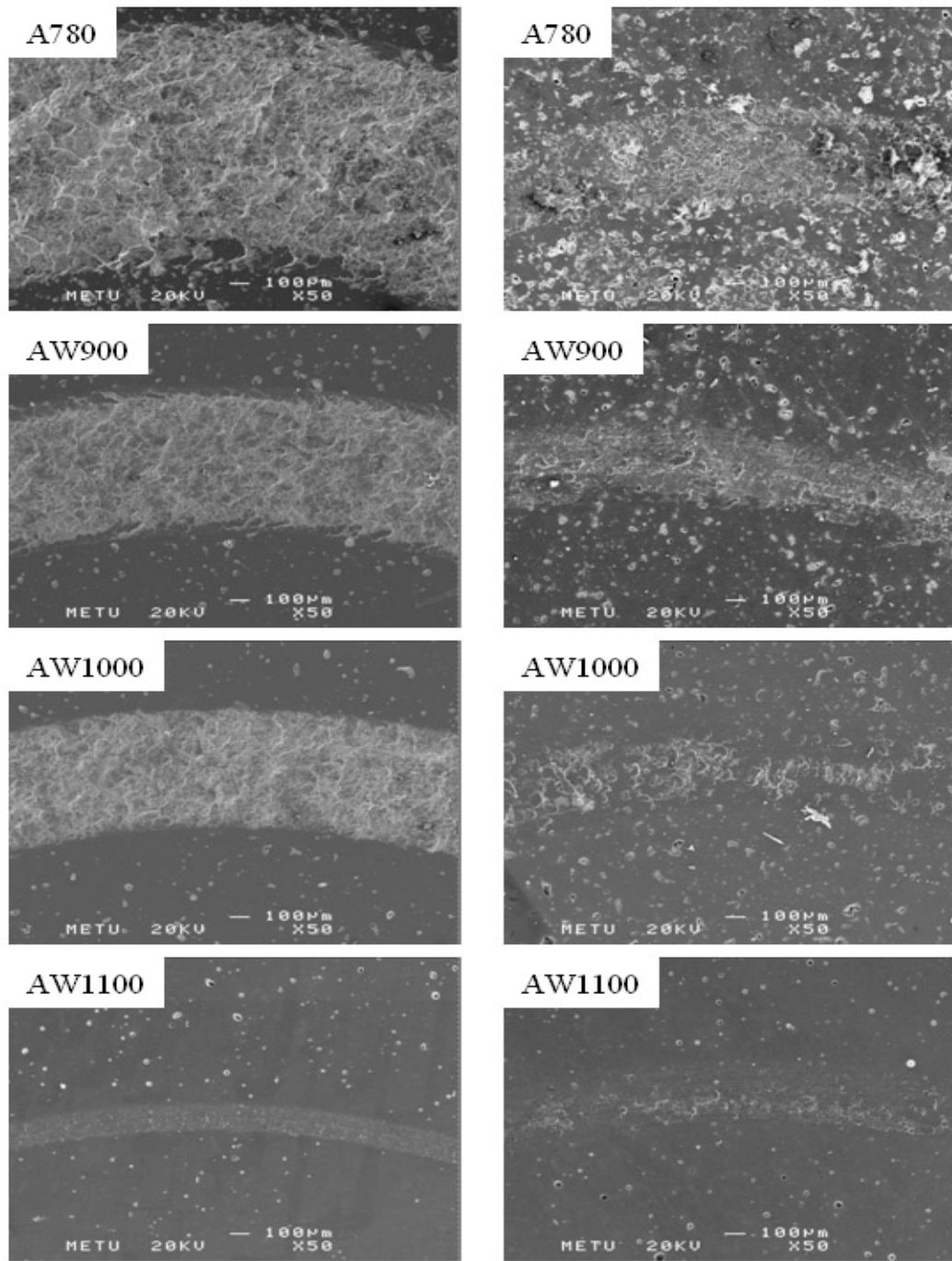


Figure 4.40 Variation in the friction coefficient with sliding distance for the commercial dental materials in dry condition and in simulated body fluid.

In general, material with lower μ is preferred in a dental restoration, because the friction can cause lateral forces on the teeth, which, if excessive, are destructive to the supporting tissues [138,140]. From that point of view, AW1000 and AW1100, whose μ is more or less the same as μ of the commercial dental materials in SBF, would be an appropriate material for dental applications.

4.5.5 Surface Characterization

SEM micrographs of the wear tracks obtained after wear tests on the alumina-added A-W glass ceramics sintered at different temperatures are shown in Figure 4.41. Differences are noticed in the appearance of wear tracks, owing to the microstructural dissimilarities among the materials and bioenvironmental test conditions. Although microcracks, wear debris and deep ploughing grooves are observed on the wear tracks, the width of the wear tracks decreases from A780 to AW1100. The images confirm the tribological findings signifying that the glass ceramic becomes more wear resistant as the sintering temperature is increased.



(a)

(b)

Figure 4.41 SEM micrographs of the wear track for alumina-added A-W glass ceramics. The tracks were obtained after wear tests (a) in dry condition (b) in SBF.

Significant differences are observed on the wear tracks obtained in dry condition and in SBF. Wear tracks are rather clear and visible in dry condition but become imperceptible in SBF. Wear tracks of the commercial dental materials illustrated also similar features. In dry conditions, the wear tracks are coarse and harsh, while in SBF they are light and pale as seen in Figure 4.42. The grooves and signs of materials loss are clearly seen in all of the materials investigated.

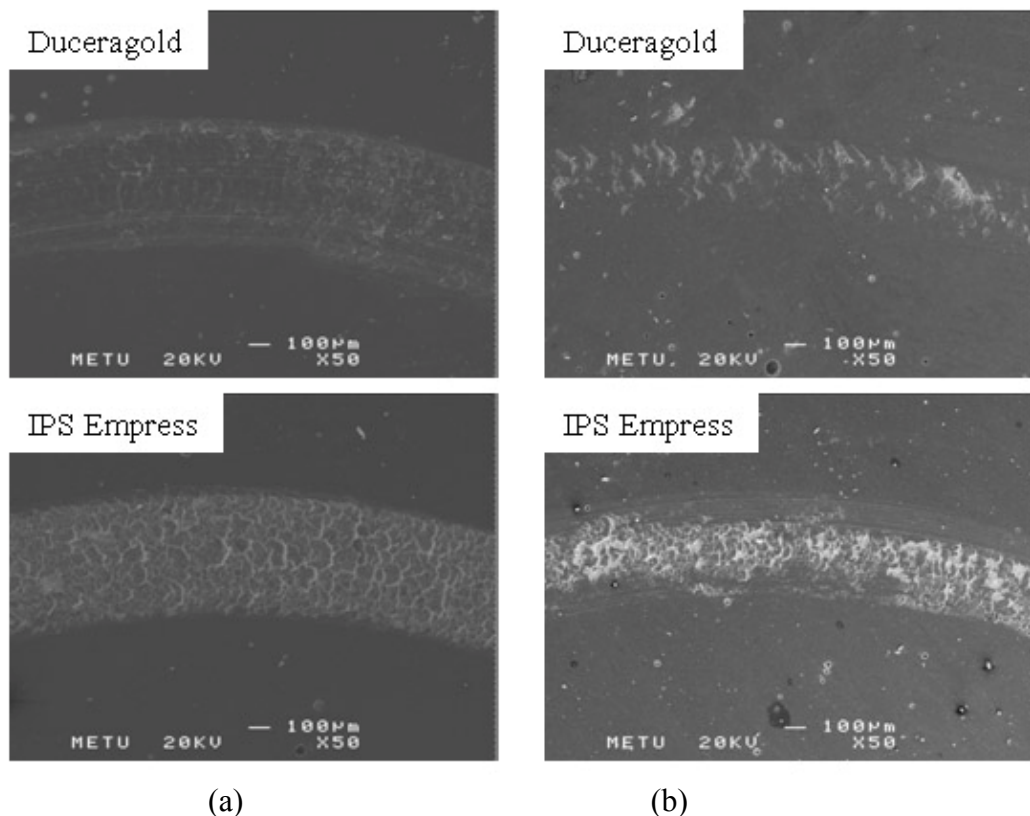


Figure 4.42 SEM micrographs of the wear track for commercial dental materials. The tracks were obtained after wear tests (a) in dry condition (b) in SBF.

SEM micrographs of the wear tracks suggest that different failure modes occur at the wear surfaces during wear test. Wear debris in the form of particles or blocks observed on the wear tracks imply that abrasive and adhesive wear mechanisms have occurred during wear test. The propagation of the fissures on the surface and the loss of material reveal that the dominant wear mechanism is abrasion in A780. However, in the samples sintered at higher temperature the primary wear

mechanisms involved was adhesion. The deep ploughing grooves, ridges and chips observed on the wear tracks are the features of abrasive and adhesive wear [62]. As seen in the micrographs in Figure 4.42, one of the wear mechanisms involved in the commercial dental materials was fatigue, caused by fissure nucleation on the subsurface and its propagation as a result of the repeated cycles.

More ploughed marks and debris were observed on the wear track of the materials having relatively higher values of wear rate, friction coefficient and lower values of hardness. The wear track profiles shown in Figures 4.43 and 4.44 supported these findings. Wear track profiles shown in Figure 4.43 reveal that the depth and width of the wear track as well as the wear area decreased steadily with increasing sintering temperature. Wear profiles obtained in dry condition illustrate relatively deeper and wider plough than those obtained in SBF for all of the materials investigated.

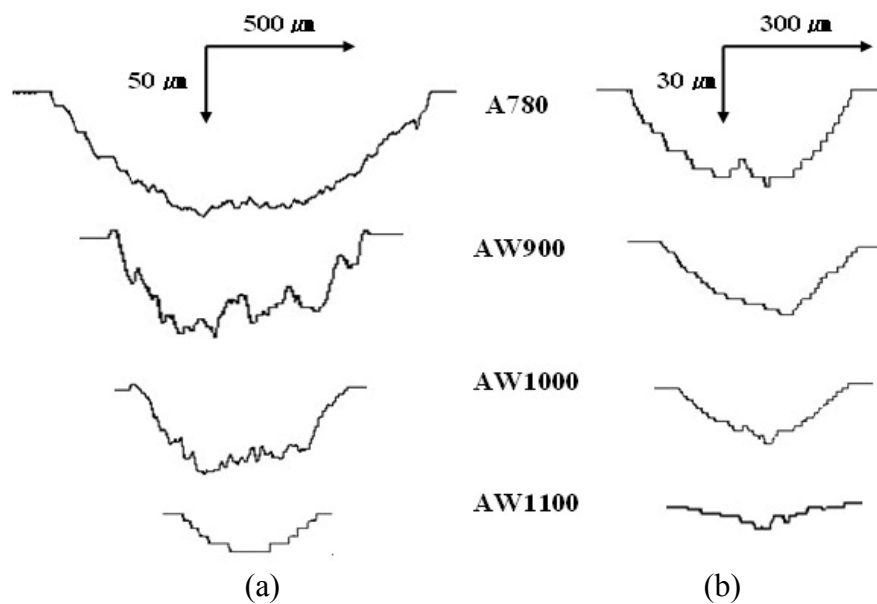


Figure 4.43 Wear track profiles for alumina-added A-W glass ceramics. The profiles were obtained after wear tests (a) in dry condition (b) in SBF.

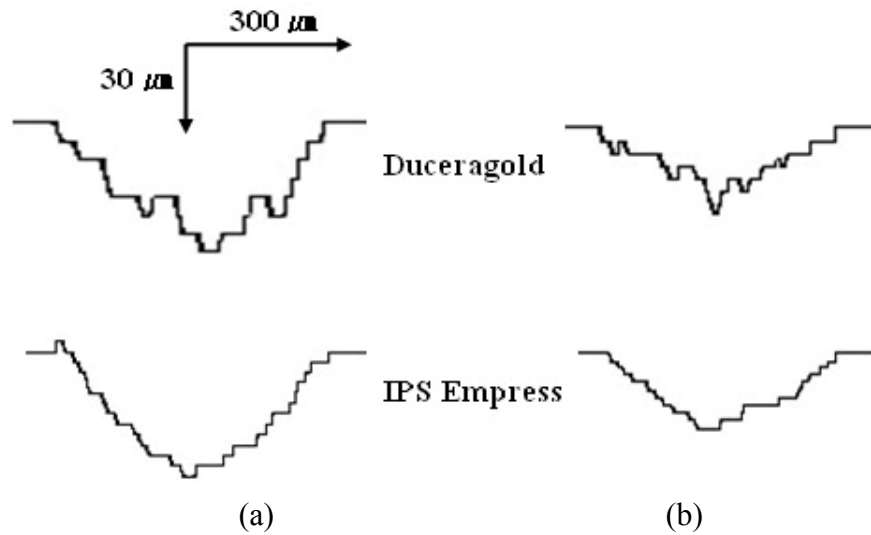


Figure 4.44 Wear track profiles for commercial dental materials. The profiles were obtained after wear tests (a) in dry condition (b) in SBF.

4.6 BIOACTIVITY OF A-W GLASS-CERAMICS PRODUCED BY MELT-CASTING

4.6.1 General

In this section, the data gathered from the experimental study conducted on bioactivity of the A-W glass-ceramics is presented. The results are discussed and compared with the results of the previous studies published in the literature.

Previous studies [34-40] have shown that A-W glass-ceramic produced by powder packing process has uniform microstructure and the ability to bond spontaneously to living bone in a short period in a body environment. It has been presented in Section 4.1 that the A-W glass-ceramic produced by melt casting process has a heterogeneous microstructure consisting of apatite and wollastonite crystals randomly distributed throughout a glass matrix and shows structure oriented changes in the properties. Determination of the biological behavior of the A-W glass-ceramic produced by melt casting process is essential to understand the biological performance of this material in various biomedical applications.

The purpose of the present study was to determine bioactivity of the A-W glass-ceramic produced in the MgO-CaO-SiO₂-P₂O₅-F system by melt casting process. Bioactivity tests were accomplished in a simulated body fluid (SBF). Formation of an apatite phase has been investigated to see whether the production process influences the bioactivity of A-W glass-ceramic. The rate and extent of formation of the apatite has been considered as a measure of bioactivity.

The glass blocks obtained in the MgO-CaO-SiO₂-P₂O₅-F system according to the procedure as described in Section 3.6.1 were colorless and indicated no unmolten batch materials or crystallinity. The blocks were carefully heat treated as described in Section 3.6.2 to obtain A-W glass-ceramics through melt casting process.

4.6.2 X-ray Diffraction Analysis

Figures 4.45 and 4.46 illustrate the XRD patterns obtained from the surfaces of the glass ceramics A and A-W, respectively before and after immersing in the SBF solution for 1, 10, and 20 days. The figures suggest that the crystal structure on the surface of the samples was changed when they are immersed in SBF for certain period of time.

In sample A, apatite crystals are clearly detected in the XRD pattern before it is soaked in SBF. The intensity of apatite peak decreased and patterns became weak as the immerse time is increased. After being soaked for 1 day, not much change was observed. However, significant change was seen after being soaked for 10 days. The proportion of amorphous phase increased and crystallinity decreased. After being soaked 20 days, the apatite peaks became visible in the XRD pattern at 2θ of between $\sim 30^\circ$ and 35° , since the ions in the coated film might be arranged during immerse. The detected XRD patterns of apatite phase is the evidence of the formation of apatite film on the surface of sample A after being immersed in SBF.

In sample A-W, apatite and wollastonite crystals are clearly detected in the XRD pattern before being immersed in SBF. The (002) plane of wollastonite at 2θ of $\sim 25.6^\circ$ is the highest peak among others. This is attributed to the surface crystallization of wollastonite crystals and orientated crystal growth from free surface to interior as discussed in section 4.3. After being soaked in SBF, the intensity of the (002) plane decreased with soaking time. Meanwhile, not many changes have been detected in the pattern of apatite crystals until the sample was soaked for 20 days. A change in the patterns of apatite crystals in 2θ of between 30° and 35° was observed after the sample was soaked for 20 days. The pattern suggests that the proportion of the amorphous phase increased and crystallinity decreased. It is expected that the bioactive layer was coated on the surface of sample A-W. The film covered also the wollastonite crystals which were oriented in one direction, and reduced the intensity of the pattern. However, the coated layer was so thin or small that the effect was relatively smaller than in sample A.

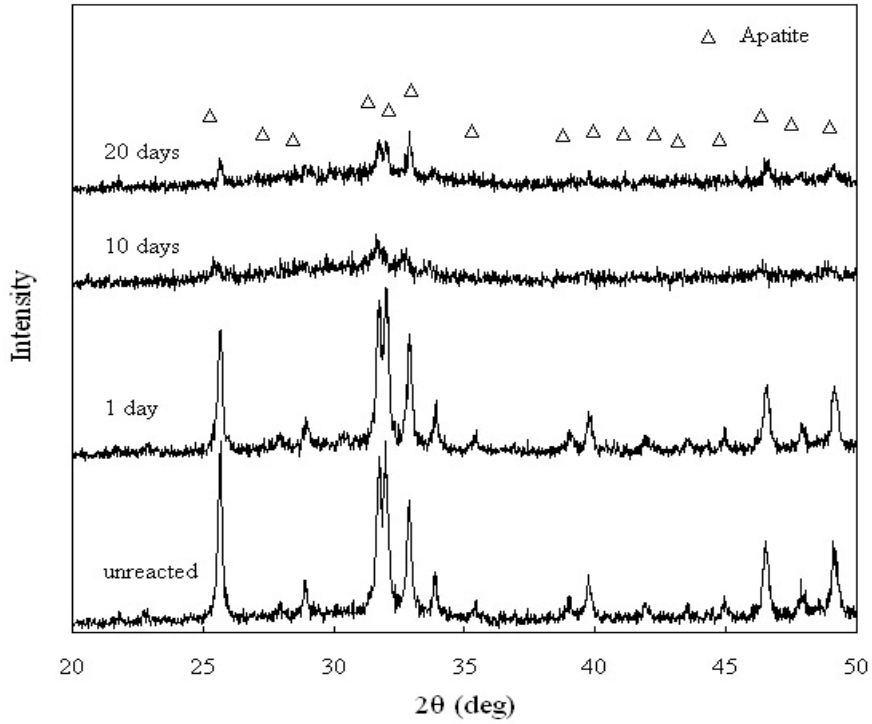


Figure 4.45 XRD patterns obtained from the surface of the glass ceramic A before and after immersing in the SBF solution for 1, 10, and 20 days.

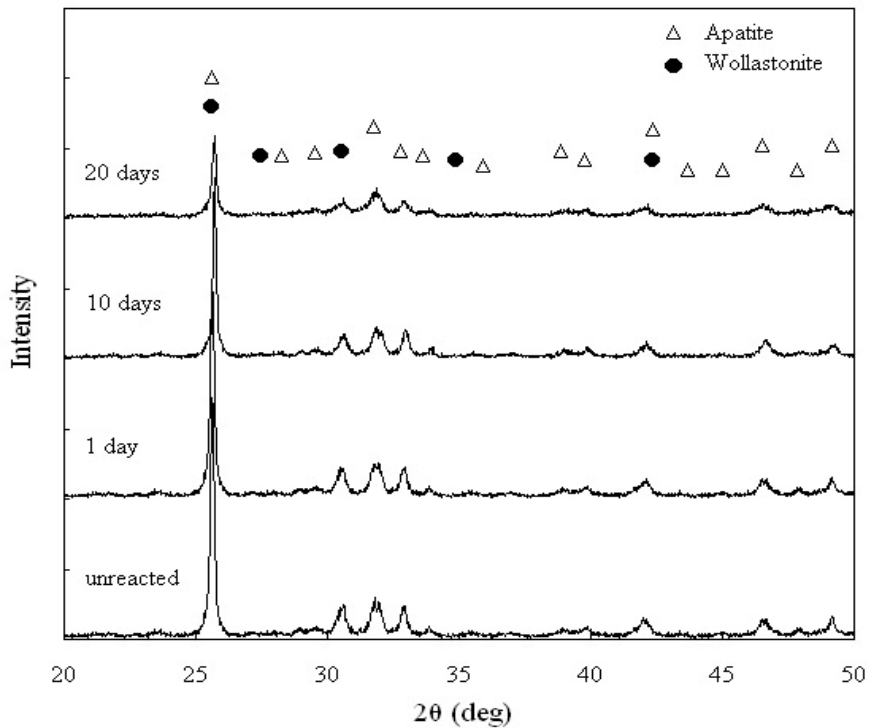
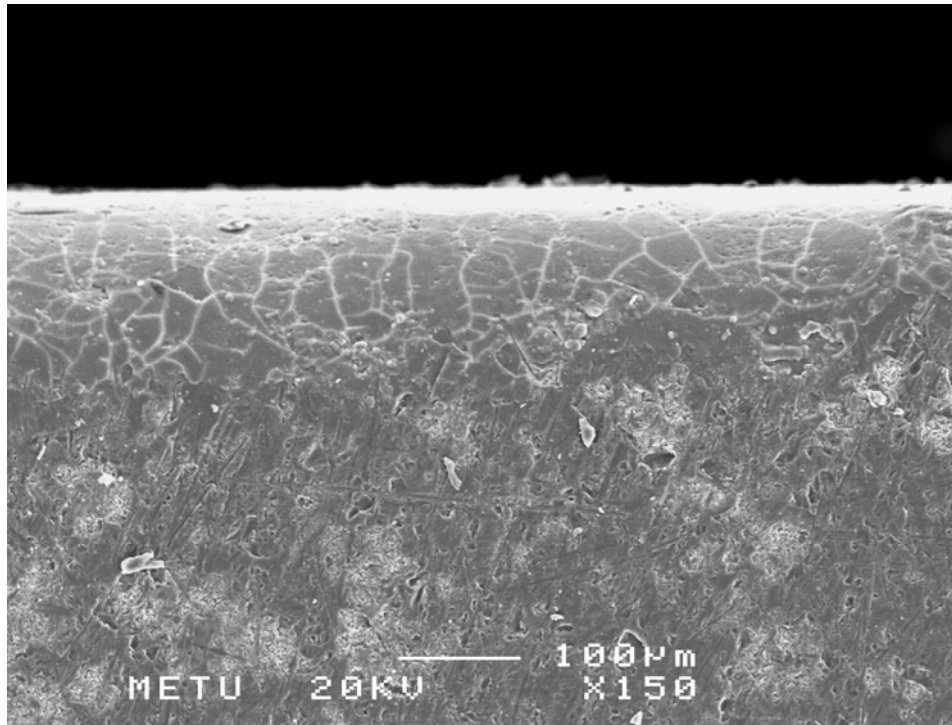


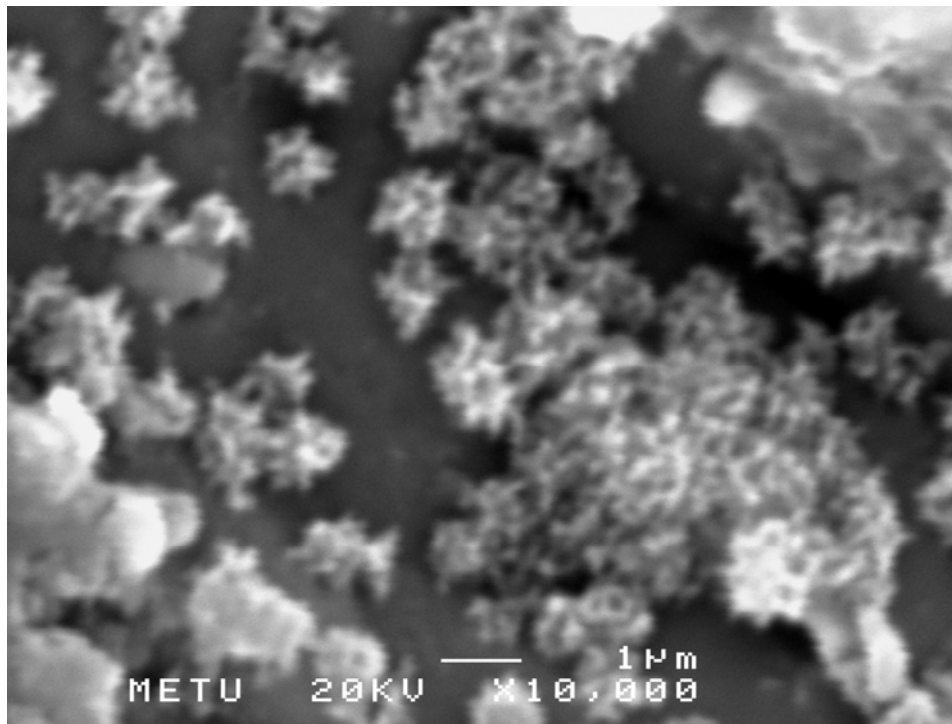
Figure 4.46 XRD patterns obtained from the surface of the glass ceramic A-W before and after immersing in the SBF solution for 1, 10, and 20 days.

4.6.3 Scanning Electron Microscopy

SEM micrographs in Figures 4.47 to 4.49 show the microstructure of the surface of sample A after being immersed for 1, 10 and 20 days, respectively. The deposition layer on the surface can be seen in the sample for all immerse durations. The morphology of the layer is similar to that formed on bioactive glasses and glass-ceramics presented in the literature [33,34,38.]. The cracks observed on the coated layer are assumed to form due to the capillary stress developed during drying. Even after being immersed 1 day in SBF, the layer was deposited on the whole surface of sample as seen in Figure 4.47. Apatite crystal appeared like a small ball with leaf-like surface on it as seen in larger magnification of the layer in Figure 4.47 (b). The thickness of the layer was about 2 μm . With increasing soaking time up to 10 days, the apatite layer became dense and the thickness of the layer increased to 4 μm as recognized in Figure 4.48. The layer looked like a thick and dense layer. The apatite layer covers the overall surface of the sample, but it has not been rearranged well to crystalline. Somehow, it plays as an amorphous layer as shown in the XRD pattern in Figure 4.45. When the immerse duration was increased to 20 days, the thickness of apatite layer increased to 12 μm as seen in Figure 4.49.

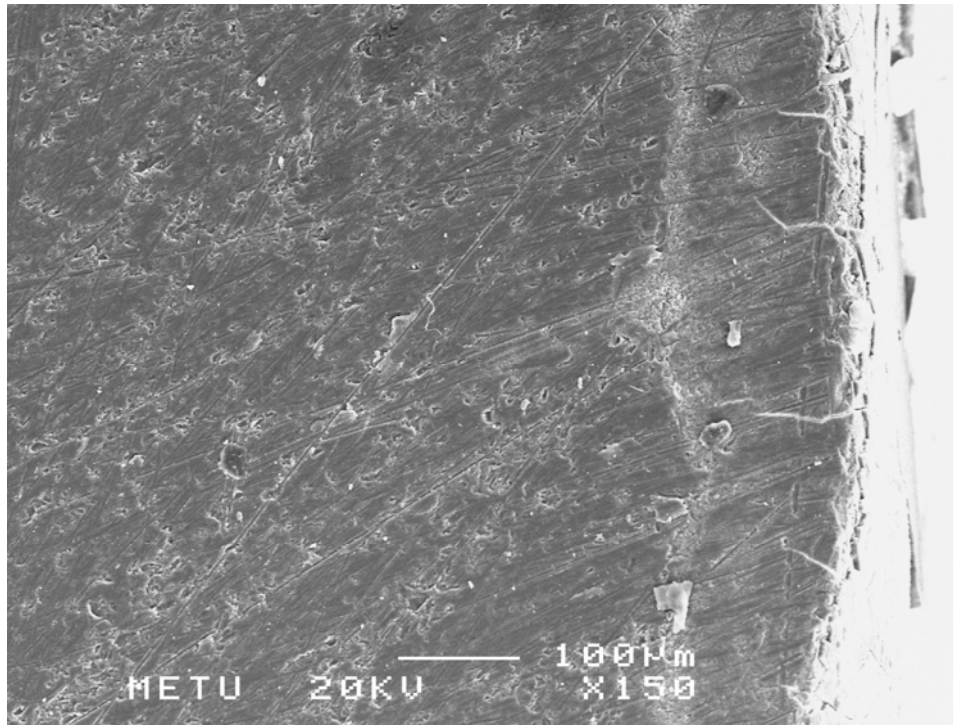


(a)

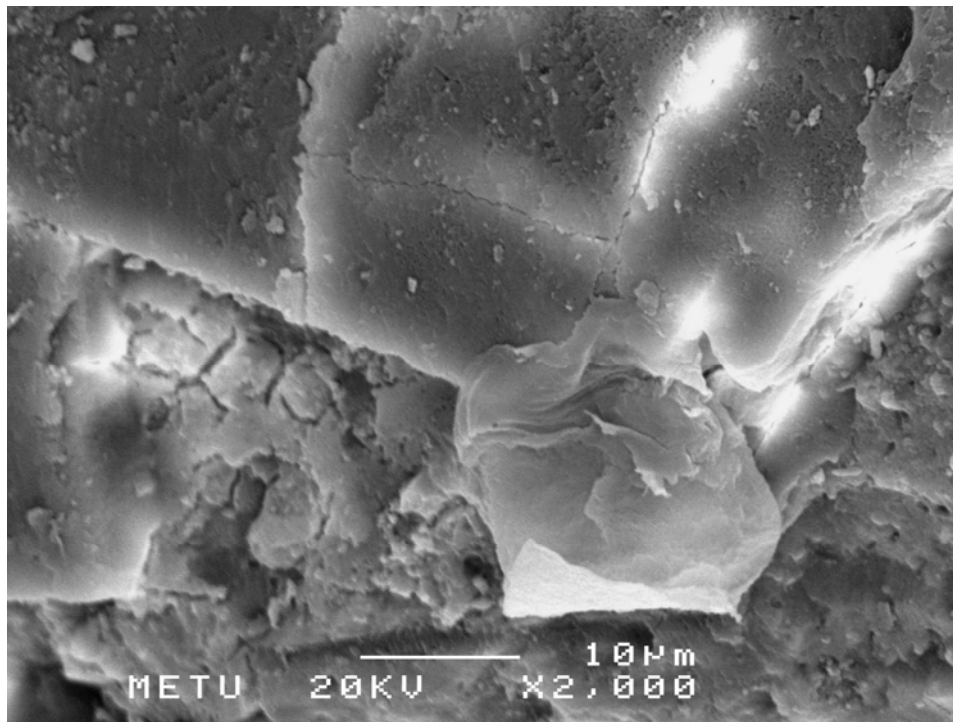


(b)

Figure 4.47 SEM micrographs taken from (a) fracture surface, (b) surface of the coated later of sample A after being immersed in the SBF for 1 day.

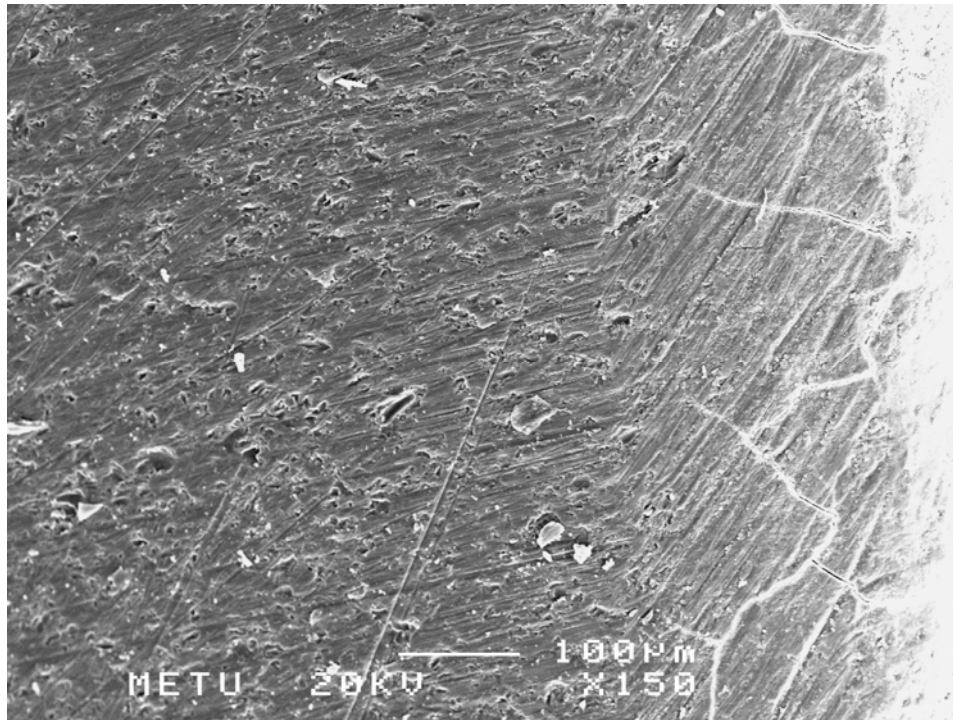


(a)

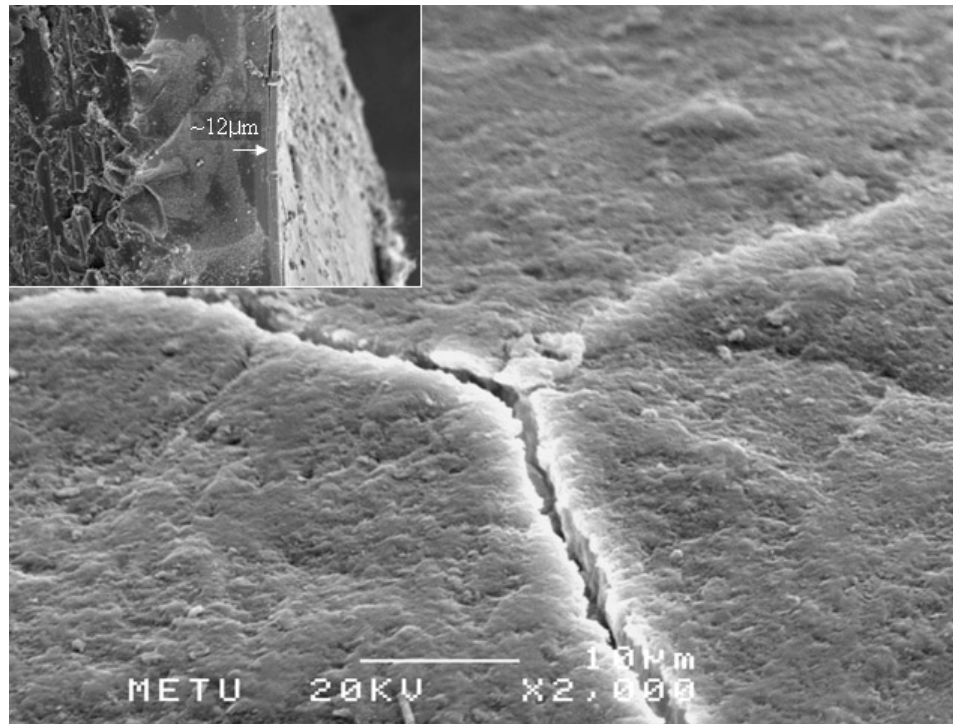


(b)

Figure 4.48 SEM micrographs taken from (a) fracture surface, (b) surface of the coated later of sample A after being immersed in the SBF for 10 days.



(a)



(b)

Figure 4.49 SEM micrographs taken from (a) fracture surface, (b) surface of the coated later of sample A after being immersed in the SBF for 20 days.

Figure 4.50 shows the variation of the surface apatite layer thickness with immerse duration. It is obvious that the thickness of the apatite layer increased as the immerse duration is increased. Also, the apatite layer deposition rate increased with increasing immerse duration. As mentioned in section 2.3.3, Kokubo *et al.*[34] reported that Ca and Si ions dissolve from A-W glass-ceramic to form an apatite layer. Ca and Si ions dissolve from both of the wollastonite and glassy phase. In sample A, however, most of Ca and Si ions are dissolved from the glassy phase since it has only apatite crystals which would not provide Ca and Si ions.

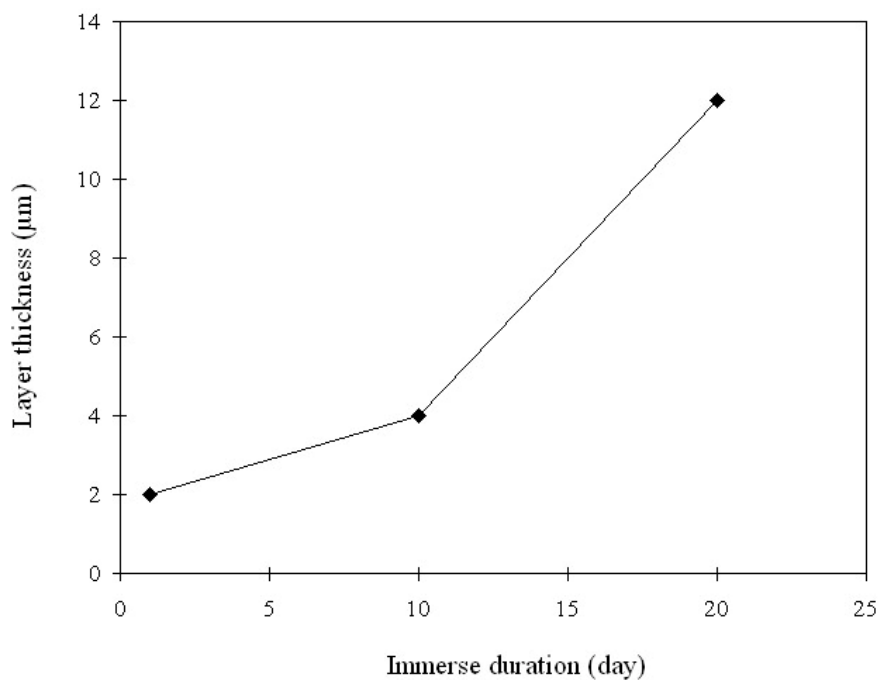


Figure 4.50 The variation of the surface apatite layer thickness with immerse duration for sample A.

The dissolution of Ca and Si ions from glassy phase induced stress which damaged the sample and led to the propagation of cracks. As seen in Figure 4.48 (a), cracks propagated from surface towards interior with size of about 70 µm, just below the apatite deposition layer. The crack length increased to 150 µm in Figure 4.49 (a) which was taken from the sample immersed in SBF for 20 days. These cracks were not detected on the sample after it was immersed in SBF for 1 day.

The variation of the crack propagation rate with immerse duration was shown in Figure 4.51. The more apatite layer is deposited, the more crack propagation occurs.

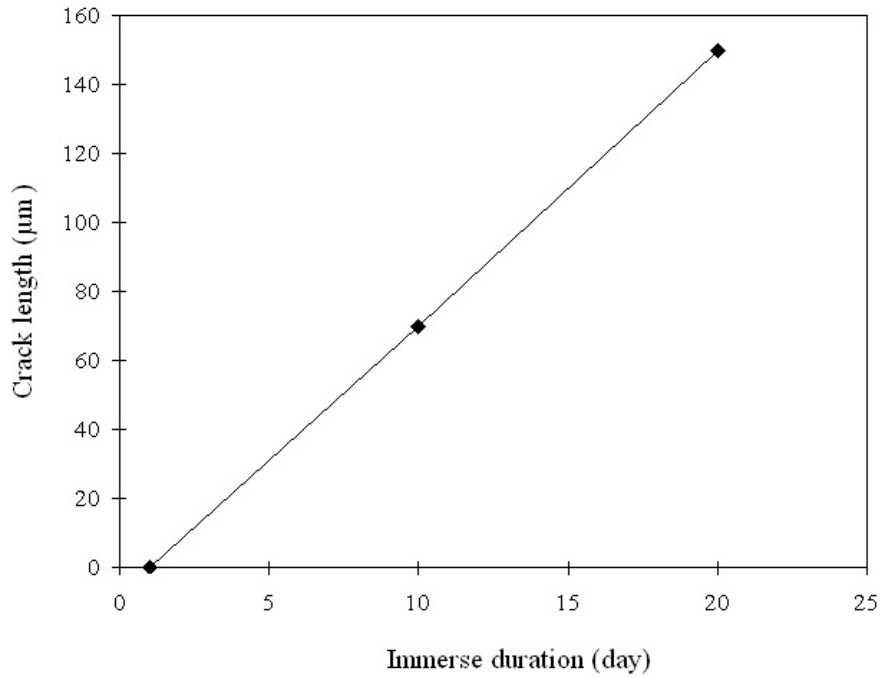


Figure 4.51 The variation of the crack length with immerse duration for sample A.

Sample A-W showed different behavior as compared to sample A. Figures 4.52 to 4.54 illustrate SEM micrographs showing the surface morphology of the sample A-W after being immersed in SBF for 1, 10 and 20 days, respectively. Apatite layer could not be detected on the surface after being immersed in SBF for 1 day as seen in Figure 4.52. The apatite layer could not be observed on the surface even after immersing the sample in SBF for 10 days as seen in Figure 4.53. When the immerse duration is increased to 20 days, a thin apatite layer of about 1 µm thickness could be noticed on the surface as seen in Figure 4.54. The findings agree very well with the XRD patterns presented in Figure 4.46. The deposited apatite layer was so thin that it could not have a profound effect on the XRD patterns. It has only decreased the maximum intensity of wollastonite phase which was mainly crystallized and oriented on the surface.

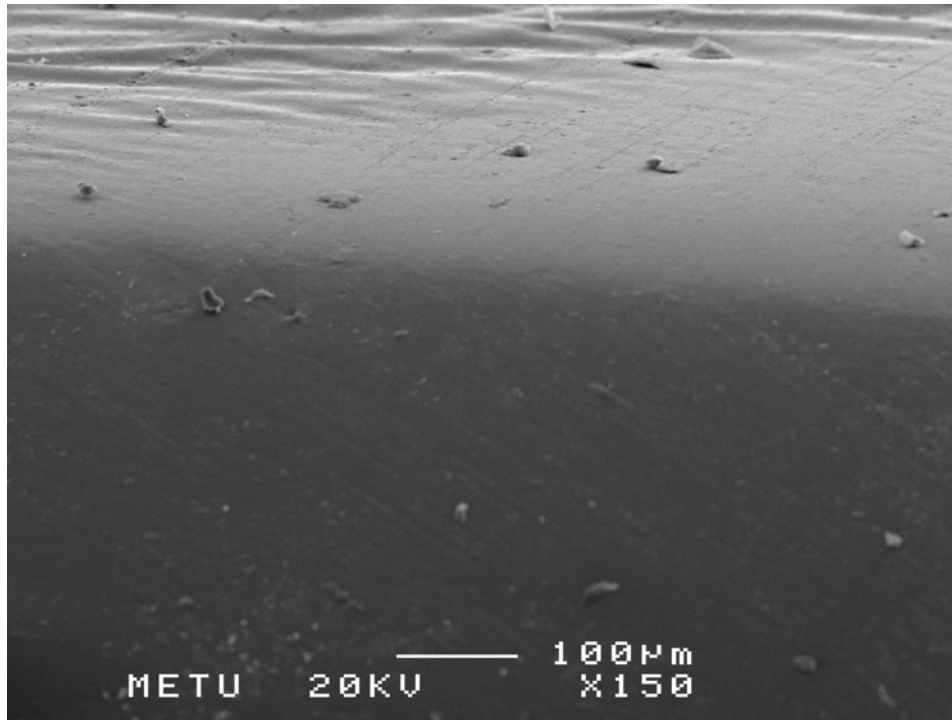


Figure 4.52 SEM micrograph of sample A-W after being immersed in SBF for 1 day.

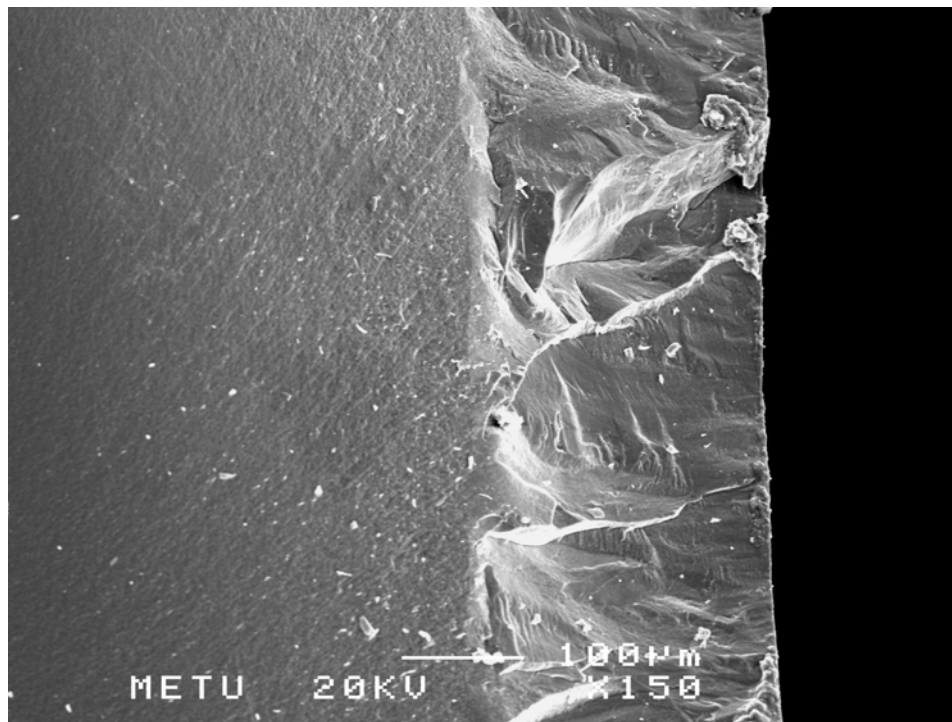


Figure 4.53 SEM micrograph of sample A-W after being immersed in SBF for 10 days.

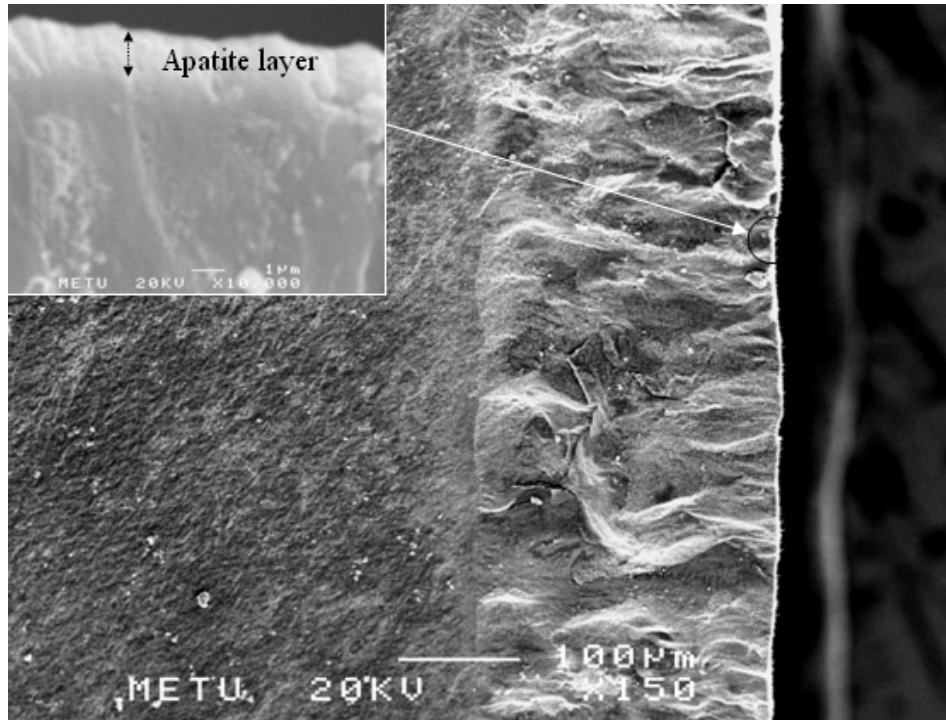


Figure 4.54 SEM micrograph of sample A-W after being immersed in SBF for 20 days.

The difference in the reaction behavior between sample A and sample A-W is assumed to be caused by the difference in type and proportion of the crystals precipitated in the glassy matrix. Sample A has enough glassy phase which can dissolve Ca and Si ions for new apatite layer formation. Sample A-W has relatively less glassy phase. Although the source of leached Ca and Si ions are reported as glassy phase and wollastonite crystal [39,40], it has been consistently observed in this study that the glassy phase is more effective than wollastonite. Therefore, relatively thicker apatite layer is formed on sample A as compared to sample A-W.

Another difference of reaction behavior between sample A and sample A-W is the crack propagation on the surface. No crack propagation has been detected on the surface of the sample A-W. It is an indication of relatively less and slow dissolution of Ca and Si ions in sample A-W as compared to sample A. The A-W glass-ceramic is assumed to be more chemical resistant to SBF solution. The variation of the surface apatite layer thickness with immerse duration is shown in

Figure 4.55. Kokubo *et al.*[34] reported that the thickness of apatite layer formed on the A-W glass ceramic produced by powder packing process was 7 μm in 10 days. However, the thickness of the layer formed in this study by melt casting process was 1 μm in 20 days. The formation of lesser apatite layer is attributed to the difference in the production process of the A-W glass ceramics. Although the test conditions were not identical, the bioactivity of glass-ceramic produced by melt casting decreased over 90% as compared to that produced by powder packing process by Kokubo [40]. The reason why the A-W glass ceramics produced by melt casting process has less bioactivity as compared to that produced by powder packing process may be explained as these; the A-W glass-ceramic produced by melt casting process has pore-free dense microstructure, hence it has less ion dissolution during immersion test, followed by less nucleation of apatite crystal on the surface of glass-ceramic.

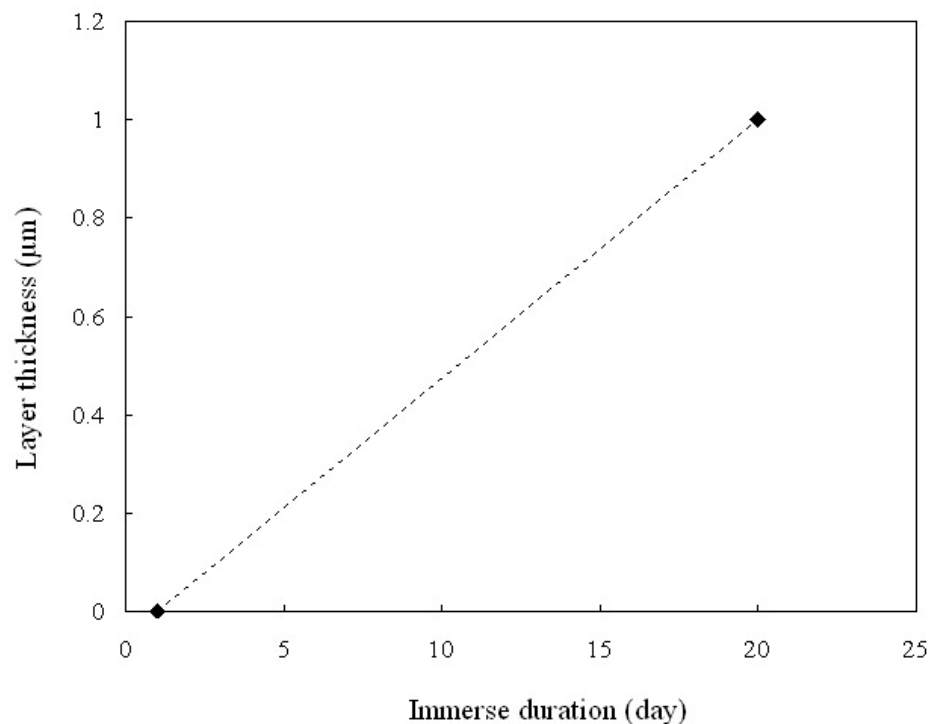


Figure 4.55 The variation of the surface apatite layer thickness with immerse duration for sample A-W.

4.6.4 Electron Dispersive Spectroscopy Analysis

The elemental analysis of the deposition layer was done by using Electron Dispersive Spectroscopy (EDS). The deposition layer on the surface of sample A is composed of mainly Ca and P ions with a trace amount of Si and Mg ions as seen in Figure 4.56. The spectrum suggests that the coated layer formed on the surface after immersion test is predominantly apatite crystals. It is thought that a small amount of Si and Mg ions have been leached together with Ca ions from the glass-ceramic. Hench and Wilson [22] and Kokubo [39] explained that silica-rich gel layer forms at the glass-solution interface, and then the apatite layer would be deposited on top of that. The detection of the Si ions of the deposition layer agrees well with the bioactive kinetic theory [22].

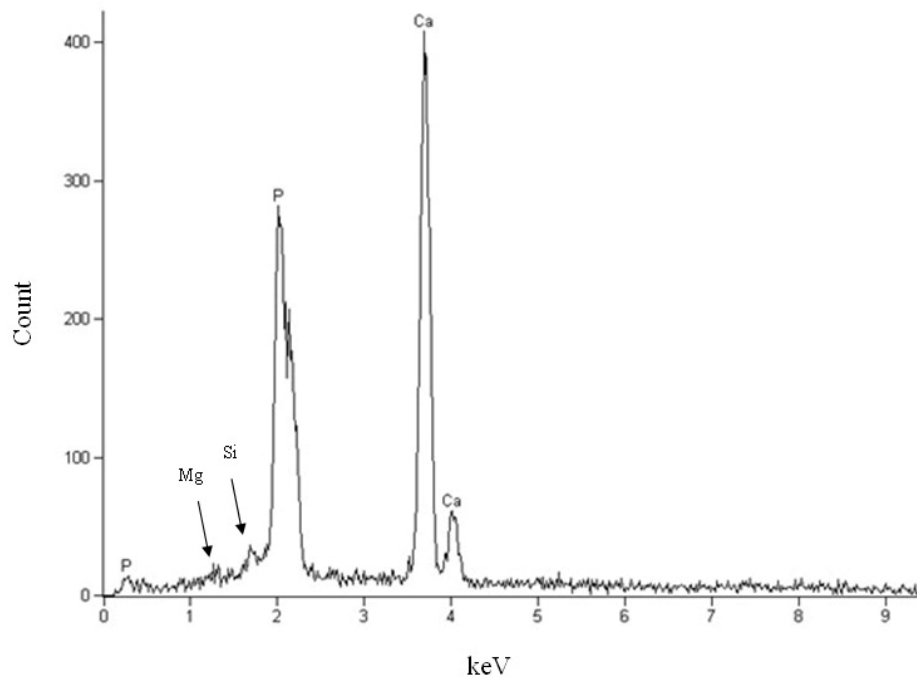


Figure 4.56 EDS spectrum of the apatite layer on the surface of the sample A after being immersed 10 days.

In sample A, crack propagation was observed as a result of exceptional ion leaching. The variation of element composition with distance from the interface between glass-ceramic and apatite layer in sample A is shown in Figure 4.57. The sample was immersed in SBF for 20 days. The elemental analysis was performed at various distances. In particular, the change in the atomic concentrations of Ca, P, and Si ions with distance was plotted and compared between close and remote places from the free surface of the sample. Five different points were selected for element analysis. Point 1 is about 500 μm away from the interface of sample A with apatite layer. Points 2 and 3 are 50 μm and 5 μm , respectively away from the interface towards interior of the glass-ceramic. Point 4 is at the interface and point 5 is 5 μm away from the interface towards the apatite layer.

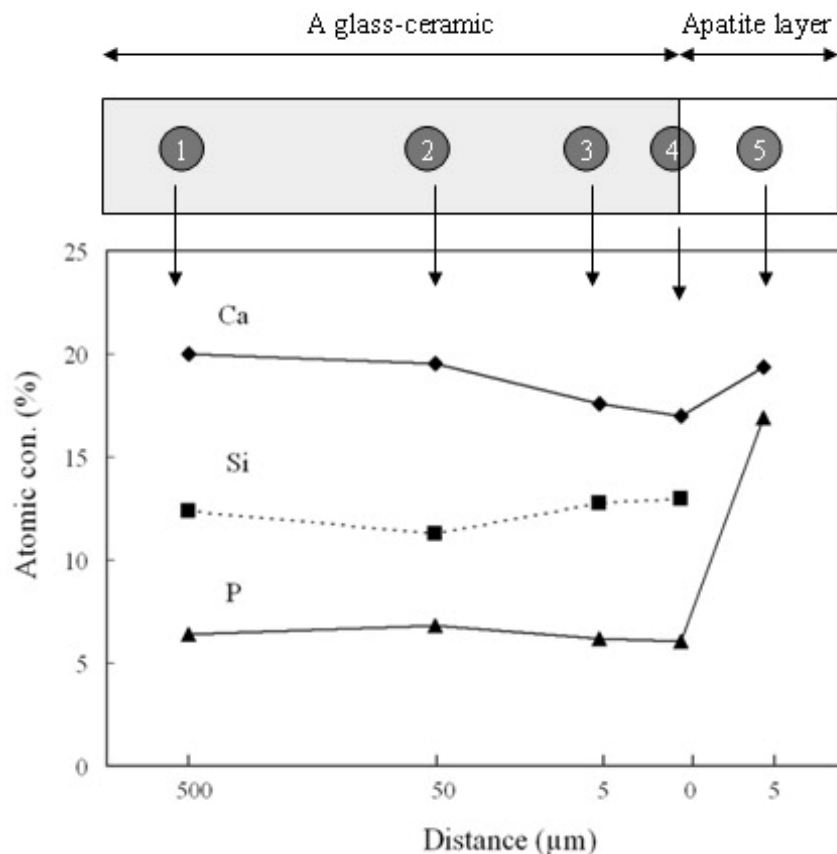


Figure 4.57 The variation of element composition with distance from the interface between A glass-ceramic and apatite layer. The sample was immersed in SBF for 20 days.

Each ion concentration showed slightly different behavior with distance from the interface between glass-ceramic and apatite layer. Ca ion decreased from point 1 and became minimum at point 4, and then increased at point 5. Similarly, P ion decreased from point 1 and became minimum at point 4, and then increased at point 5. However, Si ion showed a maximum at point 4 and was not detected at all in point 5.

The decrease in Ca ions can be explained by Hench's theory [22]. Ca ions were easily leached, and became the basic component of the deposited layer on the surface. P ions were leached with quite little amount, but P ion concentration was very high. It means that P ions in the deposited layer are mostly supplied from the SBF solution. Si ions were leached from the glass-ceramic and made silanol layer on the surface. They played only as a favorable site for apatite formation not evolved as component of the apatite crystal. Therefore, Si concentration showed a maximum on the interface and did not appear in the deposited apatite layer. Especially the concentration of P ions increased abruptly in point 5. Figure 4.58 shows the variation of Ca/P ratio at each point. At point 1, the ratio was 3.13 and decreased to 2.81 at point 4, and finally became 1.15 at point 5, implying that the layer is Ca-deficient apatite crystal.

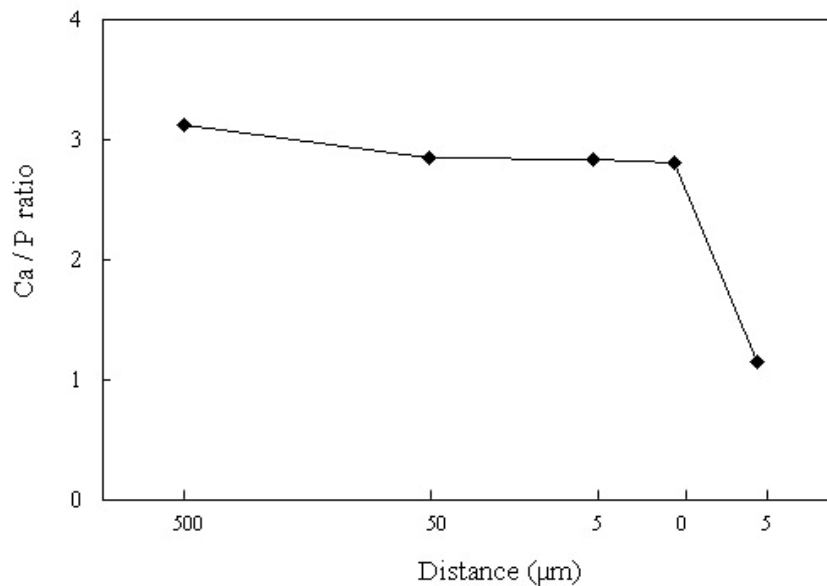


Figure 4.58 The variation of Ca/P atomic ratio with distance from the interface between A glass-ceramic and apatite layer.

For sample A-W, the EDS analysis reveals that the deposited layer is an apatite composed with mainly Ca and P ions as shown in Figure 4.59. There are also small amounts of Si and Mg ions, but their intensities are very low as compared to those of sample A. The change in the atomic concentrations of Ca, P and Si ions with distance are graphed in Figure 4.60. The tendency of the variation of each ion is similar to that of ions observed in sample A in Figure 4.57. The concentration of Ca and P became minimum at the interface with apatite layer where the concentration of Si ion became maximum. The variation of Ca/P atomic ratio with distance from the interface between A-W glass-ceramic and apatite layer is shown in Figure 4.61. The Ca/P atomic ratio of the apatite layer at point 5 was 1.56 which is still below the stoichiometric value (1.67) of hydroxyapatite. It means that the deposited layer is Ca-deficient apatite. However the value is greater than that for sample A, and shows a lower amount of P ions are deposited. As a result, the A-W sample shows low bioactivity in SBF solution. It is believed that the crystallization both of apatite and wollastonite crystals reduces the residual glassy phase content. The amount of glassy phase for leaching of Ca and Si ions are decreased. Therefore, fewer Si ions can be released from the substrate which in turn decreases the amount of Si-rich gel needed as a favorable site for the surface apatite formation [39].

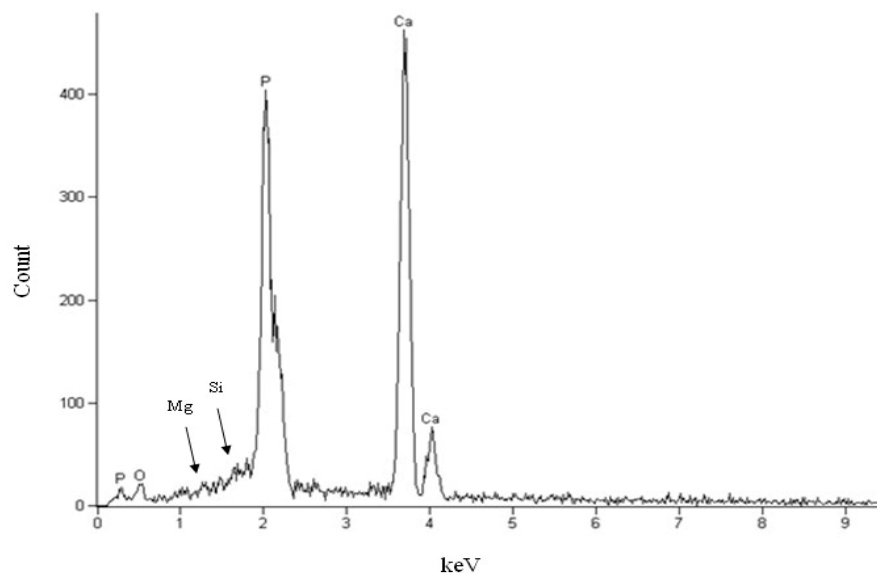


Figure 4.59 EDS spectrum of the apatite layer on the surface of the sample A-W after being immersed 20 days.

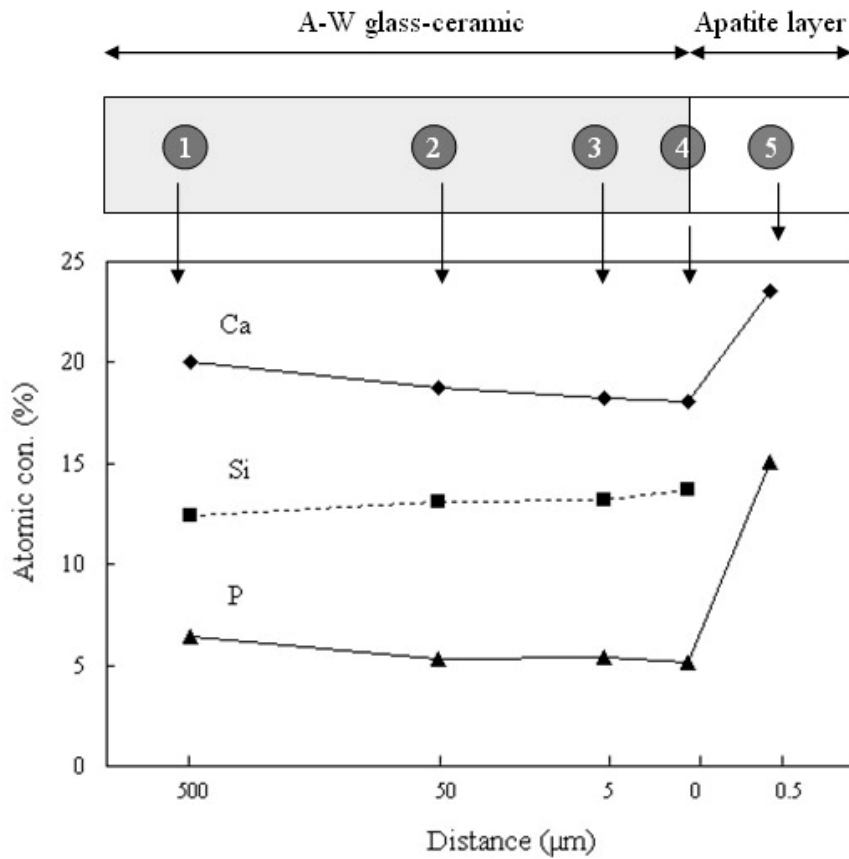


Figure 4.60 The variation of element composition with distance from the interface between A-W glass-ceramic and apatite layer. The sample was immersed in SBF for 20 days.

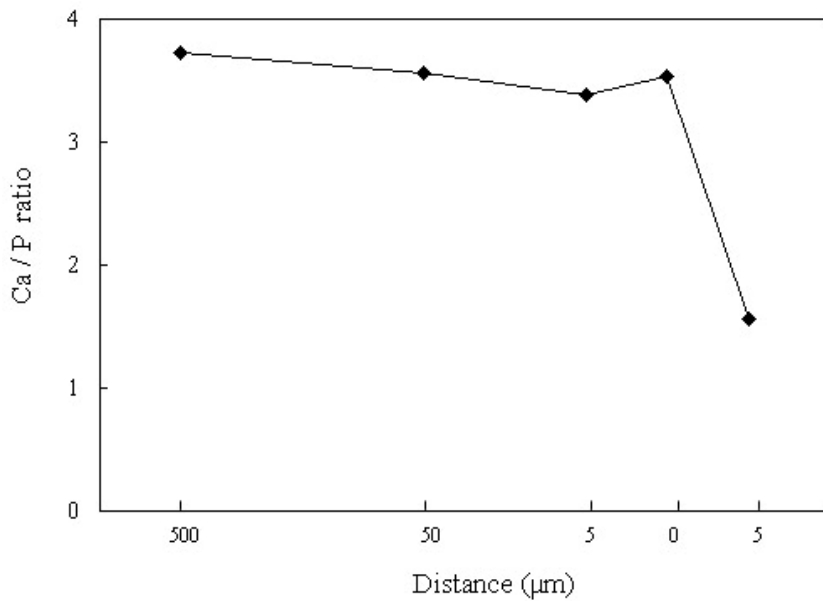


Figure 4.61 The variation of Ca/P atomic ratio with distance from the interface between A-W glass-ceramic and apatite layer.

CHAPTER 5

CONCLUSIONS

1. An investigation on the nucleation and crystallization kinetics of a glass in the MgO-CaO-SiO₂-P₂O₅-F system has revealed that the optimum temperature for the nucleation of apatite phase is 780 °C, and for the growth of wollastonite phase is 900 °C. The crystallization mechanism of apatite was a three dimensional bulk process with the reaction order, $n \approx 3$, while that of the wollastonite is a two-dimensional surface process with $n \approx 2$. The peak temperature of the crystallization exotherm of apatite phase had no significant change, but that of wollastonite phase shifted to lower temperatures, as the particle size of the glass powder decreased. The activation energy for crystallization and frequency factor for apatite and wollastonite are 460 kJ/mol and 433 kJ/mol, and 1.74×10^{22} and 2.25×10^{17} , respectively.

2. Small amount of TiO₂ additions did not have much influence on, but aided the crystallization of apatite and wollastonite phases. The activation energy for crystallization of apatite and wollastonite decreased to a minimum of 408 and 320 kJ/mol, respectively when 4 wt% TiO₂ was incorporated. The results imply that TiO₂ is an effective nucleating agent in the MgO-CaO-SiO₂-P₂O₅-F system for promoting the crystallization of apatite and wollastonite. It is expected that the wollastonite content and the properties of apatite-wollastonite (A-W) glass ceramics may be altered by changing the TiO₂ content.

3. The indentation microhardness and tribological properties of A-W glass-ceramic produced by melt casting process are strongly dependent on the microstructure developed during the crystallization process. Structure oriented changes in properties were evidenced. The presence, proportion, and orientation

of wollastonite phase had a profound effect on the microhardness and wear rate of the A-W glass-ceramics. The A-W glass-ceramic studied exhibit relatively high hardness and wear resistance as compared to commercial dental ceramic materials. Therefore, it may be used as an alternative dental material.

4. The investigation on the tribological properties of the A-W glass-ceramics has revealed the possibility of utilization of the A-W glass-ceramics in restorative dentistry when fabricating restorations that require moderate wear rate and hardness. It has been observed that the wear rate, friction coefficient, and wear mechanisms are similar to currently used artificial dental materials. The tribological properties on the free surface of this glass ceramic are close to the dentin porcelain materials, while those of the interior are comparable to enamel porcelain materials.

5. Addition of a small amount of alumina to a glass in the MgO-CaO-SiO₂-P₂O₅-F system hinders the bioactivity of the resultant glass ceramic. The tribological properties and microhardness of the alumina-added A-W glass-ceramics depend strongly on the crystals precipitated and microstructure developed during sintering. The tribological test environment had a profound effect on the wear rate and mean friction coefficient. Wear rate and mean friction coefficient obtained in simulated body fluid (SBF) are always lower than those obtained in dry condition. Strong correlation exists between mean friction coefficient, wear rate and microhardness of alumina-added A-W glass-ceramics. The tribological properties and microhardness of the alumina-added A-W glass-ceramics are comparable to those of selected commercial dental materials when they are sintered at 1000 °C or higher temperatures.

6. Glass-ceramics containing apatite and A-W showed bio-reaction after being immersed in SBF solution for a given time. Apatite containing glass-ceramic has a relatively higher reaction rate and thicker apatite layer on the surface than A-W glass-ceramic. The reaction of bioactivity strongly depends on the types of crystals developed and their proportion. Apatite and A-W containing glass-

ceramics produced by melt casting process showed lower bioactivity as compared to the A-W glass ceramics produced by powder packing process. The glass-ceramic produced by melt casting has pore-free and dense surface morphology that prohibited the ions leaching for apatite formation on the surface, and resulted in lower bioactivity, without adding additions to chemical composition.

REFERENCES

1. P.W. McMillan, "Glass-Ceramics", Academic Press, London, 1964, pp: 1-2.
2. D. Parsell, "Optimization of a glass-ceramic heat treatment schedule through thermal analysis", in Nucleation and Crystallization in Liquids and Glass, ed. by M.C. Weinberg, The American Ceramic Society, Ohio, 1993, pp: 285-291.
3. G. Partridge, C.A. Elyard and M.I. Budd, "Glass-Ceramics in substrate applications", in Glass and Glass-Ceramics, ed. by M.H. Lewis, Chapman and Hall, New York, 1989, pp: 226-271.
4. Z. Strnad, "Glass-Ceramic Materials", Elsevier Science Publishers, Amsterdam, 1986, pp: 114-140.
5. G.H. Beall, "Glass-Ceramics: Recent Developments and Applications", in Nucleation and Crystallization in Liquids and Glass, ed. by M.C. Weinberg, The American Ceramic Society, Ohio, 1993, pp: 241-266.
6. M. Vaverka and L. Hrabalek, "Anterior cervical dissection with intervertebral bioactive glass-ceramic prostheses replacement", International Congress Series, Vol. 1247 (2002), pp: 587-589.
7. Y.S. Chang, M. Kobayashi, Z.L. Li, M. Oka and T. Nakamura, "Significance of peak value and duration of the interfacial shear load in evaluation of the bone-implant interface", Clinical Biomechanics, Vol. 18 (2003), pp: 773-779.
8. A.G. Dias, I.R. Gibson, J.D. Santos and M.A. Lopes, "Physicochemical degradation studies of calcium phosphate glass ceramic in the CaO-P₂O₅-MgO-TiO₂ system", Acta Biomaterialia, Vol. 3 (2007), pp: 263-269.
9. V.G. Sukumaran and N. Bharadwaj, "Ceramics in Dental Applications", Trends in Biomaterials and Artificial Organs, Vol. 20 (2006), pp: 7-11.

10. J.G. Ironside and M.V. Swain, "A Review and critical issues of Dental Ceramics", *Journal of the Australasian Ceramic Society*, Vol. 34 (1998), pp: 78-91.
11. L.A. George and F.C. Eichmiller, "Dental applications of Ceramics", *Bioceramics: Materials and Applications*, Ceramic Transactions Volume 48, ed. by G. Fischman, A. Clare and L. Hench, American Ceramic Society, Westerville, Ohio (1995), pp: 157-172.
12. J.R. Kelly, "Ceramics in Restorative and Prosthetic Dentistry", *Annual Review of Materials Science*, Vol. 27 (1997), pp: 443-468.
13. P.W. Piche, W.J. O'Brien, C.L. Groh and K.M. Boenke, "Leucite content of selected dental porcelains", *Journal of Biomedical Materials Research*, Vol. 28 (1994), pp: 603-609.
14. J.W. McLean and M.I. Kedge, "High-strength ceramics", *Quintessence International*, Vol. 18 (1987), pp: 97-106.
15. W.J. O'Brien, C.L. Groh, K.M. Boenke, G.P. Mora and T.Y. Tien, "The strengthening mechanism of a magnesia core ceramic", *Dental Materials*, Vol. 9, pp: 242-245.
16. R.R. Seghi, T. Daher and A. Caputo, "Relative flexural strength of dental restorative ceramics", *Dental Materials*, Vol.6 (1990), pp: 181-184.
17. S.D. Stookey, "Catalyzed Crystallization of Glass in Theory and Practice", *Industrial and Engineering Chemistry*, Vol. 51 (1959), pp: 805-808.
18. T. Yamamuro, T. Nakamura, H. Iida, K. Kawanabe, Y. Matsuda, K. Ido, J. Tamura and Y. Senaha, "Development of bioactive bone cement and its clinical applications", *Biomaterials*, Vol. 19 (1998), pp: 1479-1482.
19. Q.Z. Chen, I.D. Thompson and A.R. Boccaccini, "45S5 Bioglass®-derived glass-ceramic scaffolds for bone tissue engineering", *Biomaterials*, Vol. 27 (2006), pp: 2414-2425.
20. W. Höland, "Biocompatible and bioactive glass-ceramics - state of the art and new directions", *Journal of Non-Crystalline Solids*, Vol. 219 (1997), pp: 192-197.

21. L.L. Hench, R.J. Splinter, W.C. Allen and T.K. Greenlee, "Bonding mechanisms at the interface of ceramic prosthetic materials", *Journal of Biomedical Materials Research*, Vol. 5 (1971), pp: 117-141.
22. L.L. Hench and J. Wilson, "Bioactive Glasses and Glass-Ceramics: A 25-Year Restrospective", in *Bioceramics: Materials and Applications*, ed. by G. Fischman, A. Clare and L. Hench, The American Ceramic Society, Ohio, 1995, pp: 11-22.
23. W. Höland, M. Frank and V. Rheinberger, "Surface crystallization of leucite in glasses", *Journal of Non-Crystalline Solids*, Vol. 180 (1995), pp: 292-307.
24. K.A. Malament and S.S. Socransky, "Survival of Dicor glass-ceramic dental restorations over 16 years. Part III: Effect of luting agent and tooth or tooth-substitute core structure", *The Journal of Prosthetic Dentistry*, Vol. 86 (2001), pp: 511-519.
25. J.R. Kelly, I. Nishimura and S.D. Campbell, "Ceramics in dentistry: historical roots and current perspectives", *Journal of Prosthetic Dentistry*, Vol. 75 (1996), pp: 18-32.
26. J.M. Tzeng, J.G. Duh, K.H. Chung and C.C. Chan, "Al₂O₃-and ZrO₂-modified dental glass ceramics", *Journal of Material Science*, Vol. 28 (1993), pp: 6127-6135.
27. D. Zikk, Y. Rapoport, J. Bloom and M. Z. Himelfarb, "Auditory brain-stem responses in guinea pigs following middle ear implantation of Ceravital", *European Archives of Oto-Rhino-Laryngology*, Vol. 248 (1990), pp: 102-104.
28. C. Ohtsuki, H. Kushitani, T. Kokubo, S. Kotani and T. Yamamuro, "Apatite formation on the surface of ceravital-type glass-ceramic in the body", *Journal of Biomedical Materials Research*, Vol. 25 (1991), pp: 1363-1370.
29. W. Höland and W. Vogel, "Machineable and phosphate glass-ceramics", in *An Introduction to Bioceramics*, ed. by L.L. Hench and J. Wilson, World Scientific, Singapore, 1993, pp. 125-137.
30. O. Peitl, E.D. Zanotto and L.L. Hench, "Highly bioactive P₂O₅-Na₂O-CaO-SiO₂ glass-ceramics", *Journal of Non-Crystalline Solids*, Vol. 292 (2001), pp: 115-126.

31. V.A. Dubok, "Bioceramics - Yesterday, Today, Tomorrow", Powder Metallurgy and Metal Ceramics, Vol. 39 (2000), pp: 381-394.
32. T. Kokubo, M. Shigematsu, Y. Nagashima, M. Tashiro, T. Nakamura and S. Higashi, "Apatite and wollastonite containing glass-ceramics for prosthetic application", Bulletin of Institute for Chemical Research, Kyoto University, Vo. 60 (1982), pp: 260-268.
33. T. Kokubo, S. Ito, S. Sakka, and T. Yamamuro, "Formation of a High-Strength Bioactive Glass-Ceramic in the System $MgO-CaO-SiO_2-P_2O_5$ ", Journal of Material Science, Vol. 21 (1986), pp: 536-540.
34. T. Kokubo, "Bioactive Glass-Ceramics: Properties and Applications", Biomaterials, Vol. 12 (1991), pp: 155-163.
35. T. Kokubo, S. Ito, M. Shigematsu, S. Sakka and T. Yamamuro, "Mechanical properties of a new type of apatite-containing glass-ceramic for prosthetic application", Journal of Material Science, Vol. 20 (1985), pp: 2001-2004.
36. T. Kokubo, S. Ito, S. Sakka, M. Shigematsu and T. Yamamuro, "Fatigue and Life-time of Bioactive glass-ceramic A-W containing Apatite and Wollastonite", Journal of Materials Science, Vol. 22 (1987), pp: 4067-4070.
37. T. Kitsugi, T. Yamamuro, T. Nakamura and T. Kokubo, "The bonding of glass ceramics to bone", International Orthopaedics, Vol.13 (1989), pp: 199-206.
38. T. Yamamuro, "A/W Glass-Ceramic: Clinical Applications", in An Introduction to Bioceramics, ed. by L.L. Hench and J. Wilson, World Scientific, 1993, pp: 89-103.
39. T. Kokubo, "Surface Chemistry of Bioactive Glass-Ceramics", Journal of Non-Crystalline Solids, Vol.120 (1990), pp: 138-151.
40. T. Kokubo, "A/W Glass-Ceramic: Processing and Properties", in An Introduction to Bioceramics, ed. by L.L. Hench and J. Wilson, World Scientific, 1993, pp: 75-88.
41. T. Kokubo, S. Ito, Z.T. Huang, T. Hayashi, S. Sakka, T. Kitsugi and T. Yamamuro, "Ca, P rich layer formed on high-strength bioactive glass-ceramic A-W", Journal of Biomedical Materials Research, Vol. 24 (1990), pp: 331-343.

42. T. Kitsugi, T. Yamamuro and T. Nakamura, "Bone bonding behavior of MgO-CaO-SiO₂-P₂O₅-CaF₂ glass", Journal of Biomedical Materials Research, Vol. 23 (1989), pp: 631-648.
43. T. Kitsugi, T. Yumamuro, T. Nakamura, S.Yoshii, T. Kokubo, M.Takagi and T. Shibuya, "Influence of substituting B₂O₃ for CaF₂ on the bonding behavior to bone of glass-ceramics containing apatite and wollastonite", Biomaterials, Vol.13 (1992), pp: 393-399.
44. J.J. Shyu and J.M. Wu, "Effects of composition changes on the crystallization behavior of MgO-CaO-SiO₂-P₂O₅ Glass Ceramics", Journal of American Ceramic Society, Vol. 74 (1991), pp: 536-540.
45. S. Kihara and A. Watanabe, "Calcium phosphate glass-ceramic crown prepared by lost-wax technique", Journal of American Ceramic Society, Vol. 67 (1984), pp: C100-C101.
46. K. Ohura, T. Kakanura, T. Yamamuro, Y. Ebisawa, T. Kokubo, Y. Kotoura and M. Oka, "Bioactivity of CaO.SiO₂ added with various ions", Journal of Material Science: Materials in Medicine, Vol. 3 (1992), pp: 95-100.
47. Y. Ebisawa, T. Kokubo, K. Ohura and T. Yamamuro, "Bioactivity of CaO.SiO₂-based glasses: in vitro evaluation", Journal of Material Science: Materials in Medicine, Vol. 1 (1990), pp: 239-244.
48. C. Ohtsuki, T. Kokubo and T. Yamamuro, "Compositional Dependence of Bioactivity of Glasses in the system CaO-SiO₂-Al₂O₃: Its *in vitro* Evaluation", Journal of Materials Science: Materials in Medicine, Vol. 3 (1992), pp: 119-125.
49. K. Ono, T. Yamamuro, T. Nakamura, Y. Kakutani, T. Kitsugi, K. Hyakuna, T. Kokubo, M. Oka and Y. Kotoura, "Apatite-wollastonite containing glass ceramic-fibrin mixture as a bone defect filler", Journal of Biomedical Materials Research, Vol. 22 (1988), pp: 869-885.
50. T. Kitsugi, T. Yamamuro and T. Kokubo, "Bonding behavior of a glass-ceramic containing apatite and wollastonite in segmental replacement of the rabbit tibia under load-bearing conditions", The Journal of Bone and Joint Surgery, Vol. 71 (1989), pp: 264-272.
51. N. Ikeda, K. Kawanabe and T. Nakamura, "Quantitative comparison of osteoconduction of porous, dense A-W glass-ceramic and hydroxyapatite granules (effects of granule and pore sizes)", Biomaterials, Vol. 20 (1999), pp: 1087-1095.

52. T. Kitsugi, T. Yamamuro, T. Nakamura, S. Kotani and T. Kokubo, "Effect of Varying Amounts of Al_2O_3 on the bond between A-W Glass Ceramics and Bone", in *Bioceramics (Proceeding of 1st International Bioceramic Symposium)*, ed. by H. Oonishi, H. Aoki and K. Sawai, Ishiyaku EuroAmerica Inc., St. Louis, 1989, pp: 169-174.
53. K. Nishio, M. Neo, H. Akiyama, Y. Okada, T. Kokubo and T. Nakamura, "Effects of apatite and wollastonite containing glass-ceramic powder and two types of alumina powder in composites on osteoblastic differentiation of bone marrow cells", *Journal of Biomedical Materials Research*, Vol. 55 (2001), pp: 164-176.
54. S. Shinzato, M. Kobayashi, W.F. Mousa, M. Kamimura, M. Neo, Y. Kitamura, T. Kokubo and T. Nakamura, "Bioactive polymethyl methacrylate-based bone cement: Comparison of glass beads, apatite-and wollastonite containing glass-ceramic, and hydroxyapatite fillers on mechanical and biological properties", *Journal of Biomedical Materials Research*, Vol. 51 (2000), pp: 258-272.
55. S. Shinzato, T. Nakamura, T. Kokubo and Y. Kitamura, "Bioactive bone cement: Effect of filler size on mechanical properties and osteoconductivity", *Journal of Biomedical Materials Research*, Vol. 56 (2001), pp: 571-577.
56. J.A. Juhasz, S.M. Best, W. Bonfield, M. Kawashita, N. Miyata, T. Kokubo and T. Nakamura, "Apatite-forming ability of glass-ceramic apatite-wollastonite-polyethylene composite: effect of fill content", *Journal of Materials Science: Materials in Medicine*, Vol. 14 (2003), pp: 489-495.
57. J.A. Juhasz, S.M. Best, R. Brook, M. Kawashita, N. Miyata, T. Kokubo, T. Nakamura and W. Bonfield, "Mechanical properties of glass-ceramic A-W-polyethylene composite: effect of filler content and particle size", *Biomaterials*, Vol. 25 (2004), pp: 949-955.
58. C. Schuh, E.J. Kinast, E. Mezzomo and M.P. Kapcainski, "Effect of glazed and polished surface finishes on the friction coefficient of two low-fusing ceramics", *The Journal of Prosthetic Dentistry*, Vol. 93 (2005), pp: 245-252.
59. W. Pompe and M. Gelinsky, "Biological Materials: Failure of Bone and Teeth", in *Encyclopedia of Materials: Science and Technology*, ed. by K.H.J. Buschow, R.W. Cahan, M.C. Flemings, B. Ilschner, E.J. Kramer and S. Mahajan, Elsevier, Oxford, 2001, pp: 580-584.

60. S. Cho, F. Miyaji, T. Kokubo and T. Nakamura, "Induction of bioactivity of a non-bioactive glass-ceramic by a chemical treatment", *Biomaterials*, Vol. 18 (1997), pp: 1479-1485.
61. U. Gross and V. Strunz, "The Interface of various Glasses and Glass Ceramics with a bony implantation bed", *Journal of Biomedical Materials Research*, Vol. 19 (1985), pp: 251-271.
62. S. Jahanmir and X. Dong, "Wear mechanism of a dental glass-ceramic", *Wear*, Vol. 181-183 (1995), pp: 821-825.
63. A.D. Sarkar, "Friction and wear", Academic Press, London, 1980, pp: 1-4.
64. R. DeLong, "Intra-oral restorative materials wear: Rethinking the current approaches: How to measure wear", *Dental Materials*, Vol. 22 (2006), pp: 702-711.
65. R. DeLonga, C. Sasikb, M.R. Pintadoa and W.H. Douglas, "The wear of enamel when opposed by ceramic systems", *Dental Materials*, Vol. 5 (1989), pp: 266-271.
66. L.H. Mair, "Wear in dentistry-current terminology", *Journal of Dentistry*, Vol. 20 (1992), pp: 104-144.
67. P. Lambrechts, E. Debels, K.V. Landuyt, M. Peumans and B.V. Meerbeek, "How to simulate wear? Overview of existing methods", *Dental Materials*, Vol. 22 (2006), pp: 693-701.
68. L.H. Mair, T.A. Stolarski, R.W. Vowles and C.H. Lloyd, "Wear: mechanisms, manifestations and measurement. Report of a workshop", *Journal of Dentistry*, Vol.24 (1996), pp: 141-148.
69. P. Lambrechts, K. Goovaerts, D. Bharadwaj, J. De Munck, L. Bergamans, M. Peumans and B.V. Meerbeek, "Degradation of tooth structure and restorative materials: A review", *Wear*, Vol. 261 (2006), pp: 980-986.
70. W. Wang, A.T. DiBenedetto and A.J. Goldberg, "Abrasive wear testing of dental restorative materials", *Wear*, Vol. 219 (1998), pp: 213-219.
71. S. Bahadur and I. Iskanda, "Effect of Test Variables on the Friction and Wear of Alumina", in *Wear Testing of Advanced Materials*, ed. by R. Divakar and P.J. Blau, ASTM, Philadelphia, 1992, pp: 7-23.

72. CSM Instruments, Tribology test standards, No.18, September 2002.
73. J.J. Shyu and J.M. Wu, "Crystallisation of MgO-CaO-SiO₂-P₂O₅ Glass", Journal of American Ceramic Society, Vol. 73 (1990), pp: 1062-1068.
74. J. Park and A. Ozturk, "Tribological properties of MgO-CaO-SiO₂-P₂O₅-F-based glass-ceramic for dental applications", Materials Letters, Vol. 61 (2007), pp: 1916-1921.
75. S. Likitvanichkul and W.C. Lacourse, "Apatite-wollastonite glass-ceramics Part 1 Crystallization kinetics by differential thermal analysis", Journal of Materials Science, Vol. 33 (1998), pp: 5901-5904.
76. M. Rezvani, B. Eftekhari-Yekta, M. Solati-Hashjin and K. Marghussian, "Effect of Cr₂O₃, Fe₂O₃ and TiO₂ nucleants on the crystallisation behaviour of SiO₂-Al₂O₃-CaO-MgO(R₂O) glass-ceramics", Ceramic International, Vol. 31 (2005) pp: 75-80.
77. C.H. Gür and A. Öztürk, "Determination of the influence of TiO₂ on the elastic properties of a mica based glass ceramic by ultrasonic velocity measurements", Journal of Non-Crystalline Solids, Vol. 351 (2005), pp: 3655-3662.
78. J.O. Isad, P.E. James and A.H. Ramsden, "An investigation of the possibility that electric fields could affect the nucleation of glass ceramics", Physics and Chemistry of Glasses, Vol. 19 (1978), pp: 9-13.
79. R.G. Duan, K.M. Liang and S.R. Gu, "Effect of changing TiO₂ content on structure and crystallisation of CaO-Al₂O₃-SiO₂ system glasses", The Journal of European Ceramic Society, Vol. 18 (1998), pp: 1729-1735.
80. P.W. McMillan, "Glass-Ceramics", Academic Press, London, 1964, pp: 63-65, 85-123.
81. M. Avrami, "Kinetics of phase change I: General Theory", Journal of Chemical Physics, Vol. 7 (1939), pp: 1103-1112.
82. J.A. Augis and J.E. Bennett, "Calculation of the Avrami parameters for heterogeneous solids reactions using a modified of the Kissinger method", Journal of the Thermal Analysis, Vol.13 (1978), pp: 283-292.
83. H.E. Kissinger, "Reaction kinetics in Differential Thermal Analysis", Analytical Chemistry, Vol. 29 (1959), pp: 1702-1706.

84. C.S. Ray and D.E. Day, "Nucleation and crystallization in glasses as determined by DTA", in *Nucleation and crystallization in liquids and glasses*, ed. by M.C. Weinberg, The American Ceramic Society, Westerville, Ohio, 1992, pp: 207-223.
85. S.F. Hulbert, L.L. Hench, D. Forbers and L.S. Bowman, "History of bioceramics", *Ceramics International*, Vol. 8 (1982), pp: 131-140.
86. L.L. Hench, "Bioceramics and the origin of life", *Journal of Biomedical Materials Research*, Vol. 23 (1989), pp: 685-703.
87. L.L. Hench and O. Andersson, "Bioactive Glasses", in *An Introduction to Bioceramics*, ed. by L.L. Hench and J. Wilson, World Scientific, Singapore, 1993, pp: 41-62.
88. L.L. Hench, "Bioceramics: From Concept to Clinic", *Journal of the American Ceramic Society*, Vol. 74 (1991), pp: 1487-1510.
89. U.M. Gross, C. Muller-Mai and C. Voigt, "Ceravital® Bioactive Glass-Ceramics", in *An Introduction to Bioceramics*, ed. by L.L. Hench and J. Wilson, World Scientific, Singapore, 1993, pp: 105-123.
90. D.G. Grossman, "Machinable glass-ceramic based on tetrasilicic mica", *Journal of American Ceramic Society*, Vol. 55 (1972), pp: 446-449.
91. W. Vogel, W. Höland and K. Naumann, "Development of machinable glass-ceramic for prosthetic application", *Journal of Non-Crystalline Solids*, Vol. 80 (1986), pp: 34-52.
92. F.H. Lin and M.H. Hon, "A study on bioglass ceramics in the Na₂O-CaO-SiO₂-P₂O₅ system", *Journal of Material Science*, Vol. 23 (1989), pp: 4295-4299.
93. D.M. Liu and H.M. Chou, "Formation of a new bioactive glass-ceramic", *Journal of Materials Science: Materials in Medicine*, Vol. 5 (1994), pp: 7-10.
94. W. Höland, M. Schweiger, M. Frank and V. Rheinberger, "A comparison of the microstructure and properties of the IPS Empress®2 and the IPS Empress® glass-ceramics", *Journal of Biomedical Materials Research*, Vol. 53 (2000), pp: 297-303.

95. H.W. Kim, Y.H. Koh, S.B. Seo and H.E. Kim, "Properties of fluoridated hydroxyapatite-alumina biological composites densified with addition of CaF_2 ", *Materials Science and Engineering C*, Vol. 23 (2003), pp: 515-521.
96. A.S. Posner, E.D. Eanes, R.A. Harper and I. Zipkin, "X-ray diffraction analysis of the effect of fluoride on human bone apatite", *Archives of Oral Biology*, Vol.8 (1963), pp: 549-570.
97. A. Bloch-Zupan, "Is the Fluoride Concentration Limit of 1500 ppm in Cosmetics (EU Guideline) Still Up-to-Date?", *Caries Research*, Vol. 35, Suppl.1, (2001), pp: 22-25.
98. C.Y. Kim, A.E. Clark and L.L. Hench, "Early stage of calcium-phosphate layer formation in bioglasses", *Journal of Non-Crystalline Solids*, Vol. 113 (1989), pp: 195-202.
99. T. Kitsugi, T. Nakamura, T. Yamamuro, T. Kokubo, T. Shinbuya and T. Takagi, "SEM-EPMA observation of three types of apatite-containing glass-ceramics implanted in bone: the variance of a Ca-P-rich layer", *Journal of Biomedical Materials Research*, Vol. 21 (1987), pp: 1255-1271.
100. H.M. Kim, "Ceramic bioactivity and related biomimetic strategy", *Current Opinion in Solid State and Materials Science*, Vol. 7 (2003), pp: 289-299.
101. Y. Abe, T. Kokubo and T. Yamamuro, "Apatite Coating on Ceramics, Metals and Polymers Utilizing a Biological Process", *Journal of Materials Science: Materials in Medicine*, Vol. 1 (1990), pp: 233-238.
102. M.A. Meyers, P.Y. Chen, A.Y.M. Lin and Y. Seki, "Biological materials: Structure and Mechanical Properties", *Progress in Materials Science*, Vol. 53 (2008), pp: 1-208.
103. L.H. Hong and M.V. Swain, "Influence of environment on mechanical behavior of mature human enamel", *Biomaterials*, Vol. 28 (2007), pp: 4512-4520.
104. J.H. Kinney, S.J. Marshall and G.W. Marshall, "The Mechanical Properties of Human Dentin: A Critical Review and Re-evaluation of The Dental Literature", *Critical Reviews in Oral Biology and Medicine*, Vol. 14 (2003), pp: 13-29.

105. W. Höland, V. Rheinberger, E. Apel, C. van't Hoen, M. Holand, A. Dommann, M. Obrecht, C. Mauth and U. Graf-Hausner, "Clinical applications of glass-ceramics in dentistry", *Journal of Materials Science: Materials in Medicine*, Vol. 17 (2006), pp: 1037-1042.
106. H. Fischer, M. Hemelik, R. Telle and R. Marx, "Influence of annealing temperature on the strength of dental glass ceramic material", *Dental Material*, Vol. 21 (2005), pp: 671-677.
107. S.C. Oh, J.K. Dong, H. Luthy and P. Scharer, "Strength and Microstructure of IPS Empress2 Glass-Ceramic after different treatments", *International Journal of Prosthodontics*, Vol. 13 (2000), pp: 468-472.
108. A.M. Lacy, "Ceramics in restorative dentistry-past, present and Future at Bioceramics: materials and applications", ed. by G. Fishman, A. Clare and L. Hench, *Ceramic transactions Vol. 48*, The American Ceramic Soc. Westerville, Ohio, 1995, pp: 35-41.
109. J.Y. Thompson, S.C. Bayne and H.O. Heymann, "Mechanical properties of a new mica-based machinable glass ceramic for CAD/CAM restorations", *The Journal of Prosthetic Dentistry*, Vol. 76 (1996), pp: 619-623.
110. T. Sato, K. Tsuji, N. Kawashima, H. Sato and Y. Nakamura, "Effect of defect size on fracture strength of dental low fusion porcelain", *Colloids and Surfaces B: Biointerfaces*, Vol. 38 (2004), pp: 77-82.
111. K. Kato and K. Adachi, "Wear Mechanism", in *Morden Tribology Handbook Vol. 1*, ed. by B. Bhushan, CRC Press, USA, 2001, pp: 273-300.
112. K.C. Ludema, "Friction", *Morden Tribology Handbook, Vol.1*, ed. by B. Bhushan, CRC Press, USA, 2001, pp: 205-233.
113. ASTM G99, "Standard test method for wear testing with a pin-on-disk apparatus", *Annual Book of ASTM Standards*, 1999, pp: 401-405.
114. S.K. Chen and H.S. Liu, "FTIR, DTA and XRD study of sphene (CaTiSiO₅) crystallization in a ceramic frit and a non-borate base glass", *Journal of Materials Science*, Vol.29 (1994), pp: 2921-2930.
115. K.T. Metzler, R.D. Woody, A.W. Miller III and B.H. Miller, "In vitro investigation of the wear of human enamel by dental porcelain", *Journal of Prosthetic Dentistry*, Vol. 81 (1999), pp: 356-364.

116. K.J. Anusavice, "Phillips' science of dental materials", 10th ed., Philadelphia, WB Saunders, 1996, pp: 33, 69-71, 598-600.
117. T. Kokubo, H. Kushitani, S. Sakka, T. Kitsugi and T. Yamamuro, "Solutions able to reproduce in vivo surface-structure changes in bioactive glass-ceramic A-W", *Journal of Biomedical Materials Research*, Vol. 24 (1990), pp: 721-734.
118. B.D. Cullity, "Elements of x-ray diffraction", Addison-Wesley Pub., Philippine, 1978, pp: 394-395.
119. C. Klein and C.S. Hurlbut, "Manual of mineralogy" (after J. D. Dana), 21st ed., John Wiley & Sons, New York, 1993, pp: 434-435, 484-486.
120. N. Mehta, R.S. Tiwari and A. Kumar, "Glass forming ability and thermal stability of some Se-Sb glassy alloys", *Materials Research Bulletin*, Vol. 41 (2006), pp: 1664-1672.
121. A. Goel, E.R. Shaban, F.C.L. Melo, M.J. Ribeiro and J.M.F. Ferreira, "Non-isothermal crystallization kinetic studies on MgO-Al₂O₃-SiO₂-TiO₂ glass", *Journal of Non-Crystalline Solids*, Vol. 353 (2007), pp: 2383-2391.
122. H.F. Wu, C.C. Lin and P.Y. Shen, "Structure and dissolution of CaO-ZrO₂-TiO₂-Al₂O₃-B₂O₃-SiO₂ glass", *Journal of Non-Crystalline Solids*, Vol. 209 (1997), pp: 76-86.
123. R.B. Rao, D.K. Rao and N. Veeraiyah, "The role of titanium ions on structural, dielectric and optical properties of Li₂O-MgO-B₂O₃ glass system", *Materials Chemistry and Physics*, Vol. 87 (2004), pp: 357-369.
124. A. Shaim and M. Et-tabirou, "Role of titanium in sodium titanophosphate glasses and a model of structural units", *Materials Chemistry and Physics*, Vol. 80 (2003), pp: 63-67.
125. L. Koudelka, P. Mosner, M. Zeyer and C. Jager, "Lead borophosphate glasses doped with titanium dioxide", *Journal of Non-Crystalline Solids*, Vol. 326&327 (2003), pp: 72-76.
126. B. Yu, K. Liang, A. Hu and S. Gu, "Influence of different TiO₂ content on crystallization of CaO-MgO-P₂O₅-SiO₂ system glasses", *Materials Letters*, Vol. 56 (2002), pp: 539-542.

- 127.S. Fu, P. Wu and Z. Han, "Tensile strength and rupture energy of hybrid poly(methylvinylsiloxane) composites reinforced with short PET fibers and wollastonite whiskers", *Composites Science and Technology*, Vol. 62 (2002), pp: 3-8.
- 128.R. Adams and P.W. McMillan, "The characterization of high-strength surface-crystallized glasses", *Journal of Materials Science*, Vol. 17 (1982), pp: 2727-2735.
- 129.I. Krejci, F. Lutz, M. Reimer and J.L. Heinzmann, "Wear of ceramic inlays, their enamel antagonists, and luting cements", *Journal of Prosthetic Dentistry*, Vol. 69 (1993), pp: 425-430.
- 130.M. Albakry, M. Guazzato and M.V. Swain, "Fracture toughness and hardness evaluation of three pressable all-ceramic dental materials", *Journal of Dentistry*, Vol. 31(2003), pp: 181-188.
- 131.C.H. Hacker, W.C. Wagner and M.E. Razzoog, "An in vitro investigation of the wear of enamel on porcelain and gold in saliva", *Journal of Prosthetic Dentistry*, Vol. 75 (1996), pp: 14-17.
- 132.I.L. Denry and J.A. Holloway, "Elastic constants, Vickers hardness, and fracture toughness of fluorrichterite-based glass-ceramics", *Dental Materials*, Vol. 20 (2004), pp: 213-219.
- 133.N.L. Clelland, V. Agarwala, L.A. Knobloch and R.R. Seghi, "Relative wear of enamel opposing low-fusing dental porcelain", *Journal of Prosthodontics*, Vol. 12(2003), pp: 168-175.
- 134.F. Borgioli, E. Galvanetto, F. Iozzelli and G. Pradelli, "Improvement of wear resistance of Ti-6Al-4V alloy by means of thermal oxidation", *Materials Letters*, Vol. 59 (2005), pp: 2159-2162.
- 135.E.S. Reeh, W.H. Douglas and M.J. Levine, "Lubrication of saliva substitutes at enamel-to-enamel contacts in an artificial mouth", *Journal of Prosthetic Dentistry*, Vol. 75 (1996), pp: 649-656.
- 136.E.W. Tillitson, R.G. Craig and F.A. Peyton "Friction and wear of restorative dental materials", *Journal of Dentistry Research*, Vol. 50 (1971), pp: 149-154.

137. C. Schuh, E.J. Kinast, E. Mezzomo and M.P. Kapczinski, "Effect of glazed and polished surface finishes on the friction coefficient of two low-fusing ceramics", *The Journal of Prosthetic Dentistry*, 93 (2005), pp: 245-252.
138. T.R. Katona, "A mathematical analysis of the role of friction in occlusal trauma", *The Journal of Prosthetic Dentistry*, Vol. 86 (2001), pp: 636-643.
139. R.R. Seghi, S.F. Rosenstiel and P. Bauer, "Abrasion of human enamel by different dental ceramics in vitro", *Journal of Dental Research*, 70 (1991) 221-225.
140. T.R. Katona, "A mathematical analysis of the role of friction in occlusal trauma", *The Journal of Prosthetic Dentistry*, Vol. 86 (2001), pp: 636-643.

CURRICULUM VITAE

PERSONAL INFORMATION

SURNAME, NAME: PARK, JONGEE

Nationality: Korean

Date and Place of Birth: 10 February 1971, SEOUL

Martial Status: Married

Phone: +90 312 287 0603

Mobil: +90 536 513 3264

email: e127227@metu.edu.tr

EDUCATION

Degree	Institution	Year of Graduation
MS	Hanyang Univ. Inorganic material Eng. Seoul, Korea	1995
BS	Hanyang Univ. Inorganic material Eng. Seoul, Korea	1993

WORK EXPERIENCE

Year	Place	Enrollment
2005-present	Department Metallurgical and Materials Eng. METU, Turkey	Project Researcher
2000-2001	Nano co. Ltd, Korea	R&D engineer
1995-2000	Hankook Titanium co. Ltd., Korea	R&D engineer
1994-1995	Inorganic materials Eng. Dep. Hanyang Univ. Seoul, Korea	Research Assistant
1993-1994	Korea Electron and Technology Institute	R&D researcher

PUBLICATION

1. Jongee Park and Abdullah Ozturk, "Effect of TiO₂ addition on the crystallization and tribological properties of MgO-CaO-SiO₂-P₂O₅-F glasses", *Thermochimica Acta*, doi:10.1016/j.tca.2008.01.018.
2. Jongee Park, Gurel Pekkan and Abdullah Ozturk, "Wear of MgO-CaO-SiO₂-P₂O₅-F Based Glass Ceramics Compared to Selected Dental Ceramics", *Research Letters in Materials Sciences*, Vol. 2007, doi:10.1155/2007/69897.
3. Jongee Park and Abdullah Ozturk, "Tribological Properties of MgO-CaO-SiO₂-P₂O₅-F Based Glass Ceramic for Dental Applications", *Materials Letters*, Vol.61 (2007), pp: 1916-1921.

CONFERENCE PRESENTATIONS

1. Jongee Park, Kaan Soysal and Abdullah Ozturk, "Comparison of Tribological properties of A-W glass-ceramics produced by Melt-casting and Powder-packing Processes", *SERES IV. Ceramic, Cam, Emaye, Sır ve Boya Semineri, Eskişehir, Turkey, 2007*, pp: 550-556.
2. Cektar Vakifahmetoglu, Jongee Park, Feza Korkusuz, Abdullah Ozturk and Muharrem Timucin, "Production and properties of apatite-wollastonite ceramics for biomedical applications", *11th CCT (International Congress on Ceramics, Cells and Tissues) Nanotechnology for Functional Repair and Regenerative Medicine, Faenza, Italy, 2007*.
3. Jongee Park and Abdullah Ozturk, "Determination of the crystallization kinetic parameters in MgO-CaO-SiO₂-P₂O₅-F glass", *Poster, 13th Interantional Metallurgical and Materials Congress, Istanbul, Turkey, 2006*.
4. Jongee Park and Abdullah Ozturk, "MgO-CaO-SiO₂-P₂O₅-F Camında Kristalleşme Kinetik Parametrelerinin Belirlenmesi", *III. Seramik, Cam, Emaye, Sır, ve Boya Semineri, Eskişehir, Turkey, 2005*, pp: 711-719.
5. Jongee Park and Abdullah Ozturk, "Tribological Properties of a Mica Containing Glass Ceramic", *Poster, Autumn Meeting of the Korean Ceramic Society, Dajon, South Korea, Oct., 2003*.
6. Jongee Park and Eun Sang Lee, "A study on the dielectric, piezoelectric and pyroelectric properties of PT-PCW ", *Presentation, Autumn Meeting of the Korean Ceramic Society, Seoul, South Korea, 1994*.

7. Jongee Park and Eun Sang Lee, “A study on the sintered property of PT-PCW system in high temperature”, Presentation, Spring Meeting of the Korean Ceramic Society, Seoul, South Korea, 1993.

PATENT

1. Jongee Park, Sungho Park and Wonjai Han, “The synthetic method of potassium titanate whisker”, KOR-156676, 1998.